

TRANSVERSE SUSCEPTIBILITY STUDIES OF RECORDING MEDIA

by

Richard David Cookson

A thesis submitted in partial fulfilment of the requirements of the University of Central
Lancashire for the degree of Doctor of Philosophy

at

Centre for Materials Science
University of Central Lancashire
Preston

December 2002

Supervisors:

Prof. P.R. Bissell

Dr. J.A. Gotaas

Acknowledgements

I would like to thank Prof. Phil Bissell for his supervision and support throughout my studies at the University of Central Lancashire. Thanks also to Professor K. O'Grady and Mr J.J. Blackwell of the University of York Magnetism Group for the provision and preparation of AMP powder samples.

I am indebted to the University of Central Lancashire for financial support and provision of laboratory and computing facilities. Members of support staff have also been of great assistance, particularly Barbara for rescuing my data on 'bad computer' days, and Roy for fixing 'blown' instrument components on "That wasn't supposed to happen" days during the instrumentation development.

Thanks are due to the other residents of the basement, in particular Tim, Gill and Marian for their friendship and discussions on magnetism and other subjects.

Finally, thanks to my family, and especially to Joanne, for putting-up with my lack of activity decorating the house, digging the garden, mowing the lawns etc. for the first 14 months of our marriage and for never questioning or doubting my sudden change in career or my ability to find work following it.

Abstract

A highly sensitive transverse susceptometer has been developed for the investigation of magnetic recording media. The susceptometer was based on the design of Pareti and Turilli[4] with modifications to the solenoid and sensing coils. The modifications have resulted in an improvement in the signal to baseline ratio of a factor of 525, and a reduction in random noise.

The increase in the sensitivity of the susceptometer allowed the investigation of Advanced Metal Particle (AMP) tapes and the measurement of the imaginary component of the transverse susceptibility (TS) proposed by Papusoi[5]. Also, a modification was developed which allowed the investigation of the non-linear TS, proposed by Chantrell *et al*[7]. The work reported for the latter two techniques was the first experimental demonstration of these measurements on magnetic recording media. Samples of Co- γ -Fe₂O₃, CrO₂, mixed γ -Fe₂O₃ / CrO₂ and AMP tapes were investigated, as were γ -Fe₂O₃, CrO₂ and AMP powders. The investigations suggested that the incoherent reversal mode was dominant in the systems containing CrO₂, with coherent reversal dominant in the remaining systems. The anisotropy peaks measured using the non-linear TS were found to be less dependent on sample texture than those of the traditional linear measurement. In particular the anisotropy peaks of the non-linear TS for incoherently reversing systems appeared to be independent of texture and it was proposed that these were a direct measure of the anisotropy field distribution, although independent verification was not performed.

The determination of magnetic coating thickness after Sollis and Bissell[6] was extended to allow the measurement of AMP tapes. A computer model was developed to investigate the error in the technique due to the particulate nature of the coating. The results of the model indicated that the error increased as coating thickness and volume packing fraction decreased. Correction factors were determined for MP3 and MP4 particle based systems.

The detection of the imaginary component of TS and its close agreement with the theoretical predictions of Papusoi suggested that the classification of TS as a 'stiffness' method of anisotropy field determination might be in error.

Table of Contents

| | |
|---|-----------|
| List of Figures | iv |
| List of Tables | ix |
| 1 Introduction | 1 |
| 1.1 Overview of Thesis | 1 |
| 1.2 Magnetic hysteresis | 3 |
| 1.3 Magnetic anisotropy | 5 |
| 1.4 Magnetic domains | 7 |
| 1.5 Stoner-Wohlfarth model | 8 |
| 1.5.1 Effect of the applied field direction, α | 10 |
| 1.5.2 Comparison with real systems | 15 |
| 1.5.3 Interactions | 15 |
| 1.6 Incoherent reversals | 16 |
| 1.7 Magnetic recording | 25 |
| 1.7.1 The recording process | 26 |
| 1.7.2 The design of recording media | 28 |
| 1.8 Magnetic characterisation of recording media | 31 |
| 1.8.1 Hysteresis parameters | 32 |
| 1.8.2 Orientation ratio | 32 |
| 1.8.3 IRM and DCD curves | 32 |
| 1.8.4 Anisotropy field | 34 |
| 2 Transverse susceptometer development | 39 |
| 2.1 Existing equipment | 39 |
| 2.1.1 Theory of design | 41 |
| 2.1.2 Limitations of existing equipment | 43 |
| 2.2 Design Development – Oscillator circuit | 45 |
| 2.3 Modifications to existing susceptometer | 48 |
| 2.3.1 Symmetry of sense coils | 49 |
| 2.3.2 Reduction of baseline | 52 |
| 2.3.3 Coaxial coils | 61 |

| | | |
|----------|--|------------|
| 2.3.4 | Balancing circuit | 64 |
| 2.4 | Solenoid de-coupling | 66 |
| 2.4.1 | Solenoid design | 66 |
| 2.5 | High field system | 71 |
| 2.6 | Control system | 75 |
| 2.6.1 | Field calibration routine | 76 |
| 2.6.2 | Field control routine | 76 |
| 2.6.3 | Loop control routine | 77 |
| 2.7 | Discussion | 77 |
| 3 | Linear transverse susceptibility | 79 |
| 3.1 | Previous work | 80 |
| 3.2 | Theory | 82 |
| 3.3 | Response to variation of ac field | 86 |
| 3.4 | Investigation of tape and powder samples | 88 |
| 3.4.1 | Metal particle tapes | 94 |
| 3.5 | Powders | 96 |
| 3.6 | Variation in response with sample alignment | 104 |
| 3.7 | Imaginary components | 107 |
| 3.8 | Discussion | 112 |
| 4 | Magnetic layer thickness measurement | 117 |
| 4.1 | Previous work | 118 |
| 4.2 | Application of technique to modern media | 120 |
| 4.3 | Effects of stacking samples | 121 |
| 4.4 | Measurement of MP samples | 123 |
| 4.5 | Demagnetising field model | 126 |
| 4.5.1 | Design of model | 127 |
| 4.5.2 | Calculation of effective demagnetising field | 128 |
| 4.5.3 | Programming model | 133 |
| 4.5.4 | Calculation of volume packing fraction | 136 |
| 4.5.5 | Results of model | 138 |
| 4.6 | Interpretation of model results | 142 |
| 4.6.1 | Corrected thickness values | 143 |

| | | |
|----------|--|------------|
| 4.7 | Other magnetic methods of determining layer thickness..... | 144 |
| 4.8 | Discussion..... | 145 |
| 5 | Non-linear transverse susceptibility | 147 |
| 5.1 | Theory..... | 148 |
| 5.2 | Modification of susceptometer | 151 |
| 5.3 | Response to variation of ac field..... | 152 |
| 5.4 | Investigation of tape and powder samples | 154 |
| 5.4.1 | Powders..... | 162 |
| 5.5 | Variation in response with sample alignment..... | 172 |
| 5.6 | Discussion..... | 175 |
| 6 | Conclusions & further work..... | 179 |
| | Appendix – Susceptometer control system software..... | 201 |

List of Figures

| | |
|--|----|
| Figure 1-1 Major hysteresis loop of a ferromagnetic material showing parameters used to characterise loop (after Sharrock[8]) | 4 |
| Figure 1-2 Closure domains in a cubic crystal..... | 8 |
| Figure 1-3 Stoner-Wohlfarth particle coordinates (after Cullity) | 9 |
| Figure 1-4 Energy as a function of h and θ for a particle with $\alpha=180^\circ$ | 11 |
| Figure 1-5 Energy as a function of h and θ for a particle with $\alpha=90^\circ$ | 12 |
| Figure 1-6 Energy as a function of h and θ for a particle with $\alpha=135^\circ$ | 13 |
| Figure 1-7 Switching field, h_c , as a function of switching angle, θ_c | 14 |
| Figure 1-8 Comparison of A) Fanning and B) Coherent modes of reversal for a chain of spheres (after Cullity[14])..... | 17 |
| Figure 1-9 curling and coherent rotation modes, b) and d) are cross sections normal to the z axis (after Cullity[14])..... | 18 |
| Figure 1-10 Coercivity as a function of angle between applied field and easy axis for different switching modes (after Bottoni[16]) | 25 |
| Figure 1-11 a) Schematic of digital recording process using an inductive ring head. b) Schematic write and read waveforms (after Chantrell & O'Grady)[9] | 27 |
| Figure 1-12 Hysteresis loop of an ideal recording medium..... | 29 |
| Figure 1-13 Typical IRM and DCD curves after Spratt <i>et al</i> [19]..... | 34 |
| Figure 2-1 Layout of existing transverse susceptometer | 40 |
| Figure 2-2 Balancing circuit | 41 |
| Figure 2-3 Oscillator χ_t circuit | 46 |
| Figure 2-4 Susceptometer initial baseline..... | 49 |
| Figure 2-5 Baseline with centred coils..... | 50 |
| Figure 2-6 Centred-coil baseline with control sample | 51 |
| Figure 2-7 Original baseline with control sample..... | 52 |
| Figure 2-8 Conservation of flux normal to surface, and field parallel to surface, at a boundary | 55 |
| Figure 2-9 Flux refraction at a boundary | 55 |
| Figure 2-10 – Model design of electromagnet yoke and solenoid..... | 57 |

| | |
|---|----|
| Figure 2-11 Solenoid flux density plot - core with permeability of unsaturated soft iron | 58 |
| Figure 2-12 – Solenoid flux density plot - core with $\mu_r = 5$ | 58 |
| Figure 2-13 – Solenoid flux density plot - core with $\mu_r = 2$ | 59 |
| Figure 2-14 Ac flux at sensing coil as a function of core and pole-piece permeability | 59 |
| Figure 2-15 Cross-section through coaxial coil assembly | 61 |
| Figure 2-16 Separate sensing coils system – control sample and baseline | 63 |
| Figure 2-17 Coaxial sensing coils system – control sample and baseline | 63 |
| Figure 2-18 – Operational amplifier active balancing circuit | 65 |
| Figure 2-19 Operational amplifier printed circuit design | 65 |
| Figure 2-20 MP tape control sample with baseline for single solenoid system | 69 |
| Figure 2-21 MP tape control sample with baseline for double solenoid system | 69 |
| Figure 2-22 Single-solenoid signal and baseline for low-field susceptometer (after Heuser[77]) | 70 |
| Figure 2-23 Concentric-solenoid signal and baseline for low-field susceptometer (after Heuser[77]) | 70 |
| Figure 2-24 Switching unit double pole crossover | 72 |
| Figure 2-25 Reversing unit direction indicator | 73 |
| Figure 2-26 Reversing unit indicator printed circuit board | 74 |
| Figure 2-27 Reversing unit comparator | 74 |
| Figure 2-28 Reversing unit comparator printed circuit board | 75 |
| Figure 2-29 Block diagram of transverse susceptometer control system | 76 |
| Figure 3-1 Sketch of energy minimum showing relationship between shape of curve, ac field energy, ΔE_{ac} , and oscillation angle, $\Delta\theta$ | 83 |
| Figure 3-2 Energy as a function of θ at $H_{dc}=0.95H_c$, arrow indicates broad minimum. | 85 |
| Figure 3-3 Expanded view of broad minimum | 85 |
| Figure 3-4 Orientation of particles giving dominant response | 87 |
| Figure 3-5 Susceptibility is measured by change in moment in the ac field direction | 87 |
| Figure 3-6 Response of χ_t signal to changing probe field | 88 |
| Figure 3-7 Co modified γ -Fe ₂ O ₃ VHS video tape χ_t plot | 91 |
| Figure 3-8 γ -Fe ₂ O ₃ / CrO ₂ mixed VHS video tape χ_t plot | 91 |
| Figure 3-9 CrO ₂ TK50 data tape χ_t plot | 93 |

| | |
|--|-----|
| Figure 3-10 MP tape χ_t plots. Zero's offset to separate traces | 95 |
| Figure 3-11 Normalised χ_t plots for MP tapes superimposed to show similarity of shape | 96 |
| Figure 3-12 Randomly oriented CrO ₂ powder χ_t plot..... | 97 |
| Figure 3-13 Randomly oriented CrO ₂ powder and aligned hand-spread after Sollis <i>et al</i> [86]..... | 97 |
| Figure 3-14 Randomly oriented γ -Fe ₂ O ₃ powder χ_t plot | 98 |
| Figure 3-15 Randomly oriented Co- γ -Fe ₂ O ₃ powder and aligned hand-spread after Sollis <i>et al</i> [86]..... | 98 |
| Figure 3-16 MP powder sample 1 χ_t plot | 100 |
| Figure 3-17 MP powder sample 2 χ_t plot | 101 |
| Figure 3-18 MP powder sample 3 χ_t plot | 101 |
| Figure 3-19 MP powder sample 4 χ_t plot | 102 |
| Figure 3-20 Theoretical curve for random easy axis distribution with coherent switching, $H_k=2100$ Oe, $\sigma_H=0.1$ Oe. After Hoare <i>et al</i> [79]..... | 103 |
| Figure 3-21 Theoretical curve for random easy axes switching by incoherent fanning after Berkov and Chantrell[93]..... | 104 |
| Figure 3-22 Alignment angle, β , of sample easy axis with respect to ac field direction | 105 |
| Figure 3-23 Aligned γ -Fe ₂ O ₃ hand spread, χ_t as a function of angle between sample alignment and ac field direction (β)..... | 106 |
| Figure 3-24 CrO ₂ TK50 tape, χ_t as a function of angle between sample alignment and ac field direction (β)..... | 106 |
| Figure 3-25 Real (solid line) and imaginary (dashed line) components of χ_t as a function of reduced field for a particle where $\alpha=90^\circ$ - after Papusoi[5]..... | 107 |
| Figure 3-26 Real (solid line) and imaginary (dashed line) components of χ_t for $\alpha=89.9^\circ$ - after Papusoi | 108 |
| Figure 3-27 Real (solid line) and imaginary (dashed line) components of χ_t for $\alpha=89.8^\circ$ - after Papusoi | 109 |
| Figure 3-28 Comparison of real and imaginary signal for a typical ($M_t = 6$) MP tape l 10 | |
| Figure 3-29 Imaginary transverse susceptibility plot for CrO ₂ TK50 tape..... | 110 |

| | |
|---|-----|
| Figure 3-30 Development MP tape imaginary [$\Im(\chi_t)$] plots. Zero's offset to separate traces | 111 |
| Figure 3-31 Shape difference of real and scaled-imaginary component of signal for a typical sample ($M_r t=6$)..... | 112 |
| Figure 4-1 Sample orientations for magnetic layer thickness determination | 118 |
| Figure 4-2 Anisotropy peaks for a typical sample a) in orientation 1 and b) in orientation 2..... | 119 |
| Figure 4-3 Flux is normal to sample plane so field at surfaces of cylinder is given by B/μ | 121 |
| Figure 4-4 B/μ is the same for both ends of the cylinder so the external field is unchanged by the sample | 122 |
| Figure 4-5 Transverse susceptibility response of layered samples showing peak position independent of number of layers..... | 123 |
| Figure 4-6 Typical measurement (sample $M_r t6$) showing change in peak position | 124 |
| Figure 4-7 Comparison of calculated thickness with $M_r t$ values..... | 126 |
| Figure 4-8 Axis definition and particle layout for demagnetising field model | 127 |
| Figure 4-9 Four-sheet magnetic layer (particle of interest shaded) | 129 |
| Figure 4-10 MP3 and MP4 particle shapes (not to scale)..... | 131 |
| Figure 4-11– Symmetry of particle sheet..... | 134 |
| Figure 4-12 Error in dipole estimate as a function of particle distance..... | 135 |
| Figure 4-13 MP3 particles effective demagnetising factor against VPF for varying layer thickness | 139 |
| Figure 4-14 MP4 particles effective demagnetising factor against VPF for varying layer thickness | 140 |
| Figure 4-15 Effective N_d vs. thickness for VPF=0.4 (assumed typical) | 142 |
| Figure 4-16 Comparison of magnetic thickness evaluation techniques after Bissell <i>et al</i> | 145 |
| Figure 5-1 Change in moment in dc field direction due to action of ac field | 148 |
| Figure 5-2 Coordinate system for particle with easy axis direction E after Chantrell <i>et al</i> [7]..... | 149 |
| Figure 5-3 Modelled comparison of $\chi_{nl}/10$ (solid line) to χ_t (dashed line) after Chantrell <i>et al</i> [7]..... | 150 |

| | |
|---|-----|
| Figure 5-4 Modelled comparison of $\chi_{nl}/10$ to χ_t with texture symmetry axis at 5° to ac field after Chantrell <i>et al</i> [7] | 150 |
| Figure 5-5 Sensing and compensating coil layout for χ_{nl} measurement | 152 |
| Figure 5-6 χ_q sense coil voltage as a function of ac solenoid current..... | 154 |
| Figure 5-7 Comparison of χ_t and χ_{nl} plots for CrO ₂ TK50 data tape | 155 |
| Figure 5-8 Phase change in measurement with moment switching..... | 157 |
| Figure 5-9 Co- γ -Fe ₂ O ₃ commercial VHS tape χ_{nl} plot | 158 |
| Figure 5-10 Mixed γ -Fe ₂ O ₃ / CrO ₂ commercial VHS tape χ_{nl} plot | 159 |
| Figure 5-11 Commercial CrO ₂ TK50 data tape χ_{nl} plot..... | 159 |
| Figure 5-12 γ Fe ₂ O ₃ powder χ_{nl} plot..... | 163 |
| Figure 5-13 CrO ₂ powder χ_{nl} plot..... | 163 |
| Figure 5-14 MP powder sample 1 χ_{nl} plot | 164 |
| Figure 5-15 MP powder sample 2 χ_{nl} plot..... | 165 |
| Figure 5-16 MP powder sample 3 χ_{nl} plot..... | 165 |
| Figure 5-17 MP powder sample 4 χ_{nl} plot..... | 166 |
| Figure 5-18 χ_{nl} difference curves for MP powder samples showing irreversible response | 167 |
| Figure 5-19 χ_t difference curves for MP powder samples showing irreversible response | 168 |
| Figure 5-20 Idealised form of mean χ_{nl} curve (solid line), dashed lines show underlying features..... | 169 |
| Figure 5-21 Mean χ_{nl} curves for MP powder samples 1, 3 and 4..... | 169 |
| Figure 5-22 Mean χ_{nl} plot for MP powder sample 2 | 170 |
| Figure 5-23 Energy diagram for particle aligned with dc field | 171 |
| Figure 5-24 Predicted susceptibility of a particle with easy axis parallel to the dc field direction | 171 |
| Figure 5-25 Co- γ -Fe ₂ O ₃ VHS video tape, variation of χ_{nl} response with sample alignment..... | 173 |
| Figure 5-26 Co- γ -Fe ₂ O ₃ VHS video tape, alignment angle $\beta = 90^\circ$ | 174 |
| Figure 5-27 CrO ₂ TK50 data tape, variation of χ_{nl} response with sample alignment... | 174 |

List of Tables

| | |
|--|-----|
| Table 2-1 Changes in signal-to-noise ratio | 78 |
| Table 3-1 Characteristics of commercial tape samples..... | 92 |
| Table 3-2 Commercial tape - ratio of anisotropy peak values to coercivity | 92 |
| Table 3-3 Characteristics of development MP tape samples | 94 |
| Table 3-4 Anisotropy peak value as a function of nominal M_t value..... | 94 |
| Table 3-5 Characteristics of MP powder samples | 99 |
| Table 4-1 Static characteristics of tape samples | 124 |
| Table 4-2 Results of demagnetising field and magnetic layer thickness calculations.. | 125 |
| Table 4-3 Particle parameters for demagnetising field model | 138 |
| Table 4-4 Magnetic layer thickness (/nm) for MP3 particle model..... | 141 |
| Table 4-5 Magnetic layer thickness (/nm) for MP4 particle model..... | 141 |
| Table 4-6 Correction of thickness iterations for $M_t=3$ | 143 |
| Table 4-7 Thickness measurements corrected using results of model..... | 143 |
| Table 5-1 Comparison of χ_{nl} peak values with χ_t peaks and VSM measurements..... | 160 |
| Table 5-2 Comparison of anisotropy and switching peak values for $\gamma\text{-Fe}_2\text{O}_3$ and CrO_2 powders | 162 |
| Table 5-3 χ_{nl} peak positions of metal particle powder samples..... | 166 |
| Table 6-1 Calculated coercivities of typical recording particles for Stoner-Wohlfarth (C), chain-of-spheres coherent (B) and chain-of-spheres 'fanning' (A) reversal modes | 181 |

1 Introduction

This thesis is concerned with the theory, measurement and applications of the transverse susceptibility of magnetic recording media. The transverse susceptibility of magnetic materials was first discussed by Gans in 1909[1] but was not of major interest to experimentalists until the publication of the Stoner-Wohlfarth[2] model of magnetic hysteresis for uniaxial, single domain particles in 1947. The Stoner-Wohlfarth model allowed the hysteretic behaviour of uniaxial, single domain particles to be defined completely from the knowledge of two particle parameters, the saturation magnetisation and the anisotropy field. The saturation magnetisation could relatively easily be determined for bulk materials but the anisotropy field was different for each particle and its measurement depended on precise knowledge of the particle orientation with respect to an applied field. The theoretical work of Aharoni *et al*[3] in 1957 suggested that the transverse susceptibility of a system of Stoner-Wohlfarth type particles would contain information about the distribution of anisotropy fields and this was confirmed experimentally by Pareti and Turilli[4] in 1987.

Since the initial experiment of Pareti and Turilli considerable further theoretical and experimental development has been carried out with the aim of developing a fast and practical method of using transverse susceptibility for the measurement of anisotropy field distributions of samples of magnetic recording media and this thesis is concerned with recent developments to the technique made at the University of Central Lancashire.

1.1 Overview of Thesis

The thesis is split into six chapters as follows:

Chapter 1. Introduction. This chapter gives an overview of the content of the thesis and contains background information required for a full understanding of the remainder of the thesis. The background information includes,

- An overview of magnetic hysteresis, magnetic anisotropy and magnetic domains.

- An overview of the Stoner-Wohlfarth model of hysteresis for single domain, uniaxial particles and a brief discussion of some of the limitations of the model.
- A discussion of the incoherent reversal of single domain, uniaxial particles.
- An overview of the design and manufacture of magnetic recording media.
- An overview of the methods used to characterise magnetic recording media.
- An overview of the methods used to determine the anisotropy field distribution of magnetic recording media.

Chapter 2. Transverse Susceptometer Development. This chapter contains a description of the susceptometer previously developed at Preston based on the design of Pareti and Turilli. The chapter goes on to describe a number of design developments which were made to improve the performance of the susceptometer for use with modern magnetic recording media. The developments described include improvements to the signal processing electronics, mechanical isolation of vibration, coil and solenoid geometry and positioning, implementation of a high-field electromagnet, de-coupling of the ac solenoid field from the electromagnet and the design of an automated computer control system.

Chapter 3. Linear Transverse Susceptibility. This chapter outlines the theory of the linear transverse susceptibility and reviews previous research in the field. The chapter goes on to describe investigations made to test the response of the susceptometer against that predicted by theory, and investigations of samples of magnetic recording media. Investigations are presented of commercial and development recording tapes and of particle powders and an investigation is made on the effect of measuring the sample at different angles with respect to the sample easy axis. A further investigation is made to determine the existence of the imaginary component of the transverse susceptibility which was proposed in the theoretical paper of Papusoi[5]. The results of the investigations are discussed.

Chapter 4. Magnetic Layer Thickness Measurement. This chapter reviews the technique of magnetic layer thickness measurement reported by Sollis and Bissell[6] and details the application of the technique to modern media. The investigation of a series of dual coated metal particle tapes is reported, for which traditional mechanical measurement techniques could not be used. A numerical computer model is also developed to determine the error in the assumption that particulate magnetic layers can be treated as homogeneously magnetised sheets in the calculation of out-of-plane demagnetising factors for particulate recording media. The results of the model are discussed and corrections are applied to the magnetic layer thickness measurements.

Chapter 5. Non-linear Transverse Susceptibility. The theory of non-linear transverse susceptibility and its proposal by Chantrell *et al*[7] as an improved method for the detection of anisotropy information in magnetic recording media is reviewed. The modification of the susceptometer to investigate non-linear transverse susceptibility is detailed and the response of the susceptometer is compared to that predicted by theory. A number of magnetic recording tapes and magnetic particle powders are investigated and the effect of sample measurement angle for an aligned system of particles is reported. The results are discussed and comparison is made with the traditional linear transverse susceptibility.

Chapter 6. Conclusions and Further Work. The conclusions of the previous chapters are drawn together and applications of the various techniques are discussed. Areas of further work are identified which would further extend the usefulness of the techniques detailed.

1.2 Magnetic hysteresis

Magnetic hysteresis is the process by which, after the application and removal of a magnetic field to a ferromagnetic material, a residual or remanent magnetisation remains and the magnetisation does not fall back to its original level.

Relatively small field applications show hysteresis in magnetic materials by permanently changing the magnetisation of a small fraction of the material, but the measured change in magnetisation in these cases is dependent on the ‘magnetic history’

of the material prior to application of the field. In order to characterise the magnetic behaviour of a material in a repeatable manner, large fields are used to first ‘saturate’ the material (i.e. to apply a large field such that all of the magnetic moment vectors within the sample align with the applied field and a maximum magnetisation is reached which does not increase significantly with further increases in the applied field). The applied field is then swept from the positive saturation value to the negative saturation value and back again, whilst the magnetisation of the sample is recorded as a function of the applied field. The resulting plot of magnetisation against field is known as the ‘major hysteresis loop’ and gives the most important parameters by which magnetic recording media are characterised. Figure 1-1, after Sharrock[8], shows a typical major hysteresis loop and defines the main hysteresis parameters.

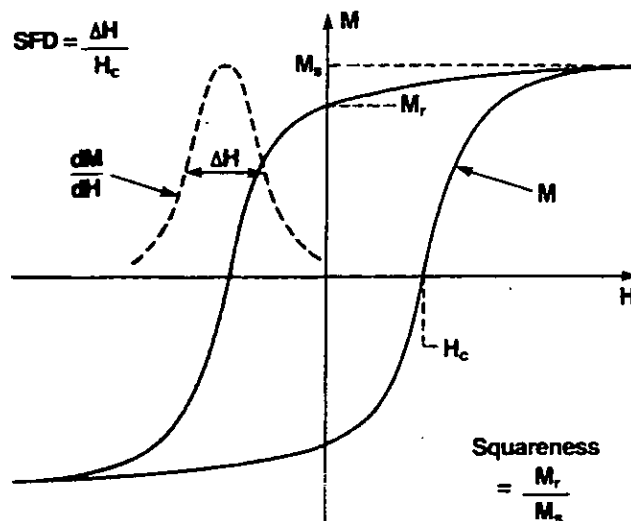


Figure 1-1 Major hysteresis loop of a ferromagnetic material showing parameters used to characterise loop (after Sharrock[8])

The loop parameters shown in Figure 1-1 are as follows:

- The saturation magnetisation, M_s , which is the magnetisation at the maximum applied field. Although the M_s value does not increase significantly with further increases in applied field a small reversible increase will occur. For this reason it is important when comparing values of M_s that the saturation is measured at the same applied field value.
- The remanent magnetisation, M_r , is the residual magnetisation of the sample when the applied field is reduced to zero following saturation.

- The coercivity, H_c , is the reverse field which must be applied to the sample following saturation which causes the magnetisation of the sample to reduce to zero.
- The Switching Field Distribution (SFD) is a measure of the spread of switching field values at which irreversible magnetisation changes take place in the sample. The SFD is obtained by differentiating the hysteresis loop to obtain the rate of change of magnetisation about the coercivity, and taking the full-width at half-maximum value of the distribution. The SFD can either be expressed directly as a field interval, or divided by the coercivity (as shown in Figure 1-1) to obtain a dimensionless reduced value.
- The squareness is a measure of the shape of the loop which expresses the fraction of saturation magnetisation retained after removal of the applied field. The squareness is obtained by dividing the remanent magnetisation, M_r , by the saturation magnetisation, M_s .

Care must also be taken when comparing parameters obtained from hysteresis loops that the rate of change of the applied field is similar for the loops compared. Magnetic particles within a sample that are in a metastable state close to their switching value may be switched by thermal effects introducing a time dependence to the magnetisation, known as 'magnetic viscosity'. Hysteresis loops are measured by a number of instruments including BH loopers and Vibrating Sample Magnetometers (VSMs). BH loopers use an ac supply at typically 50~60 Hz to directly drive the field, resulting in the field executing a full cycle in $\sim 1/50$ second, whereas a VSM with a highly inductive electromagnet may take many minutes to perform the same cycle, resulting in differences in the shape of the loop and in the measured parameters such as H_c [9].

1.3 Magnetic anisotropy

Magnetic anisotropy[10] is the way in which the magnetic properties of a material are dependent on the direction in which they are measured. In practical terms we find that many materials are easier to magnetise in one direction than they are in another. The directions of easy magnetisation are referred to as easy axes and those of hard magnetisation, hard axes.

The magnetic anisotropy of magnetic materials is found to have a number of different origins, two of which are important in the design of magnetic recording media:

- Crystal anisotropy – preferred easy directions of magnetisation with respect to the crystal lattice. These are due to quantum coupling effects between electron spin moments in the crystal.
- Shape anisotropy – preferred easy directions of magnetisation with respect to the shape of the magnetised body. These are due to the minimisation of magnetostatic energy and are analogous to the distribution of electrical charge on a charged body to minimise electrostatic energy.

As magnetising a material in a hard axis direction requires work to be done on the material, magnetic anisotropy is associated with a stored energy. If we take a cubic crystal and apply a saturating field to it such that its magnetisation vector, M_s , makes angles a, b, c with the crystal axes the crystalline anisotropy energy is given by the series,

$$E = K_0 + K_1 (\alpha_1^2 \alpha_2^2 + \alpha_2^2 \alpha_3^2 + \alpha_3^2 \alpha_1^2) + K_2 (\alpha_1^2 \alpha_2^2 \alpha_3^2) + \dots, [10] \quad (1.1)$$

where $\alpha_1, \alpha_2, \alpha_3$ are the cosines of angles a, b, c respectively. The K_0 term is a constant and so can be neglected, as can the higher terms above K_2 . If we neglect these terms and consider a crystal which has uniaxial anisotropy the above equation becomes,

$$E = K_1 \sin^2 \theta + K_2 \sin^4 \theta. \quad (1.2)$$

Shape anisotropy is again expressed as the energy stored in the system by the deviation of the magnetisation vector from the easy axis direction. If we take a crystal which is magnetically isotropic and form it into a prolate spheroid it becomes uniaxially anisotropic due to its shape and it can be shown that its anisotropy energy is given,

$$E = K_s \sin^2 \theta, \quad (1.3)$$

where θ is the angle between the particle moment and the easy axis. We can see that this has the same form as the first term of equation (1.2) for uniaxial crystalline anisotropy.

If we mix shape and crystalline anisotropies by producing a prolate spheroid from an anisotropic crystal we find that the resultant particle also has uniaxial anisotropy, with the easy axis somewhere between the shape easy axis and the closest crystal easy axis. The mixed uniaxial anisotropy may be expressed,

$$E = K_u \sin^2 \theta, \quad (1.4)$$

which is the uniaxial anisotropy upon which the Stoner-Wohlfarth model of uniaxial particle rotation and switching is based. The above equation and the Stoner-Wohlfarth model must be used with some caution as the K_2 term of the crystal anisotropy is neglected which may lead to errors when dealing with materials which have a high value of K_2 .

1.4 Magnetic domains

Section 1.3 introduced the preference of magnetic materials to magnetise in some particular direction with respect to the crystal axis. In addition to these intrinsic properties, the direction of the magnetic moment is also influenced by interactions with the moments of the surrounding material, which take two different forms. Exchange interactions are due to a short-range quantum effect, by which it is energetically preferable if the electron-spin magnetic moments line up parallel to their neighbours. The effect of this is that neighbouring magnetic moments tend to align in the same direction along one of the crystal easy axes. If exchange were the only interaction effect, a crystal of magnetic material would spontaneously magnetise to its saturation magnetisation along one of the easy axis directions without the application of an external field. The other interaction effect between the magnetic moments is the long-range magnetostatic interaction. This effect seeks to reduce the total magnetostatic energy of the magnetic field by 'flux closure' (the formation of closed loops of flux within the material to reduce the stray flux outside the magnetic material).

Small particles of ferromagnetic material are dominated by short-range exchange forces which keep the electron-spin magnetic moments parallel resulting in a particle with a constant absolute magnetisation equal to its saturation magnetisation. These are known as 'single domain' particles and are important in the manufacture of recording media and permanent magnets. As particles become larger, the longer-range magnetostatic forces become dominant and the particle forms magnetic domains. These are small volumes within which the magnetic moments remain parallel along the easy magnetisation axes of the crystal but which have different magnetisation directions relative to one another. The domain magnetisation directions are arranged to minimise stray flux such that the whole particle has zero net magnetic moment (see Figure 1-2).

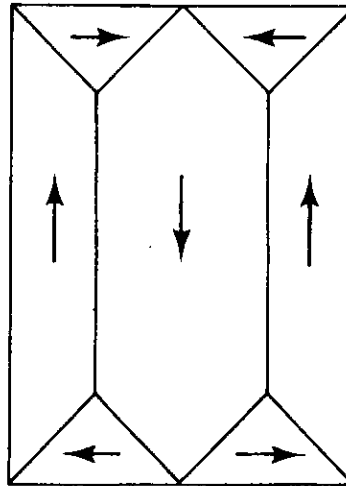


Figure 1-2 Closure domains in a cubic crystal

When such a material is subjected to an applied magnetic field it is magnetised first by the process of domain wall motion. Domains that are close to the direction of magnetisation grow, whilst those opposing it shrink. In this way the material has a net moment in the direction of magnetisation whilst all the individual domain moments remain in the easy axis directions of the crystal. As the applied field is further increased the domain aligned most closely with the field will continue to grow until all of the crystal is magnetised in this direction. Subsequent increases in the applied field rotate moments out of the easy axis direction, into the direction of the applied field, saturating the crystal. With the removal of a saturating field the moments will rotate back to the nearest easy axis direction to minimise magnetostatic energy. A field applied in the reverse direction allows domain walls to propagate and move until the magnetisation has been fully reversed.

1.5 Stoner-Wohlfarth model

The model proposed by Stoner and Wohlfarth[2] in 1948 attempted to explain the hysteretic behaviour of many magnetic materials by determining the energy of a small, single domain, uniaxial magnetic particle as a function of applied field and the angle of the magnetisation vector. The model assumes that the magnetic moments within the particle remain parallel to one-another (coherent) during rotation and switching. Hence, the particle will have a constant intensity of magnetisation, which changes only in direction. By finding the total energy minima it is possible to predict the magnetisation rotation and switching behaviour of the particle under the influence of an applied field.

Bulk magnetic materials may be modelled by using assemblies of these particles with varied distributions of easy axis direction, anisotropy and spacing. In some conditions particles within a magnetic material will rotate incoherently in order to minimise local magnetostatic energy and in these circumstances the Stoner-Wohlfarth model breaks down.

In the original Stoner-Wohlfarth paper, the applied field direction is taken as the datum from which the particle easy-axis and magnetic moment vector angles are defined. For the modelling of magnetic materials this is very convenient as it allows the easy axis distribution of a system of particles to be easily expressed as a distribution of angles compared to the applied field. When considering a single particle however, it is often more convenient to treat the easy-axis direction as the datum, leading to a simplified notation and coordinate system. The outline of the model herein, after Cullity[11], is expressed in such a coordinate system;

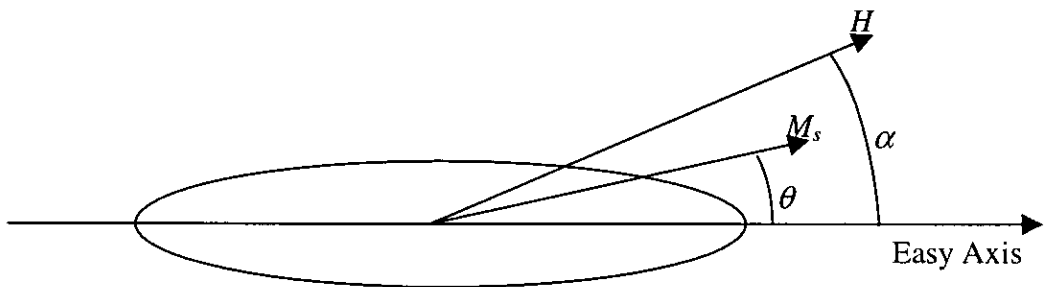


Figure 1-3 Stoner-Wohlfarth particle coordinates (after Cullity)

In the system shown in Figure 1-3, which represents a single domain, uniaxial particle, the anisotropy energy can be expressed as,

$$E_a = K_u \sin^2 \theta. \quad (1.5)$$

Where K_u is a constant which characterises the shape, stress and crystalline anisotropy of the particle, and θ is the angle between M_s and the easy axis direction (see equation (1.4)).

The potential energy, E_p , as a result of applying an external field H at angle α with respect to the easy axis direction is,

$$E_p = -H \cdot M_s \cos(\alpha - \theta). [11] \quad (1.6)$$

Hence, the total energy is given by,

$$E = K_u \sin^2 \theta - H \cdot M_s \cos(\alpha - \theta). \quad (1.7)$$

The anisotropy field, H_k , is defined as the field value at which the particle saturates with the field applied in the direction normal to the easy axis. It can be shown that the value of the anisotropy field is given by,

$$H_k = \frac{2K_u}{M_s}. \quad (1.8)$$

If we express H in terms of 'reduced field', $h = H/H_k$, equation (1.7) becomes,

$$E = H_k \cdot M_s \left(\frac{1}{2} \sin^2 \theta - h \cos[\alpha - \theta] \right). \quad (1.9)$$

Equation (1.9) allows us to plot the energy for a field applied at angle α as a function of h and θ , hence the θ values of the local energy minima give the stable equilibrium directions of the magnetisation vector. In this way the stable equilibria of M_s may be defined as those where the conditions $dE/d\theta = 0$ and $d^2E/d\theta^2 > 0$ are met.

We can now deal with a number of specific cases for different values of α .

1.5.1 Effect of the applied field direction, α

a) Particles where $\alpha = 180^\circ$

For a particle where $\alpha = 180^\circ$ (i.e. the applied field is antiparallel to the direction of magnetisation along the easy axis) the energy as a function of θ is shown in Figure 1-4.

With zero applied field ($h=0$) the energy function has two minima, at $\theta = 0^\circ$ and $\theta = 180^\circ$. As we increase the field the depth of the energy well at $\theta = 0^\circ$ reduces. We can see that the stable equilibrium at $\theta = 0^\circ$, changes to become an unstable equilibrium at a field value of $h = 1$. Above this field, a moment with an angle $\theta = 0^\circ$ would switch to the $\theta = 180^\circ$ position. The value of h at which this occurs is known as the switching field, h_c . For Figure 1-4, where $\alpha = 180^\circ$, we can see that $h_c = H_k$.

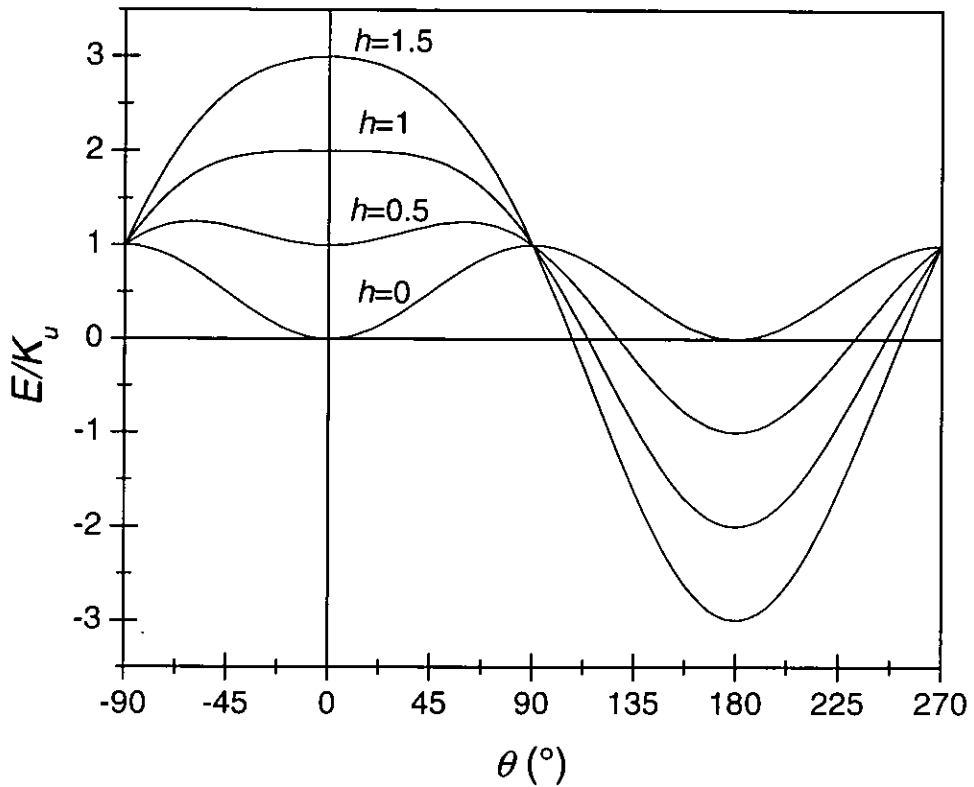


Figure 1-4 Energy as a function of h and θ for a particle with $\alpha=180^\circ$

b) Particles where $\alpha = 90^\circ$

If we consider a particle where a field is applied perpendicular to the easy axis direction, (i.e. $\alpha = 90^\circ$) the energy function is as shown in Figure 1-5. Here we can see that as the field is increased the angular position of the minima change, causing the magnetisation vector to rotate. Neither of the minima disappear at higher fields, instead they merge to form a single minima at $\theta = 90^\circ$ when $h=1$. The effect of this is that the magnetisation will rotate continuously from the easy axis to the hard axis direction without any switching behaviour. The particle moment will be aligned with the applied field (hard axis direction) at an applied field of $h \geq 1$ ($H \geq H_k$).

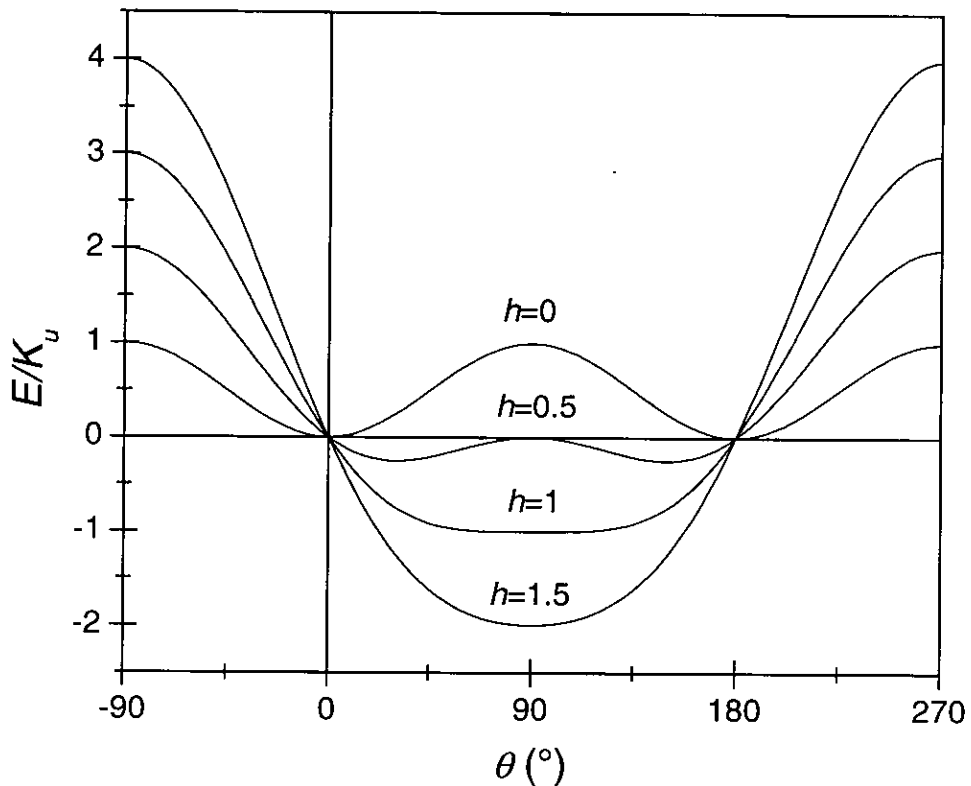


Figure 1-5 Energy as a function of h and θ for a particle with $\alpha=90^\circ$

c) Particles where $90^\circ < \alpha < 270^\circ$

For a particle where a field is applied at an angle greater than 90° from the easy axis direction a combination of rotation and switching governs the magnetisation of the particle (with $\alpha = 180^\circ$ as a special case where the reversible rotation component is zero). Figure 1-6 shows the energy function for a particle where $\alpha = 135^\circ$. In this case we can see that the angular position of the minimum at $\theta = 0$ starts to change as the field is applied, causing the magnetisation vector to rotate. At a field value somewhere between $h=0.4$ and $h=0.6$ (actually at $h=0.5$ for this particular angle) the minimum changes to a point of inflection and at this point the magnetisation will switch to the remaining minimum. Subsequent increases in the field continue to rotate the magnetisation vector towards the field direction but saturation in the direction of the field ($\theta = \alpha$) will only be achieved when $h = \infty$. Note that in this case the switching occurs at a field where $h < 1$ and nothing significant happens at the field value $h=1$.

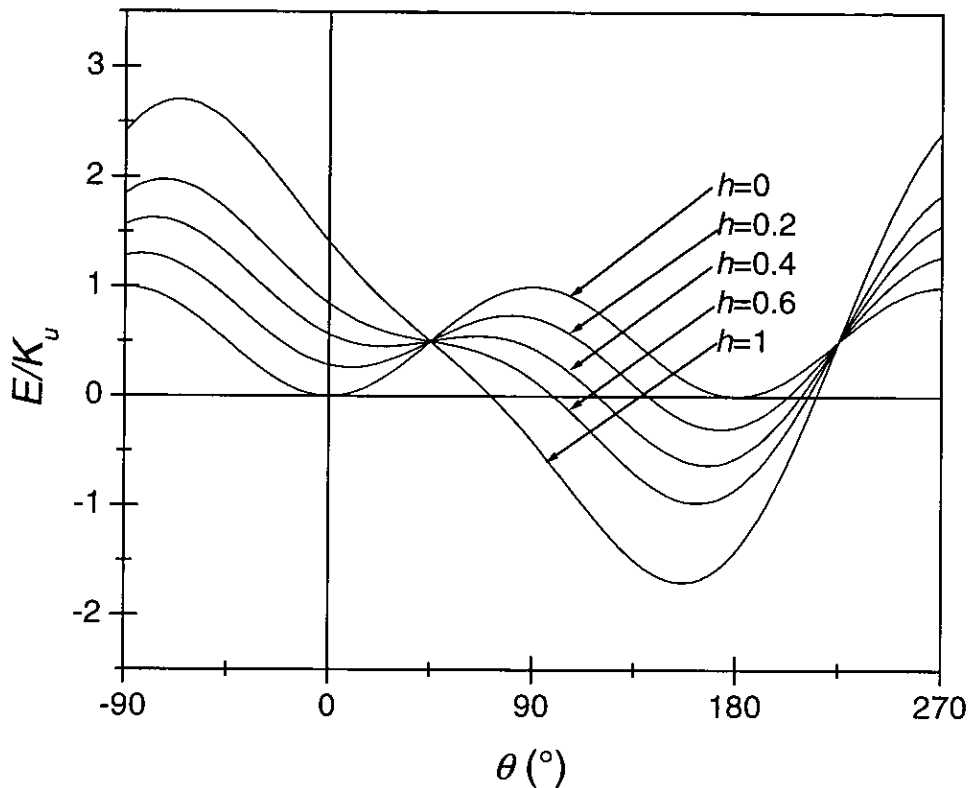


Figure 1-6 Energy as a function of h and θ for a particle with $\alpha=135^\circ$

d) General case

For the special case where $\alpha = 180^\circ$ there is no change in the magnetisation vector as a result of increasing field until the field reaches $h=1$, when the particle switches and the magnetisation is subsequently saturated in the field direction. Also, for the special case where $\alpha = 90^\circ$ the magnetisation rotates continuously with increasing field until the field reaches $h=1$, at which point the magnetisation vector is aligned with the applied field and the magnetisation is saturated in the field direction. For all other cases the magnetisation rotates towards the applied field direction tending to saturate in the field direction as the field approaches infinity. Where the magnetic moment direction at $h=0$ is greater than 90° from the direction of the applied field a switching event will also occur at some point during the rotation.

In order to determine at what angle, θ_c , and at what field, h_c , a switching event will occur we consider the conditions for switching. In order for a moment to switch, the energy minimum in which the moment rests must become a flat

point-of-inflection. Hence $dE/d\theta = 0$ and $d^2E/d\theta^2 = 0$. The solution of equation (1.9) for these conditions gives the following two equations[11],

$$\tan^3 \theta_c = -\tan \alpha, \quad (1.10)$$

$$h_c^2 = 1 - \frac{3}{4} \sin^2 2\theta_c. \quad (1.11)$$

From these equations it is possible to determine the switching angle as a function of the applied field angle, and the switching field as a function of the switching angle.

The latter equation is an interesting result as it shows that the maximum switching field is equal to H_k and occurs only where the switching angle θ_c , is parallel, or orthogonal to the easy axis direction. The switching field, h_c , as a function of the switching angle, θ_c , is shown in Figure 1-7.

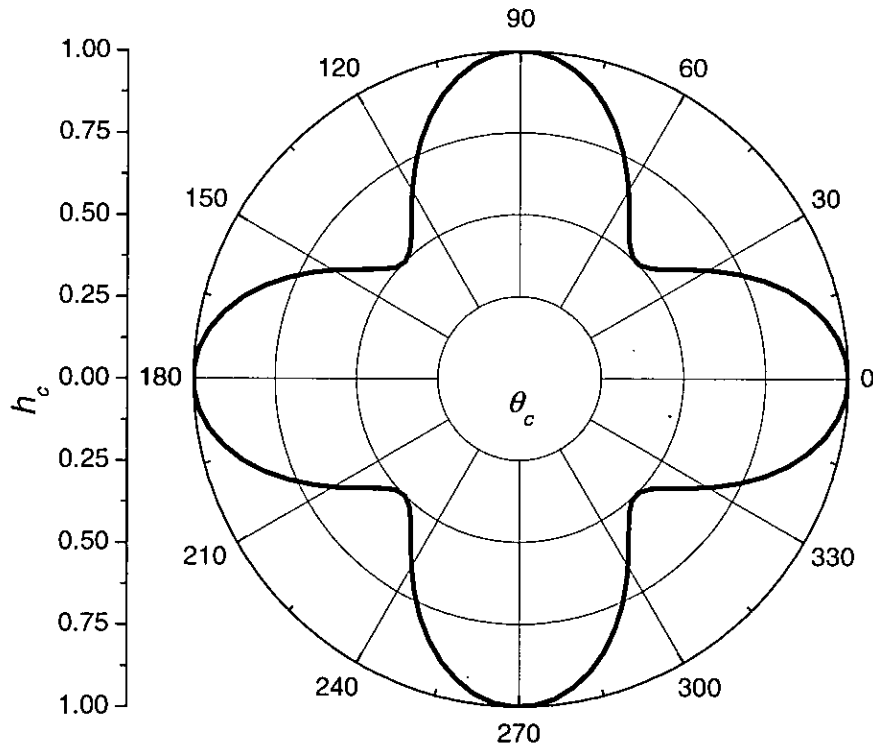


Figure 1-7 Switching field, h_c , as a function of switching angle, θ_c

The Stoner-Wohlfarth model has proved to be invaluable in the theoretical modelling of systems of magnetic particles such as those used in magnetic recording media. By reference to equation (1.5) we see that the behaviour of a Stoner-Wohlfarth particle can be completely described by defining the two parameters, M_s and H_k .

1.5.2 Comparison with real systems

In order to compare models developed using the Stoner-Wohlfarth equations with real magnetic systems we must determine the saturation magnetisation, M_s , and the anisotropy field, H_k , distribution for the particular material.

The M_s value is constant for a given material and is relatively easily obtained from measurements of the bulk material, however, H_k is a function of the particle shape, the material, the alignment of the crystal lattice axes with the particle axes, the particle stress and a number of other parameters which contribute to the particle anisotropy. As such the anisotropy fields of particles in a real system must be expressed as a distribution. H_k is only measurable from the switching behaviour of particles where the applied field is either parallel or orthogonal to the particle easy axis. As a real material will contain a distribution of particle shapes, sizes and orientations with respect to any applied field the switching of the particles will take place over a range of field values making it difficult to determine which particles are switching at their anisotropy field value and which are switching at a lower field.

A number of techniques have been developed in an attempt to measure the anisotropy field distribution of magnetic recording media, the most common of which are detailed in section 1.8.4.

1.5.3 Interactions

Simple magnetic models based on Stoner-Wohlfarth particles can be made by assuming a particular distribution of easy-axis directions and anisotropies and summing the resulting magnetisation vectors for a particular applied field.

In a real system the local magnetic field at a particular particle will be the result of the applied field, and the field due to the magnetisation of the other particles. As the magnetisation of the surrounding particles changes, so will the local field. These effects due to the changing magnetic moment of the surrounding particles, are known as magnetostatic interactions. Various iterative numerical modelling techniques may be used to dynamically calculate the local field values in a changing system. However, in simple models these effects are often neglected. If more accurate results are required these effects must be taken into account by producing a more complex model using micro-magnetic modelling techniques. Comparisons of modelled coercivity values for

systems of particles with experimental measurements tend to suggest that bulk system H_c values are lowered by the effect of interactions and hence vary as a function of the packing fraction of the magnetic particles in the media[12,13].

There are also interactions known as ‘exchange interactions’ that are due to a quantum effect which favours the parallel alignment of electron spin magnetic moments. These exchange interactions are very short-ranged and are generally not considered to have a significant inter-particle effect. They do, however, have an effect on the switching behaviour within the particle and in the Stoner-Wohlfarth model it is assumed that the exchange interactions are sufficiently high that the particles reverse coherently.

1.6 Incoherent reversals

The publication of the Stoner-Wohlfarth model stimulated a great deal of research and development into the production of fine particle magnetic systems as the theory predicted very high coercivity magnets could be produced from systems of aligned single-domain uniaxial particles. When techniques for the manufacture of fine iron particles by electrodeposition in mercury were finally developed, the coercivity of magnets made from these fine particles was found to be much less than that predicted by the Stoner-Wohlfarth model. In order to explain this discrepancy, a number of modifications to the Stoner-Wohlfarth model were proposed, and experimental techniques were developed to test these proposals. The modifications to the Stoner-Wohlfarth model questioned the assumption that the magnetic moment of a single domain particle would remain invariant during switching and proposed that in some circumstances flux closure would occur within the particles during reversal, increasing exchange energy and decreasing magnetostatic energy in order to minimise the total energy of the particle. The strength of exchange interaction is a function of the particular material and is difficult to determine other than by empirical methods. In 1955, Jacobs and Bean[14] developed the chain-of-spheres model.

The theory was developed to model the switching of electrodeposited iron particles, which were observed to be ‘peanut’ shaped, i.e., roughly cylindrical with periodic bulges. The particles were represented by chains of spheres, such that each sphere had a point contact with its neighbour and the moment of each sphere was considered to rotate coherently. With zero applied field, the particle energy was minimised when the

moments of the spheres aligned parallel to the long axis of the particle. Jacobs and Bean then calculated the field required to reverse the magnetisation of the particle, making the assumption that exchange interactions dominated within each sphere, so each sphere rotated coherently, but no exchange interaction existed between neighbouring spheres (i.e. a point contact was assumed). Two modes of reversal were investigated, coherent, where the moments of every sphere remained parallel during reversal, and ‘fanning’, where the moments of neighbouring spheres rotated in opposite directions to one-another. Figure 1-8 shows a comparison of fanning and coherent modes of rotation for a chain of two spheres after Cullity.

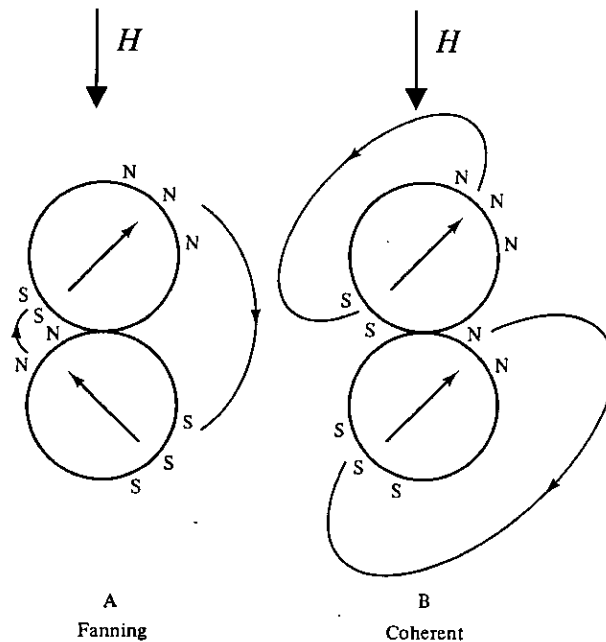


Figure 1-8 Comparison of A) Fanning and B) Coherent modes of reversal for a chain of spheres (after Cullity[15])

The coercivity predicted by the chain of spheres model was much closer to that observed experimentally for the electrodeposited iron particles. The fanning model is however unrealistic in that the spheres are considered to be in point contact allowing exchange interactions between spheres to be neglected. Also, advances in particle morphology produced particles with much more regular shapes which still had coercivities lower than those predicted by the Stoner-Wohlfarth model but which could not reasonably be represented by chains of spheres in point contact. In 1957 Frei, Shtrikman and Treves[16] used analytical techniques to determine the lowest energy reversal mode for an infinite cylinder. The three possible modes of rotation were found

to be coherent, 'buckling' and 'curling'. The 'buckling' mode was later discounted for particles of a useful length[17]. In the curling mode of reversal, as the particle moments reversed they 'curled' around to form closed rings around the particle axis. Figure 1-9 shows a section through a particle undergoing curling and coherent modes of switching.

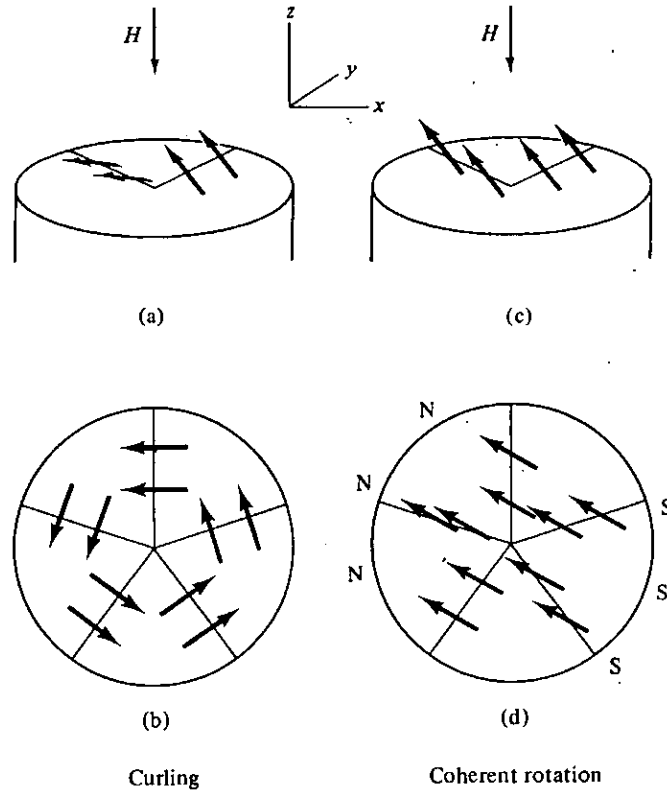


Figure 1-9 curling and coherent rotation modes, b) and d) are cross sections normal to the z axis (after Cullity[15])

From Figure 1-9 it can be seen how curling reduces the stray flux outside the particle, however, it is also clear that exchange interactions must be overcome for curling to occur. This condition results in a critical particle diameter, d_0 , which must be exceeded for curling to occur. For particles below the critical diameter, coherent reversal is energetically favourable.

In 1957 Jacobs & Luborsky[18] used aligned dilute systems of electrodeposited metal particles to determine the coercivity of systems as a function of angle and found that the coercivity initially increased as the angle between the easy axis and the applied field increased, in line with the chain-of-spheres 'fanning' model. The rotational hysteresis integral was also found to be consistent with chain-of-spheres 'fanning'. However, analysis of high-field torque curves and rotational hysteresis gave values between those

predicted for chain-of-spheres coherent rotation and Stoner-Wohlfarth rotation. Also in 1957, Brown and Morrish[19] showed that cavities within high coercivity particles could lower the coercivity from that predicted by reversal models.

In 1959 Aharoni[20] showed that small imperfections in particle shape from the ideals assumed by models could cause large reductions in the switching field, Johnson and Brown[21] showed that the magnetocrystalline anisotropy (previously neglected by the Stoner-Wohlfarth model) contributed to particle anisotropy for low aspect ratio particles and Wohlfarth[22] showed that the angular dependence of coercivity of a partially aligned system could not definitively differentiate between reversal modes unless the specific easy axis distribution was known.

Luborsky's review of fine particle magnetism published in 1961[23] reviewed previous experimental results for electrodeposited iron and iron-cobalt particles and found them broadly consistent with the chain-of-spheres 'fanning' model.

In 1972 Bottoni *et al*[24] showed the effect of the packing density of systems on various magnetic parameters including the rotational hysteresis integral. It was found that the rotational hysteresis integral increased with increasing dilution. The results were interpreted as evidence that the rotational hysteresis integral could only be considered as an indicator of the individual particle reversal mode at extreme dilutions.

From 1978 to 1981 Knowles published work[25] which studied the reversal of individual particles of $\gamma\text{-Fe}_2\text{O}_3$, CrO_2 and metal powders by dispersing the particles in a viscous fluid and applying pulsed fields to them. The results were analysed as a function of switching field and applied angle. The results were broadly consistent with chain-of-spheres 'fanning' for $\gamma\text{-Fe}_2\text{O}_3$ and Fe particles, 'buckling' for Co modified $\gamma\text{-Fe}_2\text{O}_3$ particles and curling for CrO_2 particles. There was a wide variation found between individual particles of nominally the same form indicating the importance of morphology on the reversal mechanism. The morphology of the individual particles could not be observed with the optical microscope used and it was believed that a high proportion of the particles observed were actually multiple particles lying side by side. Sharrock and McKinney[26] found that the measured coercivity of a magnetic material was dependent on the time scale of the measurement due to thermally assisted reversal of magnetic domains, and that a 'typical' $\gamma\text{-Fe}_2\text{O}_3$ tape measured using a VSM would show a coercivity approximately 0.75 of the OK value.

In 1984 Sharrock published further work[27] which used the coercivity variation with time to determine the switching volume of various $\gamma\text{-Fe}_2\text{O}_3$, $\text{Co-}\gamma\text{-Fe}_2\text{O}_3$ and MP tape system particles using a model which assumed chain-of-spheres ‘fanning’ reversal. The switching volumes were found to be similar to the physical volumes of the particles determined by transmission electron microscopy (TEM) for all samples except the largest metal particles where the switching volume was less than $1/6^{\text{th}}$ of the physical volume. Bottoni *et al* investigated low aspect-ratio $\text{Co-}\gamma\text{-Fe}_2\text{O}_3$ particles by hysteresis parameters as a function of temperature, and rotational hysteresis integral[28]. The rotational hysteresis integral was again found to be affected by the packing density and the measured rotational hysteresis integral did not agree with the values for any of the pre-existing reversal models.

In 1986 Andress *et al* published a study of $\gamma\text{-Fe}_2\text{O}_3$ particle systems analysed by TEM, Xray scattering and print-through characteristics[29]. The Xray scattering results and the calculation of activation volumes from print-through characteristics suggested smaller structures than the physical particle volumes measured by TEM. It was proposed that the particles were made up of a number of ‘microcrystallites’, rather than a single crystal, which were likely to affect the reversal mechanism.

In 1987 Ishii and Sato[30] proposed a modification to the chain-of-spheres model whereby the point contact between spheres was replaced by a finite area of contact which gave a more realistic representation of particles made up of multiple ‘crystallites’. Calculation of the rotational hysteresis integral for this model gave a wide range of results dependent on contact area for ‘fanning’ reversal which were consistent with the measurements of Bottoni *et al*[28]. Flanders and Sharrock analysed the time dependent magnetization, coercivity and print-through of $\gamma\text{-Fe}_2\text{O}_3$ and $\text{Co-}\gamma\text{-Fe}_2\text{O}_3$ tapes. The activation volumes of the systems were calculated from the samples (assuming ‘fanning’ reversal) and it was found that the activation volumes of the $\gamma\text{-Fe}_2\text{O}_3$ systems were approximately two times the physical particle volume (determined by TEM), implying agglomerations of particles which interacted during reversal. The activation volumes of $\text{Co-}\gamma\text{-Fe}_2\text{O}_3$ were found to be approximately half of the physical particle volumes. The activation volume was interpreted as that volume of a particle which reverses coincidentally, and not necessarily an indication of reversal mode.

In 1988 Richter and Hempel published an extension to the chain-of-spheres model for two spheres which also took into account the effects of magnetocrystalline anisotropy within the spheres[31]. The model predicted that the rotation would tend from 'fanning' to coherent as the magnetocrystalline anisotropy increased. Schabes and Bertram used a micromagnetic model to investigate the reversal of square section prisms with aspect ratios 3 and 5 and the crystal parameters on $\gamma\text{-Fe}_2\text{O}_3$ [32]. The particles were found to reverse by a complicated mode whereby a vortex (similar to curling) formed at each end of the crystal, sweeping towards the centre reversibly until the centre of the particle reversed. The angular dependence of the switching field was found to be similar to that for other incoherent reversal modes.

In 1990 de Witte *et al* developed a thermal activation model based on hypothetical fluctuation fields[33]. The model was used to calculate activation volumes as a function of applied fields from time dependent measurements of Co- $\gamma\text{-Fe}_2\text{O}_3$, CrO_2 and metal particles. The variation of fluctuation field with applied field did not agree with the predictions of the model for the magnetic recording particles which was interpreted as an indication of incoherent reversal as the model was based on Stoner-Wohlfarth energy barriers. The activation volumes calculated at H_c for the Co- $\gamma\text{-Fe}_2\text{O}_3$, CrO_2 and MP particles were 0.17, 0.04 and 0.08 of the physical volume respectively.

In 1991 Pankhurst published a study of barium ferrite and Co- $\gamma\text{-Fe}_2\text{O}_3$ reversal field as a function of applied field direction measured by applied-field Mössbauer spectroscopy[34]. Using a mean field model the results gave a monotonically decreasing critical switching field with applied field angle consistent with coherent reversal. Also in 1991 Bottoni published a study of reversal modes in $\gamma\text{-Fe}_2\text{O}_3$ and Co- $\gamma\text{-Fe}_2\text{O}_3$ particles as a function of interactions[35]. The reversal modes were investigated by rotational hysteresis measurements and by the angular dependence of coercivity. Interactions were investigated by the measurement of remanence curves. The study found that as interactions increased the parameters indicating the reversal mode tended to values more consistent with coherent reversal, whilst H_c decreased. The author postulated that increased interactions led to a greater percentage of the particles reversing by coherent processes in $\gamma\text{-Fe}_2\text{O}_3$ and Co- $\gamma\text{-Fe}_2\text{O}_3$ systems.

In 1994 Salling *et al* published an investigation of the reversal of two individual ellipsoidal $\gamma\text{-Fe}_2\text{O}_3$ particles[13] using pulsed fields to switch the particles and TEM to

determine the particle morphology and switching (using Foucault mode Lorentz microscopy). The critical switching field as a function of angle was found to be similar in shape to that for Stoner-Wohlfarth coherent reversal, but the switching field values were only 0.75 and 0.94 of the predicted Stoner-Wohlfarth values for the two particles. Also the coercivity of the bulk powder was found to be much lower than the lowest values measured from the two particles, indicating considerable reduction in coercivity due to inter-particle interactions. Lederman *et al* published a study of the time dependence of thermal switching in single particles, analysed by magnetic force microscopy (MFM)[36]. The results questioned the validity of the Néel statistics commonly used for the study of thermally activated reversal and the determination of activation volumes.

Also in 1993 and 1994 Braun and Bertram published a model of incoherent reversal using a statistical mechanics approach to thermal switching independent of the Néel theory[37,38]. The model produced a switching curve similar in shape to that of the Stoner-Wohlfarth model, but with a greatly reduced coercivity consistent with the results of Salling *et al*[13].

Parker *et al*[12] measured the first quadrant of the hysteresis loop of γ -Fe₂O₃, Co- γ -Fe₂O₃, CrO₂, Fe particles and barium ferrite systems as a function of temperature. Room temperature Mössbauer spectra were also recorded. Curves were fitted to the experimental results using Stoner-Wohlfarth assumptions and assumed log-normal anisotropy field distributions. Extension of the model in to the second quadrant allowed H_c values to be calculated using the measured thermal activation and H_k distribution parameters from the first quadrant. The calculated H_c values for coherent reversal and 'fanning' were found to be very similar and were both consistent with the experimentally measured values.

In 1995 Morales *et al* published a study of the activation volumes of spherical and elongated γ -Fe₂O₃ particles as a function of packing density[39]. The study used hysteresis parameters and time dependent measurements to determine the fluctuation field and activation volumes of the samples. The study found that the spheres changed from multidomain to single domain as the packing density increased. The elongated particles activation volume increased from 0.018 to 0.023 of the physical volume. The

author proposed that the change in properties as a function of packing indicated a significant effect of interactions on the reversal mechanism of these particles.

Bottoni's study of the rotational hysteresis of pure and doped $\gamma\text{-Fe}_2\text{O}_3$, CrO_2 and Ba ferrite particles[40] showed that the rotational hysteresis of doped particles tended more to that of incoherently reversing systems than did that of the undoped particles (i.e. the rotational hysteresis integral was increased by doping).

The 1997 study of McConochie *et al*[41] used a similar technique to that of Knowles[25] to study the reversal of single particles of $\gamma\text{-Fe}_2\text{O}_3$ removed from an audio tape by dissolving the organic binder. The results of the study showed an increasing switching field as the angle between the applied field and easy-axis direction was increased, consistent with the predicted switching function for incoherent reversal. The morphology of the particles was not known.

In 1998 Keller and Schmidbauer published a study of the reversal mode of Fe-doped CrO_2 single domain recording particles[42]. The particles were studied in tape, compacted powder and dispersed powder form by rotational hysteresis integral, Mössbauer spectroscopy, hysteresis parameters and remanence parameters. The results of the study concluded that the low-field behaviour of the particles deviated from the Stoner-Wohlfarth behaviour which was consistent with 'curling' type reversal, possibly modified by the formation of agglomerates in the dispersed samples and the effects of superposed shape and magnetocrystalline anisotropy which are neglected in the curling model. At high-fields the results suggest that the magnetocrystalline anisotropy direction is the same as the shape anisotropy.

In the 1998 paper of Morales *et al*[43] five commercial and development recording metal particle samples were investigated using a variety of techniques. Xray diffraction showed smaller crystal sizes than those observed by TEM and these were assumed to be due to crystallites corresponding to observed variations in contrast on TEM images. Activation volumes calculated from time-dependent measurements ranged from 0.18 to 0.63 of the physical particle volume. The author postulated that the presence of these crystallites could encourage incoherent reversal, accounting for the lower than expected coercivity of the particles.

The different properties of 'spindle' and 'needle' shaped metal particles were compared in the 1998 paper of Igaki *et al*[44]. The particles were investigated by hysteresis

analysis, rotational hysteresis integral and torque analysis. No significant difference was observed in the anisotropy field or saturation magnetisation measurements. The switching field of the 'spindle' type particles was observed to be 10-15% higher than that of the 'needle' shaped particles, however, this difference was not sufficient to suggest that the spindle shaped particles reversed by a different mechanism and the rotational hysteresis integral indicated a value between that of Stoner-Wohlfarth rotation and 'buckling'.

In 1999 Bottoni published an investigation of the reversal modes and activation volumes of $\gamma\text{-Fe}_2\text{O}_3$, barium ferrite, Co- $\gamma\text{-Fe}_2\text{O}_3$, CrO_2 and metal particle samples[45]. The study used time-decay of magnetisation to determine activation volumes and the rotational hysteresis integral as an indication of the reversal mechanism. The $\gamma\text{-Fe}_2\text{O}_3$ particles included 'ordinary' particles and non-polar (NP) $\gamma\text{-Fe}_2\text{O}_3$ particles which were manufactured by a process which was supposed to produce single crystal particles with low porosity and good morphology. The rotational hysteresis integral suggested that the NP particles reversed coherently and those particles also had an activation volume close to their physical volume. The results also showed $\gamma\text{-Fe}_2\text{O}_3$ particles to have a similar activation volume to their physical volume although the rotational hysteresis integral indicated that these particles were likely to reverse incoherently.

Sharrock's review of recent advances in metal particulate media, published in 2000 [46], showed that the most recent metal particles had activation volumes similar to the physical (core) volumes of the particles, although the coercivity of these particles was still lower than the expected Stoner-Wohlfarth value.

The comparison of the properties of traditional metal particles (MP) with the most recent advanced metal particles (AMP) by Bottoni *et al*[47] found that the rotational hysteresis integral of AMP particles did not conform to the modified chain-of-spheres fanning model[30] as that of MP particles did. Studies of thermal switching indicated a similar activation volume for AMP particles as traditional MP particles whilst the physical volume of AMP particles was much reduced. The rotational hysteresis integral indicated some reversal mode between the chain-of-spheres 'fanning' and coherent rotation.

Generally, incoherent reversal is only energetically favourable when the applied field is parallel to, or at a small angle to, the particle easy axis. When the switching field is

applied at a larger angle to the particle easy axis we can see that incoherent modes such as curling or fanning would require some of the moments to align antiparallel to the applied field, increasing the total energy. At such angles coherent switching becomes energetically favourable.

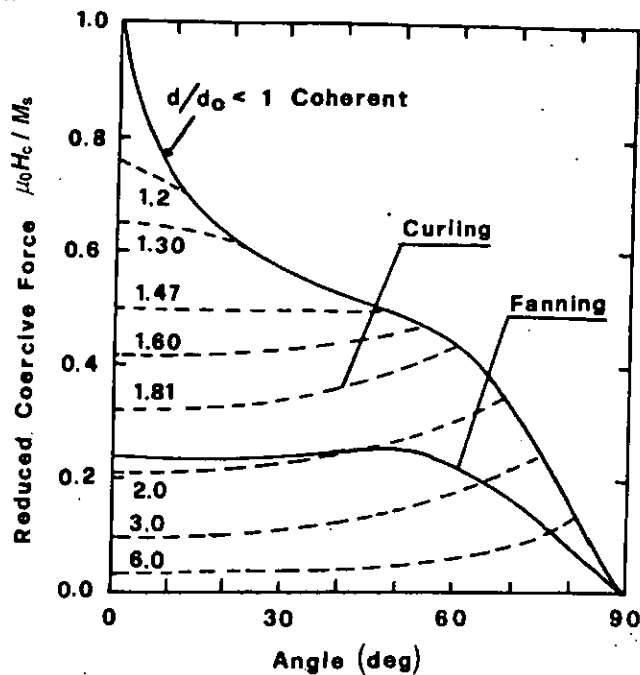


Figure 1-10 Coercivity as a function of angle between applied field and easy axis for different switching modes (after Bottoni[35])

Attempts to experimentally determine switching modes have largely focussed on the effect of incoherent modes of reversal on the coercivity of particles and attempts to match measured coercivities to those predicted by the various reversal modes, although it is difficult to isolate these from the effects of interactions on the coercivity. Figure 1-10 after Bottoni[35] shows the predicted coercivities as a function of applied field angle for the different switching modes and particle diameters.

1.7 Magnetic recording

The earliest magnetic recording device was invented and patented by a telephone engineer, Valdemar Poulsen, in 1898. His device was designed to record telephone and telegraph messages by using the telephone signals to magnetise a steel wire. Poulsen's 1899 UK patent[48] covered recording using magnetic media including 'a steel band ...

supported by insulating material, *'a disk of magnetisable material'* and *'a strip or sheet of some insulating material ... covered with a magnetisable metallic dust'*. In the century since Poulsen's patent the basic techniques he described have become the mainstays of the magnetic recording industry, which is described by Sharrock[8] as 'one of the two foundations of the expansion in computer power... *with ...an economic importance that is comparable to that of semiconductor devices.*'

The basis of any information storage is that the recording medium must exhibit a memory process, such that the recording process permanently alters the state of the system in a way that can later be detected. An added advantage is gained if the stored information can subsequently be erased and the medium re-used. Magnetic recording uses the hysteresis of ferromagnetic materials to achieve these objectives, whereby when a ferromagnetic material is magnetised by the application of a magnetic field, a residual or remanent magnetisation remains after the field is removed and the magnetisation does not fall back to its original level unless it is demagnetised by the application of a field in the opposite direction or by some sort of annealing process. This remanent magnetisation is detected in the read-back process and is used to reconstruct the recorded information.

1.7.1 The recording process

The method of recording digital signals is illustrated in Figure 1-11 (after Chantrell and O'Grady[9]). The schematic illustrates longitudinal recording in which each bit is represented by the magnetisation of a section of tape in a direction parallel to the plane of the tape and parallel to the direction of motion. The state of the bit (i.e. 1 or 0) is determined by the specific direction of the magnetisation, either parallel or antiparallel to the 'play' direction of the medium. The transition between two bits magnetised in opposite directions gives rise to stray flux at the surface of the tape which induces a signal such as that shown in Figure 1-11 *b*) on read-back by the same, or a similar head. Electronic processing is used to retrieve the original signal.

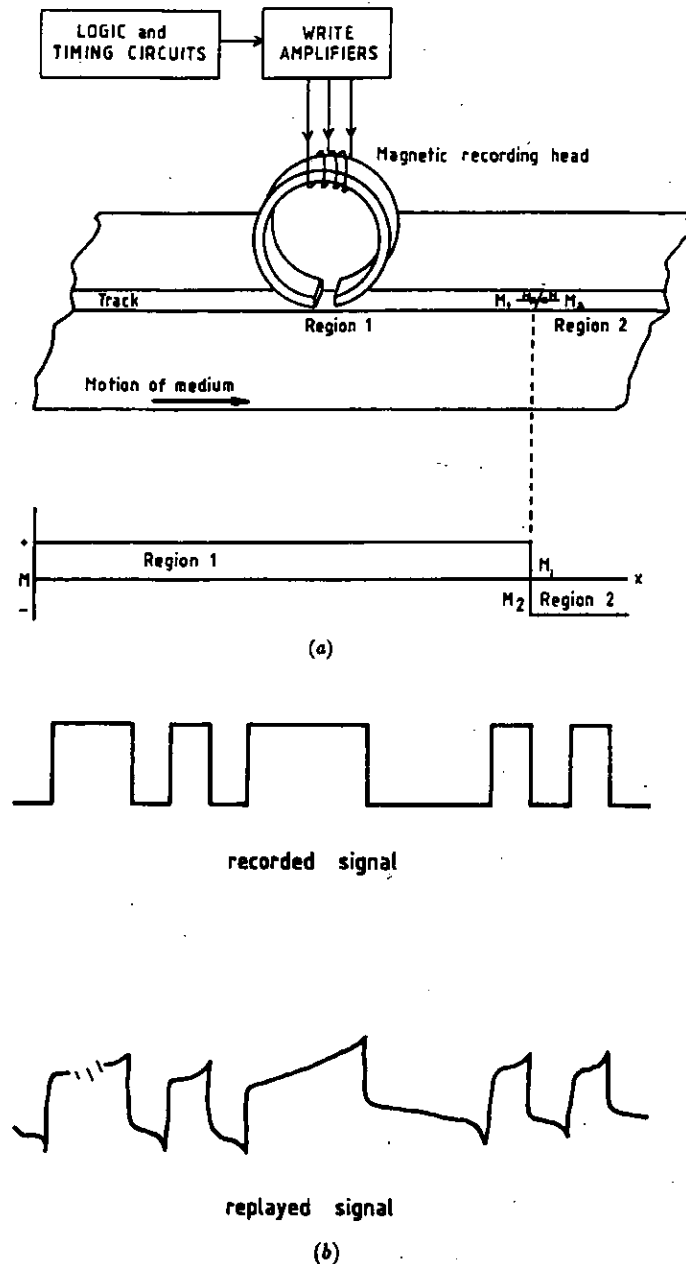


Figure 1-11 a) Schematic of digital recording process using an inductive ring head. b) Schematic write and read waveforms (after Chantrell & O'Grady)[9]

In the case of analogue recording of sound or video the suitably amplified signal is fed through the recording head causing the size of the fringing field to modulate and partially magnetising the tape to a value proportional to the signal strength which is then reproduced on playback. Analogue recording is complicated by the non-linearity (due to hysteresis) of the magnetisation of media from the demagnetised state. This is generally overcome by applying an ac 'bias' signal as well as the required dc signal. The ac signal

is then reduced (by the motion of the tape) resulting in the removal of the hysteresis effect and a linearisation of the magnetisation with respect to the signal.

Although the recording processes for analogue and digital signals are different, the general requirements for media design remain the same for both processes.

1.7.2 The design of recording media

The required magnetic properties of recording media can be determined by considering an ideal recording medium. In such a medium the magnetisation vector would only exist in two states, fully magnetised (i.e. saturated) in the positive direction, or fully magnetised in the negative direction, and the transition between the two states would occur at a single specified field value. Also the switching value would be low enough to be produced by the fringing field of a recording head, but sufficiently high to prevent erasure by self-fields and by long-term thermal switching effects. It turns out that the hysteresis loop of such an ideal sample is 'square'. Figure 1-12 shows a sketch of such an idealised loop and we can see that the magnetisation switches instantly from positive saturation to negative saturation at the application of a reverse field greater than H_c . We can also note that the squareness of this ideal loop is 1 and the SFD is zero (see section 1.2). In practice such a square loop cannot be achieved but the basic task of the media designer is to achieve squareness as close to 1 as possible and a SFD close to zero.

In order to increase the capacity of recording media the bit density must be increased. This requires shorter bit-lengths which will increase the self-demagnetising field of the bits if the same magnetic layer thickness is maintained. Hence, as bit lengths decrease the magnetic layer is made thinner and the coercivity is increased to prevent the erasure of the data by its own self-field. This thinning of the magnetic layer reduces its magnetic moment making the signals more difficult to read back. Also, the increase in coercivity requires higher fields to be produced by the write head, particularly for writing at high speeds as the magnetic viscosity effects require a much higher field to be applied at the write frequency than the quasi-static measurement of H_c using a VSM. Overall the design process is a compromise between creating a sufficiently high coercivity to write at a high bit-density whilst being able to write at high speeds with the write head field available.

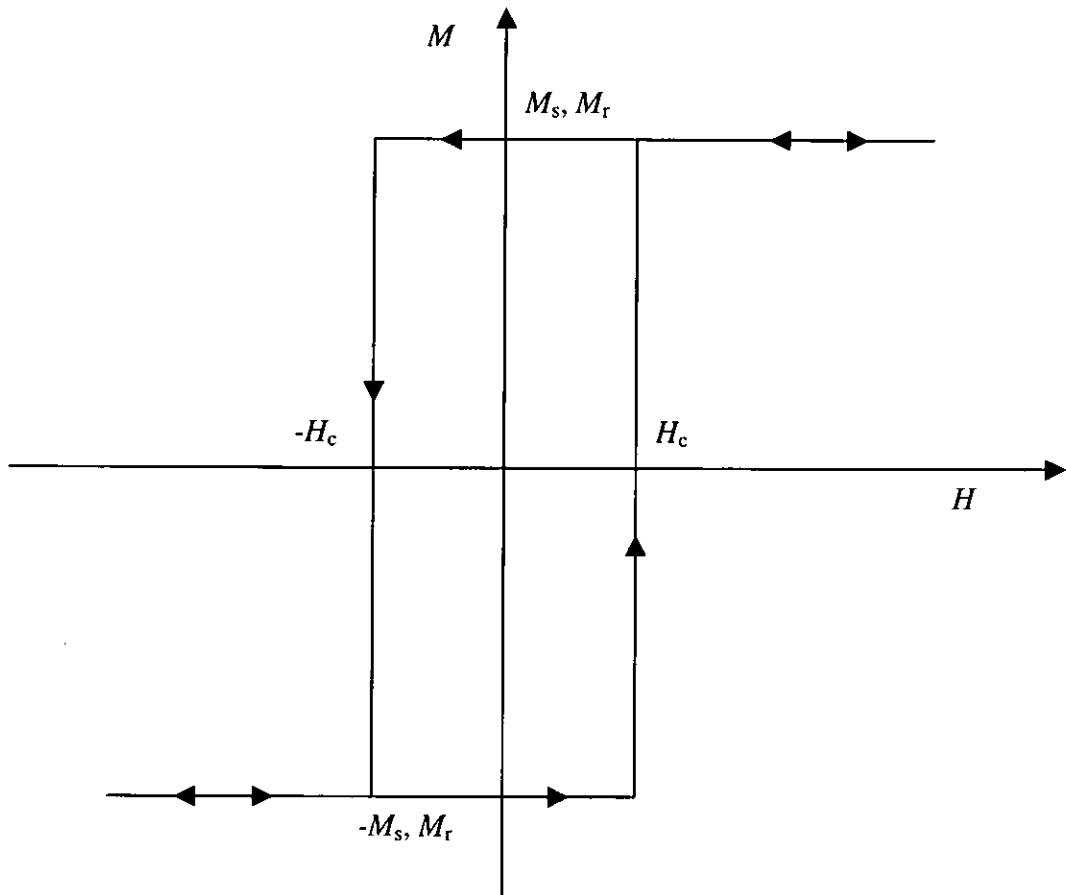


Figure 1-12 Hysteresis loop of an ideal recording medium

Although the first magnetic recording equipment used steel wires as recording media, the use of such bulk materials is far from ideal. Measurements of the hysteresis of such media show a low squareness value which results in relatively low signals on read-back and a wide SFD which results in self erasure and ‘write through’ problems for the low switching field fraction, and problems in erasing and overwriting the high switching field fraction. The reason for these characteristics is the formation of magnetic domains in the material.

In order to produce recording media with hysteresis properties nearer to the ideal shown in Figure 1-12 it is necessary to prevent the formation of magnetic domains. This is achieved by manufacturing magnetic media in which the magnetic layer is divided up into small grains of material that are below the size at which domain formation becomes energetically favourable. Such grains form a single magnetic domain and have a net magnetic moment equal to their saturation moment at all times. Permanent changes in

the magnetisation of these substances are effected by switching individual grains to their other easy axis directions.

1.7.2.1 Particulate media

Particulate magnetic recording media consist of small single domain particles of magnetic material which are dispersed in an organic resin and coated onto a non-magnetic backing film to form magnetic tape or magnetic disks. The particles are manufactured to have uniaxial anisotropy, due to either crystalline anisotropy, shape anisotropy or a mixture of both. Using uniaxial, single domain particles allows the Stoner-Wohlfarth model to be used to predict and engineer the magnetic behaviour of the media. During the coating process the particle easy axes are aligned with the tape play direction by the application of a magnetic field. From the model we find that a Stoner-Wohlfarth particle with its easy axis exactly aligned with the applied field direction (see Figure 1-4) has a 'square' loop of the form shown in Figure 1-12. Hence, if we can produce particles which are identical, and align them perfectly with the tape play direction, we would have an ideal recording medium with a square hysteresis loop. In practice, particles have a size, shape, anisotropy and alignment distribution which prevent the ideal medium being achieved. Also the perfect dispersion of the particles in the coating is problematic and coatings often contain agglomerations of particles as well as those which are mono-dispersed. In addition to these basic difficulties the requirement to produce ever thinner magnetic coatings has resulted in reduced particle size resulting in the use of higher-moment metal particles, and the development of double coating techniques.

1.7.2.2 Thin films

Magnetic thin films consist of thin layers of Cobalt alloys deposited to form a thin, polycrystalline layer on the surface of a rigid disk of metal, glass or silicon substrate. Typically, for computer hard-disk applications the substrate material is an aluminium alloy onto which a layer of Chromium is deposited by sputtering. The pressure of the sputtering deposition and the substrate disk temperature can be varied to determine the grain size and orientation of the surface. Low pressures and high substrate temperatures favour a greater mobility of the deposited atoms resulting in a larger degree of orientation. The magnetic layer is generally a thin layer of Co-Cr alloy such as Co-Cr-

Ta or Co-Cr-Pt. This is sputtered on top of the layer of Cr and the similarity of inter-atomic spacing in the crystal lattices cause the magnetic layer to take up the same crystal structure as the Cr 'seed' layer with the easy axis orientation of the Cr parallel to the plane of the disk. Further protective and lubricant layers are deposited on top of the magnetic layer.

The fine crystal structure of the magnetic layer tends to reduce the exchange interaction between the grains and some of the additions to the alloy are thought to form non-magnetic layers around the grains which further reduce the exchange interaction. In practice the thin film acts like a fine particulate and the ability to grow the layer with the crystal easy axis aligned with the plane of the disk and uniform sized grains allows films to be produced which have very square magnetic hysteresis in the plane of the disk.

Further details of magnetic thin films are beyond the scope of this thesis. The investigation of thin films, using the transverse susceptibility techniques detailed in the body the thesis, was attempted but the expected anisotropy and switching features could not be detected. The reason for the technique failing for thin films is not known but may be due to a breakdown in some of the Stoner-Wohlfarth assumptions of transverse susceptibility theory when used to measure Cobalt based magnetic materials which have a high K_2 [49] anisotropy constant (neglected in Stoner-Wohlfarth theory) compared with materials traditionally used in particulate media[10].

1.8 Magnetic characterisation of recording media

In order to quantify developments made to the design of magnetic recording media, introduce quality control into production processes and share research findings in the advancement of magnetic recording it is necessary to define a number of standard characteristics and methods of determining these which can be used experimentally to compare the magnetic properties of samples of recording media. The most basic of these are the static parameters described in this section. In addition to these there are dynamic techniques whereby signals are written to magnetic media then read back and analysed to determine dynamic characteristics such as signal noise and write frequency effects. These dynamic characterisations are not discussed in this thesis.

1.8.1 Hysteresis parameters

The parameters most widely used to characterise magnetic recording media are those obtained from the major hysteresis loop of the media: saturation magnetisation, remanent magnetisation, coercivity, switching field distribution and squareness. The definitions of these parameters have already been given in section 1.2. The parameters are obtained from a hysteresis loop of the sample which is typically measured using a VSM or a BH looper with due care being taken to account for any magnetic viscosity differences between measurement techniques due to different rates of change of the applied field. The samples are measured with their easy axes parallel to the applied field. For samples with a low aspect ratio of length to thickness some correction for demagnetising fields within the sample must also be made.

1.8.2 Orientation ratio

The orientation ratio (OR) is the ratio of the remanent magnetisation measured with the sample easy-axis parallel to the applied field direction, to the remanent magnetisation measured with the sample easy axis transverse to the applied field direction.

$$OR = \frac{M_r}{M_{r\perp}}. \quad (1.12)$$

The remanent magnetisation with the sample easy axis transverse to the applied field is obtained in the same way as the parallel remanent magnetisation, but from a major hysteresis loop measured with the sample easy axis transverse to the applied field direction, ensuring that the applied field is parallel to the plane of the sample.

The OR gives a measure of the particle easy axis distribution within the sample, a higher OR indicating a narrower distribution of easy axes about the nominal easy axis direction.

1.8.3 IRM and DCD curves

The major hysteresis loop of a sample only gives the remanent magnetisation for a sample which has previously been saturated so that all of the moments are switched into the same nominal direction. The remanent states of a sample after applications of fields lower than the saturation value are important as such fields often exist at track edges and in areas adjacent to those being written in the recording process.

The isothermal remanent magnetisation (IRM) curve is obtained from a sample which is initially in the demagnetised state. This is achieved by either ac demagnetisation or dc rotational demagnetisation. The demagnetised sample is mounted in a VSM with the easy axis parallel to the applied field direction and a small field is applied to the sample then the field is returned to zero and the sample remanence is measured. A slightly larger field is then applied and reduced to zero and the remanence re-measured. The process is repeated with incrementally larger fields until the sample is saturated (i.e. the remanence value shows no further increase). The curve is plotted as the remanent magnetisation against the applied field value.

The dc demagnetisation (DCD) curve is produced in a similar way to the IRM curve, the difference being that the sample is first saturated, then incrementally increasing negative fields are applied and the remanent state is measured after each application.

The negative fields are increased until the sample reaches negative saturation.

Care must be taken when measuring IRM and DCD curves that the remanent magnetisation is measured at a true zero applied field. Electromagnets have a small remanent field which is dependent on their previous field settings. In order to obtain a true zero the control system must reverse the electromagnet polarity and apply a small reverse field to offset the remanent field.

Typical IRM and DCD curves [$I_r(H)$ and $I_d(H)$ respectively] after Spratt *et al*[50] are shown in Figure 1-13. It can be shown that for a system of independent, non-interacting particles, the reduced curves are related by,

$$\bar{I}_d(H) = 1 - 2\bar{I}_r(H), [51] \quad (1.13)$$

and we can see from this relationship that the field where the I_r curve is at 50% of the saturation value should be coincident with the field where the I_d curve crosses zero.

These points are known as the remanent coercivities H_r and H_r' and we can see from the example of Figure 1-13 that they are not coincident, which indicates that the particles are not switching independently of one another and are interacting.

By subtracting the right hand side of equation (1.13) from the measured value of \bar{I}_d we can obtain a plot of the interaction strength as the system switches which is known as a δI or δM plot[52]. The δM plot is positive at fields where interactions within the system

are ‘magnetising’ and tend to reinforce the magnetisation of the sample, and negative at fields where interactions are ‘demagnetising’. Micromagnetic modelling[53,54] and experimental measurements[52,55] have shown that ‘positive’ or ‘magnetising’ interactions are typically associated with exchange coupling between grains in thin-films, which tend to promote cooperative reversal, whereas ‘negative’ or ‘demagnetising’ interactions are typically associated with magnetostatic effects between isolated particles.

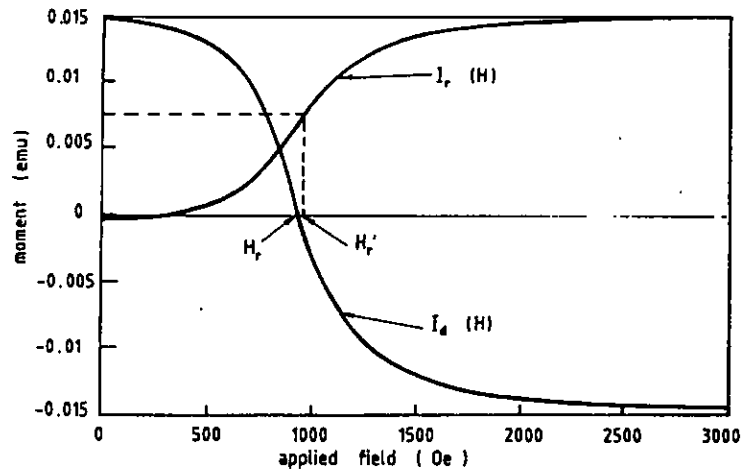


Figure 1-13 Typical IRM and DCD curves after Spratt *et al*[50]

1.8.4 Anisotropy field

As defined in section 1.5 the anisotropy field is the field that applied at 90° to the easy axis direction of a uniaxial single domain particle, is just sufficient to saturate the particle in the hard direction. It is also the field required to make a particle switch magnetisation if it is applied at 180° to the occupied easy axis direction or at an angle just below 90° from the occupied easy axis direction (see sections 1.5.1 and Figure 1-7). The anisotropy field is a constant of the particular particle but it causes no detectable physical event when the applied field is at any other angle to the particle than 90° or 180° from the currently occupied easy axis direction.

The combination of the anisotropy field potentially being different for each particle, only being directly measurable at specific angles to the particle, and the particles being oriented at a distribution of angles to the easy axis direction of the sample makes the measurement of the distribution of anisotropy fields particularly difficult. The techniques employed to measure anisotropy fields directly, need to select particles at

either 90° or 180° to the applied field direction and isolate the behaviour of those particles from the rest of the system. Other techniques relying on the response of the whole system use models to deconvolve the particle anisotropy field distribution from the response of the system. The techniques break down into two types: those that measure the switching of particles and apply theoretical relationships between H_c and H_k to determine the anisotropy field distribution, known as 'switching' techniques, and those that measure the energy required to rotate particle moments in an applied field without causing them to switch, known as 'stiffness' techniques.

1.8.4.1 Switching techniques

The technique of rotational hysteresis loss (RHL) as a method for the investigation of the switching behaviour of magnetic samples was discussed by Bean and Meiklejohn[56] in 1956 and was subsequently used widely in attempts to determine the anisotropy field distribution and switching mode of magnetic samples. [18,44,57-63]. The technique measures the anisotropy field distribution by rotating a sample disk through 360° in an applied magnetic field. The torque on the sample is recorded and the total work done in rotating the sample (the area under the torque vs. rotation angle curve) is a measure of the fraction of particles which have been switched by the field. The energy lost is a function of the discontinuity which occurs as the particles flip from one energy minima to the other. Once the field is increased beyond the local anisotropy field the particles will only rotate reversibly. Hence, any energy absorbed by them in one part of the rotation will be given up in another so that the net energy loss is associated only with the particles which switch. By taking a series of measurements at increasing applied fields it is possible to determine the proportion of particles which switch as a function of applied field and hence determine the anisotropy field distribution. As the applied field increases above the maximum anisotropy field the particles will rotate smoothly remaining aligned with the field at all times and again there will be no losses. The RHL technique does not give information about the angular dispersion of the anisotropy field distribution (i.e. it is insensitive to texture) and knowledge of the switching mode is required in order to interpret the results fully. The Flanders and Shtrikman remanence curve technique[64-68] involves switching the moments in a known direction by saturating the sample, then removing the field,

rotating the sample through a small angle, $\Delta\theta$ and applying an incrementally increasing field. By measuring the remanent magnetisation of the sample transverse to the applied field following each field application it is again possible to determine the proportion of moments which have switched as a function of field. If the rotation of the sample, $\Delta\theta$, is small, the only moments which switch will be those which are transverse ($90^\circ \pm \Delta\theta$) to the applied field, so it is possible to determine the anisotropy field distribution as a function of particle easy axis direction. The other advantage of this technique is that all of the particles switched have an applied field angle, α , near to 90° , where switching by coherent rotation is favoured and the switching field is similar to the anisotropy field.

The technique of remanent curve analysis (RC) determines the anisotropy field distribution by analysis of the initial remanent magnetisation curve or demagnetisation curve of the sample to obtain the switching field distribution from which the anisotropy field distribution is calculated. This technique has been used widely as the determination can be carried out using a standard VSM[21,60,69-71].

Variations on the above techniques exist which rely on the measurement of particle switching to determine anisotropy field distributions. These include modifications to RHL[72-74] and analysis of the variation of the bulk coercivity with temperature[68,75].

Comparison of the results of the above techniques with anisotropy determined by 'stiffness' techniques, or by measurement of individual particles, has shown that the methods involving switching generally give lower values of anisotropy than expected[60,68,75-77]. The reason for the lower values is not fully understood but is believed to be due to the effects of inter-particle interactions and thermal activation on the switching field of individual particles[60,63,68,77].

1.8.4.2 Stiffness techniques

The investigation of the torque acting on a sample rotated in a saturating magnetic field as a function of the sample angle predates the Stoner-Wohlfarth model as a method of investigating the macroscopic anisotropy of samples. Since the Stoner-Wohlfarth model the technique has been used widely in the investigation of the anisotropy field distribution of polycrystalline samples[58,62,78,79]. In order to avoid switching events the applied field must be greater than the maximum anisotropy field of the sample. The

torque curve is a measure of the macroscopic torque of the sample and knowledge of the orientational texture is required in order to deconvolve the anisotropy field distribution from the torque curve. For this reason torque curves are often used for the analysis of highly aligned systems.

The technique of singular point detection (SPD)[80-82] uses derivatives of the hysteresis loop in the reversible branch, with the applied field falling from saturation to zero. Particles with hard axes parallel to the applied field have a 'knee' in the magnetisation curve at the anisotropy field, where the particle rotates into the hard axis direction and becomes saturated. In a polycrystalline sample the curves of all the particles superimpose and the 'knee' is no longer apparent. Differentiation of the curve gives a discontinuity at the knee, which in the second derivative is a singular point. The singular points of the individual particles form a cusp in the second derivative of the sample curve at the anisotropy field. The technique generally uses pulsed field equipment, or BH loopers, with circuits to electronically differentiate the response in real-time. The suitability of the technique for use with pulsed field equipment has resulted in wide use in the characterisation of hard permanent magnet materials with high anisotropy fields. However, a number of studies have used the technique for the characterisation of recording media[60,68]. At the time when the SPD technique was developed, equipment such as VSMs recorded measurements of hysteresis manually using chart recorders and it was found that such recordings were not sufficiently accurate to obtain a reliable second derivative. With the more recent advent of computer controlled magnetometers the SPD technique has been extended by fitting curves to hysteresis loops (to smooth resolution and random errors) and numerically differentiating them [75,83-87].

Ferromagnetic resonance (FMR) is a technique whereby the precession of particle magnetic moments about an applied field is measured. A sample is placed in an applied dc field with a high frequency alternating field transverse to it. Particles aligned with the dc field precess about the field at a given resonant frequency dependent on the local field surrounding the particle. By monitoring the absorption spectrum of energy from the precessing field as a function of applied dc field it is possible to determine the local field distribution surrounding those particles aligned with the dc field from which the anisotropy field can be derived[60,79,88-91].

The torsion pendulum method[60,92-96] consists of a sample suspended on a torsion wire in an applied magnetic field. The sample is initially aligned with its easy axis parallel to the applied field and the torsion wire in a relaxed state. The sample is then displaced by a small angle from the equilibrium position and released. The subsequent oscillations about the direction of the applied field are due to a restoring force which is a combination of torque from the torsion wire and torque due to the anisotropy of the sample. By taking a series of measurements at different applied fields, and measuring the frequency of oscillation of the torque pendulum as a function of applied field, it is possible to determine the anisotropy field distribution of the sample. The torsion pendulum needs an aligned sample and knowledge of the sample texture in order to determine the anisotropy field distribution.

Transverse susceptibility is a technique whereby a small ac field is applied transverse to a dc bias field. The susceptibility of the sample in the ac field direction is measured as a function of the bias field. The susceptibility of an individual particle with the applied field at 90° to the easy axis direction becomes singular when the applied field is equal to the anisotropy field due to the flat energy minimum for particles where $\alpha=90^\circ$ (see Figure 1-5). For a polycrystalline sample with random easy axis orientation this singularity becomes a cusp[3] and the transverse susceptibility of samples of recording media show peaks associated with the anisotropy field distribution[4,75,81,87,89,90,94-102]. The equipment required to investigate transverse susceptibility is reasonably robust and inexpensive. However, samples of relatively high magnetic moment are required and the curves must be deconvolved to isolate the anisotropy field distribution from texture and switching effects. The remaining chapters of this thesis detail the development of the transverse susceptibility technique for the investigation of relatively low-moment modern recording media at the University of Central Lancashire.

A number of other techniques and variations exist for the determination of anisotropy field distributions which include Mössbauer spectroscopy[34], static field SPD measurement[103], curve matching of modelled magnetisation and hysteresis curves[71, 12], rotational hysteresis at 45° to aligned thin films[63,105,106] and transverse biased initial susceptibility (TBIS) measured by the magneto-optic Kerr effect (MOKE)[91,107].

2 Transverse susceptometer development

In order to extend previous work carried out on the use of transverse susceptibility in the characterisation of magnetic recording media it was necessary to develop and build a suitable transverse susceptometer. An earlier susceptometer had been built at Preston[108]. The software developed for driving the equipment was very basic and further changes were required to allow the measurement of modern recording media, which eventually resulted in the complete replacement of the existing equipment.

The main developments to the system detailed in this chapter include the following:

- Optimising the position of the existing sensing coils,
- Investigation of the origin of the susceptometer baseline,
- Design and manufacture of coaxial sensing coils,
- Design and manufacture of a control system and polarity switching unit for a 100A, 2.3 Tesla electromagnet,
- Decoupling of the susceptometer solenoid flux from the electromagnet yoke and pole pieces,
- Design and development of a computer control system to automate susceptometer measurements.

The most significant development was probably the identification of the interaction between the solenoid return-flux and the electromagnet as the main cause of the instrument baseline, and the subsequent decoupling of the solenoid flux from the electromagnet to minimise the baseline.

2.1 Existing equipment

The existing reversible transverse susceptometer at Preston was based on that described by Pareti and Turilli[4]. A diagram of the susceptometer is shown in Figure 2-1.

The equipment consisted of a 96-turn solenoid, producing an ac field, mounted between the pole-pieces of an electromagnet. Inside the solenoid were two identical 1000-turn sense coils connected in opposition to one-another through a passive potentiometer balancing circuit (Figure 2-2). A 10-turn low resistance 'quadrature' coil was also wound coaxially onto one of the sensing coils and short-circuited through a low value variable resistor.

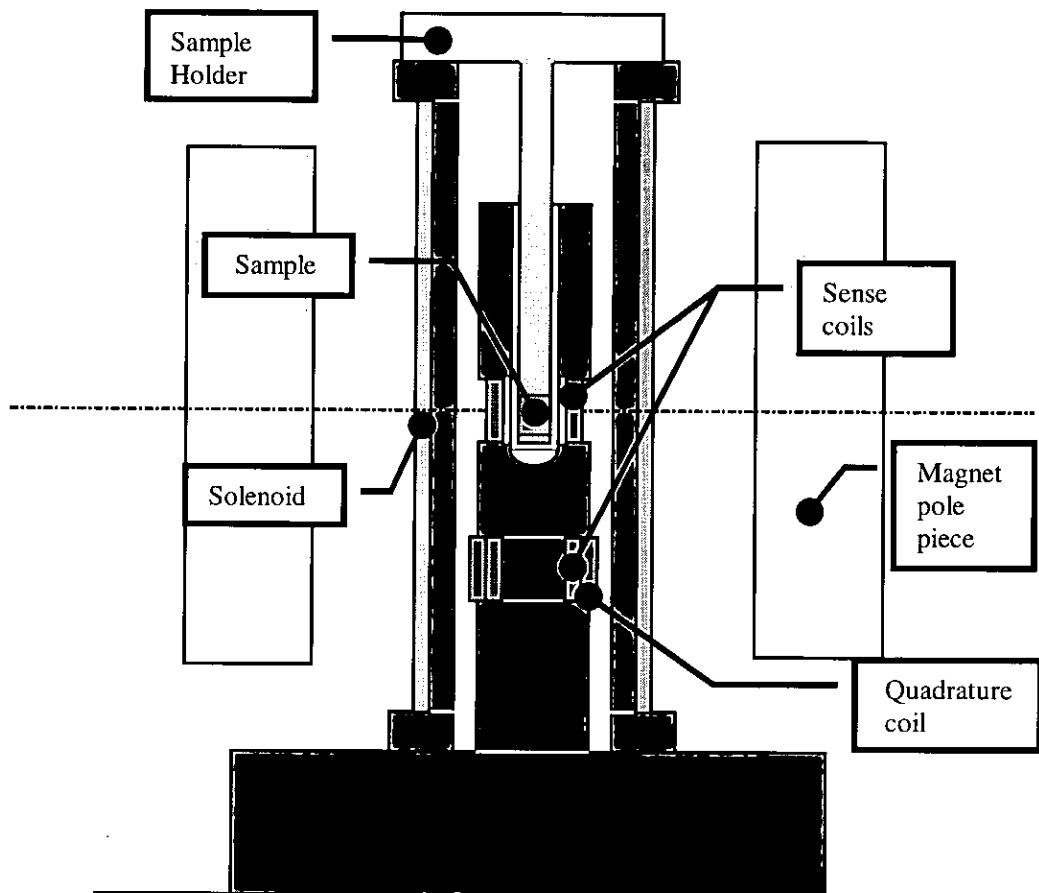


Figure 2-1 Layout of existing transverse susceptometer

An alternating current was passed through the solenoid at a frequency of 10kHz, producing an alternating field of approximately 1.6 kA/m. The sensing coil balance potentiometers and the quadrature coil variable resistor were adjusted in turn to minimise the inductive output signal from the empty sense coils and to minimise any phase difference between the two coil signals. A sample was then inserted into the centre of one of the sense coils (see Figure 2-1). The resulting change in the balanced circuit output was considered to be due to the change in the reversible transverse susceptibility of the sample. The balanced signal was fed into a lock-in amplifier that was set to extract only the component of the signal that was in phase with the ac field induced in the sample coil, thus eliminating noise at other frequencies and phases.

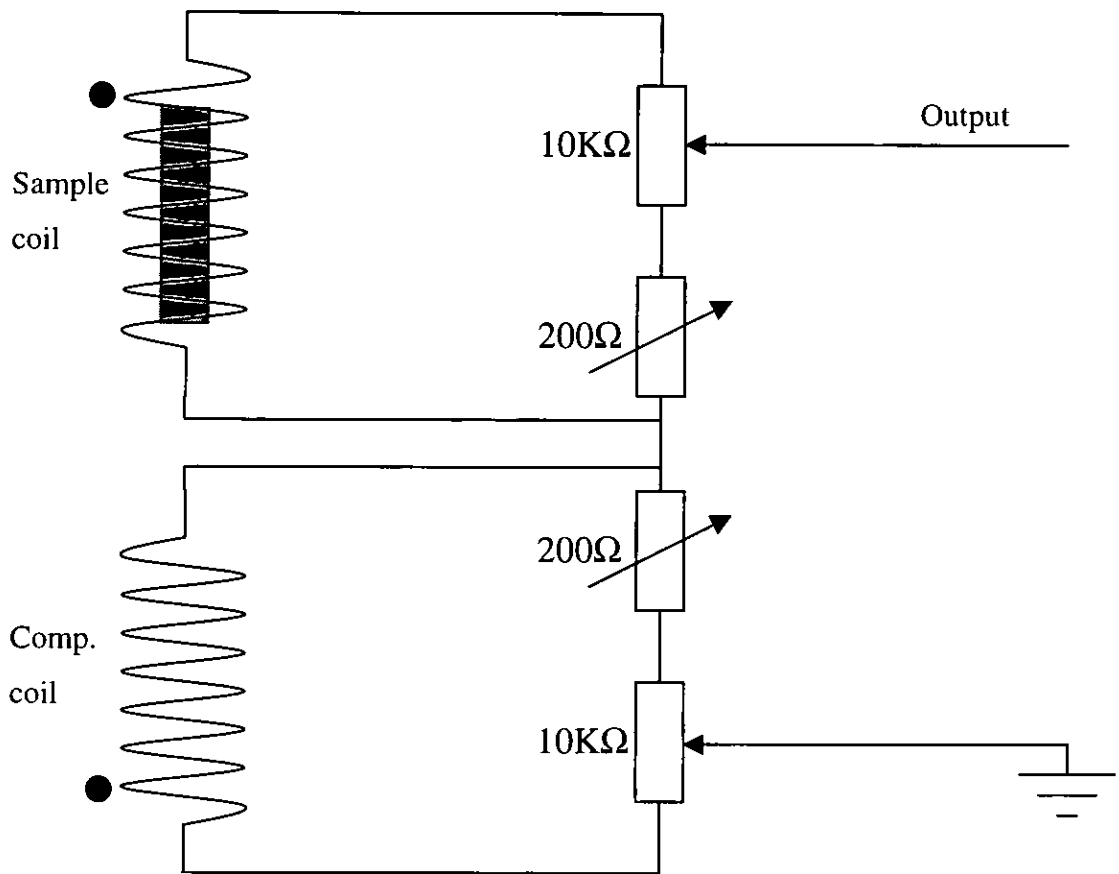


Figure 2-2 Balancing circuit

2.1.1 Theory of design

Faraday's Law gives the instantaneous emf generated by a coil placed in a changing magnetic field,

$$\epsilon = -\frac{d\Phi}{dt} \quad (2.1)$$

Flux linking the coil is given by,

$$\Phi = NBA, \quad (2.2)$$

where A is the cross-sectional area of the coil and N is the total number of turns.

So,

$$\epsilon = -NA\frac{dB}{dt} \quad (2.3)$$

For an air cored coil, $B = \mu_0 H$, so for any given air cored coil placed in a changing magnetic field,

$$\varepsilon = -NA\mu_0 \frac{dH}{dt}. \quad (2.4)$$

Now, if part of the air core is replaced by a sample of magnetic material of relative permeability μ_r , with a cross sectional area of A_s , the emf generated due to the flux through the sample is given by,

$$\varepsilon = -NA_s\mu_0\mu_r \frac{dH}{dt}. \quad (2.5)$$

Hence, by adding the emf generated in (2.4) and (2.5), remembering to subtract the flux due to the air that the sample displaces, we obtain,

$$\begin{aligned} \varepsilon &= -NA\mu_0 \frac{dH}{dt} - NA_s\mu_0\mu_r \frac{dH}{dt} + NA_s\mu_0 \frac{dH}{dt}, \\ &= -N\mu_0 \frac{dH}{dt} (A + A_s\mu_r - A_s), \\ &= -N\mu_0 \frac{dH}{dt} (A + A_s[\mu_r - 1]), \\ &= -N\mu_0 \frac{dH}{dt} (A + A_s\chi_m). \end{aligned} \quad (2.6)$$

By definition, the magnetic susceptibility of the sample, χ_m , is equal to $(\mu_r - 1)$, so by using two coils in the susceptometer, one air cored (compensating coil) and one containing the sample (sample coil), we can subtract the outputs, (2.4) from (2.6) to obtain,

$$\begin{aligned} \varepsilon &= -N\mu_0 \frac{dH}{dt} (A + A_s\chi_m) + NA\mu_0 \frac{dH}{dt}, \\ &= -N\mu_0 \frac{dH}{dt} (A + A_s\chi_m - A), \\ &= -N\mu_0 \frac{dH}{dt} A_s\chi_m. \end{aligned} \quad (2.7)$$

For a sinusoidal ac probe field we obtain a sinusoidal voltage output, of the same frequency with a phase shift of 90° , which is proportional to the susceptibility of the sample.

In practice, there were small differences in the ac field strength between the sensing coil locations (particularly in the design of Figure 2-1, where one coil is nearer to the end of the solenoid than the other). To compensate for this, the emf values were not subtracted directly; the coils were each connected to a high resistance wire-wound potentiometer (See Figure 2-2). The potentiometers were connected in opposition to one-another and were adjusted to zero the signal when both coils were empty, thus compensating for any small differences in field. This correction was independent of changes in the ac field, assuming that the proportionality between the field values at the two coil locations was maintained.

Another difference between the ideal and observed response of the instrument was that a small phase difference was observed between the signals generated in the two sensing coils. This was probably due to the effects of slightly different circuit inductances and capacitances when the coils were attached to the potentiometer measuring circuit, which resulted in phase shifts between the emf generated, and the signal detected. In order to compensate for these phase shifts, a 'quadrature' coil was added to the basic circuit. This was simply a low resistance coil wound around one of the sensing coils and shorted through a low-value variable resistor. An emf was induced in the coil as per equation (2.4). As the coil was virtually short-circuited and had a reasonably low inductance, a current flowed which was approximately in phase with the voltage. Hence the coil generated a small ac field that was 90° out-of-phase with the probe field. This in turn generated an emf in the sensing coil around which the quadrature coil was wound and by varying the series resistor of the quadrature coil it was possible to make small adjustments to the phase of the sensing coil output.

2.1.2 Limitations of existing equipment

The following limitations of the existing equipment were identified.

- Equipment accuracy - The existing equipment had been developed for the χ_t measurement of traditional magnetic recording tapes and bulk magnetic powders used in the production of magnetic tapes. As such, the χ_t signal generated by the samples was large and the sensitivity and repeatability required of the equipment was relatively low. On attempting to measure more modern recording media

using the equipment it was found that the signal was small compared to the instrument noise.

- Equipment baseline - It was found that when the susceptometer was run without a sample, a baseline response was measured. This baseline response was a repeatable function of the applied dc field and also showed some hysteresis. As the cause of the baseline was unknown it was not immediately obvious whether it would simply add to the required signal when a sample were inserted, or operate on the signal in some more complex way, such as multiplicatively. Investigation of the baseline suggested that it was a simple additive response, which was independent of the sample signal, for the following reasons,
 - A 'U' shaped baseline was recorded without a sample fitted in the susceptometer coil. If the baseline were a multiple of the sample signal, no baseline would be observed without a sample.
 - The output of the susceptometer was a measure of the imbalance between the two sensing coils. Adjustment of the balancing potentiometer to give an increased imbalance of say 1mV caused the whole of the baseline to increase by exactly the same amount.
 - Varying the sample size caused the output of the susceptometer to change. If the output were caused by the signal being multiplied by some function, we would expect the shape of the output to be constant irrespective of sample size. In practice the output signal was similar in shape to the empty susceptometer baseline for very small samples, and tended towards the theoretically predicted χ_t response of the sample (showing anisotropy and coercivity peaks) for larger samples.

Due to the above results it was concluded that the baseline was additive and the baseline was recorded periodically with the susceptometer empty. The recorded curve was then subtracted from subsequent susceptometer measurements to obtain the required signal. The size of the baseline signal was large compared with the signal generated by modern media. Hence, small changes in the baseline signal could mask the required media signal. The current theoretical model of χ_t measurement did not predict any baseline, and although the baseline

signal had been observed before [4,94,96,108] its origin remained largely unexplained.

- Limitations of dc field - The dc electromagnet used for the existing susceptometer was only capable of generating a field of approximately 875 kA/m. This field value was too low to show anisotropy peaks for modern media with high anisotropy field values. The existing electromagnet was also air-cooled and was only capable of running for one or two hours continuously before it started to heat the sample, and had to be switched off to cool for several hours.
- Control system - The software running the existing equipment was a very simple GWBasic program. The software did not give a graphical display of the measurement and was not capable of subtracting a previously measured baseline. Thus it was impossible to determine whether any signal was being detected until after a run had been completed and the data processed using other spreadsheet software. The time taken to cycle the dc field to make a measurement was approximately forty minutes and was not easily adjustable within the software. The dc field was measured using an analogue, Hall effect, instrument, the output voltage of which was measured using a proprietary ADC card fitted to the computer. Although the system could be calibrated as a whole, the analogue to digital conversion added further limitations to the resolution of the measurement.

2.2 Design Development – Oscillator circuit

A technique had recently been reported using the change in frequency of an LC oscillator circuit to measure transverse susceptibility[109]. A prototype oscillator circuit was designed and manufactured to determine whether this technique offered advantages over the existing design.

By using an oscillator circuit to measure the χ_t response, the ac field generation and the sensing mechanism could be combined in a single coil. This would eliminate the requirement for the compensating and balancing system, and would allow a much smaller single coil to be manufactured to just enclose the sample.

A similar technique had been used previously at Preston to determine the concentration of magnetic particles suspended in a column of fluid[110]. A variation of this circuit (Figure 2-3) was built in an attempt to increase the signal to noise ratio and reduce the baseline of the χ_t measurements.

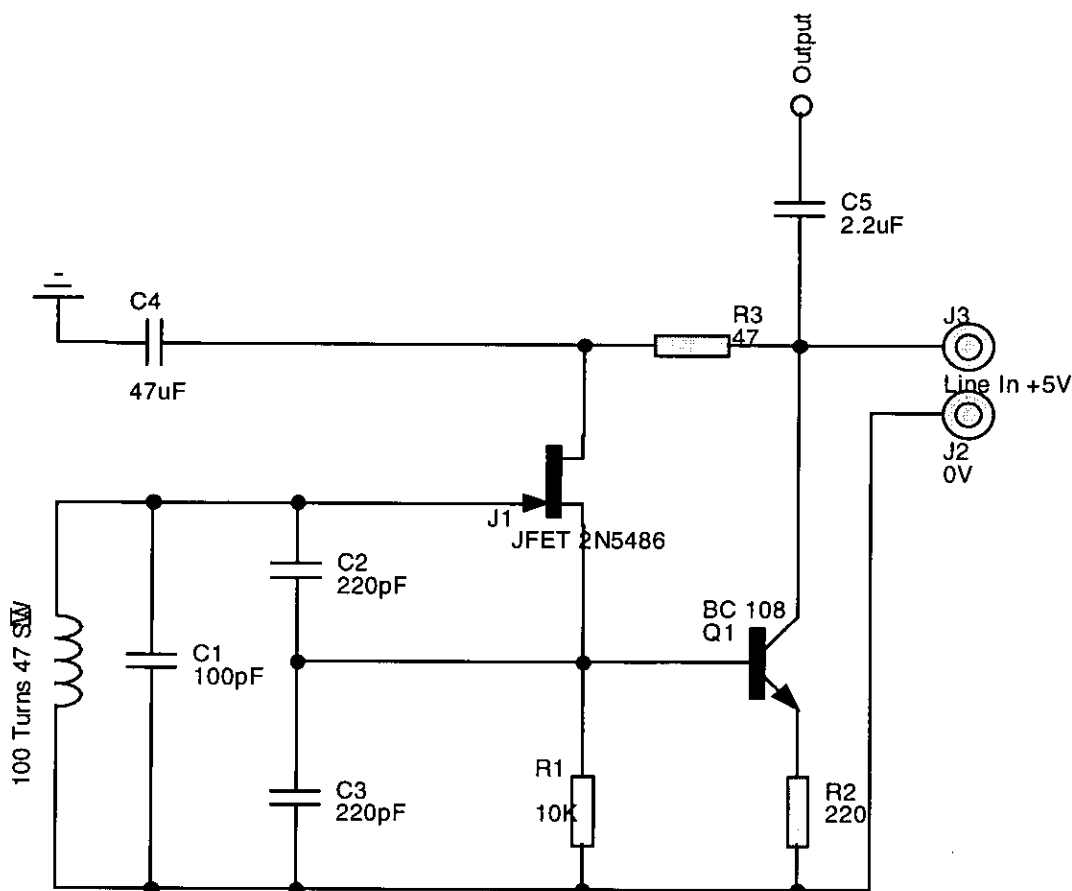


Figure 2-3 Oscillator χ_t circuit

The oscillator circuit used a Colpitts LC oscillator where the inductance was supplied by a small air-cored coil. The coil was manufactured in such a way that a sample of magnetic material could be inserted into the core. The insertion of magnetic material would change the self-inductance of the coil, which would in turn cause the operating frequency of the circuit to change. The perceived advantages of this system were that only one coil would be required both to create the perturbing ac field, and to sense the response of the magnetic material, avoiding the noise caused by the mutual inductance between the perturbing solenoid and the sensing coil on the existing equipment. Also the circuit response was in the form of a change of frequency, which is a parameter that can easily be measured to a high accuracy.

The frequency of a high Q oscillator is given by,

$$F = \frac{1}{2\pi\sqrt{LC}}. \quad (2.8)$$

The self inductance of a coil is given by,

$$L = \frac{B}{I} NA, \quad (2.9)$$

where N is the number of turns and A is the cross-sectional area of the coil.

Considering that $B = \mu_0\mu_i H$, where μ_i is the initial relative permeability of the core material, we obtain for L ,

$$L = \mu_0\mu_i \frac{H}{I} NA. \quad (2.10)$$

As H/I is a constant value related to the form of the coil, and μ_0 and A are also constants we can say,

$$L = D(1 + \chi_i), \quad (2.11)$$

where D is a constant and by definition, $\mu_r = (1 + \chi)$ for a medium.

Substituting back into (2.8) we obtain,

$$\begin{aligned} F &= \frac{1}{2\pi\sqrt{D(1 + \chi_i) \cdot C}}, \\ &= \frac{1}{2\pi\sqrt{D \cdot C} \cdot \sqrt{(1 + \chi_i)}}, \\ &= \frac{B}{\sqrt{(1 + \chi_i)}}, \end{aligned} \quad (2.12)$$

where B is a constant equal to $\frac{1}{2\pi\sqrt{D \cdot C}}$.

So,

$$\frac{dF}{d\chi_i} = -\frac{E}{(1 + \chi_i)^{3/2}}, \quad (2.13)$$

where $E = \frac{B}{2}$.

Hence, the relationship between frequency and susceptibility is not linear and we would have to use fitting techniques against known susceptibility samples to calibrate the equipment.

On testing the circuit it was not possible to observe transverse susceptibility peaks and repeat measurements showed that the signal was not repeatable. Some variation in frequency was observed, however, this was attributed to component drift caused by changes in the ambient temperature. The frequency shift due to the change in susceptibility of the sample was likely to be small as, with this technique, there was no way to compensate for the low filling factor of the sense coil. The majority of the material placed in the sense coil for the measurement of advanced magnetic tapes was non-magnetic (i.e. tape substrate and air gaps). Reports of previous χ_t measurements using an oscillator technique[109] had used a non-standard oscillator design incorporating a tunnel-diode for increased stability. Tunnel diodes are now considered an obsolete component for general electronics and are only available for specialist applications. It was felt that we did not have the necessary expertise to design and build such an oscillator and this technique was abandoned in favour of further refinements to the existing system with separate excitation and sensing coils.

2.3 Modifications to existing susceptometer

In order to measure modern media on the existing susceptometer it was necessary to improve the signal to noise ratio and reduce the baseline of the instrument. Each part of the system was addressed in turn in an attempt to optimise the susceptometer. Initially the original design was retained and existing wiring and circuitry were replaced where appropriate to improve the shielding and earthing in order to reduce external electrical noise. Modifications included the following,

- the balancing circuit was rebuilt using screened cable in a screened, die-cast enclosure.
- the cables to the sensing coils, which had been previously wired with unscreened cable, were re-wired using individually screened twisted pairs of instrument wire.

Following the above changes the random noise on the lock-in signal was reduced, although the relatively repeatable baseline signal (Figure 2-4) was still large.

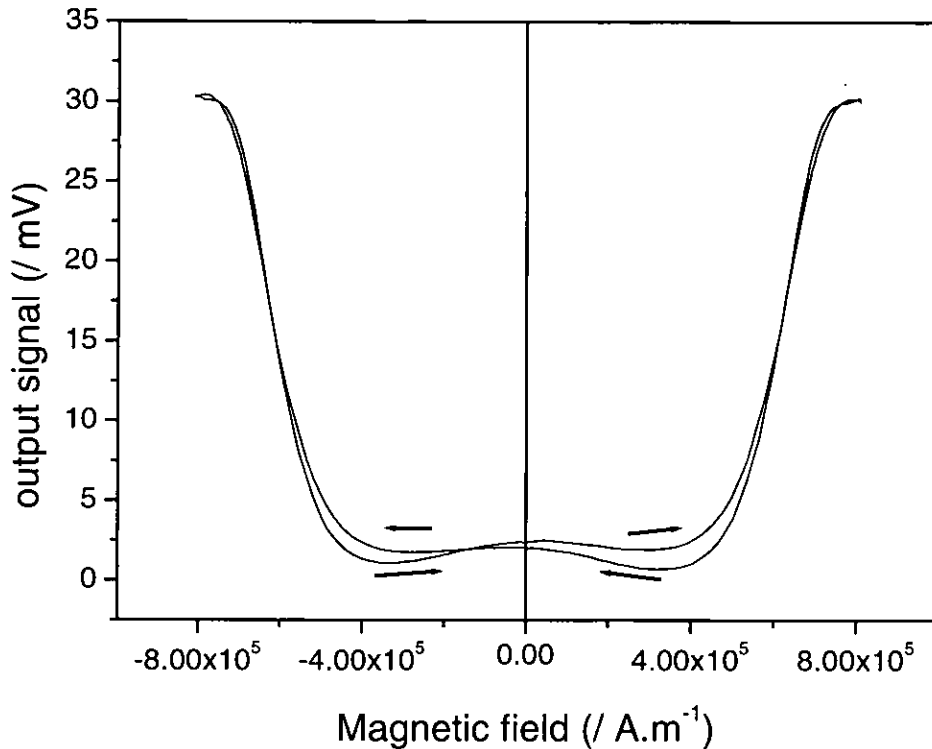


Figure 2-4 Susceptometer initial baseline

Following the optimisation of the original design a number of modifications were made to components of the system in order to further improve the signal response and reduce the baseline signal.

2.3.1 Symmetry of sense coils

The original susceptometer was built with the sample coil on the centreline of the dc electromagnet pole-pieces to give the most uniform dc field in the region of the sample. The compensating coil was also placed in the solenoid but was not in the centre of the electromagnet as theoretically it would be unaffected by the dc field.

It was clear from the baseline measured in Figure 2-4 that the dc field changed the signal from the sensing coils without any magnetic material present. It was also known that because of the geometry of the original set-up, the compensating coil would be subjected to a lower dc field than the sample coil, due to fringing effects at the edges of the pole pieces.

Although the physical mechanism of the influence of the dc field was unknown it was reasoned that the asymmetry of the original geometry might have been contributing to

the baseline signal. In order to test this hypothesis the sensing and compensating coil assembly was raised so that the coils were arranged symmetrically about the centreline of the magnet pole-pieces and the solenoid. The result showed that the baseline shape was highly dependent on the position of the sensing coils with respect to the magnet pole-pieces and the ac solenoid. Although the baseline was still significant, careful centring of the sensing coils resulted in a much-reduced response shown in Figure 2-5. If we compare Figure 2-5 with the initial baseline shown in Figure 2-4 we can see that the central area of the baseline between $\pm 5 \times 10^5 \text{ A.m}^{-1}$ is relatively unchanged. However, the steep rise in the baseline at the higher fields has been changed to a much less-steep fall, so that the baseline value for the maximum applied field is similar to that for zero applied field. It was found that this was the optimum position and further displacement, such that the compensating coil was nearer to the centreline of the electromagnet, resulted in the gradient of the outer 'falling' regions to be increased, so that the baseline became an inverted 'U' shape.

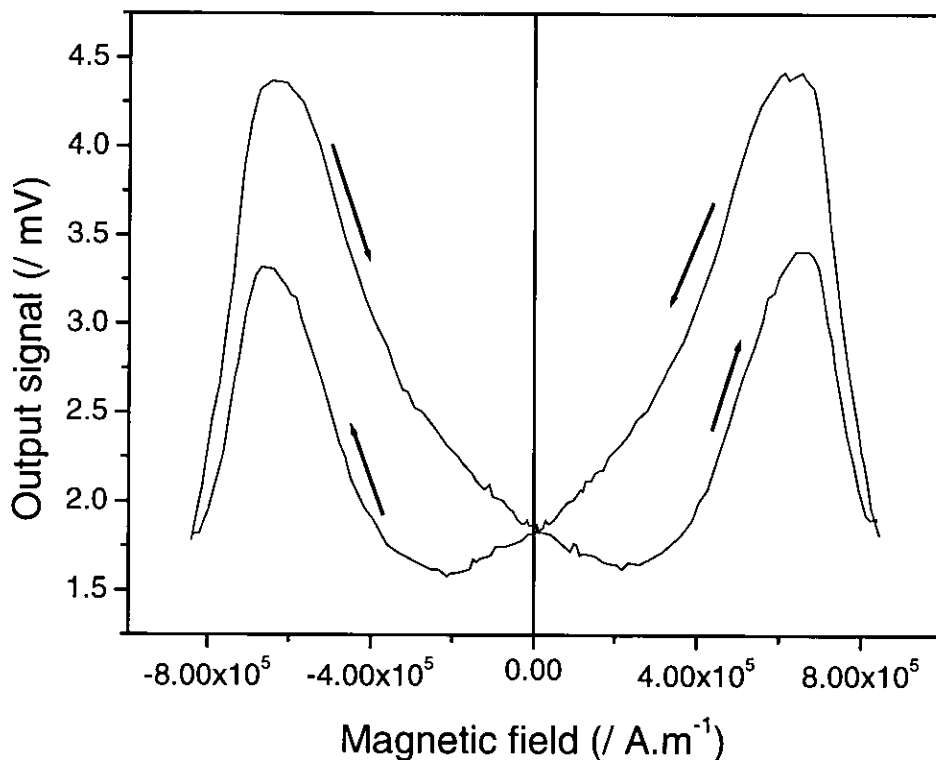


Figure 2-5 Baseline with centred coils

The reduction in the size of the baseline could not be used in isolation as an indication of the improved sensitivity of the susceptometer, as changes in the geometry also

affected the size of the measured signal for a given sample. By comparing the baseline and signal for a given sample the improvement in signal-to-baseline ratio was determined. Figure 2-6 and Figure 2-7 show the empty susceptometer baseline, and the signal due to a control sample after baseline subtraction, for the original and the centred coil set-up. By dividing the height of the sample anisotropy peak (using the signal at zero applied field as datum) by the maximum change in the baseline signal, the signal-to-baseline ratio was determined. The signal-to-baseline ratio of the original set-up (Figure 2-7) was 2.00 compared with the signal-to-baseline ratio of the system using centred coils (Figure 2-6) that was 0.16. The improvement in signal-to-baseline ratio due to centring the coils was therefore a factor of 12.5.

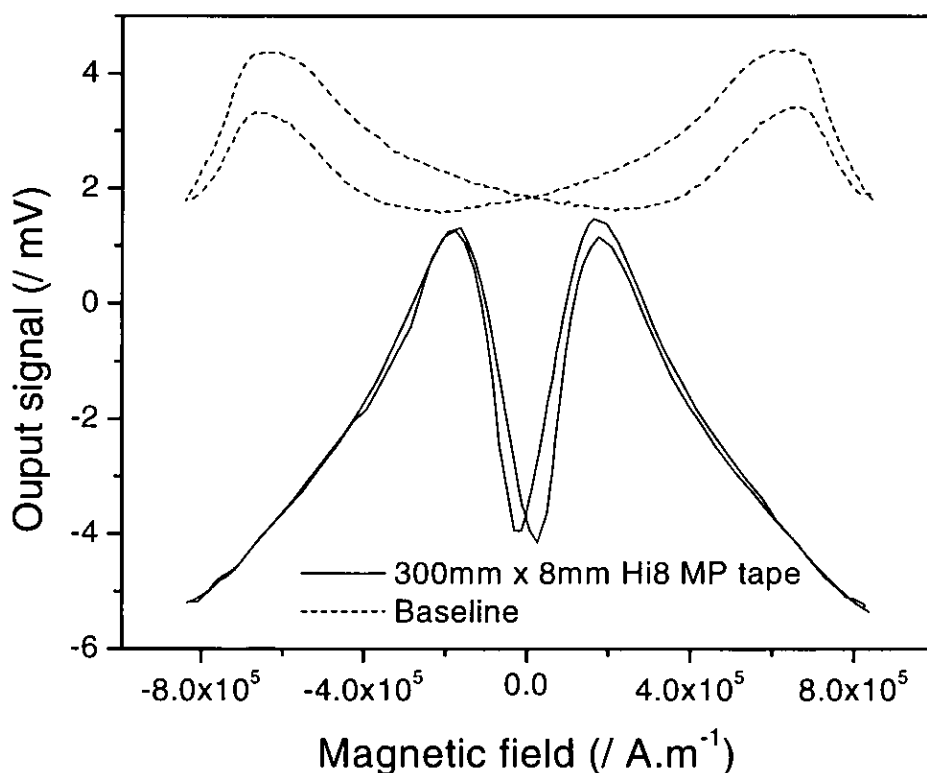


Figure 2-6 Centred-coil baseline with control sample

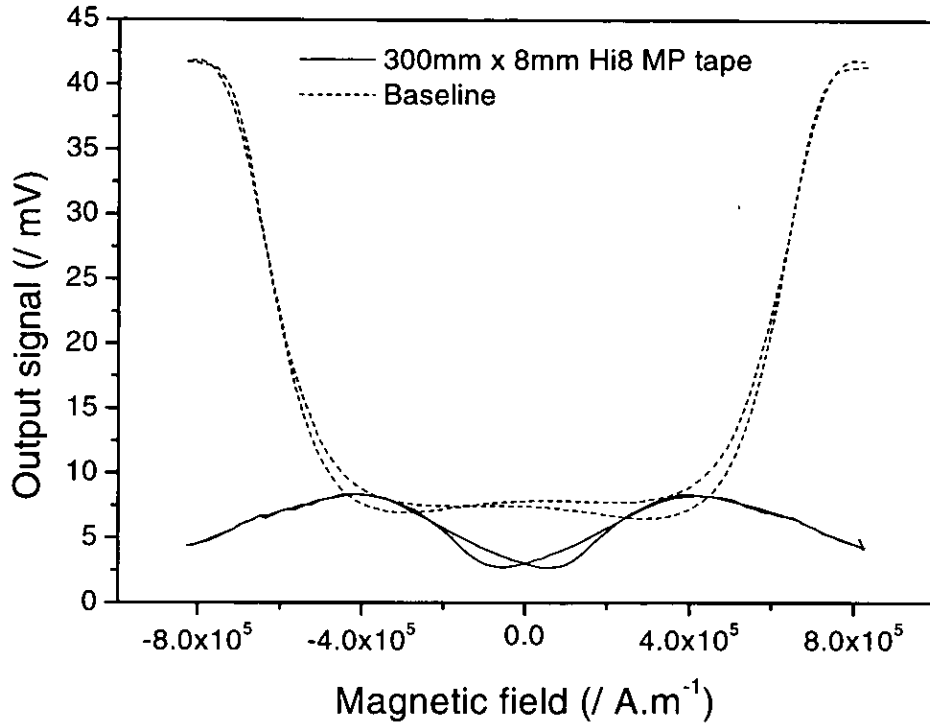


Figure 2-7 Original baseline with control sample

2.3.2 Reduction of baseline

It is well known from general electromagnetic theory that magnetic fields superpose and that the magnetic field at any point in space is the vector sum the component fields at that point. The measured output signal of a transverse susceptometer is the signal induced in the balanced sensing coils filtered by a very narrow band-pass at the same frequency as the ac excitation field, with a pre-set phase difference. As such, the lock-in amplifier filtration should remove any induction due to the very low frequency sweep of the electromagnet field. In practice we see a baseline response that is clearly a function of the electromagnet field and we must assume that this is due to some other physical effect. A number of possible causes were considered.

One of the effects caused by placing the ac field solenoid between the poles of the electromagnet is that a Lorentz force will be present on the windings of the solenoid due to the movement of charge in the magnetic field. As the solenoid acts as an oscillating dipole perpendicular to the dc field, there will be an oscillating torque on the solenoid acting about a line mutually perpendicular to the dc field and the long axis of the

solenoid. The presence of the oscillation was observed as a ‘ringing’ noise at the excitation frequency, becoming louder as the dc field was increased.

In the original susceptometer design (Figure 2-1) the ac solenoid was attached directly to a former supporting the two sensing coils. Any oscillation of the solenoid that was transmitted to the sensing coils would result in these coils oscillating in the dc field and generating an ac signal at the excitation frequency. Such a signal would vary as a function of the dc field strength and could be a cause of the instrument baseline.

In order to reduce the effects of oscillation on the sensing coils two modifications to the susceptometer were made:

- The frequency of the applied ac signal was increased from 10kHz to 20kHz. Assuming that any fundamental resonant frequency of the relatively large solenoid would be much less than this frequency, it was reasoned that an increase in the excitation frequency would reduce the amplitude of the oscillations. The ‘ringing’ sound could no longer be heard, but this may have been solely due to its frequency rising above the audible range. The baseline signal was still observed to change as a function of the dc field.
- The direct mechanical contact between the ac solenoid and the sensing coil assembly was removed. As part of the modification made to centralise the sensing coils within the solenoid (Section 2.3.1) the sensing coils were suspended from the dc electromagnet yoke independently from the solenoid attachment thereby reducing the coupling and the vibration from the solenoid through the mass of the electromagnet. Although centring the coils reduced the baseline, when the coils were placed back in their original location (but still mechanically isolated from the solenoid) the baseline was unchanged. It was concluded therefore, that although the air coupling between the coils would still be large, the observed baseline was not significantly affected by mechanical vibration.

Another effect considered as a possible cause of the baseline was the effect of the soft-iron electromagnet material on the return path of the solenoid flux. The pole-pieces and yoke of all electromagnets are manufactured from soft iron in order to give a high efficiency combined with a low remanence value. The effect of this high-permeability

material surrounding the ac solenoid would be to alter the external 'return path' of the solenoid flux.

The energy stored by a magnetic field is equal to the area under the magnetisation curve:

$$E = \int_0^B HdB , \quad (2.14)$$

where the gradient at a point on the curve is the susceptibility of the surrounding material at that particular field. Hence, we can see that for a given flux density, B , the energy of the field will be lower when the flux passes through a medium with a high susceptibility (such as unsaturated soft-iron), than when it passes through low susceptibility materials such as air. The flux in a magnetic circuit will find the path which minimises the total energy of the field. Thus, flux will preferentially pass through materials with a high permeability until the flux density is increased to a point where this is no longer energetically favourable.

As the flux from the ac solenoid enters the soft iron it will be 'refracted' due to the change in magnetic permeability between the two media. If we consider the boundary conditions shown in Figure 2-8 we can show, by integrating over a thin Gaussian surface, that the component of the magnetic flux normal to the boundary is conserved, as the integral of \mathbf{B} over a closed surface is always zero (from Maxwell's equations). Also, integrating the field around the closed path, L , shows that the field component parallel to the boundary is conserved, as the integral of \mathbf{H} around a closed path is equal to the current bounded by the path (Ampère's circuital law), which is zero in this case. From these conditions we obtain the two equations (2.15) and (2.16),

$$B_{2\perp} = B_{1\perp} , \quad (2.15)$$

$$H_{2\parallel} = H_{1\parallel} . \quad (2.16)$$

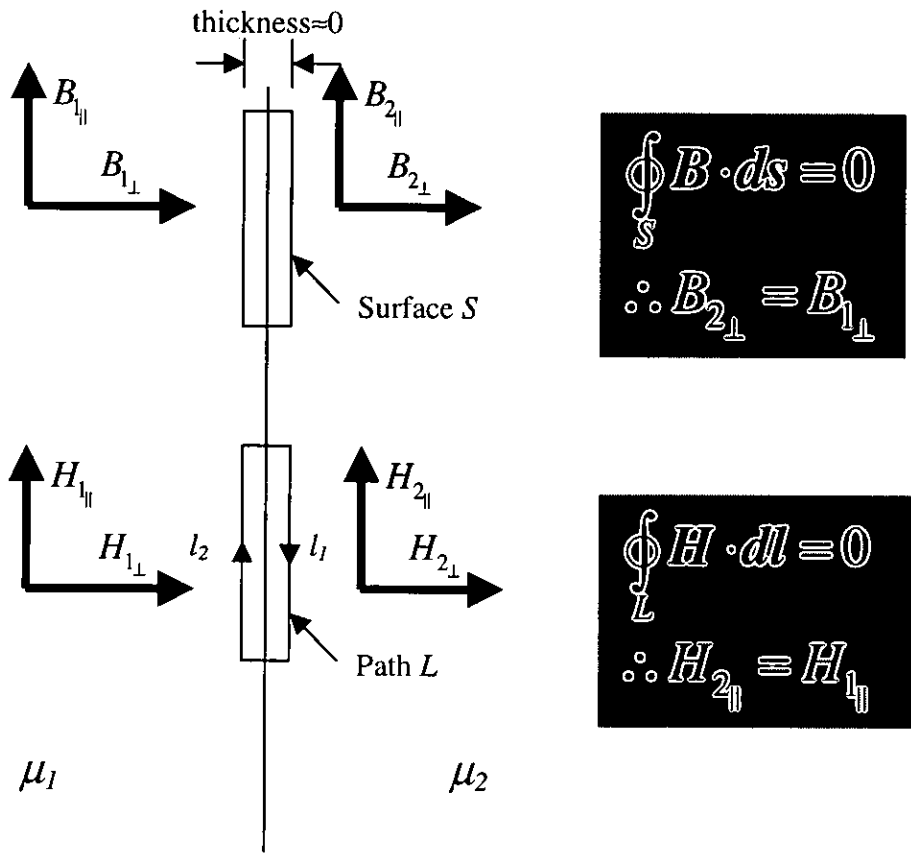


Figure 2-8 Conservation of flux normal to surface, and field parallel to surface, at a boundary

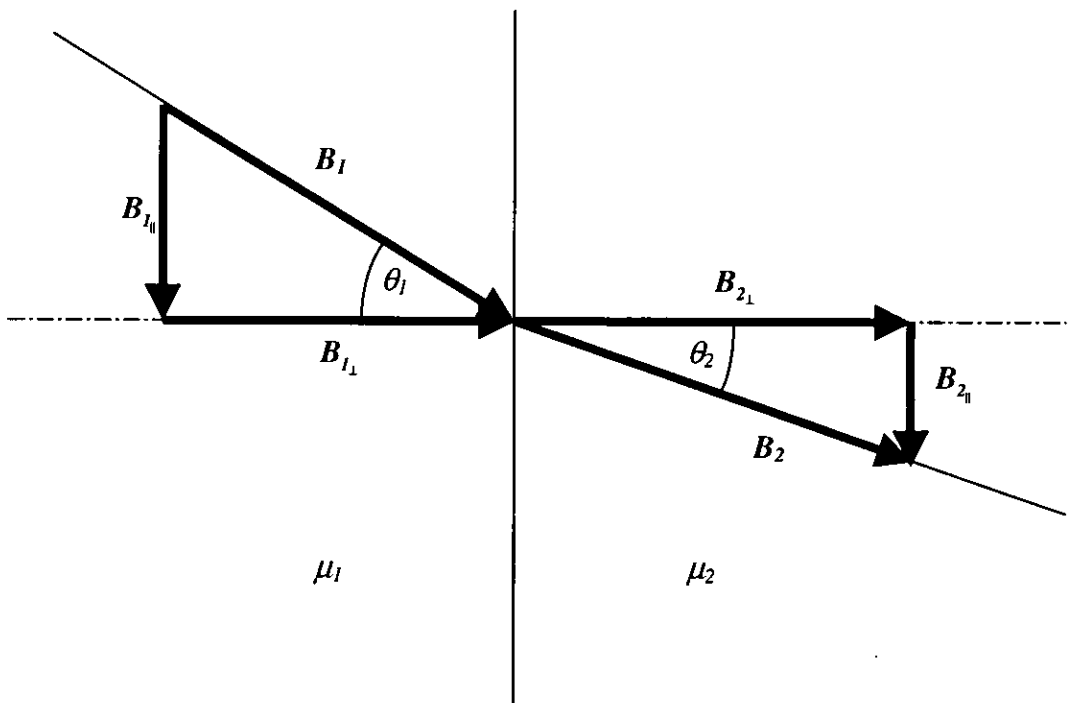


Figure 2-9 Flux refraction at a boundary

Expressing (2.15) and (2.16) in terms of B_1 , B_2 , θ_1 and θ_2 :

$$B_2 \cos \theta_2 = B_1 \cos \theta_1, \quad (2.17)$$

$$\frac{B_2 \sin \theta_2}{\mu_2} = \frac{B_1 \sin \theta_1}{\mu_1}. \quad (2.18)$$

Hence, dividing (2.18) by (2.17) we have,

$$\frac{\tan \theta_2}{\mu_2} = \frac{\tan \theta_1}{\mu_1} \quad (2.19)$$

$$\frac{\mu_1}{\mu_2} = \frac{\tan \theta_1}{\tan \theta_2}$$

Equation (2.19) shows that the line of flux will always be nearer to the surface normal on the lower permeability side of a boundary. Where the change in relative permeability is large (i.e. travelling from air into soft iron) the flux line will be constrained so that it can only enter the surface at an angle very close to the surface normal. This effect and the preference of flux to pass through high permeability materials gives rise to the concept known as magnetic images where the flux paths are the same as if a high permeability surface were replaced by a mirror image of the magnetic system placed in front of it, but with flux sources and sinks reversed.

If we consider these effects with respect to the return path of the ac solenoid flux we can see that the flux path would be changed by the proximity of the pole-pieces and hence the flux density in the centre of the solenoid would also change. If we now consider what happens to the electromagnet when a dc field is applied, we find that as the soft iron becomes magnetised its permeability starts to decrease, until at saturation the permeability tends towards the permeability of free space. As the permeability of the electromagnet decreases the return flux path will change: the soft iron becomes a less preferred flux path and the condition that flux enters the iron normal to the surface will relax. This change in the ac solenoid magnetic circuit will tend to change the flux density within the solenoid. As the transverse susceptibility response is linearly dependent on the ac solenoid field (see equation (2.7)), this is a possible cause of the susceptometer baseline and also explains why the susceptometer baseline is at a minimum when the sensing coils are arranged symmetrically within the solenoid. In order to confirm that there was an effect on the solenoid field due to changes in the pole-piece susceptibility a simple model of the electromagnet core and ac solenoid was

developed using Infolytica MagNet (proprietary magnetic modelling software). The layout of the electromagnet yoke and ac solenoid is shown in Figure 2-10. The model was run using the actual field values of the electromagnet and the peak current through the solenoid. However, it was found that the y component of the field measured at the sense coil position varied erratically, even changing sign, as the dc field was increased. It was felt that the accuracy of the numerical solution was being reduced due to the high dc field values compared to the component of interest and it was not possible to isolate the y component due to the solenoid from that due to the electromagnet. The model was simplified by considering an application of the instantaneous peak ac current through the solenoid and varying the permeability of the otherwise passive electromagnet yoke and poles to represent changes in the dc field.

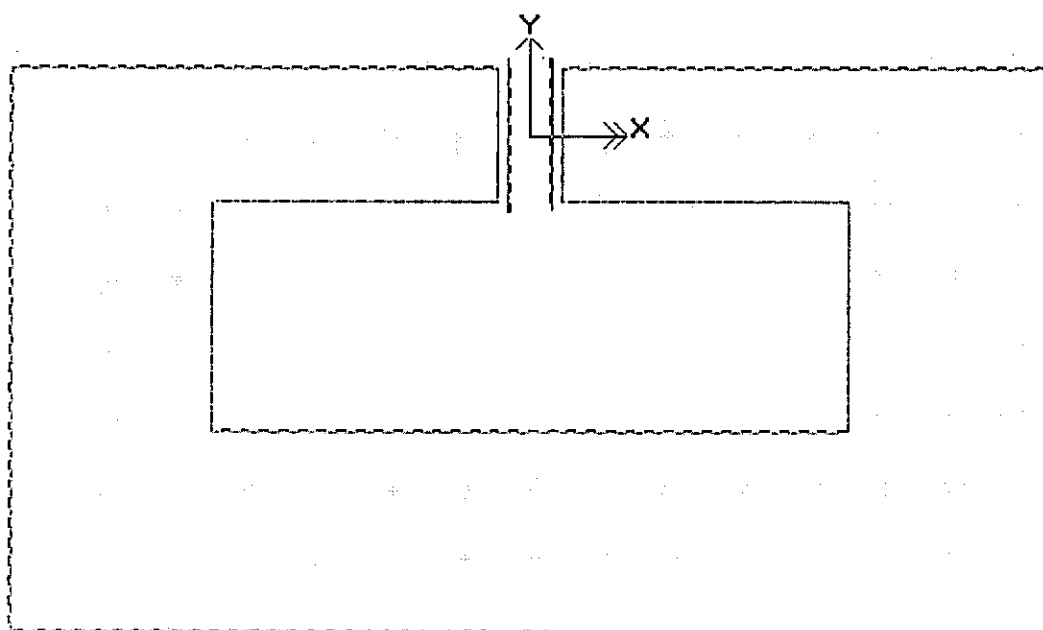


Figure 2-10 – Model design of electromagnet yoke and solenoid

The results of the model show that the field strength within the solenoid varies as a function of the effective susceptibility of the magnet core. The contour plots of the magnetic flux density around the solenoid (Figure 2-11, Figure 2-12 and Figure 2-13) show how the flux density changes as a function of the permeability of the magnet core and pole-pieces.

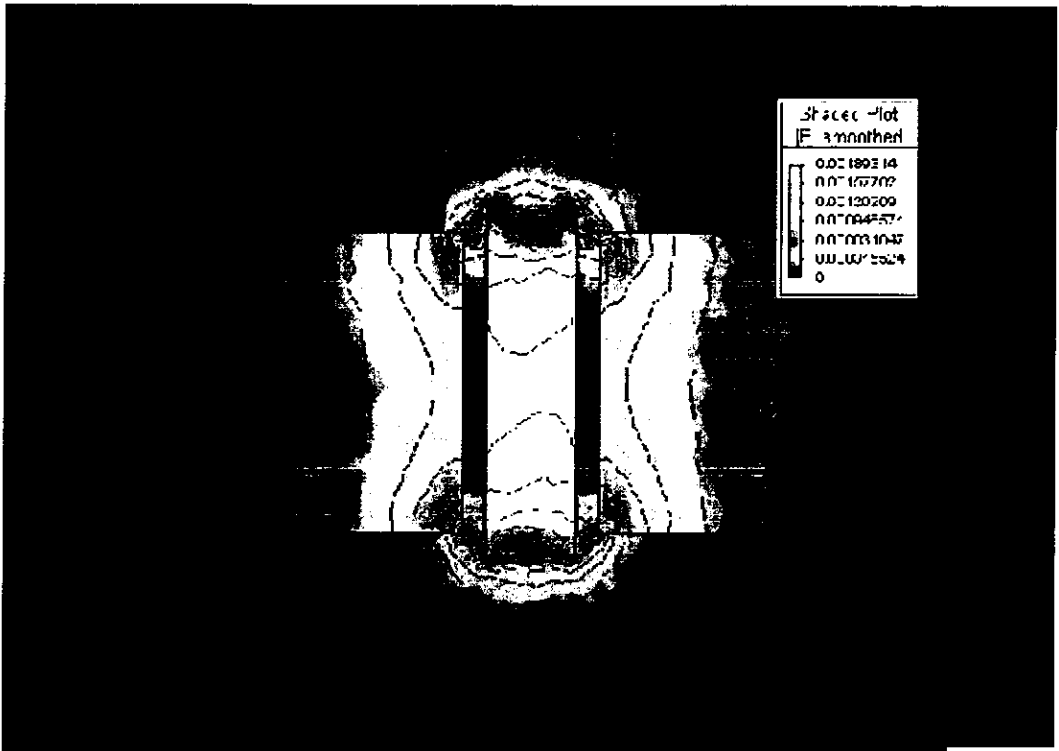


Figure 2-11 Solenoid flux density plot - core with permeability of unsaturated soft iron

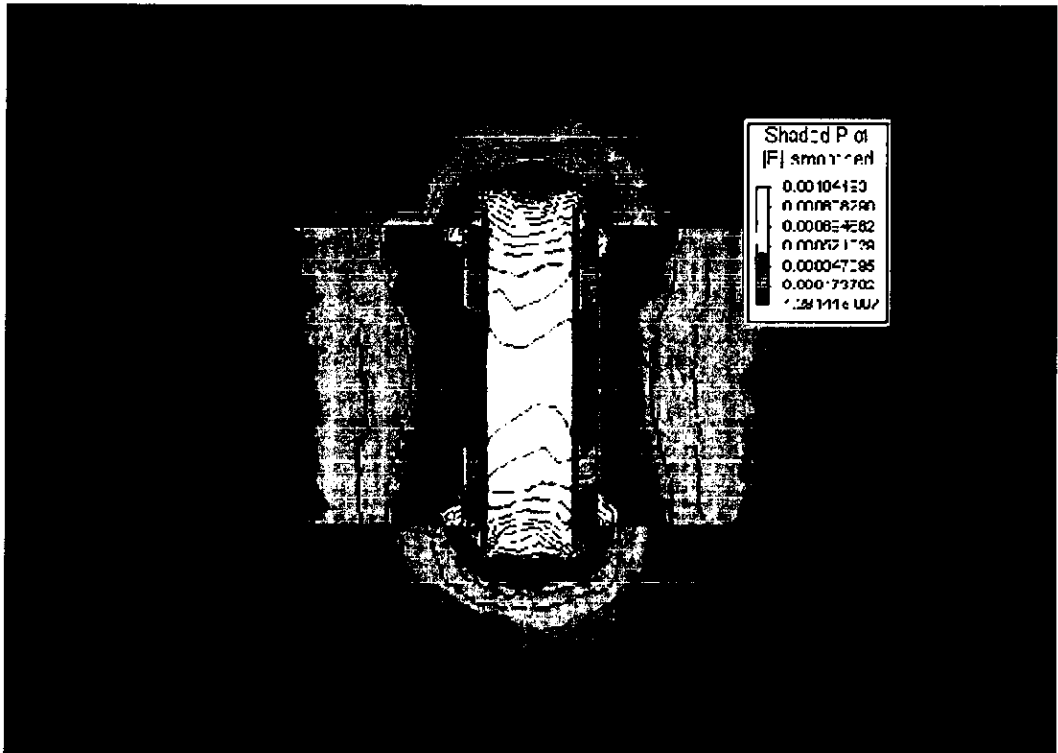


Figure 2-12 – Solenoid flux density plot - core with $\mu = 5$

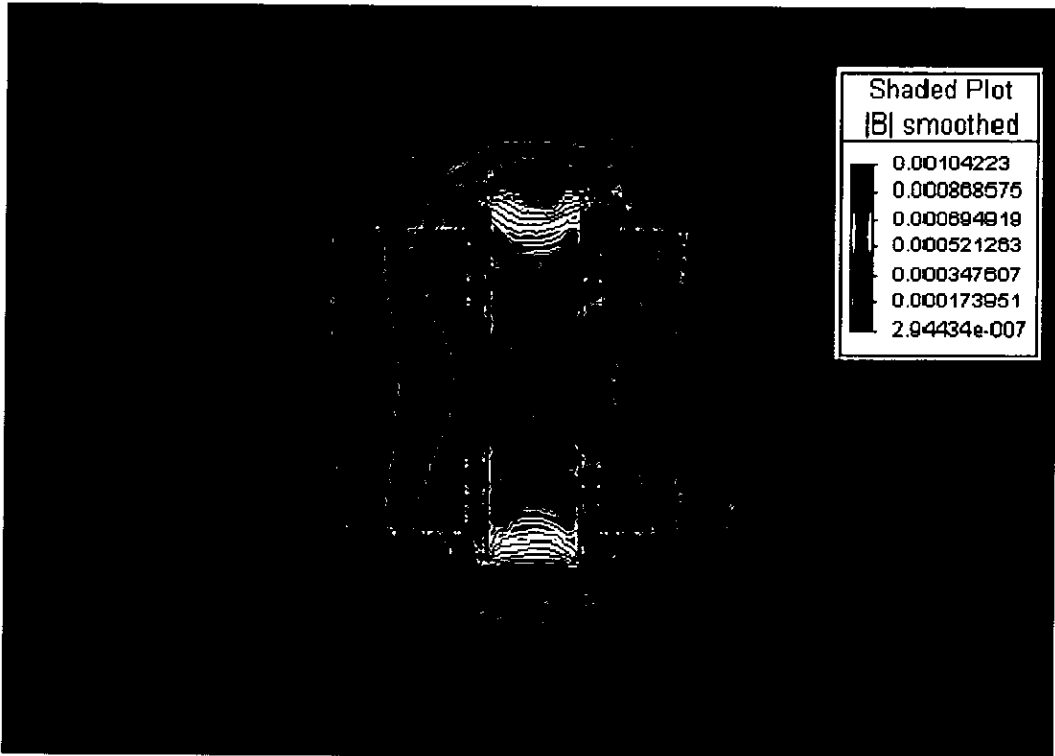


Figure 2-13 – Solenoid flux density plot - core with $\mu_r = 2$

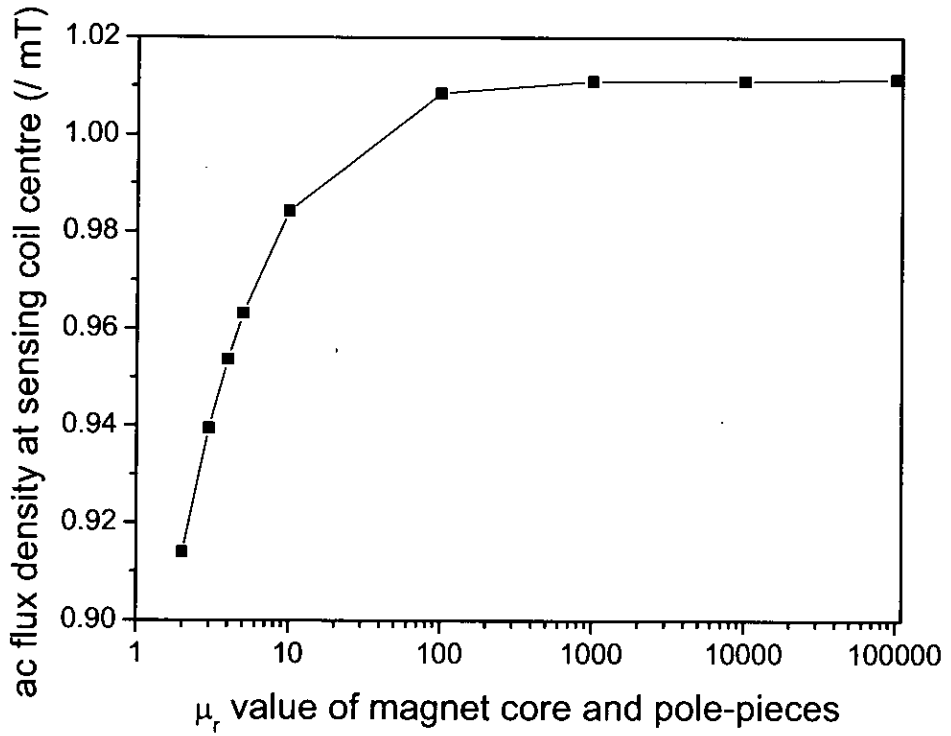


Figure 2-14 Ac flux at sensing coil as a function of core and pole-piece permeability

It is clear from the difference between the flux density plots that the changing permeability of the electromagnet core will cause changes in the ac probe field generated by the solenoid and hence changes in the transverse susceptibility signal. The changes in ac probe field at the position of the sensing coils (assuming the symmetrical arrangement) as a function of the core permeability are shown in Figure 2-14. This was confirmed by measurement of the ac field in the centre of the solenoid as a function of the dc field. The r.m.s. field value was found to increase by 1% as the dc field was swept from zero to 800 kA/m. Although the fractional change in the field was small the compensation factor of the susceptometer was greater than 1000. Hence, small imbalances of field between the two compensating coil positions would cause large effects on the instrument baseline.

With the knowledge of this effect we can now re-evaluate the features of the baseline. The reversible features of the baseline may be attributed to relative changes in the ac probe field between the sensing and compensating coils, as these coils are located in different positions within the ac solenoid. The irreversible features may be attributed to hysteresis effects within the electromagnet core, pole pieces and other fittings which all contribute to subtle changes in the ac probe field.

The above model is also a simplification in that it assumes that the ac solenoid current remains constant. In order to model the changes in the ac field fully it would be necessary to take into account changes in the inductance of the solenoid and the impedance of the solenoid power-amplifier, which would lead to changes in the ac field and phase as a function of the dc field.

As this thesis is primarily concerned with the experimental development of transverse susceptibility measurement techniques, further refinement of the model was not undertaken. It was deemed sufficient to note that the changes in susceptibility of the electromagnet components would cause changes in the ac probe field and that further reductions in the baseline were dependent on,

- Reducing the proportion of the solenoid return flux passing through the electromagnet components
- Positioning the sensing coil and the compensating coil in such a position that any changes in ac field were similar for both

2.3.3 Coaxial coils

In order to make changes in the ac field as similar as possible for both sense coils, an improvement to the design was made using coaxially wound sensing and compensating coils. This arrangement consisted of a formerless sensing coil with a compensating coil wound on top of it and connected in the opposite sense. The coaxial arrangement allowed both coils to be placed at the centre of the ac solenoid thus reducing any end effects and ensuring that the field through both coils was as closely matched as possible. The disadvantage of the coaxial arrangement was that in subtracting the compensating coil signal, part of the sample response was also subtracted, so the balanced signal was much smaller than that achieved using separate coils.

The coils were manufactured using a rectangular cross section former so that a flat packet of tape would fill a greater proportion of the sensing coil than was the case with coils of a circular cross-section (See Figure 2-15). The improved filling factor minimised the air-linkage between the ac solenoid and the sensing coils.

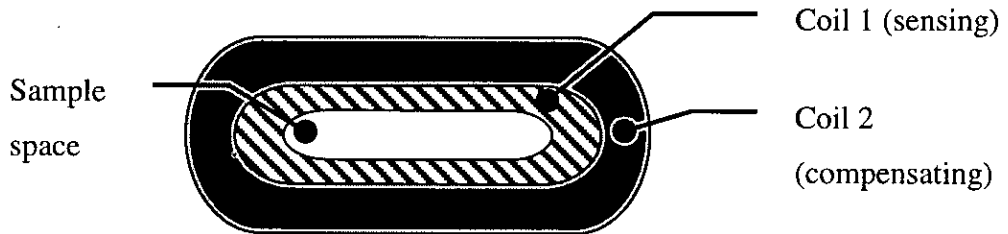


Figure 2-15 Cross-section through coaxial coil assembly

The signal generated by the coaxial coil assembly is detailed below.

We know from equation (2.4) that the emf of a coil placed in a changing magnetic field is given by,

$$\varepsilon = NA\mu_0 \frac{dH}{dt} \quad (2.20)$$

In order for the two coils (Figure 2-15) to balance (i.e. give zero output) when they are connected in opposition to one-another we must satisfy the condition $\varepsilon_1 = \varepsilon_2$. So, from equation (2.20),

$$N_1 A_1 \mu_0 \frac{dH}{dt} = N_2 A_2 \mu_0 \frac{dH}{dt},$$

$$\therefore N_1 A_1 = N_2 A_2 \quad (2.21)$$

In the case of coaxial coils the mean cross-sectional area of the outer coil is greater than that of the inner coil, hence the outer coil must have a proportionately smaller number of turns in order to meet the condition expressed in (2.21).

In practice the coils were manufactured with a similar value of N_1A_1 compared with N_2A_2 , but these parameters could not be accurately measured and the potential divider balancing circuit used previously (Figure 2-2) was used to balance the outputs when the sample coil was empty.

When a sample was inserted into the assembly, the induced emf was changed for each coil due to the difference between the permeability of the sample and the permeability of the air that it displaced. It is assumed that the permeability of air may be approximated by the permeability of free space, μ_0 . So the emf generated by each coil is now given by,

$$\begin{aligned}
 \varepsilon_i &= N_i(A_i - A_s)\mu_0 \frac{dH}{dt} + N_iA_s\mu_r\mu_0 \frac{dH}{dt}, \\
 &= N_i\mu_0 \frac{dH}{dt} [(A_i - A_s) + \mu_r A_s], \\
 &= N_i\mu_0 \frac{dH}{dt} [A_i + A_s(\mu_r - 1)], \\
 \varepsilon_i &= N_i\mu_0 \frac{dH}{dt} [A_i + A_s\chi_s].
 \end{aligned} \tag{2.22}$$

Where A_s is the cross sectional area of the sample, μ_r is the relative magnetic permeability of the sample and χ_s is the magnetic susceptibility of the sample.

If we now consider a balanced pair of coils the output is given by,

$$\begin{aligned}
 \varepsilon_1 - \varepsilon_2 &= N_1\mu_0 \frac{dH}{dt} [A_1 + A_s\chi_s] - N_2\mu_0 \frac{dH}{dt} [A_2 + A_s\chi_s], \\
 &= \mu_0 \frac{dH}{dt} (N_1[A_1 + A_s\chi_s] - N_2[A_2 + A_s\chi_s]), \\
 &= \mu_0 \frac{dH}{dt} (N_1A_1 + N_1A_s\chi_s - N_2A_2 - N_2A_s\chi_s).
 \end{aligned} \tag{2.23}$$

As the coils are balanced, $N_1A_1 = N_2A_2$, so we have,

$$\varepsilon_1 - \varepsilon_2 = \mu_0 \frac{dH}{dt} (A_s\chi_s [N_1 - N_2]). \tag{2.24}$$

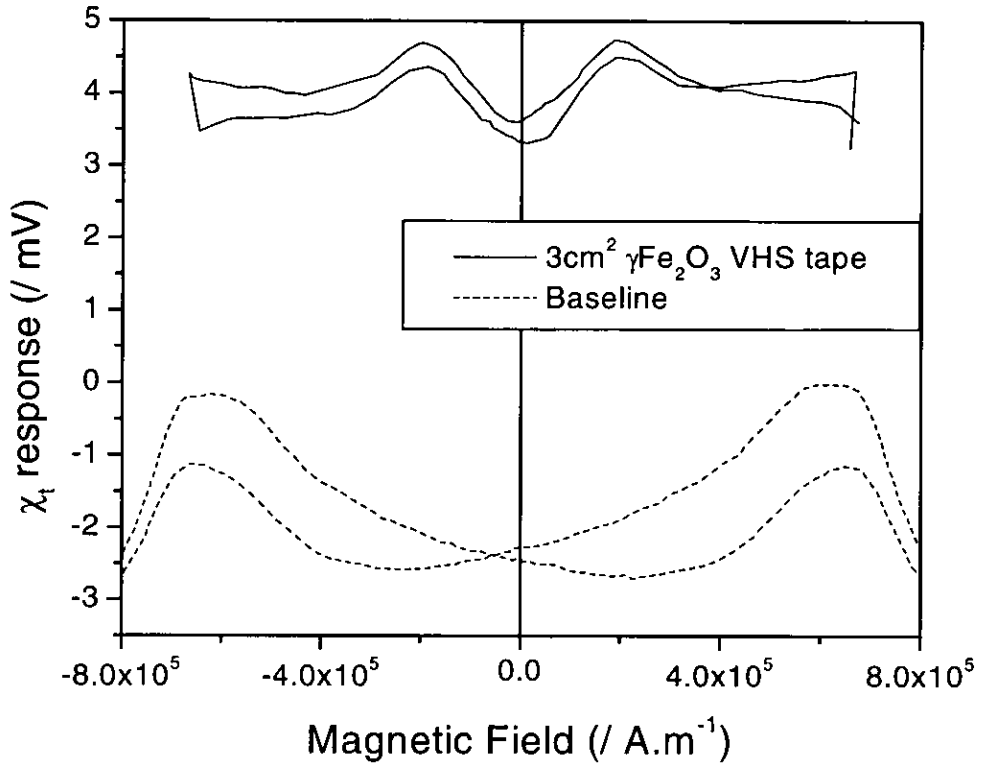


Figure 2-16 Separate sensing coils system – control sample and baseline

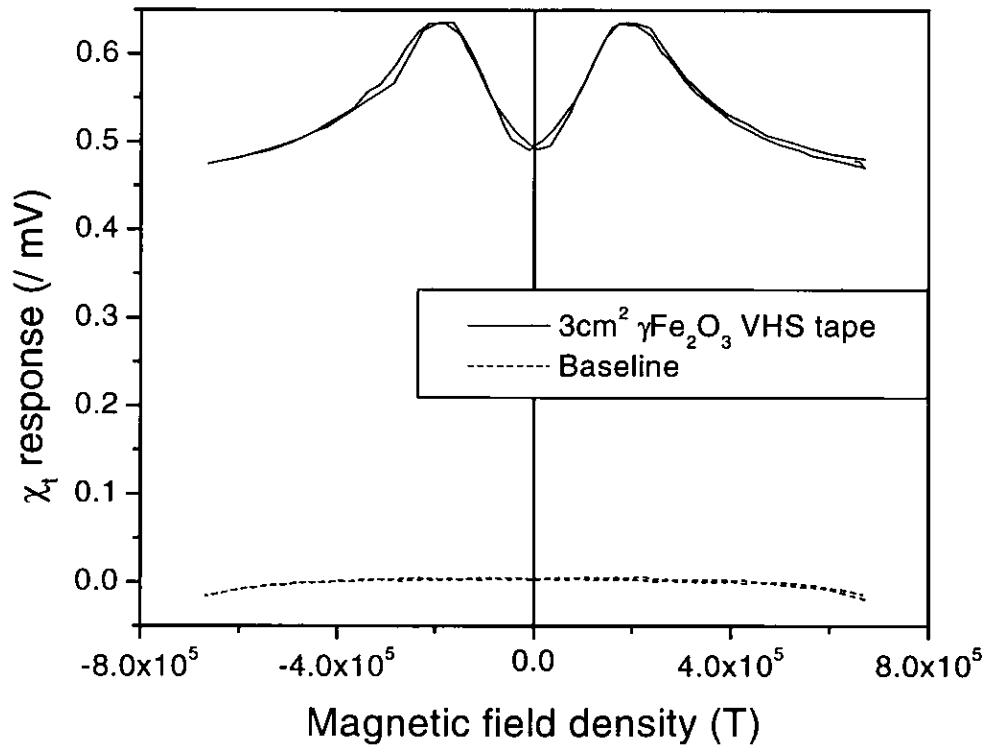


Figure 2-17 Coaxial sensing coils system – control sample and baseline

Hence, the signal is proportional to the susceptibility of the sample and is also proportional to the difference in the number of turns on the two coils.

Comparison of the response of the initial (separate coil) system in Figure 2-16 with the coaxial sense coil system Figure 2-17 demonstrates the reduction in size of the baseline compared to the signal and also the increased stability in the coaxial arrangement resulting in less random noise apparent on the measured response. Although the size of the signal was reduced by a factor of 10, the signal-to-baseline ratio was increased by a further factor of 12 giving a cumulative improvement of a factor of 150 compared to the original system.

2.3.4 Balancing circuit

The change of the sensing coils to a coaxial arrangement meant that a quadrature coil could no longer be used to eliminate any small phase differences between the signal and compensating coils. Although the difference in phase between the coils was generally small, this became significant when the coils were balanced and was still quite large compared to the measured signal. Although the out-of-phase signal was removed by the lock-in-amplifier, the input pre-amplifiers of the instrument became saturated if the input signal was larger than the maximum value of the selected range. Hence the out-of-phase component limited the sensitivity to which the lock-in amplifier could be set. In order to reduce the out-of-phase component of the signal the existing potentiometer circuit was replaced by an active summing amplifier circuit. Use of an active circuit allowed part of the signal to be differentiated to produce an out-of-phase component that could then be used in place of the quadrature coil signal.

The design of the balancing circuit is shown in Figure 2-18.

The balancing circuit was manufactured using an LM348 quad operational amplifier integrated circuit and an LM258 dual operational amplifier integrated circuit mounted on an etched printed circuit board, shown in Figure 2-19.

Although the individual amplified signals from the signal coil and the compensating coil looked clean and distortion free when monitored with an oscilloscope, their sum output displayed unexpected spikes. Despite attempts to remove these by adjusting the circuit resistances the spikes persisted and the active circuit was abandoned as it was found to create more noise on the final output than the quadrature signal that it was

designed to remove. Instead of this, the original passive balancing circuit was used and adjustments were made to the number of turns on the coils to reduce the inherent imbalance.

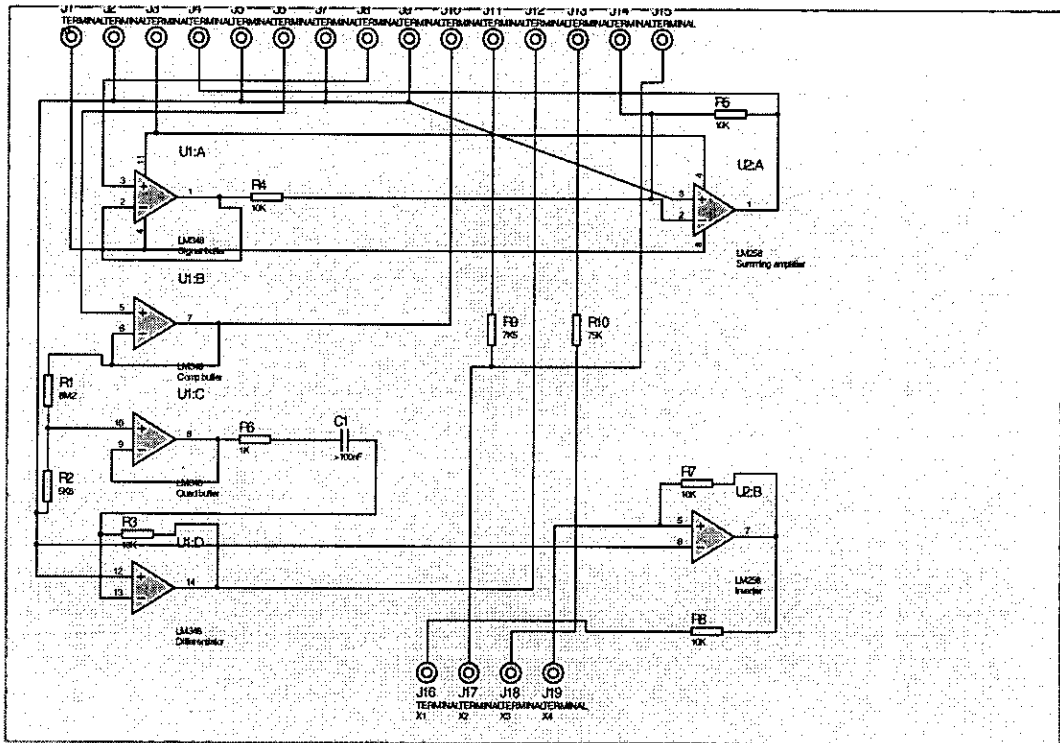


Figure 2-18 – Operational amplifier active balancing circuit

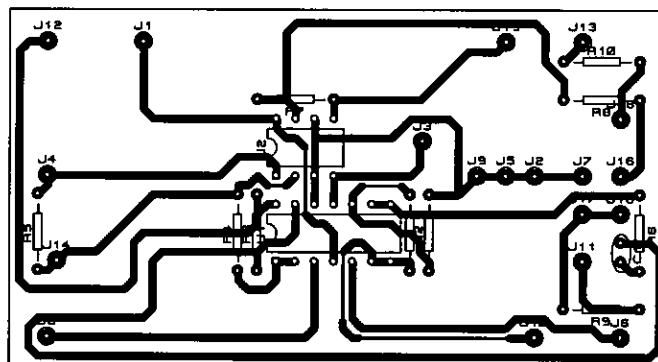


Figure 2-19 Operational amplifier printed circuit design

The origin of the out-of-phase ‘quadrature’ signal was reasoned to be due to small physical differences between the signal and compensating coil windings and wiring. Differences in the inductance and capacitance of the circuit would change the phase angle of the response of the circuit with respect to the phase of the applied field. In order to minimise the out-of-phase component of the signal the coils were replaced a number of times using slightly adjusted turns ratios between the signal and

compensating coil and the wiring was replaced using exactly matched cables for each coil until a system was obtained which needed minimal adjustment of the balancing circuit to obtain a zero signal. This system was found to have a quadrature signal that was small enough not to saturate the input of the lock-in amplifier.

2.4 Solenoid de-coupling

As the interaction between the ac solenoid and the electromagnet had been identified as a major cause of the instrument baseline, the solenoid was re-designed to minimise the interaction with the soft iron of the electromagnet on the outside of the solenoid, thus reducing the influence of the magnet susceptibility over the ac field strength.

The new solenoid design was implemented on the high-field susceptometer described in section 2.5, and consisted of an inner and an outer solenoid wound onto a former. The solenoids were connected in series in an opposite sense to one another and balanced so that the total flux through each solenoid was equal. Although the total flux was the same through each, because of their differing cross-sectional areas the inner solenoid produced a greater flux density than the outer. The effective result of this was a small net field in the inner solenoid with a return path between the inner and outer solenoids, thus minimising stray flux on the outside of the outer solenoid.

Initially the two solenoids were wound on top of one another using the same (0.5mm enamelled copper) wire. These were then connected in parallel via a potentiometer in order to balance the current through each solenoid. It was found, however, that these solenoids could not be balanced because their self-inductances were significantly different and resulted in a different phase-shift through each.

A second assembly was made with different gauge wires used to give a different turn density for each solenoid. The packing between the inner and outer solenoids was accurately matched so that they would balance when they were connected in series. The outer solenoid was wound in the opposite sense to the inner, and the wires were joined at one end to connect them in series.

2.4.1 Solenoid design

The flux density within a long air-cored solenoid is approximated by,

$$B = \mu_0 nI , \quad (2.25)$$

where n is the number of turns of wire per unit length and I is the current through the wire. Hence, the total flux generated by the solenoid is given by,

$$\begin{aligned}\Phi &= BA, \\ \Phi &= \mu_0 n I A,\end{aligned}\tag{2.26}$$

where A is the cross sectional area of the solenoid.

In order for the same flux to flow through two solenoids carrying the same current we must satisfy the condition,

$$\begin{aligned}\mu_0 n_1 I A_1 &= \mu_0 n_2 I A_2, \\ n_1 A_1 &= n_2 A_2.\end{aligned}\tag{2.27}$$

As the cross sectional area is proportional to d^2 for a circular section solenoid we have,

$$n_1 d_1^2 = n_2 d_2^2\tag{2.28}$$

The former for the solenoid was a standard piece of plastic electrical conduit with an outside diameter of 25mm. The clearance between the magnet pole-pieces was 35mm. The wire gauges for the inner and outer solenoid were selected to make best use of the space between the pole-pieces whilst still allowing sufficient clearance to fit and remove the solenoid from the magnet.

The selected wire gauges were 0.5mm \varnothing for the inner solenoid and 0.71mm \varnothing for the outer solenoid. So, for closely wound solenoids, $n_1 = 20 \text{ cm}^{-1}$ and $n_2 = 14.08 \text{ cm}^{-1}$. From equation (2.28) d_2 is given by,

$$d_2 = \sqrt{\frac{n_1}{n_2}} \times d_1,\tag{2.29}$$

which gives a value for the diameter of the outer solenoid former of $d_2 = 29.8\text{mm}$.

The solenoid was manufactured by winding the 0.5mm wire onto the former to 100mm length. Packing material was then wound around the solenoid to a diameter of 30mm and the 0.71mm wire was wound on top in the reverse direction to the inner solenoid. The windings were bonded in place using an epoxy resin adhesive and were connected at one end to give a continuous series circuit around the solenoid assembly.

The solenoid assembly was placed inside a large test solenoid to measure the stray field detected. It was found that the stray field decreased to less than 1% of the value measured when a single solenoid was used.

The use of the two balanced solenoids also resulted in a reduction of the internal field of the solenoid. However, it was found that baseline drift and noise compared with the measured signal was at a minimum for a relatively low solenoid current, $I = 0.04\text{A}$. The field of the combined solenoid assembly was given by,

$$H = nl , \quad (2.30)$$

where n in this case is the effective number of turns per unit length (i.e. the difference between n_1 and n_2). So,

$$\begin{aligned} H &= (20 - 14.08) \times 10^2 \times 0.04 \\ &\approx 24\text{Am}^{-1} . \end{aligned} \quad (2.31)$$

The effect of the double-solenoid assembly on the signal-to-baseline ratio was an increase by a factor of 3.5 when compared with the single-solenoid for the high-field system (described in section 2.5). Also the random noise on the signal was reduced. Both of these improvements can be observed by comparing Figure 2-20 and Figure 2-21. The concentric solenoid was initially developed on the high-field system. A subsequent modification to the low-field system solenoid was carried out by an exchange student, T. Heuser, which gave an improvement in signal-to-baseline ratio of a factor of 2.6 on that system [111] (See Figure 2-22 and Figure 2-23).

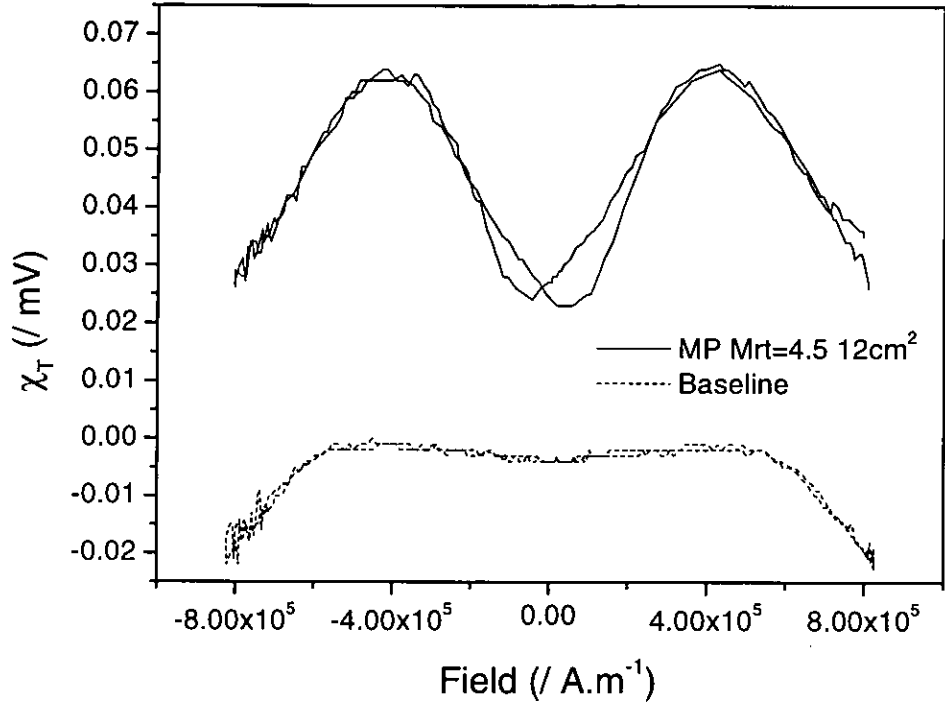


Figure 2-20 MP tape control sample with baseline for single solenoid system

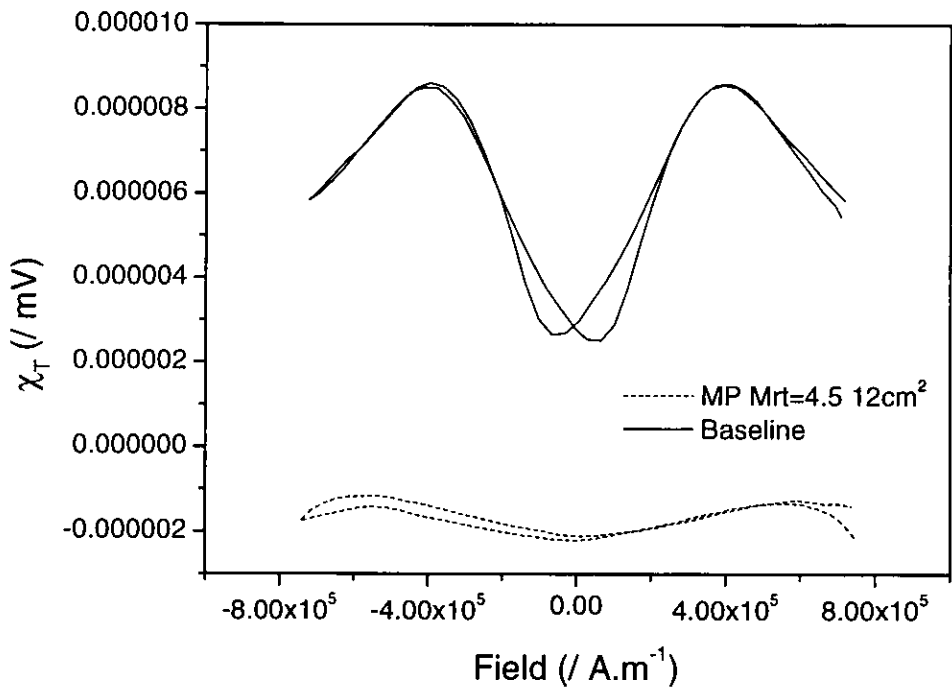


Figure 2-21 MP tape control sample with baseline for double solenoid system

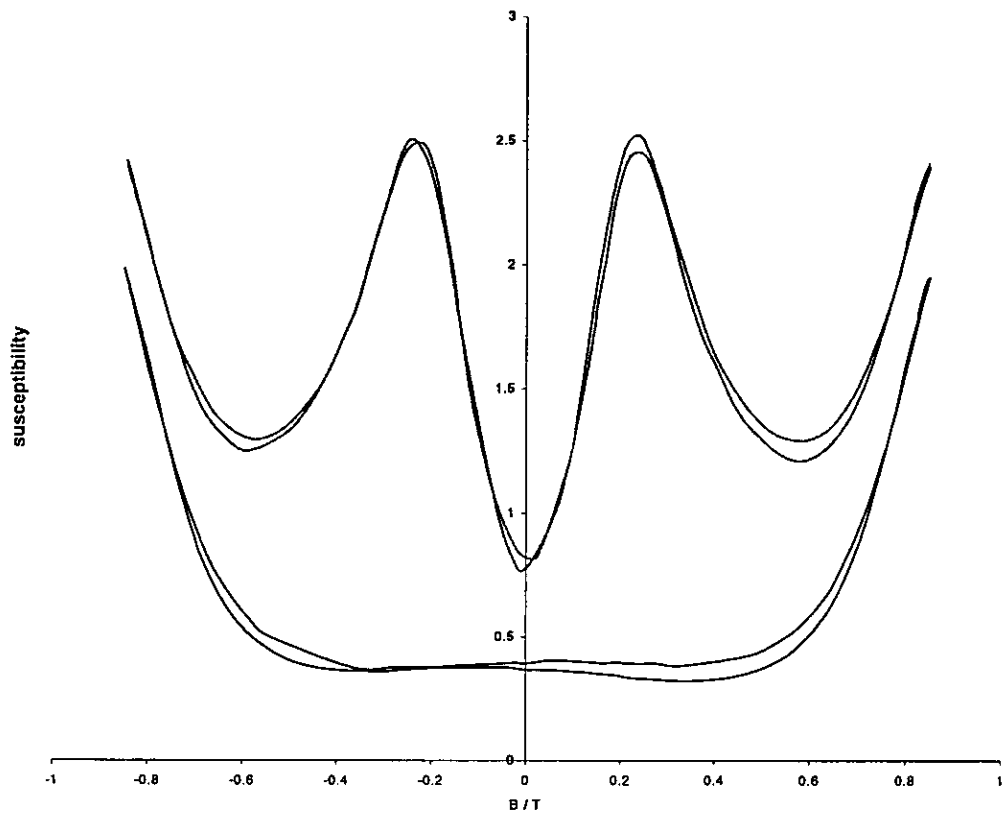


Figure 2-22 Single-solenoid signal and baseline for low-field susceptometer (after Heuser[111])

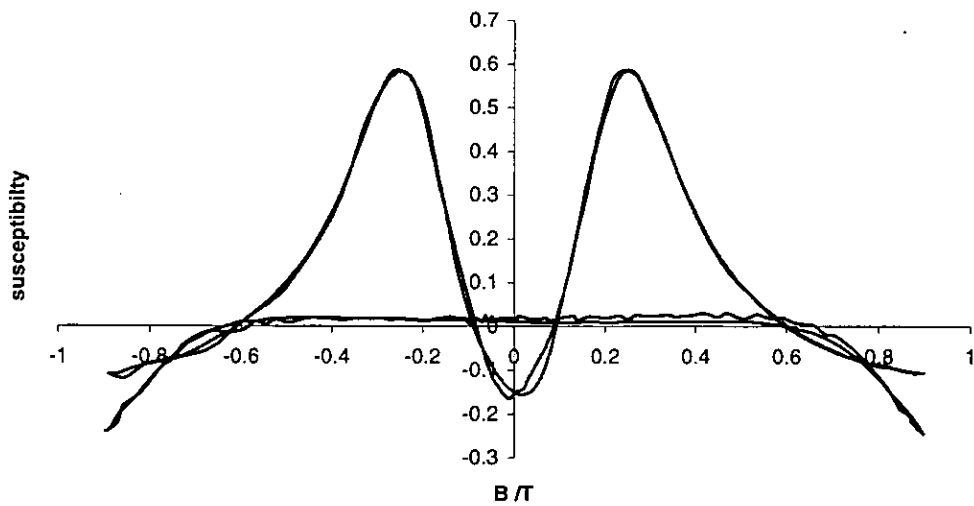


Figure 2-23 Concentric-solenoid signal and baseline for low-field susceptometer (after Heuser[111])

The cumulative improvement factor was 525 when comparing the high-field concentric-solenoid system with the original system.

2.5 High field system

Following the modifications to the existing equipment detailed in the previous sections the sensitivity of the susceptometer was considerably increased. However, the anisotropy fields of modern media were at the high-field limit of the existing electromagnet, which was only capable of producing a maximum field of 875 kA/m. The susceptometer was rebuilt, based on the improvements already made but using a larger and higher-field electromagnet.

The magnet used to rebuild the susceptometer was part of a Jeol NMR spectrometer. The magnet windings were rated up to 100A and the magnet was fitted with a power supply console and re-circulating chiller unit. Unfortunately the existing power supply and chiller were designed with the intention that the magnet would be used continuously at a high field value. The constant cooling of the water supply to the magnet was not required and the power supply was incapable of supplying currents of less than 30A to the magnet. The power supply was also only designed for manual operation and would not allow the development of an automated control system to sweep the field.

The pole pieces of the magnet were much larger, being approximately 300mm diameter (over twice as large as the existing system), which would result in a more constant field at the centre of the poles. The maximum field of the magnet was 1.8 MA/m (2.3T in the air gap).

A power supply was required which could supply a variable current between 0 and 100A and could also be controlled remotely by a computer to allow the system to be automated. As no bespoke 100A supplies were available in the laboratory and the magnet coil was a single winding which could not be split into lower current sections two Farnell model H 60/50 50A supplies were wired in parallel with one another. These supplies had the facility to act as a master / slave pair and be controlled by a remote voltage to give a constant current output. Hence, a single control voltage was used to control the output of the master supply whilst the second supply was configured as a slave to match the output of the master. The input to the master supply was calibrated so that a 0 to 10V signal at the control terminals controlled the output between 0 and 50A for each supply.

In order to sweep the field through a full cycle it was also necessary to be able to change the polarity of the magnet so a suitable polarity-switching unit was required.

The design of the polarity-switching unit was particularly problematic as a number of potential safety problems had to be considered and mitigated in the design. Whilst switching units had previously been built at Preston for electromagnets the high current required made many of the previous design features unsuitable.

In order to switch the supply polarity to the magnet a double pole crossover type arrangement had to be wired as shown in .

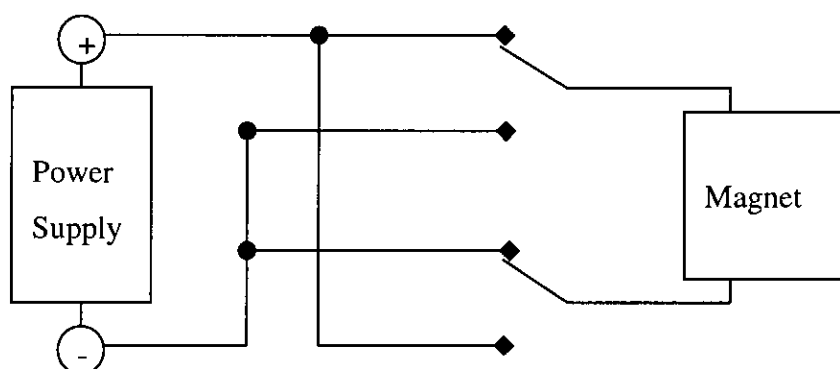


Figure 2-24 Switching unit double pole crossover

In order to perform the switching operation mechanically a double pole relay was required which was rated to carry a 100A current. Such high power rated relays are no longer widely available as they have been superseded by solid-state (thyristor based) switchgear in most industrial applications. The use of solid-state switchgear was investigated. However, this option proved unsuitable as thyristor based devices require a minimum holding current to flow to remain closed. This would prevent the fine control of the field near to zero that is required for many routine magnetometry applications (such as applying a very small current to offset the remanent field of an electromagnet). The only remaining option was to split the current into a number of parallel paths and switch each of these individually using lower current rated mechanical relays.

The switching was realised using five double-pole 20A relays wired in parallel. A 0.1 Ω series resistor was also included in each current path to equalise the current distribution. Without the series resistors the current would take the path of least resistance (i.e. the relay with the lowest contact resistance), which would lead to overloading of some of the relays. The power dissipation of the resistors at maximum loading was considerable (40W per resistor) and heat sinks and a fan were fitted to cool them.

In previous switching units the current had been switched by stacked micro-switches mounted on a proprietary 'Potter and Brumfield' mechanical actuator, whereby a voltage pulse from the lock-in amplifier auxiliary output momentarily energised the actuator, which switched the power. This system was a mechanically latched two-state switch so that once the pulse had 'switched' the unit it remained in the selected polarity even if the power was removed.

In the new system using relays, although it was not possible to arrange for the relays to stay in if power was removed, the same micro-switch actuator was used to control the relay actuator coils, and thus ensure that all the relays switched in sequence whilst only requiring a momentary pulse to change polarity. This arrangement also prevented the high field reversal of the unit following a momentary interruption of mains power. A second micro-switch was also fitted to the actuator and wired to a circuit board (see Figure 2-25 and Figure 2-26 for circuit design) that provided an LED indicator of the switch direction and a BNC voltage output so that the direction of the switching unit could be remotely monitored.

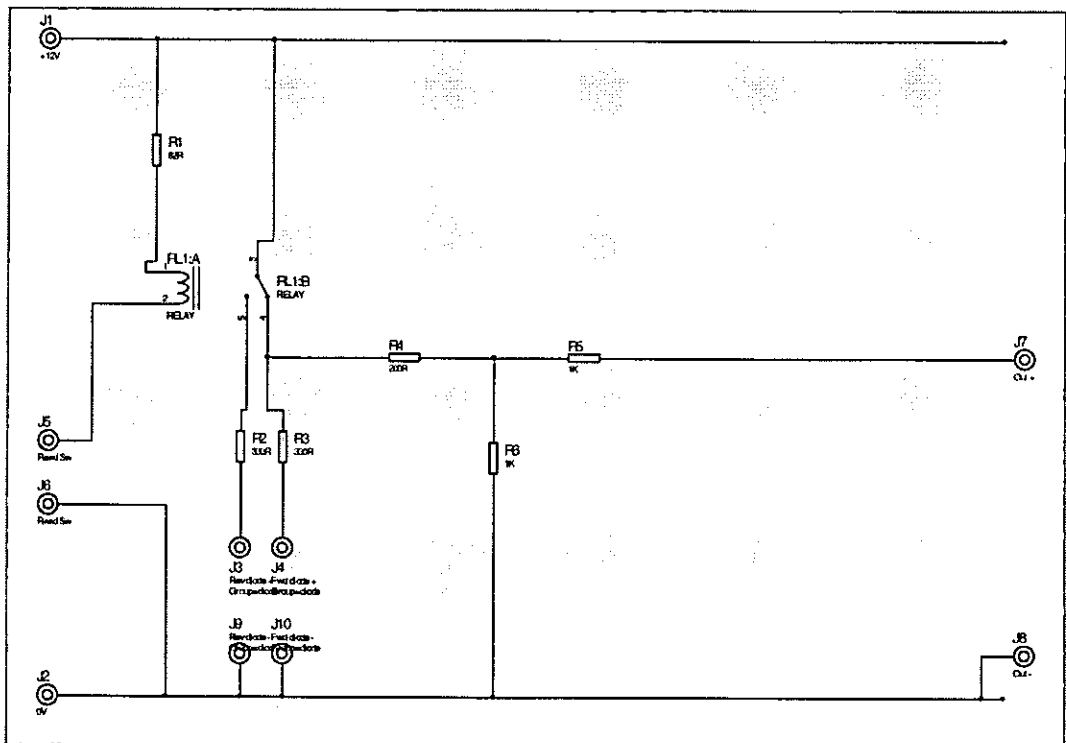


Figure 2-25 Reversing unit direction indicator

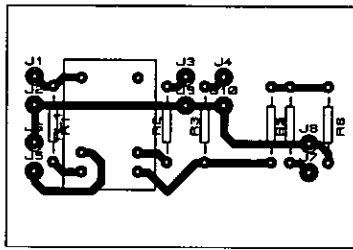


Figure 2-26 Reversing unit indicator printed circuit board

A voltage comparator circuit was designed and manufactured which monitored the voltage drop across one of the relay series resistors. The circuit was wired to prevent the switching actuator from operating when the voltage across the resistor was greater than a pre-set reference threshold. This allowed the unit to be set-up so that accidental reversals at high current were inhibited as the large inductive load of the electromagnet would make such a reversals dangerous to the controlling equipment and power supply, due to the high 'back-emf' generated.

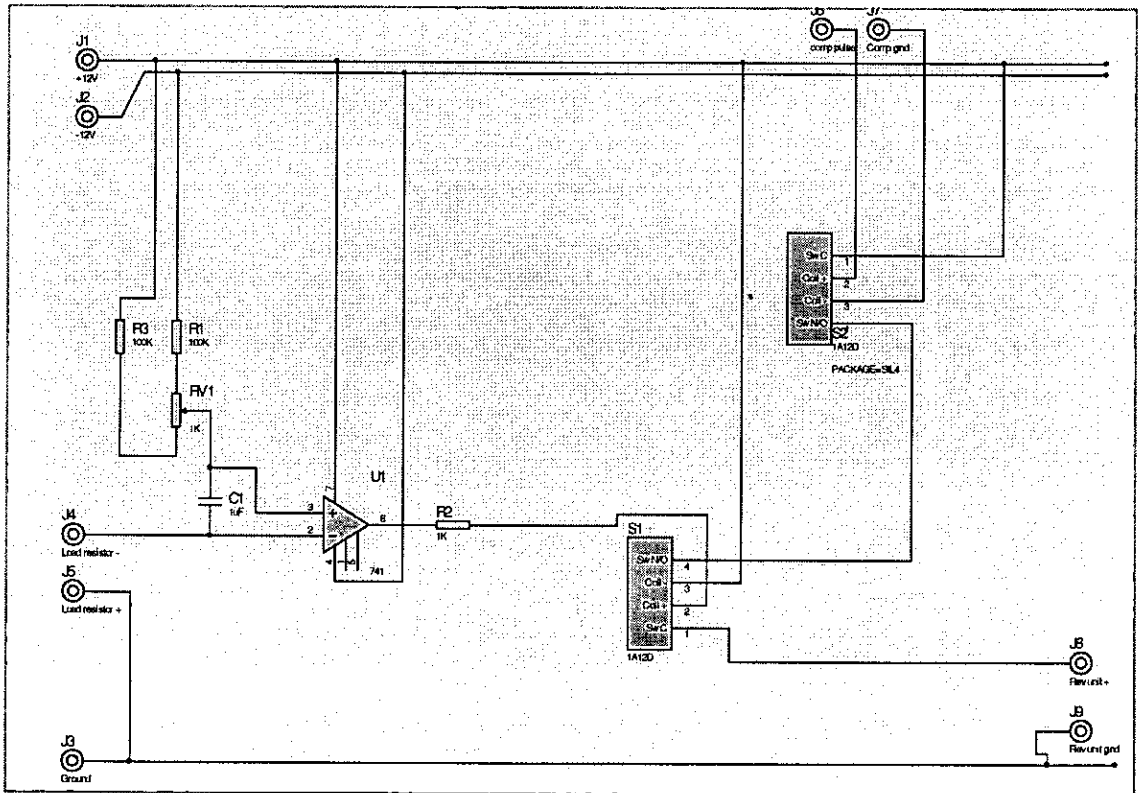


Figure 2-27 Reversing unit comparator

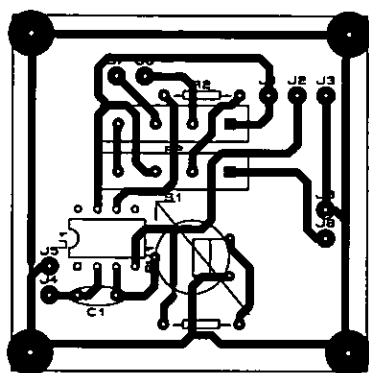


Figure 2-28 Reversing unit comparator printed circuit board

Considerable thought was given to the risk of accidental reversal of the power supply in the event of power failure to the reversing unit. Previous reversing units using mechanically actuated micro-switches had not been prone to this problem. As no simple method could be seen to make the supply truly failsafe a 90V-100A gas-discharge tube was fitted across the coil of the electromagnet. As the maximum voltage across the coil in normal operation was only approximately 40V this was seen as an ideal method to limit any high 'back-emf' to a safe value in the event of accidental reversal or interruption.

2.6 Control system

Automated control of the susceptometer was realised using a PC running National Instruments LabVIEW software. The PC was interfaced to a Bell model 6010 digital Hall effect gauss meter and to a Stanford Instruments model SR810 lock-in amplifier. The magnet power supply input and the switching unit polarity input were both wired from auxiliary voltage outputs on the lock-in amplifier whilst the switching unit polarity indicator was wired to an auxiliary input on the lock-in. In this way the PC could use the lock-in amplifier to control the field sweep whilst monitoring the susceptometer response and the dc field direction. The dc field strength was monitored via the gauss meter.

Figure 2-29 shows a block diagram of the susceptometer with the signal and power connections between components.

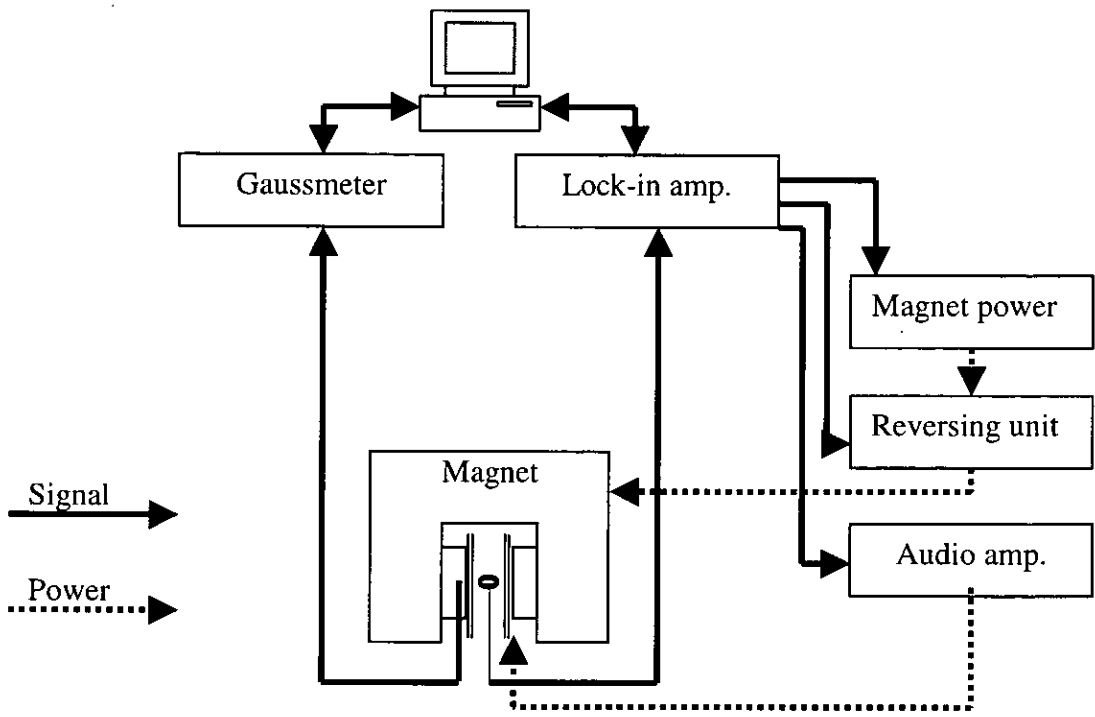


Figure 2-29 Block diagram of transverse susceptometer control system

The software to control the susceptometer was written using National Instruments LabVIEW language; a graphical language for creating control systems and instrument interfacing. The software was developed using a ‘bottom up’ approach with the most basic routines being written first then assembled in a modular approach to create a full susceptometer control program.

An overview of the software design is given below. Detailed programs are given in Appendix 1.

2.6.1 Field calibration routine

A field calibration routine was developed which incremented the control voltage to the power supply from its minimum to its maximum value over 100 steps. The resulting magnetic field as a function of control voltage was recorded in a lookup file. The lookup file was used to determine the control voltage setting for a required field, although the recorded field value was always measured directly using the digital gaussmeter to eliminate errors due to the hysteresis of the electromagnet.

2.6.2 Field control routine

A routine was developed to ‘ramp’ the magnetic field smoothly to any requested value.

The input to the routine was the absolute field value required and the ramp rate (in $V.s^{-1}$ change of the control signal).

The routine first checked the existing control signal value and the magnet polarity before determining the required value and polarity using the field calibration lookup file. The field was then swept smoothly between the two, changing polarity of the magnet at zero-field if required.

All subsequent programs used this rigorously tested routine to control the magnet field so that it was impossible for subsequent programming errors to apply dangerous step changes to the magnet control signal.

2.6.3 Loop control routine

The sweeping of the field to take transverse susceptibility measurements was controlled by a loop control routine. The routine referred to a data file containing the required field values for a particular sample. In this way the maximum field and the number of readings around areas of interest could be varied in a very flexible way. The routine also offered the option to subtract values from a previously measured baseline so that the adjusted result could be displayed and saved in real-time.

2.7 Discussion

This chapter describes improvements that were made to the existing transverse susceptometer at Preston in order to increase the sensitivity and repeatability of the equipment to allow the investigation of modern recording media.

An alternative method of measuring the susceptibility was investigated using an oscillator, but the technique was abandoned, as it could not overcome problems associated with the low filling-factor of the sense coil, which is of paramount importance for the measurement of advanced recording media.

Using coaxial sample and compensating coils to isolate the signal due to the sample from local fluctuations in the ac field achieved considerable reduction of the baseline. In a similar way the ac solenoid was isolated from the soft-iron of the electromagnet by using a coaxial, balanced-flux solenoid assembly. The effect of vibration on the baseline was found to be small, although steps were taken to mechanically isolate the sample and compensating coils from the solenoid. A summary of the improvements in signal to baseline ratio is shown in Table 2-1. In addition to this signal-noise was reduced and the

signal-repeatability was observed to increase following each modification, although this was not measured quantitatively. The sensitivity of the susceptometer was difficult to quantify, as the output of the susceptometer is in arbitrary units and the improvements made to the system have resulted in a higher sensitivity with a smaller absolute output signal. Probably the most meaningful indication of the sensitivity is the smallest sample magnetic moment from which a reliable and repeatable transverse susceptibility response could be obtained. This was less than $50\mu\text{A m}^2$.

| Modification | Improvement factor over previous design | Cumulative improvement factor |
|-----------------------------|--|--------------------------------------|
| Centring sense coils | 12.5 | 12.5 |
| Coaxial sense coils | 12 | 150 |
| De-coupled solenoid | 3.5 | 525 |

Table 2-1 Changes in signal-to-noise ratio

An active electronic balancing circuit to amplify and mix the sample and compensation coil signals was designed and built, but was found to introduce noise into the signal. Similarly, the coaxial solenoids were initially wired in parallel with a potential divider to balance the flux, but the differing inductances in the circuit caused phase differences between the solenoids. The small size of the required signal compared to the induced signal in the coils required extremely low-noise and well-shielded electronics to be used. In hindsight the most successful modifications were those which used high accuracy physical matching of components during the build of the equipment, rather than attempts to compensate for mismatched components electronically. There is scope for further increases in the sensitivity of the instrument by improvements to the balance of the sample / compensating coil assembly and the solenoid assembly. Since the coupling between ac and dc field sources is the most significant factor, use of a wide pole-gap electromagnet or possibly a super-conducting solenoid could generate significant improvements.

3 Linear transverse susceptibility

This chapter details the results of transverse susceptibility investigations made using the susceptometer described in Chapter 2. The sensing coil axes were parallel with the ac probe field to obtain the traditionally measured linear transverse susceptibility, as opposed to the non-linear transverse susceptibility described in Chapter 5.

The chapter contains a review of previous work detailing the development of transverse susceptibility as a method of characterising magnetic media and an overview of the theory. Linearity of the response with respect to the ac probe field is demonstrated.

Measurements of commercial VHS videotapes are presented which are consistent with previous measurements with the original susceptometer configuration. However, the improved sensitivity of the susceptometer allowed the measurement of smaller samples, thus reducing the peak-spreading effect caused by misalignment in samples made up of a large number of layers. Measurements of four development MP tapes were also made which were not possible previously due to their relatively low magnetic moment.

Measurements were made of CrO_2 , $\gamma\text{-Fe}_2\text{O}_3$ and four samples of metal particle powders. The anisotropy peaks were suppressed in all of the powders with the exception of the CrO_2 . A study of the transverse susceptibility of aligned samples as a function of the angle between the easy axis and the ac field direction was made for CrO_2 and $\gamma\text{-Fe}_2\text{O}_3$ systems which showed that the anisotropy peak was relatively large in the CrO_2 sample for particles aligned with the ac field, which could account for the peaks still being visible in the powder sample.

Measurement of the imaginary component of the χ_t signal, proposed by Papusoi[5], was found to be consistent with the theoretical predictions. The measurement of the imaginary component had not been possible previously due to the small signal size (approximately 1/10 of the real component). The presence of the imaginary signal challenges the assumption that thermal switching may be neglected and predicts a slight reduction in the experimentally determined H_k value compared with theory, where thermal effects are neglected.

3.1 Previous work

The reversible transverse susceptibility, RTS, was first discussed by Gans[1] in 1909. The parameter is defined as the initial susceptibility of a material measured in a transverse direction to an applied bias field.

A theoretical expression for the RTS was derived by Aharoni *et al* in 1957[3] which suggested that the RTS for a Stoner-Wohlfarth system with a random distribution of easy-axis directions would show three cusps, at the coercive field, $-H_c$, and at the anisotropy fields, $\pm H_k$ (assuming that the bias field is swept from positive to negative values). Numerous unsuccessful attempts were made to measure the transverse susceptibility of bulk materials until Pareti and Turilli[4] in 1987 demonstrated that the Aharoni model was only applicable to particulate media where the particle size was below the required volume for multiple domain formation. LeDang *et al*[97] measured the transverse susceptibility of some highly anisotropic thin films and produced a model independent of the work of Aharoni to explain the results which showed that the response was highly dependent on the alignment and easy-axis dispersion of the sample. In 1990 Richter investigated the use of transverse susceptibility in determining anisotropy information of polycrystalline permanent magnet materials[94] and randomly oriented particulate powder samples[95]. He found that, although the method was fast and robust compared with other anisotropy measurement techniques, the response was affected by particle interactions and hysteresis effects not predicted by the pre-existing theory.

In 1992 and 1993, Sollis *et al*[98,112] and Hoare *et al*[113] published experimental and theoretical studies of the effect of texture and anisotropy field distributions on the transverse susceptibility of particulate media. These showed that the shape of the χ_t plot was highly dependent on the texture of the media and that a highly aligned system enhanced the anisotropy peaks.

From 1993 to 1995, Lu *et al*[114]; Huang & Lu[115,116]; Lee *et al*[117]; and Chang & Yang[118] published extensions to transverse susceptibility theory showing the effects of thermal switching and interactions (using a mean field approach). These studies indicated that the anisotropy information in the χ_t was not affected by thermal switching, whilst the coercivity information was reduced. They also found that the

anisotropy peak shifted to lower field values and eventually merged with the coercivity peak as the interactions in the system were increased.

In 1995 Zimmermann published work investigating the influence of remanent magnetisation on the low-field χ_t [119] which showed deviations from the Stoner-Wohlfarth model due to inhomogeneous magnetisation states and particle-particle interactions.

Further experimental results published by Sollis *et al* in 1996 and 1997 highlighted that texture, rather than interactions, was the dominant factor in the suppression / enhancement of peaks in χ_t [120] and that the anisotropy peak field and the coercivity increased in accordance with previous theory when particle-particle interactions were reduced by dilution[100].

In 1998 Chantrell *et al* published a technique for extracting the anisotropy field distribution from the χ_t peak by deconvolving the orientational texture from the measurement using a numerical maximum entropy approach[121]. This technique was later extended by Jones *et al*, who used a neural network technique to perform the deconvolution [122,123].

In 1999 Spinu *et al* published work using a high-frequency oscillator based susceptometer to measure the χ_t of nanoscale particle systems as a function of temperature[102,124] which showed the loss of anisotropy information as the particles became super-paramagnetic.

The theoretical paper of Papusoi [5] proposed the existence of an imaginary part of the χ_t signal which was related to thermal relaxation of the moments at DC fields near to the anisotropy field. The paper also predicted that the real part of the χ_t signal would have a peak below the anisotropy field, not predicted by previous theory, which could shift the anisotropy peak to a lower value in some circumstances.

A comparative study of the different methods of anisotropy field determination for magnetic powders was carried out by Görnert *et al*[60]. The work compared the anisotropy of samples of BaFe₁₂O₁₉ powder using six different methods and was the first to note that the effective anisotropy field measured using 'switching' techniques (rotational hysteresis loss and remanence curves) was generally lower than that determined by 'stiffness' techniques (ferromagnetic resonance, torsion pendulum, singular-point detection and transverse susceptibility). The author suggested that the

'switching' techniques were less accurate than the 'stiffness' techniques as they did not properly account for switching due to particle interactions and thermal fluctuations. The work of Jones *et al*[75] also compared different techniques for the determination of the effective anisotropy field, this time measuring oriented tape systems using successive derivatives of the hysteresis loop, transverse susceptibility and extrapolation of the bulk coercivity to 0K. This study indicated that all of the methods were affected by changes in the texture of the media.

3.2 Theory

The linear transverse susceptibility of a material is a measure of the magnetic susceptibility (ease of magnetisation) of the material in a direction transverse to an applied bias field. In order to measure the susceptibility of the sample a small ac probe field is applied in the direction in which the susceptibility is to be measured and a coil around the sample is used to measure $\frac{d\phi}{dt}$ in this direction, which is proportional to the change in magnetisation of the sample (see section 2.1.1). The ac probe field is very small (tending to zero) so that we may assume that the measured change in magnetisation in phase with the probe field is due to reversible oscillation of the particle moments and not switching behaviour.

If we assume that the magnetic material is composed of small single-domain particles we may use the Stoner-Wohlfarth[2] model (see section 1.5) to show how the transverse susceptibility changes as a function of the applied bias field. Figure 1-4, Figure 1-5 and Figure 1-6 show the energy of a particle as a function of moment angle, θ , and reduced field, h , for different angles, α , of applied field. The application of the ac field causes a small oscillation of θ within the local energy minimum. Looking at the width of the energy minima we can see that for $\alpha=180^\circ$, just before switching, the energy minimum becomes a point of inflection the base of which becomes flat. Also, in the case where $\alpha=90^\circ$ and $h=1$ (see Figure 1-5) the two minima merge to form a single wide, flat-based minimum. In both of these cases the flat segments on the energy curve mean that there is no restoring force acting on the moment such that the transverse susceptibility becomes infinite at these points. Aharoni *et al*[3] used the Stoner-Wohlfarth model to

predict the transverse susceptibility for such a Stoner-Wohlfarth particle. The transverse susceptibility was found to be given by,

$$\frac{\chi_t}{\chi_0} = \frac{3}{2} \left[\cos^2 \phi_k \frac{\cos^2 \theta_M}{h \cos \theta_M + \cos 2(\theta_M - \theta_k)} + \sin^2 \phi_k \frac{\sin(\theta_k - \theta_M)}{h \sin \theta_k} \right], \quad (3.1)$$

where h was the reduced field, θ_M was the angle between the field and the moment direction, θ_k and ϕ_k were the coordinates of the particle easy axis and χ_0 was a constant. It can be easily shown that the equation (3.1) becomes singular at $h=1$ for $\alpha=90^\circ$, and also at $h=1$ for $\alpha=180^\circ$. The second singularity is related to the coercivity and occurs at the coercive field, h_c [equation (1.11)], for the angles $90^\circ < \alpha < 270^\circ$.

The physical origin of the features can be explained by reference to the changing shape of the energy minima in which the particle moment sits. The features related to the anisotropy field are associated with those particles with easy axes aligned with the ac field direction. Referring to Figure 1-3 this corresponds to particles with angle $\alpha = 90^\circ$. The energy as a function of reduced field, h , and moment angle, θ , is shown in Figure 1-5 and we can see that as h increases from zero, the energy minima rotate towards one another.

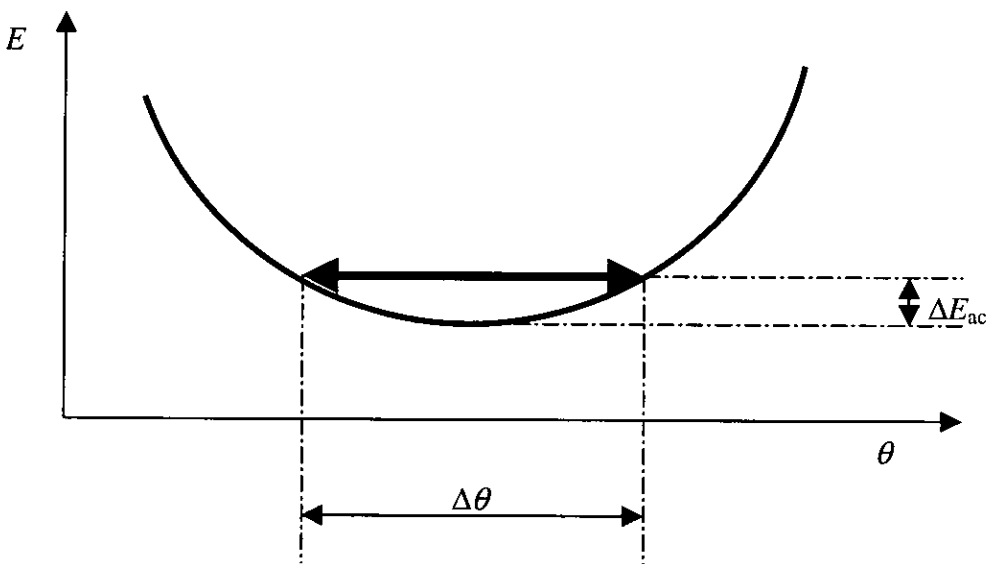


Figure 3-1 Sketch of energy minimum showing relationship between shape of curve, ac field energy, ΔE_{ac} , and oscillation angle, $\Delta \theta$

Figure 3-1 shows the relationship between the shape of the minimum, the ac field energy, ΔE_{ac} , and the moment oscillation angle, $\Delta \theta$. As the ac field is constant, changes

in the susceptometer output (which is a function of $\Delta\theta$) are solely due to changes in the shape of the minimum. For those particles with easy axes aligned with the ac field, as H_{dc} approaches H_k (i.e. as h approaches 1) the two narrow minima begin to merge until the point where $H_{dc} = H_k$, when they form one minimum with a very wide flat base (see Figure 1-5). At this point $\Delta\theta$, and the susceptometer output, become very large.

Subsequent increases in H_{dc} , to values greater than H_k , cause the single minimum to narrow reducing $\Delta\theta$. The susceptometer output goes through a sharp maximum where $H_{dc} = H_k$.

Particles with easy axes not at 90° to H_{dc} do not form this single, wide minimum.

Instead one minimum progressively deepens whilst the other becomes shallower until the shallow minimum disappears (see Figure 1-6). As no wide minimum occurs at $H_{dc} = H_k$ there is no feature in the susceptometer output associated with the anisotropy field of these particles, instead as H_{dc} approaches H_c , the shallow minima becomes wider and flatter until at $H_{dc} = H_c$ it becomes a flat point of inflection (an unstable equilibrium) and hence $\Delta\theta$ again becomes very large. As H_{dc} increases further the equilibrium position disappears and the moment switches irreversibly into the single narrow minimum causing $\Delta\theta$ to become small again.

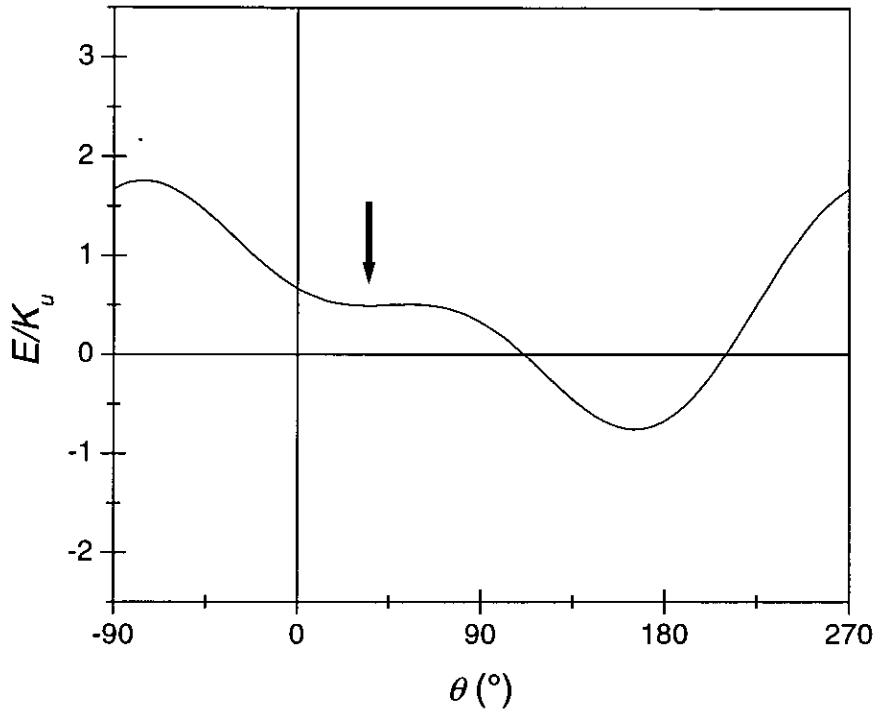


Figure 3-2 Energy as a function of θ at $H_{dc}=0.95H_c$, arrow indicates broad minimum

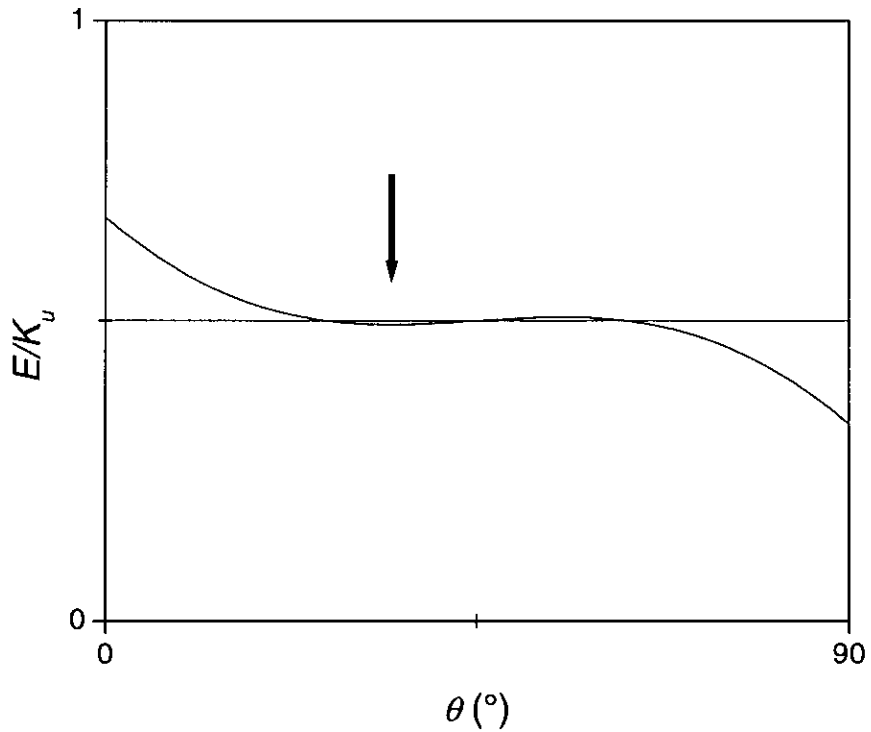


Figure 3-3 Expanded view of broad minimum

Figure 3-2 shows the energy as a function of moment angle for a particle where $H_{dc}=0.95H_c$ ($\alpha = 135^\circ$ in this example). A broad minimum exists at an angle just below

the switching angle (45° for $\alpha = 135^\circ$) and can be seen in more detail in the expanded view of Figure 3-3. In practice this causes a peak in the susceptometer output at the switching field of the particle for all particles other than those with easy axes at 90° to the dc field direction.

Aharoni *et al* went on to consider a system of identical Stoner-Wohlfarth particles with a random distribution of easy axis directions. By integrating the χ_t response over all the easy axis directions and neglecting inter-particle interactions a curve was obtained with cusps at $\pm H_k$ and at $-H_c$, where $H_c = 0.479H_k$.

Further theoretical and experimental work by LeDang *et al*[97] showed that the H_k response was dominated by particles with easy axis angles very close to $\alpha = 90^\circ$, and where the easy axis was parallel to the ac field. Hoare *et al*[113] then showed that the addition of an orientation texture distribution and particle H_k distribution to the Aharoni model gave broadened peaks rather than cusps and that the H_k peaks were enhanced in a material with a preferred orientation direction aligned with the ac field. These findings were consistent with the results of experimental measurements.

3.3 Response to variation of ac field

As discussed in section 3.2 the transverse susceptibility response is dominated by those particles with easy axes parallel to the ac field and with a transverse bias field equal to H_k applied to them. The bias field applied to these particles is just sufficient to rotate the magnetic moment into the hard axis direction. Application of a small perturbing ac field in the easy axis direction will then displace the magnetic moment by a small angle $\Delta\theta$ (see Figure 3-4).

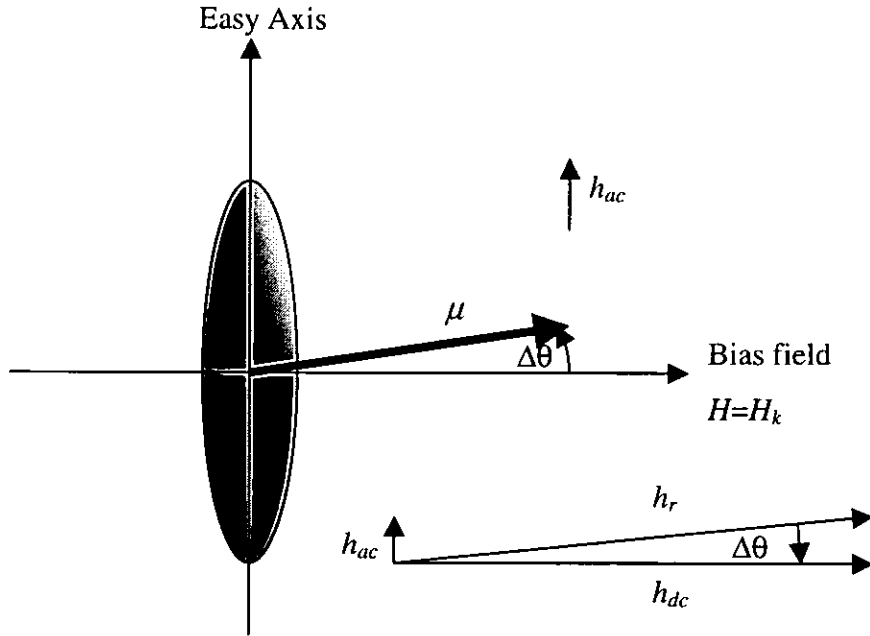


Figure 3-4 Orientation of particles giving dominant response

We may suppose that for a small perturbing field ($h_{ac} \rightarrow 0$) the displacement angle, $\Delta\theta$, will be proportional to h_{ac} , such that,

$$\Delta\theta \cong \frac{h_{ac}}{h_{dc}} . \tag{3.2}$$

The change in magnetic moment, $\Delta\mu$, measured in the easy axis direction is given by,

$$\Delta\mu = \mu \sin \Delta\theta \tag{3.3}$$

(see Figure 3-5).

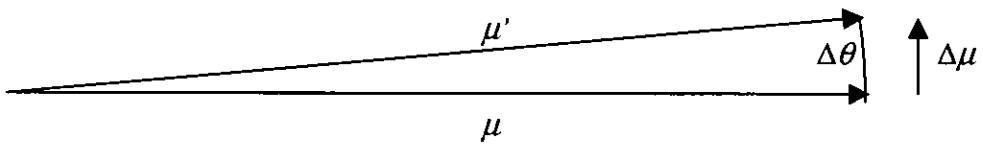


Figure 3-5 Susceptibility is measured by change in moment in the ac field direction

Using the small angle approximation, $\sin\theta \approx \theta$ as $\theta \rightarrow 0$ we have,

$$\Delta\mu = \mu \cdot \Delta\theta . \tag{3.4}$$

Substituting $\Delta\theta$ from equation (3.2),

$$\Delta\mu = k_1 \mu \cdot h_{ac} , \tag{3.5}$$

where k_1 is a constant. As the output signal of the balanced susceptometer sense coil is proportional to the change in magnetic moment, $\Delta\mu$, due to the action of the field on the sample, we can see that the output of the susceptometer is proportional to h_{ac} .

In order to test this predicted response the dc bias field was set to the anisotropy peak value of a control sample and the ac probe field was varied. The measured response of the susceptometer as a function of the probe field magnitude is shown in Figure 3-6.

The linear correlation between the χ_t response and the ac probe field was high and a least-squares linear fit gave a Pearson's correlation coefficient of $r > 0.998$.

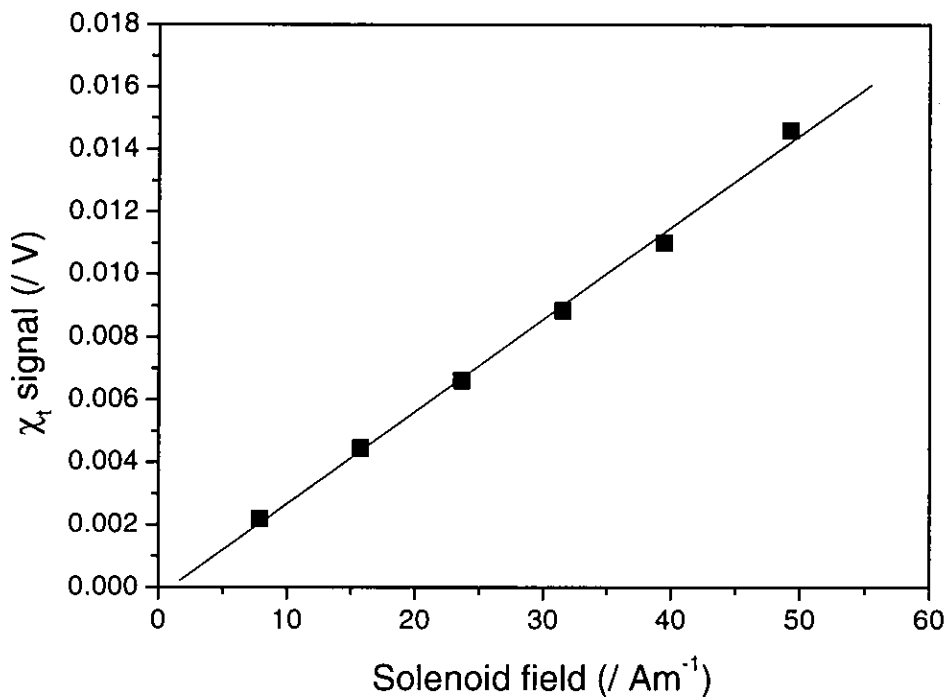


Figure 3-6 Response of χ_t signal to changing probe field

3.4 Investigation of tape and powder samples

A number of samples were investigated using the susceptometer. The improved signal-to-noise ratio of the new susceptometer design allowed characterisation using smaller samples. The samples were prepared by stacking or folding layers of tape together, so the use of smaller samples resulted in fewer layers that could be aligned more precisely. The result of this was that peak shift due to errors in sample alignment was reduced. Demagnetising field effects were neglected and in order to reduce their influence the tape samples were aligned so that the applied ac and dc fields were parallel to the plane

of the tape. As the thickness of the magnetic layer was very much smaller than the sample length it was assumed that the demagnetising field would be insignificant. The metal particle powder samples were packed into tubes to form cylindrical samples with a diameter of 2mm and a length of approximately 10mm. Because of the geometry of the sensing coils and restricted space within the ac solenoid these samples were mounted with the long axis parallel to the ac field hence the demagnetising field would tend to increase the applied field at which the anisotropy peak was observed. As no anisotropy peaks were observed in these samples no corrections were made to the results for demagnetising effects.

In order to test the correct operation of the susceptometer following the modifications detailed in chapter 2 a comparison was made with samples measured prior to the modification of the susceptometer.

Figure 3-7 and Figure 3-8 show comparisons of commercial videotape samples for the original and the modified susceptometer. The improvement in the new susceptometer configuration is not immediately apparent in Figure 3-7. However, close examination of the figure shows that the original susceptometer gave slightly broader peaks and the height of the peaks [$\chi_t(\text{max}) - \chi_t(H=0)$] was less. There was no measurable shift in the peak position. Figure 3-8 shows a comparison for a VHS tape which has a higher anisotropy peak value than the tape investigated in Figure 3-7. In this case the difference between the two measurement systems is more obvious. Again the plot measured using the original susceptometer had broader, 'lower', peaks. We can also see in this case that the peak maxima were at a lower field value when measurements were taken on the original system.

The differences between the plots from the original and modified systems shown in Figure 3-7 and Figure 3-8 are consistent with a greater misalignment between the layers of the sample in the original system. The plots show χ_t measurements for Co modified $\gamma\text{-Fe}_2\text{O}_3$ VHS tape and a VHS tape with a particle system containing a mixture of $\gamma\text{-Fe}_2\text{O}_3$ and CrO_2 particles. Although the same batches of tape were used for the original and modified susceptometer, the actual samples were different. The original susceptometer required samples of approximately 500cm^2 whereas the samples for the modified susceptometer were 20cm^2 . The effect of sample texture in χ_t measurements was investigated by Sollis *et al*[120] using samples made from stacks of aligned tape

which were deliberately misaligned to create pseudo planar-random samples. The investigation showed that the samples with a wider distribution of easy-axis angles (i.e. the pseudo random samples) had broader anisotropy peaks, lower field values for the peak maxima, and lower values of $[\chi_t(\max) - \chi_t(H=0)]$ than the closely aligned samples. From this relationship we can infer that the samples prepared for the original susceptometer were not as well aligned as the smaller samples prepared for the new susceptometer. The differences between the plots in Figure 3-7 are relatively small, with no discernable shift in the peak position, but suppression of the peak height and slight broadening is apparent in the plot from the original susceptometer. Figure 3-8 shows a much greater difference between the plots suggesting that the misalignment of layers in the sample for the original system must have been quite large.

Although the lowering of the measured H_k value for systems with broad texture distributions has been reported previously[75,120] the reason for this effect is not clear. The transverse susceptibility response has largely been considered as solely due to the singularities at $\pm H_k$ and $-H_c$, and as such the anisotropy peak in the positive descending-field branch of the curve should be independent of the switching response in the negative branch. In reality it seems that other non-singular reversible responses of particles not aligned with the ac field are sufficient to skew the H_k peak to a lower field. An example of such a reversible response is postulated in section 5.5 with respect to non-linear transverse susceptibility measurements and is sketched in Figure 5-24. As this response monotonically increases with decreasing field until the switching field is reached it would always result in the H_k peak being skewed towards a lower value. It seems likely, therefore, that the H_k value determined by transverse susceptibility will always be somewhat lower than the actual value except for the ideal case of a perfectly aligned system.

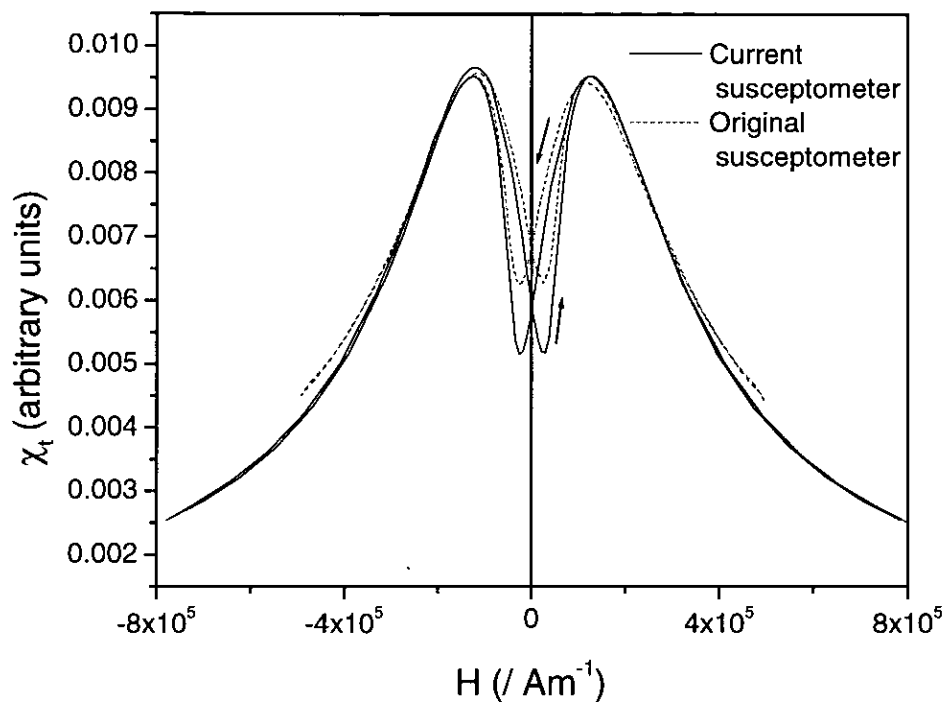


Figure 3-7 Co modified $\gamma\text{-Fe}_2\text{O}_3$ VHS video tape χ_t plot

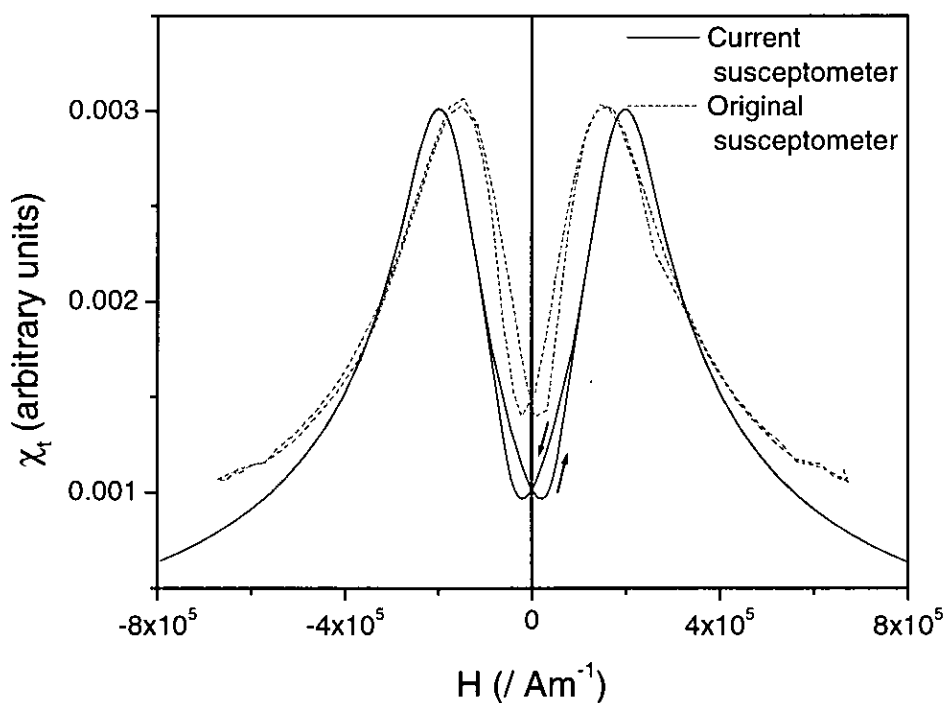


Figure 3-8 $\gamma\text{-Fe}_2\text{O}_3$ / CrO_2 mixed VHS video tape χ_t plot

Overall the plots for the original and modified susceptometer are consistent with one-another whilst the reduced sample size (by a factor of approximately 25) has resulted in a reduction in errors due to sample misalignment.

The characteristics of the two tapes were measured using a VSM and are detailed in Table 3-1.

| Tape system | H_c (/ kAm^{-1}) | SFD (/ kAm^{-1}) | Squareness | Orientation ratio |
|---|------------------------------|----------------------------|------------|-------------------|
| Co- γ -Fe ₂ O ₃ VHS | 52.8 | 25.5 | 0.76 | 1.84 |
| CrO ₂ / γ -Fe ₂ O ₃ VHS | 41.4 | 28.5 | 0.77 | 1.99 |
| CrO ₂ TK50 | 36.9 | 21.5 | 0.82 | 2.97 |

(VSM sweep rate = $3.1\text{kAm}^{-1}\text{s}^{-1}$, Maximum field 560kAm^{-1})

Table 3-1 Characteristics of commercial tape samples

Figure 3-9 shows the χ_t plot of a CrO₂ TK50 data tape, the hysteresis characteristics of which are also detailed in Table 3-1.

For systems of non-interacting Stoner-Wohlfarth particles with similar texture distributions, we would expect the ratio of H_c to H_k to be constant. For a random distribution of easy axes a theoretical value of 0.479 was obtained[2]. The values of the anisotropy peak maxima and the ratio of H_c to H_k are shown in Table 3-2.

| Tape system | H_k (/ kAm^{-1}) | H_c/H_k |
|---|------------------------------|-----------|
| Co- γ -Fe ₂ O ₃ VHS | 124.8 | 0.423 |
| CrO ₂ / γ -Fe ₂ O ₃ VHS | 199.5 | 0.208 |
| CrO ₂ TK50 | 182.9 | 0.201 |

Table 3-2 Commercial tape - ratio of anisotropy peak values to coercivity

Although the orientation ratios and squareness parameters are different for the three systems indicating different particle alignment textures, the large difference in the ratio of H_c to H_k between the systems containing CrO₂ and the system containing only Co- γ -Fe₂O₃ particles suggests that these two groups of systems switch in different ways. The ratio for the Co- γ -Fe₂O₃ is similar to the theoretical value from the Stoner-Wohlfarth model suggesting that these particles may be switching coherently. The ratios for the other systems are much lower and suggest that the particles in these systems may be switching in incoherent modes. As there is a degree of flux closure during incoherent reversal the oscillating moment detected by the transverse susceptometer would reduce

tending to suppress the switching peak. Particles with easy axes at large angles to the dc field would always switch by coherent reversal, at relatively high switching fields, which would account for the observed increase in switching-peak field compared to the coercivity in some systems. These conclusions are not definitive as it is not possible to isolate the effects of switching mode from those due to texture without modelling the specific texture distribution. Interactions are also known to affect coercivity and have not been considered in the current theoretical models of χ_t .

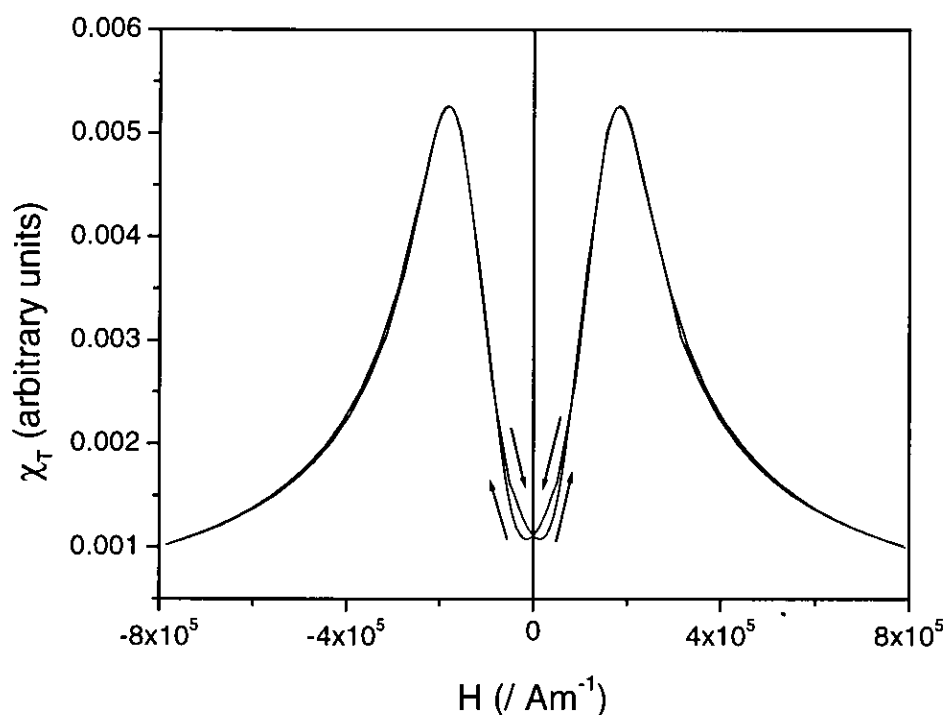


Figure 3-9 CrO₂ TK50 data tape χ_t plot

As the anisotropy peak measured is a function of the crystalline and the shape anisotropy of the particles we would not necessarily expect any correlation in the anisotropy peak values between the systems using common particle materials. The larger χ_t peak from the CrO₂ samples may be expected as the anisotropy peaks in CrO₂ measurements are typically more pronounced and less likely to be suppressed by texture effects than those of γ -Fe₂O₃[120] and the orientation ratio shows that these samples are also more highly aligned than the Co- γ -Fe₂O₃ sample.

3.4.1 Metal particle tapes

Four development MP tapes manufactured to the Linear Tape Open (LTO) format were obtained from a tape manufacturer. The tapes were manufactured each using an identical dispersion of MP3 type metal particles with the difference between the four samples being the thickness of the magnetic layer coating. The tapes were manufactured using a dual coating technique [125,126] and were referred to by the $M_r t$ values ascribed to them by the manufacturer as an indication of the magnetic layer thickness. The characteristics of the tapes were measured using a VSM and are detailed in Table 3-3.

| Sample reference | M_d (/ mA) | $M_r t$ (/ mA) | H_c (/ kAm ⁻¹) | Squareness | Orientation Ratio | |
|------------------|-----------------|-------------------|---------------------------------|------------|-------------------|--------------|
| | | | | | In-plane | Out-of-plane |
| $M_r t3$ | 40.5 | 35.3 | 154.7 | 0.87 | 2.2 | 3.2 |
| $M_r t4$ | 47.9 | 40.3 | 152.0 | 0.84 | 2.0 | 3.5 |
| $M_r t4.5$ | 54.9 | 46.0 | 151.3 | 0.84 | 2.0 | 3.3 |
| $M_r t6$ | 74.1 | 62.4 | 151.1 | 0.84 | 2.0 | 3.1 |

(VSM sweep rate = 3.1kAm⁻¹s⁻¹, Maximum field 560kAm⁻¹)

Table 3-3 Characteristics of development MP tape samples

χ_t measurements of the four development MP tapes are shown in Figure 3-10. The zero values of the χ_t axes have been offset from one-another to allow their shapes to be compared. The plots all displayed large anisotropy peaks and hysteresis effects at low field values. No coercivity peaks were apparent and the shapes of the plots were similar to those of previous particulate recording media, except that the hysteresis effects and anisotropy peaks were at comparatively higher dc field values.

The measured anisotropy peak values and H_c/H_k ratios are shown in Table 3-4.

| Nominal $M_r t$ value | Anisotropy peak value (/kAm ⁻¹) | H_c / H_k |
|-----------------------|--|-------------|
| 3 | 425 | 0.364 |
| 4 | 416 | 0.365 |
| 4.5 | 417 | 0.362 |
| 6 | 417 | 0.362 |

Table 3-4 Anisotropy peak value as a function of nominal $M_r t$ value

The measured peak values were similar to one another except for those of the $M_r t=3$ sample. As the magnetic layers of the tapes were made from the same dispersion we would expect the anisotropy field distributions and hence the anisotropy peak values to be the same. In the case of the $M_r t=3$ sample it may be that as the magnetic layer thickness was of the same order as the magnetic particle size, the texture was modified during the coating and calendering processes, causing changes in the anisotropy peak value.

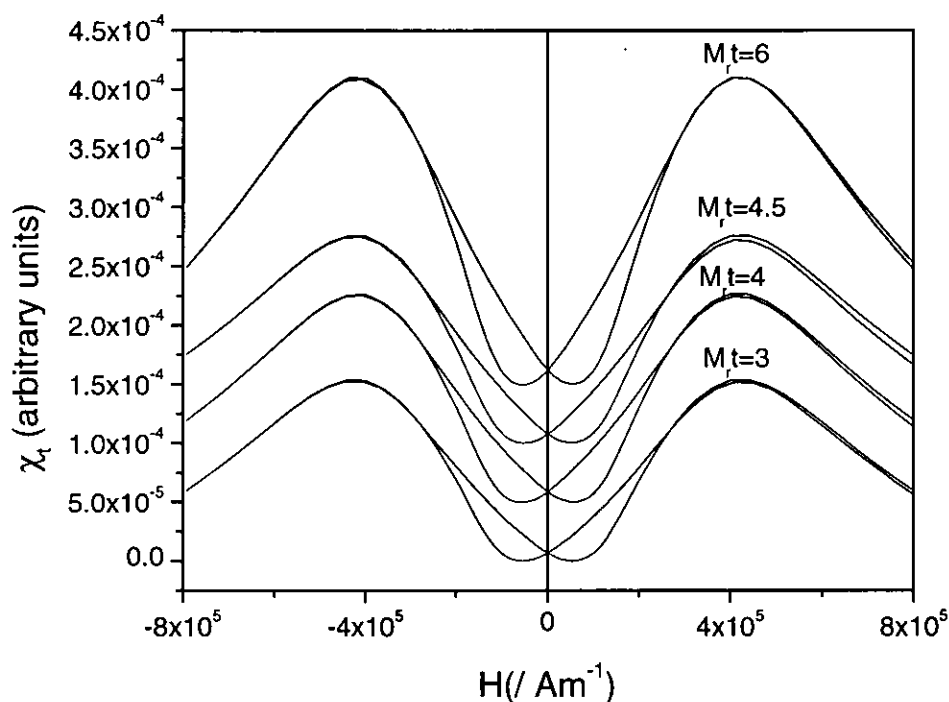


Figure 3-10 MP tape χ_t plots. Zero's offset to separate traces

Measurements of the orientation ratio, OR (see section 1.8.2), of the samples showed that the orientation of the $M_r t=3$ sample was higher than that of the other development samples (See Table 3-3), which is consistent with the observed increased anisotropy peak value for χ_t measurements due to a narrowing of the texture distribution (see Jones *et al*[75] and Sollis *et al*[120]).

The H_c / H_k ratio for the samples varied by less than 1% which we would expect for samples manufactured using the same dispersion and alignment process. The relative heights of the peaks ($\chi_t(\max) - \chi_t(H=0)$) increased as the nominal $M_r t$ value increased

which we would also expect as M_t is a measure of the moment of the sample which creates the changing flux detected by the sense coils.

The plots were normalised to compare their shapes. Figure 3-11 is a superposition of the normalised plots which shows their shapes to be virtually identical.

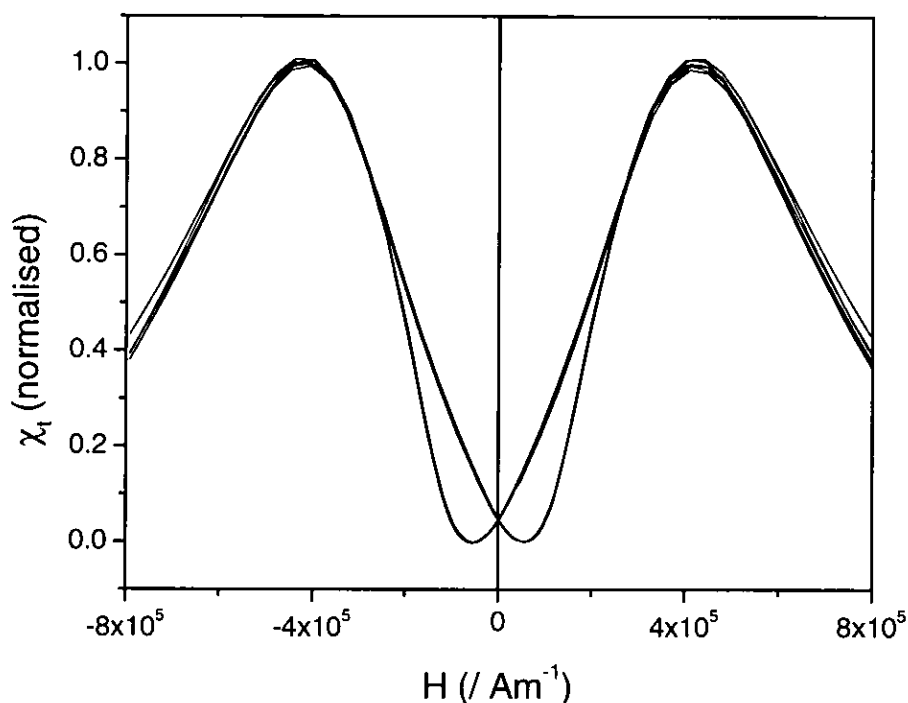


Figure 3-11 Normalised χ_t plots for MP tapes superimposed to show similarity of shape

3.5 Powders

The transverse susceptibility of bulk powders is primarily of interest in that it allows anisotropy information to be obtained from the powder. Deconvolution of the anisotropy peak can be used to obtain an anisotropy field distribution for the sample [121,122,123]. Comparison of the peaks in the powder sample with those for aligned systems of the same particles can also show the effect of texture on the χ_t measurement of a system. Due to the differences in packing fraction and clustering of particles in powder samples compared to tape dispersions it is also likely that the inter-particle interactions of the powder samples will be different from those of a tape system.

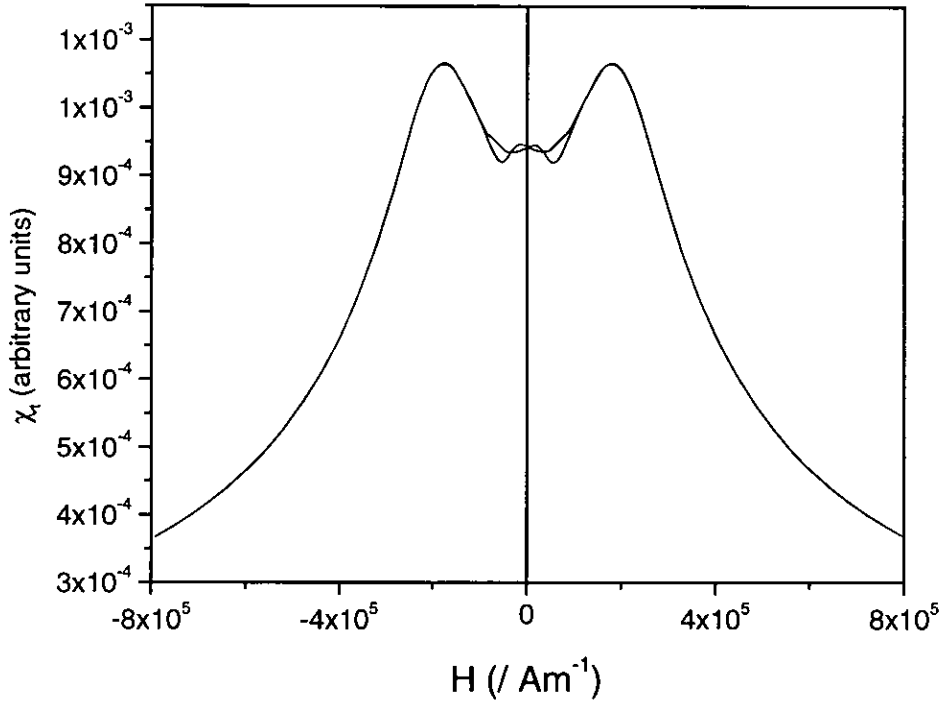


Figure 3-12 Randomly oriented CrO₂ powder χ_t plot

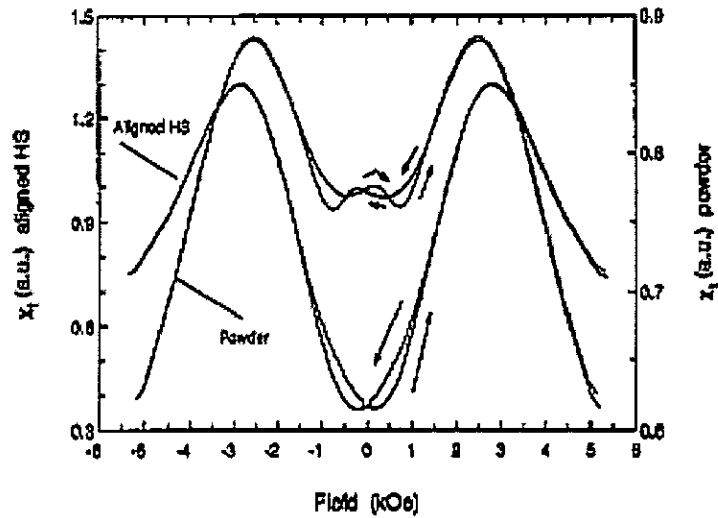


Figure 3-13 Randomly oriented CrO₂ powder and aligned hand-spread after Sollis *et al*[120]

The χ_t plot of CrO₂ powder is shown in Figure 3-12 and may be compared with the previous measurement of Sollis *et al*[120] shown in Figure 3-13. The χ_t plot of γ -Fe₂O₃ powder is shown in Figure 3-14 with the previous measurement after Sollis *et al* shown in Figure 3-15.

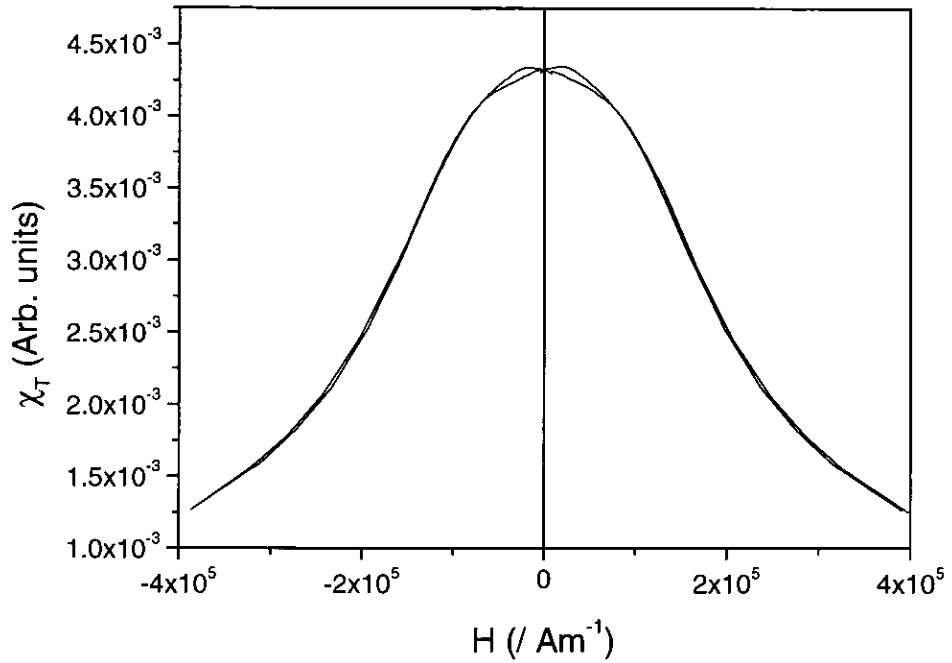


Figure 3-14 Randomly oriented $\gamma\text{-Fe}_2\text{O}_3$ powder χ_r plot

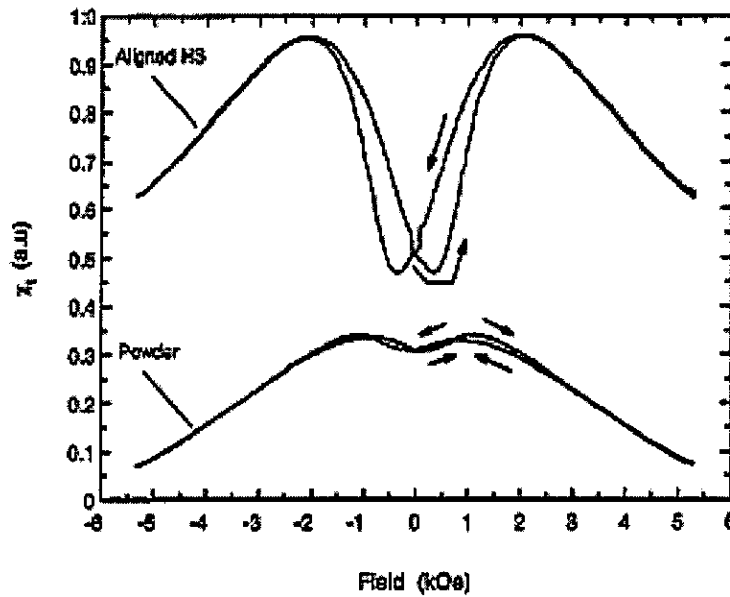


Figure 3-15 Randomly oriented Co- $\gamma\text{-Fe}_2\text{O}_3$ powder and aligned hand-spread after Sollis *et al*[120]

The CrO_2 sample showed reduced anisotropy peaks compared with the aligned CrO_2 tape system and also the form of the irreversible curve at low field values was changed with a small peak visible in the low reversed field of each sweep direction. In the $\gamma\text{-Fe}_2\text{O}_3$ plot the anisotropy peaks were completely suppressed and only the small irreversible effects remained at the low field values. Both of these results were

consistent with those previously recorded for CrO₂ and γ -Fe₂O₃ powders by Sollis *et al*[120].

Modern particulate recording media use metal particles, due to the relatively high magnetic moment and coercivity allowing smaller particles to be used to give higher recording densities. Handling of metal particles in powder form can be problematic as the powder readily oxidises when exposed to air and can even spontaneously combust, necessitating specialist equipment to handle and package the powder in an inert atmosphere. The four samples of MP powder investigated were kindly supplied by Professor K. O'Grady and prepared by J.J. Blackwell of the University of York Magnetism Group. The samples were packed to form cylinders of 2mm diameter by ~10mm long. The major hysteresis loops of the samples were measured parallel to the long axes of the samples using a VSM and the characteristics are detailed in Table 3-5.

| Sample no. | Mass (/mg) | μ_s (/nWb.m) | H_c (/kA.m ⁻¹) | Sq. | SFD (/kA.m ⁻¹) |
|------------|------------|------------------|------------------------------|------|----------------------------|
| 1 | 31 | 5.91 | 109 | 0.48 | 111 |
| 2 | 40 | 4.18 | 130 | 0.52 | 171 |
| 3 | 38 | 4.85 | 171 | 0.53 | 157 |
| 4 | 50 | 8.16 | 183 | 0.54 | 151 |

(VSM sweep rate = 3.1kAm⁻¹s⁻¹, Maximum field 560kAm⁻¹)

Table 3-5 Characteristics of MP powder samples

The demagnetising factors of the samples were neglected in the determination of the parameters detailed in Table 3-5. The squareness parameter measured for samples 2-4 is somewhat larger than the 0.5 value predicted by theory[2]. This is probably due to either inadvertent texturing of the powder during packing, tending to align the particles along the long axis of the tube, or more likely that the samples were not fully saturated in the maximum applied field of the VSM.

Transverse susceptibility measurements of the four samples are shown in Figure 3-16 to Figure 3-19. The plots of the four samples differed in the extent to which the low field non-reversible coercivity effects were apparent. In samples 1, 3 and 4 the non-reversible effects were quite pronounced whilst in sample 2 they were only just discernable. In all of the samples the peaks associated with the anisotropy information were suppressed, although there is a suggestion of a peak in the 'shoulder' of the χ_i plots for samples 3 and 4. We would expect the anisotropy field of such particles to vary as a function of

the particle volume, aspect ratio, crystalline anisotropy of the particle alloy and the crystal alignment with respect to the particle shape. These parameters were not known for the particles investigated.

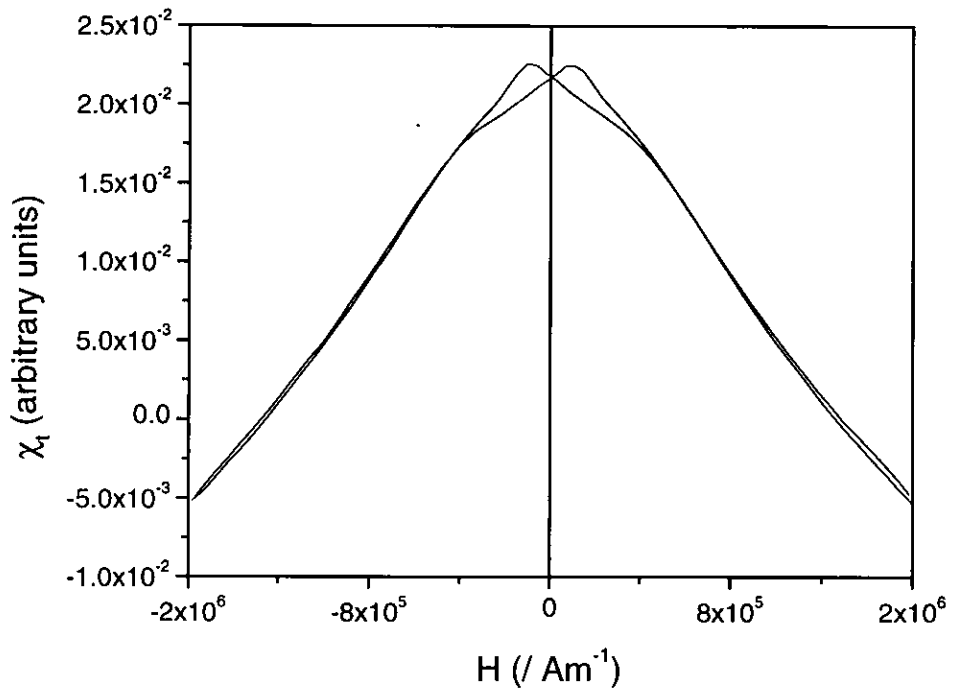


Figure 3-16 MP powder sample 1 χ_i plot

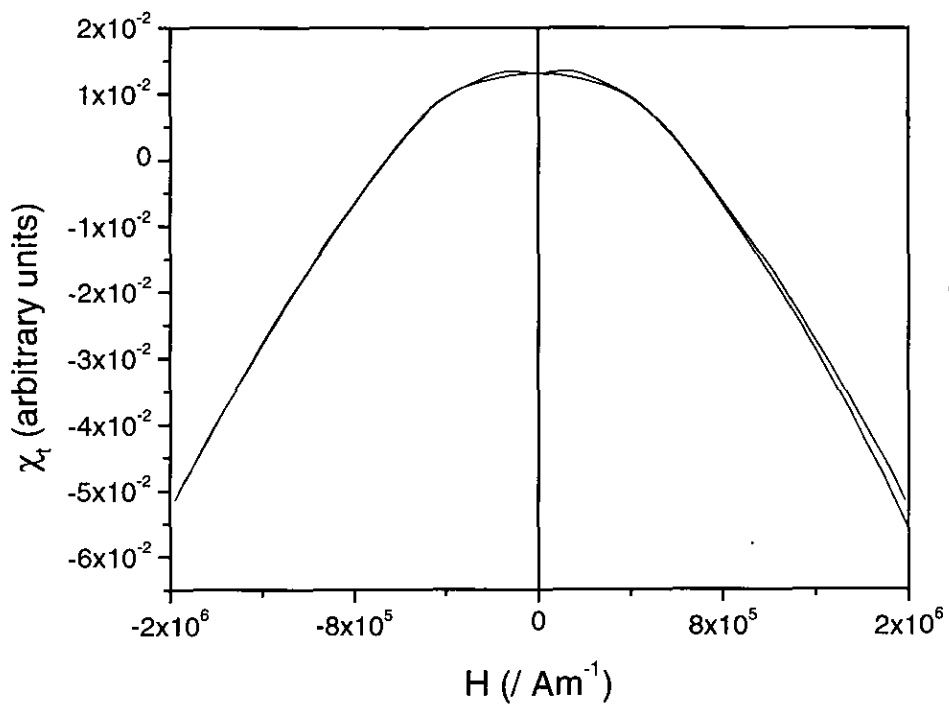


Figure 3-17 MP powder sample 2 χ_t plot

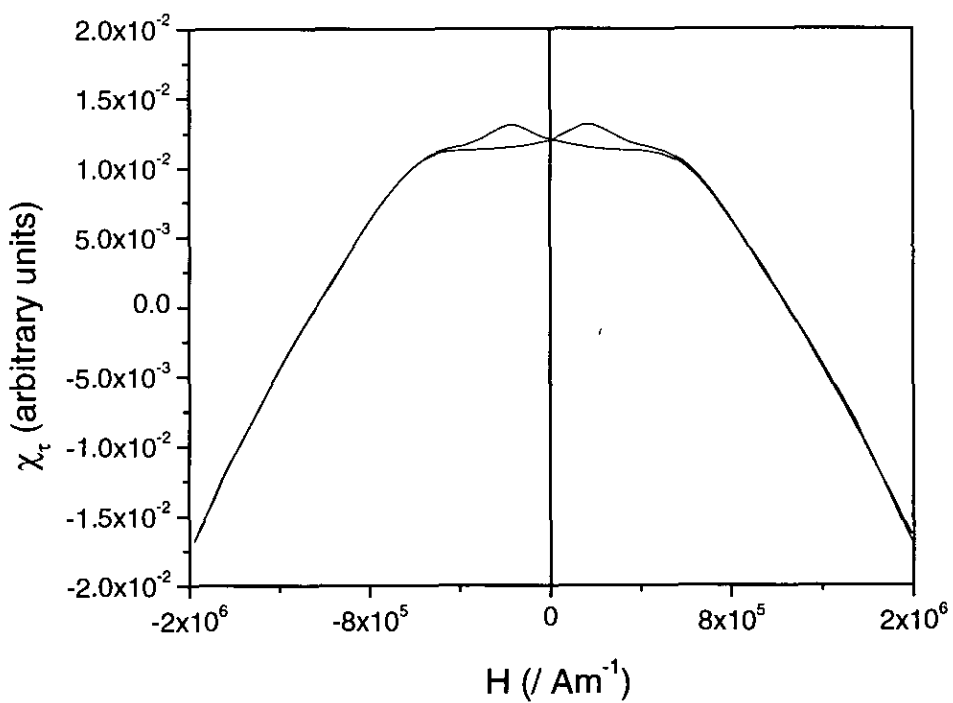


Figure 3-18 MP powder sample 3 χ_t plot

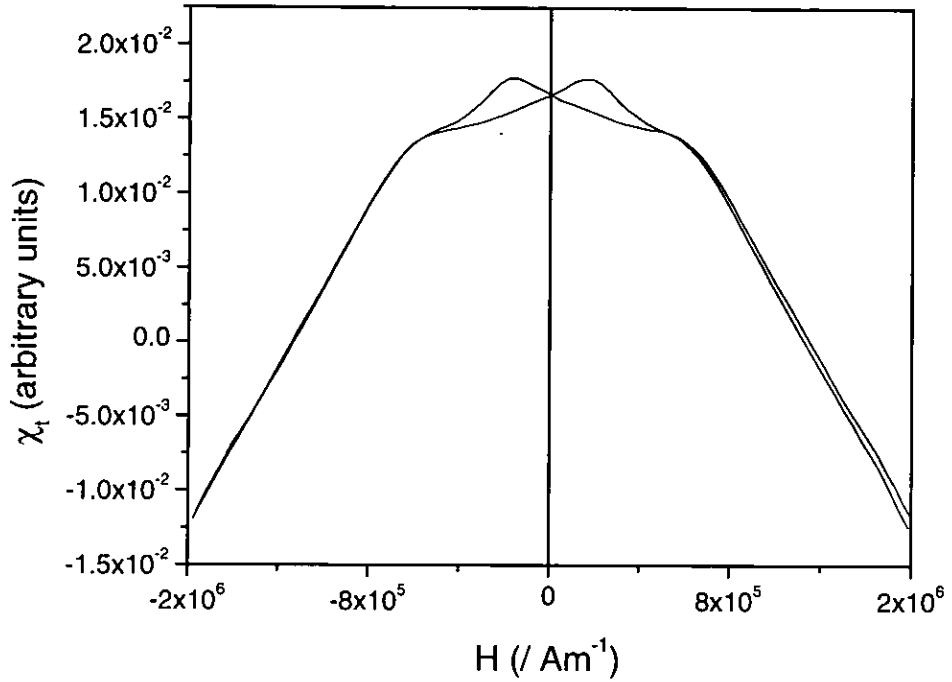


Figure 3-19 MP powder sample 4 χ_t plot

Comparing the MP powder results to those of CrO_2 and $\gamma\text{-Fe}_2\text{O}_3$ powders the shapes of the curves bear a greater similarity to those of $\gamma\text{-Fe}_2\text{O}_3$ due to the absence of any anisotropy peak. The curves of samples 1, 3 and 4 are very similar in form to the theoretical curve of Hoare *et al*[113] shown in Figure 3-20 for a system of Stoner-Wohlfarth particles with a random easy axis distribution and log-normal distribution of anisotropy field values.

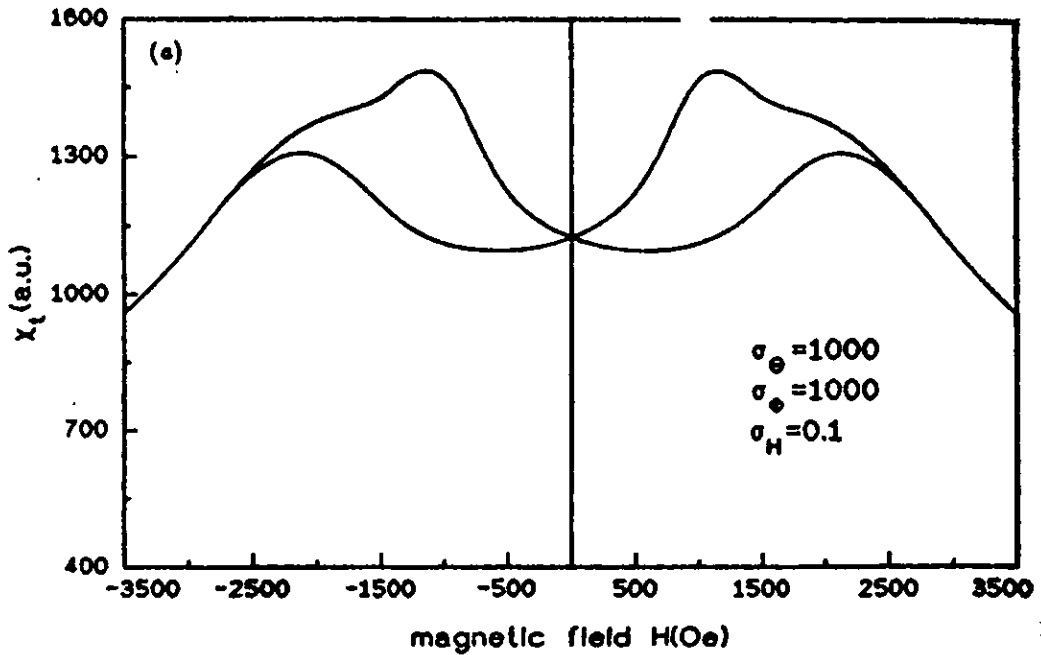


Figure 3-20 Theoretical curve for random easy axis distribution with coherent switching, $H_k=2100$ Oe, $\sigma_H=0.1$ Oe. After Hoare *et al*[113]

The enhanced anisotropy peaks of the CrO_2 powder result are not predicted by the simple Stoner-Wohlfarth treatment of uniaxial particles, however, the form of the plot does resemble the theoretical prediction for a system of particles with random easy axis directions reversing by incoherent rotation after Berkov and Chantrell[127] shown in Figure 3-21. The model of Berkov and Chantrell did not include an anisotropy field distribution and was for incoherent rotation by 'fanning' using a chain of four spheres. This is not a likely method of reversal for CrO_2 particles due to the regular shape and uniformity of the crystals. However, the results of the model show how the large coercivity peaks are suppressed by particles rotating in an incoherent mode, allowing the anisotropy peaks to manifest in the randomly textured system.

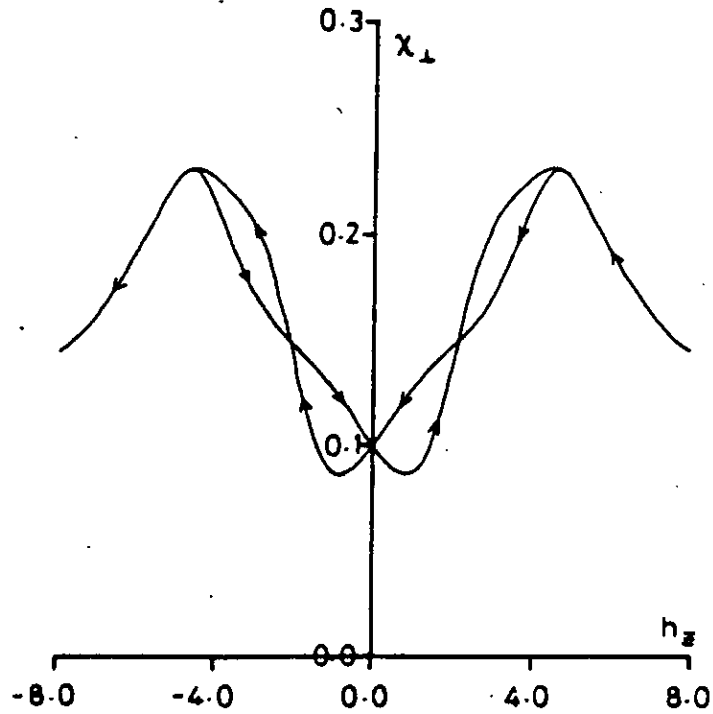


Figure 3-21 Theoretical curve for random easy axes switching by incoherent fanning after Berkov and Chantrell[127]

3.6 Variation in response with sample alignment

Comparison of the shapes of the transverse susceptibility plots of randomly oriented powders with those of aligned tapes containing similar particles showed that there was a significant effect due to the texture of the samples. Considering that we would expect the response due to a randomly orientated sample to be similar to the superposition of the response for all individual angles (assuming that interactions may be neglected) we used an aligned sample to investigate the changing response as a function of the angle, β (see Figure 3-22), between the sample easy axis and the ac field direction.

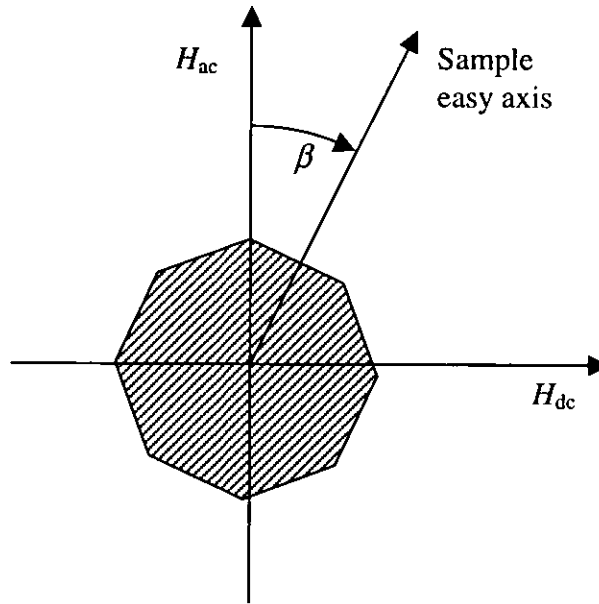


Figure 3-22 Alignment angle, β , of sample easy axis with respect to ac field direction

Figure 3-23 shows the χ_t as a function of β for an aligned hand spread of $\gamma\text{-Fe}_2\text{O}_3$ particles prepared by T. Mercer during work on particle dispersions at Preston[128]. The plot allows direct comparison with Figure 3-14 which is a χ_t plot of the random powder sample made up from the same particle base. Figure 3-24 shows the χ_t plot as a function of β for commercial CrO_2 TK50 tape. Although comparison can be made with the random CrO_2 powder plot (Figure 3-12) the particles were not from the same source. For both CrO_2 and $\gamma\text{-Fe}_2\text{O}_3$ plots the anisotropy peaks became smaller and the low-field response increased as β increased. Also the field value of the anisotropy peak reduced as β increased. Both of these effects are consistent with previous studies of the effects of texture on χ_t , which show a broadening and lowering of the anisotropy peak which eventually merges with the low field coercivity effects as the texture distribution widens. Also we can see how the sum of the curves over all angles could lead to the random powder response shown in section 3.5. Figure 3-24 shows how the anisotropy peaks are highly enhanced in CrO_2 when the easy axis is aligned with the ac field, and are well separated from the non-reversible switching effects. These are at a much lower field and are most pronounced where the easy axis is perpendicular to the ac field direction. These effects may contribute to the anisotropy peaks still being visible in the random sample of CrO_2 when compared with $\gamma\text{Fe}_2\text{O}_3$, where the peak heights are relatively constant as β is changed (see Figure 3-23).

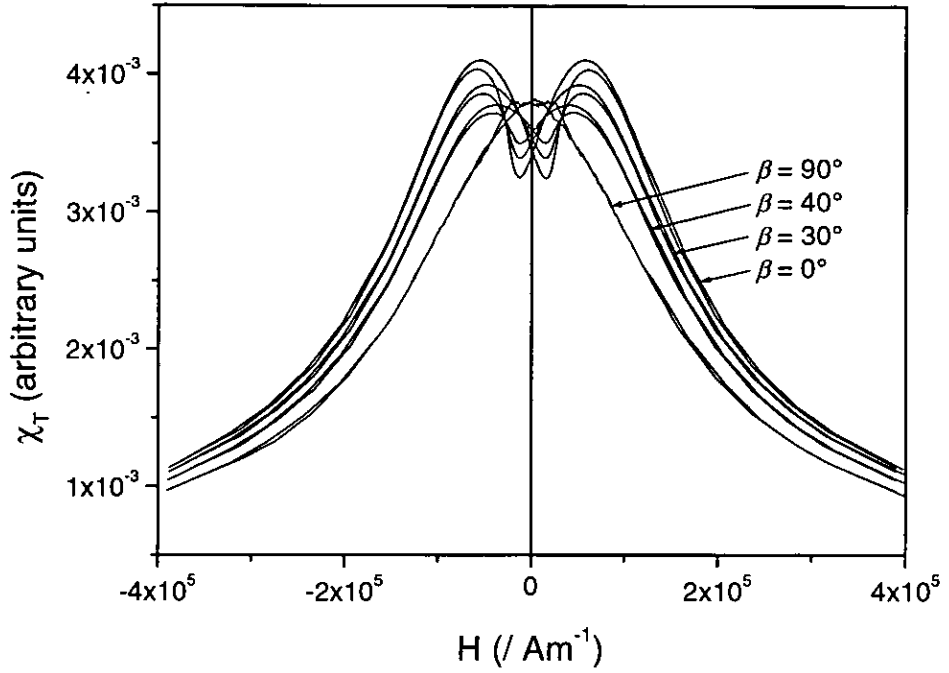


Figure 3-23 Aligned $\gamma\text{-Fe}_2\text{O}_3$ hand spread, χ_t as a function of angle between sample alignment and ac field direction (β)

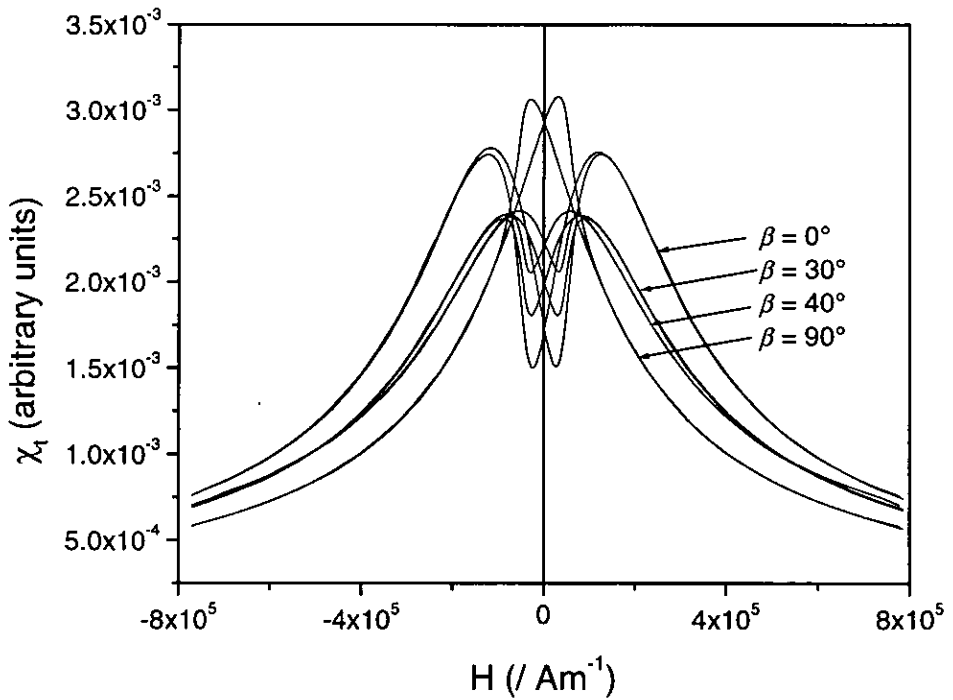


Figure 3-24 CrO_2 TK50 tape, χ_t as a function of angle between sample alignment and ac field direction (β)

3.7 Imaginary components

The paper of Papusoi[5] proposed an imaginary component of the χ_i response (i.e. a component of the ac susceptibility signal 90° out-of-phase with the ac probe field). A statistical approach is used to calculate the occupation probabilities of the two energy minima for the magnetisation direction. Thermal energy and the height of the energy barrier between the minima as a function of dc field and direction are used to calculate the relaxation time for the moment to thermally switch across the energy barrier. The author finds that for particles normally associated with the χ_i peak (i.e. those with $\alpha=90^\circ$ [see section 1.5.1]) the relaxation time is of the same order as the period of oscillation of the ac field when the dc field is just below the anisotropy field value. The implication of this is that some of the moments will start to switch across the energy barrier at a field value just below the anisotropy field. Because the energy minima are symmetrical for the case where $\alpha=90^\circ$ the thermal switching is reversible. The switching will lag the excitation field due to the thermal relaxation time, in overcoming the energy barrier, and will therefore have a real and an imaginary component with respect to the probe field phase.

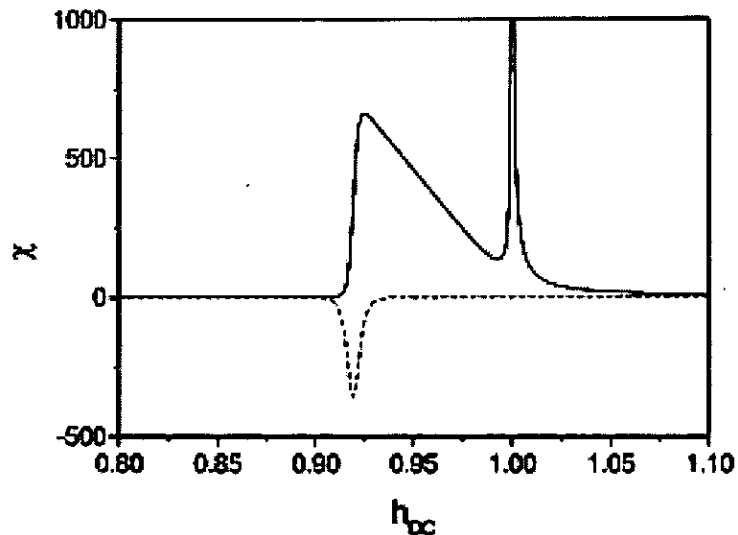


Figure 3-25 Real (solid line) and imaginary (dashed line) components of χ_i as a function of reduced field for a particle where $\alpha=90^\circ$ - after Papusoi[5]

Figure 3-25 shows the modelled real and imaginary χ_t response for a particle with easy axis parallel to the ac field. The other parameters used to model this particle were; anisotropy constant, $K = 200 \text{ kJ/m}^3$; particle diameter, $D = 45 \text{ nm}$, where volume, $V = \pi D^3 / 6$; $T = 300 \text{ K}$, $f = 10^3 \text{ Hz}$.

The plot shows a small peak in the imaginary component at approximately 92% of H_k , and also a peak in the real component of the signal at a value just below the singularity at H_k .

Papusoi went on to show that the peak in the imaginary component was more sensitive to particle alignment than that in the real component, and that the centroid of the imaginary peak is fixed where that of the real component shifts as a function of α (see Figure 3-26 and Figure 3-27).

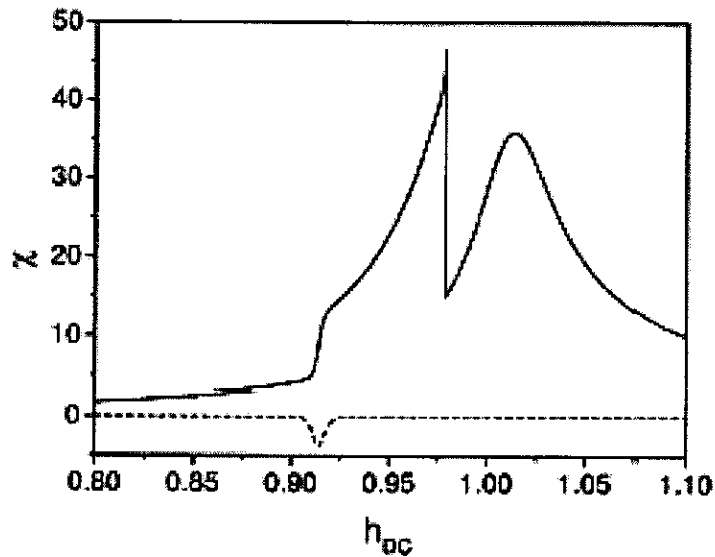


Figure 3-26 Real (solid line) and imaginary (dashed line) components of χ_t for $\alpha=89.9^\circ$ - after Papusoi

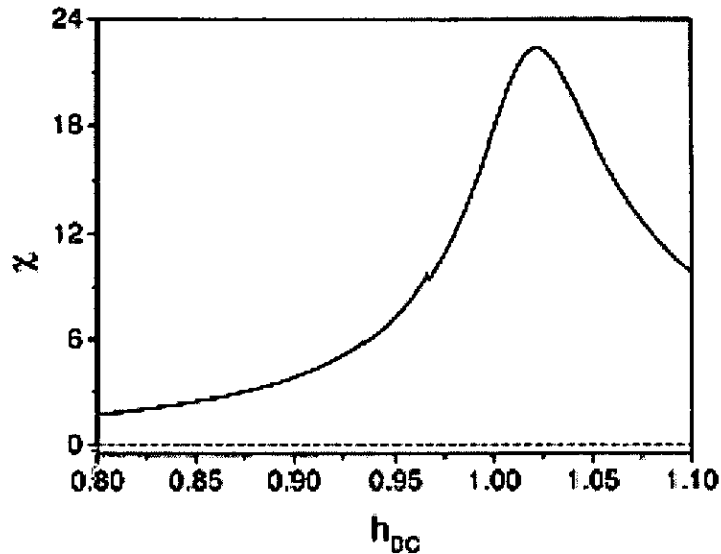


Figure 3-27 Real (solid line) and imaginary (dashed line) components of χ_i for $\alpha=89.8^\circ$ - after Papusoi

The paper of Papusoi went on to consider a system of such particles with distributions of anisotropy field value and particle volume. Inter-particle interactions were neglected and the model predicted that the anisotropy peak of the real component of χ_i , $\Re(\chi_i)$, would be shifted to a slightly lower value than that predicted by previous theory and that this shift would vary as a function of particle volume, particle anisotropy and ac probe field frequency. A peak in the imaginary component of the signal, $\Im(\chi_i)$, below the anisotropy field value was also predicted. The peak amplitude of the imaginary component was predicted to be approximately 1/10 that of the real component.

In order to test the hypotheses of the Papusoi paper, a number of measurements were made of $\Im(\chi_i)$. The imaginary component was initially measured by shifting the lock-in amplifier phase 90° from the ac field phase. Following the replacement of the original analogue lock-in amplifier, the use of a digital-signal-processing lock-in amplifier allowed the imaginary component to be measured directly, without changing the phase setting of the instrument.

Figure 3-28 is a comparison of the real and imaginary signal for a typical sample showing how the imaginary signal is much smaller than the real signal as predicted by theory. In measuring the imaginary component the susceptometer was at the limit of its

accuracy. Relatively long integration times were used at each field value resulting in some instrumentation drift over the time taken for the full measurement.

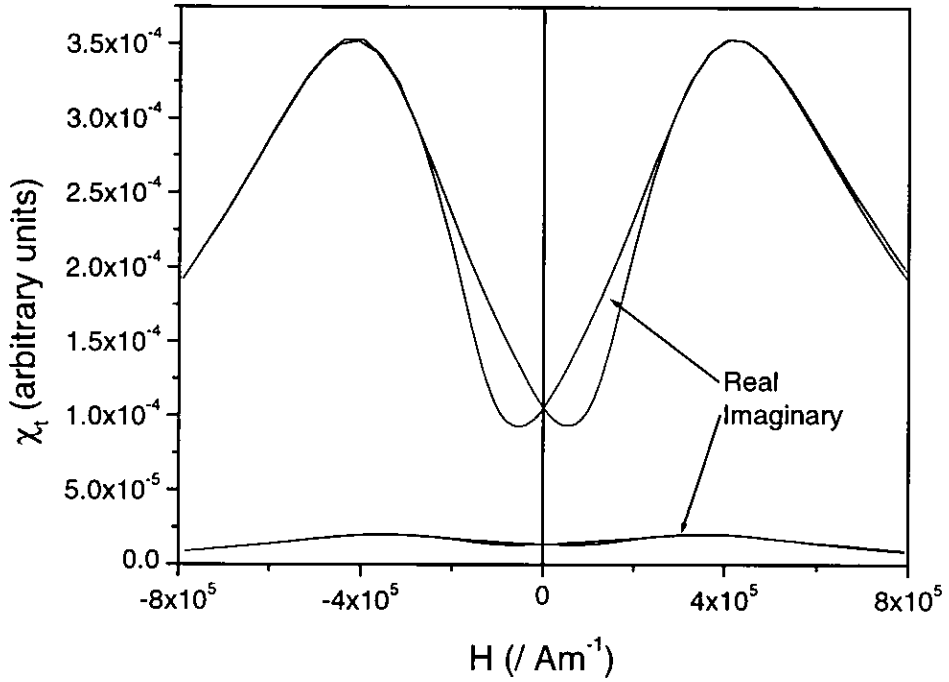


Figure 3-28 Comparison of real and imaginary signal for a typical ($M,t = 6$) MP tape

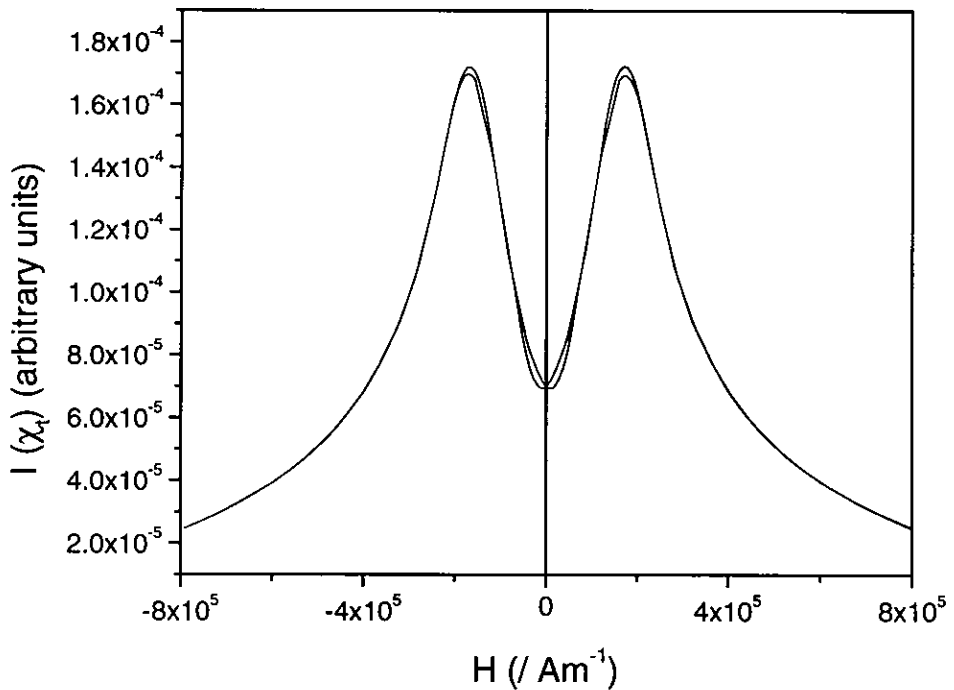


Figure 3-29 Imaginary transverse susceptibility plot for CrO_2 TK50 tape

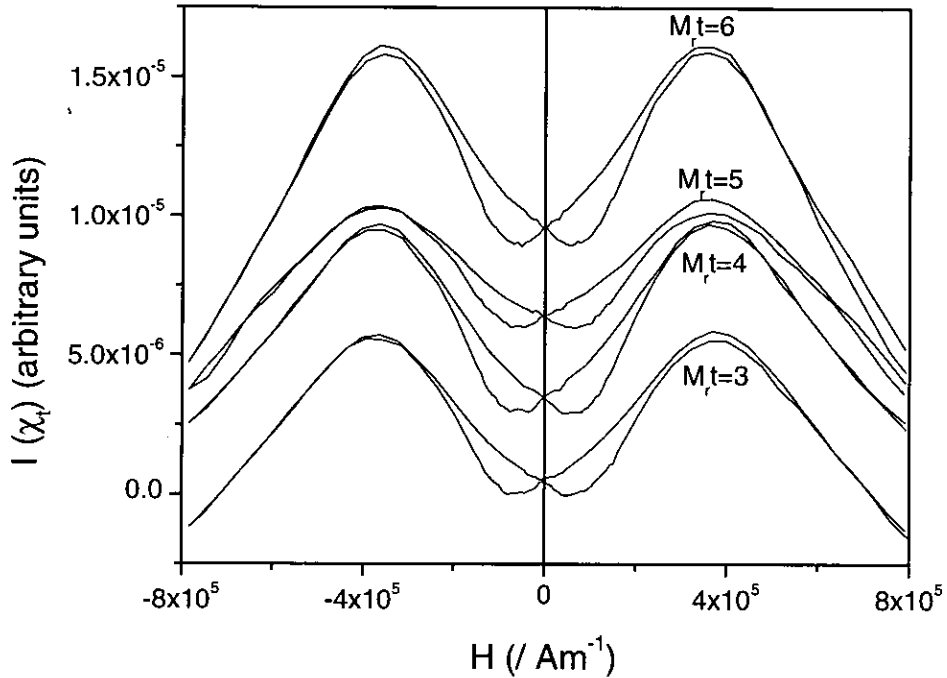


Figure 3-30 Development MP tape imaginary [χ_i] plots. Zero's offset to separate traces

Figure 3-29 shows the imaginary transverse susceptibility plot for a sample of commercial CrO₂ TK50 data tape, and Figure 3-30 shows the imaginary transverse susceptibility for the four development MP tape samples detailed earlier in section 3.4.1. Comparing the plots with those for the real component of the signal shown in Figure 3-9 and Figure 3-10 the size of the signal is considerably smaller and the slope of the peaks is steeper at high field values. The comparison between the peak shapes can be made more easily by scaling the imaginary plot to give the same $[\chi_i(\text{peak}) - \chi_i(H=0)]$ value as the real plot. Figure 3-31 shows such a scaled imaginary plot compared to the real plot for a typical sample of development tape ($M_t=6$). It can be seen that the anisotropy peak is at a slightly lower field in the imaginary plot and that the slope of the plot is much steeper in the higher field regions.

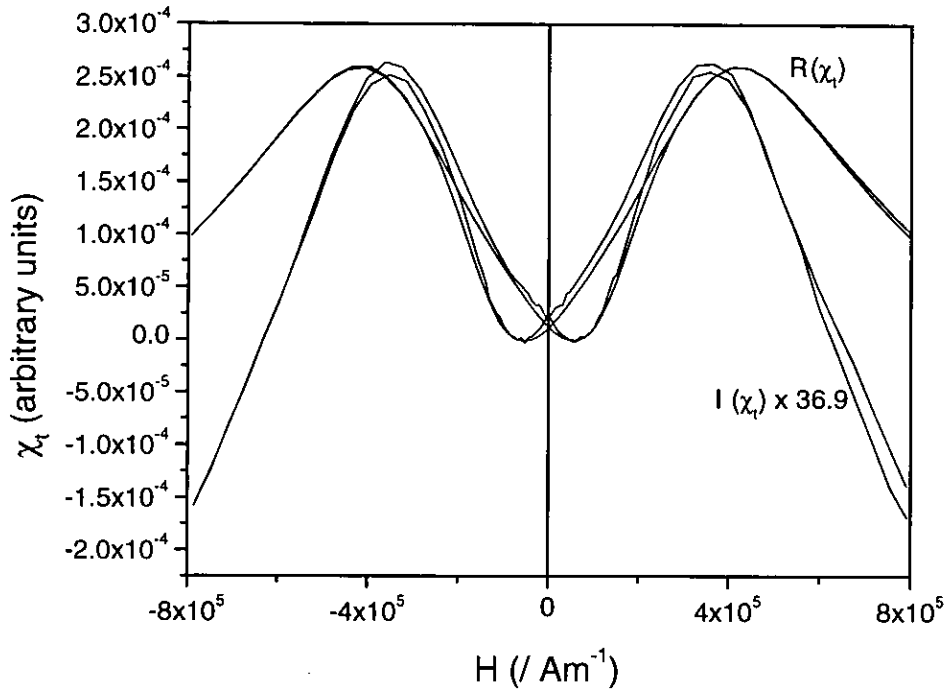


Figure 3-31 Shape difference of real and scaled-imaginary component of signal for a typical sample ($M_r t=6$)

The results are consistent with the theoretical predictions with the imaginary signal amplitude being approximately $1/10^{\text{th}}$ that of the real component. The anisotropy peak in the imaginary signal also occurs at a lower field value (approximately 85% of the real signal peak value).

The difference in the peak values is related to the distribution of anisotropies and the distribution of particle volumes within the sample and it is possible that with further theoretical development the comparison of the two components could yield information about these distributions. The consistency of the results with the predictions of the theory also lend credence to the hypothesis that part of the real χ_t signal is due to switching behaviour at fields just below the anisotropy field which could account for some of the differences between current theory and experimental measurements.

3.8 Discussion

A number of investigations have been carried out using the susceptometer described in Chapter 2. The output of the susceptometer as a function of the perturbing ac field was linear in accordance with the theoretical prediction for an infinitesimally small probe

field. The choice of probe field is a compromise between an infinitesimally small field which probes the shape of the centre of the energy minimum only, in accordance with theory, and a larger field that oscillates the moments by a sufficient amplitude to allow ease of detection. The theoretical assumption of a vanishingly small field probing only the base of the energy-well results in the linear relationship between the probe field and detected susceptibility. A larger field probing higher up the walls of the energy well would not be linear with respect to the susceptometer output and hence we can take the linearity of the response as an indication that the ac field is of an acceptable magnitude. The investigation of tape and powder samples showed the results to be consistent with those produced using earlier equipment, however, smaller samples of tape were used in the new system and this resulted in a narrower and higher anisotropy peak. Also in one case the anisotropy field was found to be higher than that determined using a previous system with a large sample size. These results are consistent with the proposition that the preparation of samples by either folding, or stacking layers of tape inevitably results in some misalignment of the layers, which effectively broadens the texture distribution of the sample. The reduction in the number of sample layers has led to an increase in the accuracy of H_k determinations, although it is inevitable that some misalignment of sample layers persists and the ideal measurement would be achieved by further improving the sensitivity of the susceptometer such that a reliable investigation could be made on a single magnetic layer.

Three samples of commercial magnetic tape were investigated comprising of a Co- γ -Fe₂O₃ VHS tape, a mixed CrO₂ / γ -Fe₂O₃ VHS tape and a pure CrO₂ TK50 data tape. Although the exact proportions of γ -Fe₂O₃ to CrO₂ particles in the mixed tape were not known it was believed from earlier work that the proportion of CrO₂ particles in the tape was relatively small[129]. This was supported by determination of the orientation ratio and squareness of the mixed tape. These were not significantly higher than those of the γ -Fe₂O₃ sample, which we would have expected them to be for a high CrO₂ system[9]. Comparison of the anisotropy peak fields showed greater similarity between the mixed CrO₂ / γ -Fe₂O₃ and the pure CrO₂ sample, but as the anisotropy is a function of the particle shape, size and composition, it does not necessarily follow that the samples with similar anisotropy fields would have the same particle composition. The H_c/H_k ratio for the CrO₂ and the mixed CrO₂ / γ -Fe₂O₃ system suggests that the particles in these

systems are switching by the same reversal mechanism, which is different to that of the Co- γ -Fe₂O₃. The suppression of H_c in these samples suggests that they are reversing incoherently as H_c is less than 50% of the value predicted for a random distribution of easy axes by Stoner and Wohlfarth, whereas the Co- γ -Fe₂O₃ coercivity is greater than 88% of the theoretical value. The H_c/H_k values of the MP tapes were all 75% of the theoretical which although lower than the Co- γ -Fe₂O₃ system was still much higher than the ratio for the mixed γ -Fe₂O₃/CrO₂ and CrO₂ system. Comparison with the value obtained by Stoner and Wohlfarth can only serve as a guide as the Stoner-Wohlfarth value is for a randomly oriented system. However, the larger deviations from the value suggest that in these samples the particles are not rotating coherently as assumed by the model. Also, as the Co- γ -Fe₂O₃ and the mixed γ -Fe₂O₃/CrO₂ samples are similar in texture the differences in H_c/H_k indicates a difference in the switching mode between these samples. If the majority particles in both of these samples are γ -Fe₂O₃ this suggests that there must be some difference in particle morphology between them to account for the different switching modes. The chain-of-spheres-coherent and 'fanning' modes of reversal have been suggested for acicular particles of γ -Fe₂O₃[130], whilst studies of ellipsoidal γ -Fe₂O₃ particles have shown the reversal to be predominantly coherent[13]. Further work is required to determine the differing particle morphology and switching mode of the samples.

The work of Parker *et al*[12] suggests that the coercivity predicted from the χ_t anisotropy peak value using the relation given by Stoner and Wohlfarth will be slightly higher than the actual value for systems with a narrow distribution of anisotropy field values, and lower than the actual value for systems with wider anisotropy field distributions. This effect may account for some of the difference between the observed ratios and theory if we assume that the anisotropy distribution is narrow.

Inter-particle-interactions are also known to lower both the anisotropy and coercivity fields of systems of particles[90,100]. However, when comparing recording media samples of similar particle packing density this effect is not likely to be significant. The investigation of the four MP tape samples showed their normalised transverse susceptibility curves to be almost identical as expected for samples manufactured using the same particle dispersion. The only sample to show any deviation from the others was the thinnest coated M_tt=3 sample. This sample had a higher anisotropy peak value

and a higher squareness and in-plane orientation ratio than the others. Initially it was thought that this may be due to the thin coating (~150nm, see Chapter 4) being close to the particle length (~ 100nm, [131]) causing a narrower distribution of easy axes in the y-z plane (where the tape is in the x-y plane and y is the play direction). However, subsequent measurement of the out-of-plane orientation ratio showed this not to be the case. The cause of the higher degree of in-plane orientation of this sample could not be determined, but the narrower texture was probably sufficient to account for the slightly higher field value of the anisotropy peak.

The investigation of CrO₂ and γ -Fe₂O₃ powder samples was consistent with earlier measurements of similar systems after Sollis *et al*[120]. Anisotropy peaks were suppressed in the γ -Fe₂O₃ system but present in the CrO₂.

Investigation of the four metal particle samples also showed the anisotropy peaks to be suppressed. Comparison with the theoretical results of Hoare *et al* showed that the predicted response for a system with a random easy axis distribution, switching by coherent rotation, was similar to the results obtained for γ -Fe₂O₃ and MP powders. The theoretical plots produced by Hoare *et al* only considered a single anisotropy field distribution (log-normal, mean = 167 kAm⁻¹ [2100 Oe], σ = 8 Am⁻¹ [0.1 Oe]) which resulted in considerable spreading of the peaks from the cusps obtained by Aharoni with a single anisotropy value. It is possible that variations in the anisotropy value and distribution width could account for the merging of the anisotropy peak with the switching peak in the cases reported herein. The result for CrO₂ powder is less similar to the theoretical predictions and suggests an enhanced response of those particles aligned with the ac field at $H = H_k$. This is supported by the study of the variation in response with sample alignment which shows the expected response for γ -Fe₂O₃ with a steady reduction in anisotropy peak height and field as the sample is rotated (Figure 3-23), whereas the response for CrO₂ shows a very rapid decrease in the anisotropy peak height as the sample is rotated away from $\beta = 0^\circ$ (Figure 3-24). It can also be seen from Figure 3-24 that the coercivity response for $\beta = 90^\circ$ is an almost exact inversion of the response for $\beta = 0^\circ$. It is likely that in the random case these effects will cancel one-another out resulting in the suppression of the coercivity peaks observed in the random powder sample (Figure 3-12). The model of Berkov and Chantrell[127]for a system of particles with a random easy axis distribution, switching by coherent fanning, also

shows enhancement of the anisotropy peaks and suppression of the coercivity peaks. Although it has been shown[17] that 'fanning' is not a preferred reversal mode for particles such as CrO₂, which have a regular shape and a lack of surface defects, it is likely that other incoherent reversal modes could also account for the suppression of switching peaks as the 'flux closure' within particles during incoherent reversal will reduce the external oscillating flux measured by the susceptometer coils. It is proposed that the enhanced anisotropy peaks and suppressed coercivity peaks in the χ_t response of the random CrO₂ system indicates that the particles in this sample are reversing by a predominantly incoherent mode.

Investigation of the imaginary component of the transverse susceptibility found the existence and behaviour of the component was consistent with the theoretical predictions of Papusoi[5]. The imaginary peak was found to be at a field rather lower, $0.85\chi_t(\text{max})$, than that predicted by Papusoi, $0.95\chi_t(\text{max})$. The existence of the imaginary peak also implied some modification to the real peak which was not taken into account by pre-existing theory and suggested that the field of the real peak would be lowered by a few percent dependent on the width of the anisotropy and particle volume distributions. The relationship between the real and imaginary peak is governed by complex relationships between the ac frequency, temperature, particle volume distribution and anisotropy field distribution. Further theoretical work is required in this area before useful characterisation data can be obtained from imaginary susceptibility investigations.

4 Magnetic layer thickness measurement

The magnetic layer of a particulate recording medium is applied as a dispersion of magnetic particles, binders, wetting agents, solvents and additives[49] which is then dried and calendered. The thickness of the magnetic layer is an important parameter which has a critical influence on the maximum bit-density of the media (See section 1.7.2).

Traditionally, the thickness of the magnetic layer has been measured using mechanical techniques, comparing the thickness of a control sample of tape with a sample from which the magnetic layer had been de-laminated. However, with the advent of dual coated tapes the mechanical measurement of the magnetic layer was no longer possible, as it could not be delaminated from the under-layer. Also it was not known to what extent magnetic particles diffused from the magnetic layer into the under-layer. In 1991 Sollis and Bissell[6] reported a magnetic, non-destructive technique to determine the coating thickness of traditional media, using transverse susceptibility measurements. This chapter details the development of the technique for use with advanced media.

The magnetic moment of single thicknesses of modern tape was found to be too low to make reliable transverse susceptibility measurements. In order to increase the moment, several layers were stacked together to produce composite samples. The effect of such stacking on the measurement of the magnetic layer thickness was not immediately apparent, as it was not clear whether the thickness of a single layer, or the composite sample would be determined. An investigation into the effect of stacked samples showed that the sample results were equivalent to those of a single layer and that the determined thickness was that of a single magnetic layer.

The thickness measurement for traditional recording media assumed that a continuous sheet of magnetically homogeneous material approximated the magnetic layer. With the trend to ever-thinner magnetic layers the particle dimensions in modern media were of a similar size to the magnetic layer thicknesses. In these cases the assumption that a homogeneously magnetised sheet could approximate the layer was questionable. A computer model of a particulate magnetic layer was developed and effective demagnetising factors of the layer were calculated as a function of layer thickness and

volume packing fraction for the current generation (MP3) and the proposed next generation (MP4) of metal particles. The experimental measurements of tape samples were corrected. Other related magnetic methods of determining layer thickness were briefly discussed including a method which can be carried out on a standard VSM.

4.1 Previous work

The technique of Sollis and Bissell was based on a determination of the demagnetising field of the magnetic layer by measuring the anisotropy peak of the transverse susceptibility in the following two orientations, (See Figure 4-1)

1. With the dc field applied at right angles to the orientation axis and parallel to the plane of the sample.
2. With the dc field applied at right angles to the orientation axis and perpendicular to the plane of the sample.

As the length and width of the magnetic layer were very much larger than its thickness it was assumed that the demagnetising factors were approximated by those of an infinite sheet, with $N_{d1} = 0$ (for the field applied parallel to the plane of the sample) and $N_{d2} = 1$ (for the field applied normal to the plane of the sample).

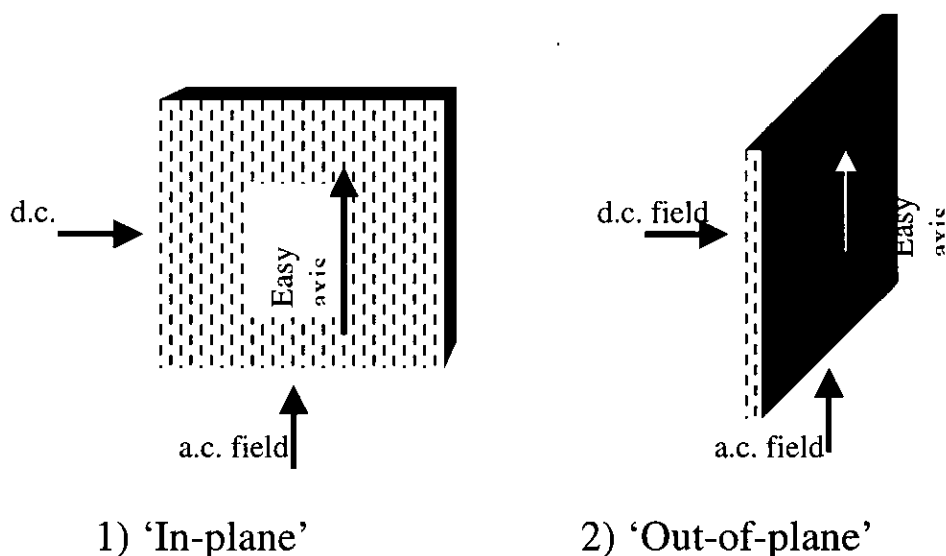


Figure 4-1 Sample orientations for magnetic layer thickness determination

The value of N_d characterises the relationship between the magnetisation M and the demagnetising field H_d for a shape magnetised in a particular direction, such that,

$$H_d = -N_d M . \quad (4.1)$$

So, with the assumption that the demagnetising factors were those of an infinite sheet, the demagnetising fields associated with the two orientations were,

$$H_{d2} = -M , \quad (4.2)$$

and

$$H_{d1} = 0 . \quad (4.3)$$

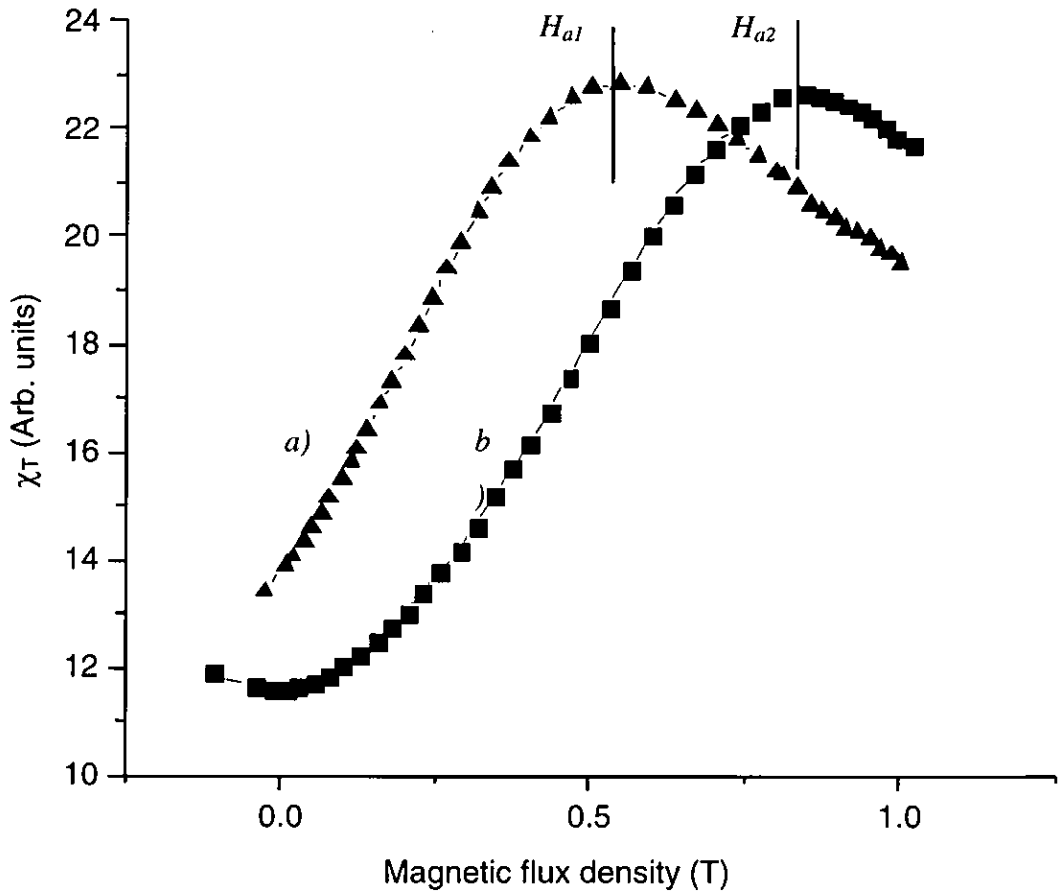


Figure 4-2 Anisotropy peaks for a typical sample a) in orientation 1 and b) in orientation 2

Work by LeDang *et al* showed that the transverse susceptibility response was largely due to the response of particles closely aligned with the ac field[97]. Hence it was assumed that the two anisotropy peaks obtained were due to the response of similarly oriented particles and occurred at the same total (internal) field value.

$$H_{a1} + H_{d1} = H_{a2} + H_{d2} \quad (4.4)$$

where H_{a1} and H_{a2} were the applied field values of the anisotropy peaks in orientations 1 and 2 respectively (see Figure 4-2).

Substituting equations (4.3) and (4.4) into (4.2) we obtain a value for M ,

$$M = H_{a2} - H_{a1} . \quad (4.5)$$

The value of M obtained is the magnetisation of the magnetic layer at an applied field of H_{a1} in orientation 1 or an applied field of H_{a2} in orientation 2.

In order to determine the magnetic layer thickness, one of the above orientation and applied field combinations was replicated with the sample mounted in a VSM (vibrating sample magnetometer). The magnetic moment of the sample, μ , was measured in this condition and related to the sample area, A , and the magnetisation, M , to determine the magnetic layer thickness, t ,

$$\begin{aligned} \mu &= MA t , \\ t &= \frac{\mu}{MA} . \end{aligned} \quad (4.6)$$

4.2 Application of technique to modern media

The magnetic measurement technique described in section 4.1 had been demonstrated successfully for traditional recording tapes. However, the technique had not been widely used due to the limited availability of commercial transverse susceptometry and the relative ease of mechanical techniques for measuring the layer thickness by delaminating the tape. With the advent of modern, dual coated, metal particle tapes[125,126] the magnetic layer thickness could not be measured by simple mechanical methods as the magnetic layer alone could not be delaminated from the under-layer. Measurements of the layer thickness by electron micrographs of sections of the tape were possible, but these were difficult to prepare without causing damage to the tape during sectioning. The transverse susceptibility technique appeared to be ideal for this task. However, the magnetic moment of modern MP tape samples was much less than that of those previously measured due to the thinner and magnetically more 'dilute' coating. This resulted in a much smaller transverse susceptibility signal that could not be measured from a single thickness sample. In order to increase the sample moment and therefore, to increase the transverse susceptibility signal, a composite sample was made by stacking a number of layers of tape together and treating these as a single

sample. It was not immediately apparent what the effect of such stacking would be on the out-of-plane demagnetising field compared to that of a single layer.

4.3 Effects of stacking samples

From Maxwell's equation, $\nabla \cdot \mathbf{B} = 0$, we know that magnetic flux is not divergent, therefore for a closed surface S we can say,

$$\oint_S \mathbf{B} \cdot d\mathbf{a} = 0. \quad (4.7)$$

If we apply a magnetic field, H_a , normal to the sample plane we induce a magnetic flux B . As we have assumed that the sample may be approximated by an infinite sheet, the lines of flux will remain normal to the surface. Hence the value of B at the upper surface of the Gaussian cylinder shown in Figure 4-3 (within the sample) is the same as that at the lower surface.

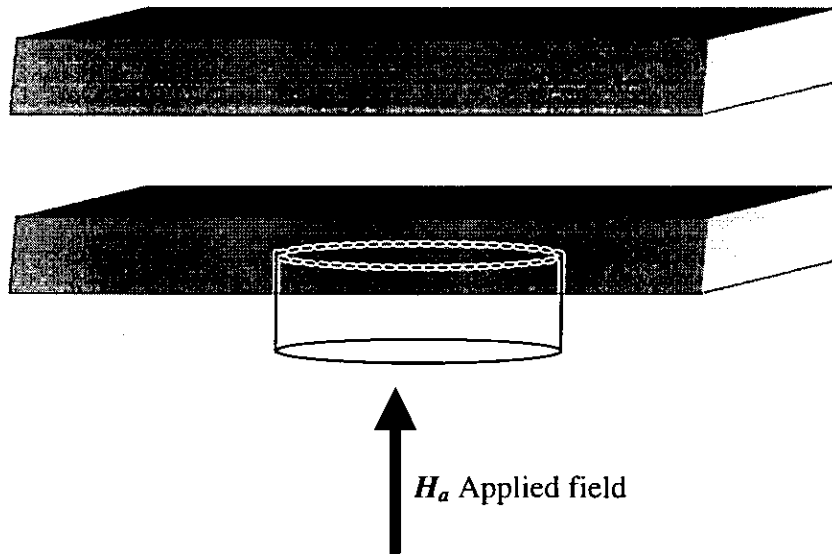


Figure 4-3 Flux is normal to sample plane so field at surfaces of cylinder is given by B/μ

B at the lower surface of the cylinder is related to H_a by,

$$B = \mu_0 H_a. \quad (4.8)$$

The field within the sample medium, H_s , is given by,

$$H_s = \frac{1}{\mu_0 \mu_r} B, \quad (4.9)$$

where μ_r is the relative magnetic permeability of the sample. Hence,

$$H_s = \frac{1}{\mu_r} H_a \quad (4.10)$$

For a ferromagnetic sample where $\mu_r > 1$, we can see that the field within the sample is reduced.

If we now consider the cylinder shown in Figure 4-4 we can again assume that the value of B for the upper and lower surfaces of the cylinder will be the same. This time however, the permeability at both surfaces is the same also, so the value of H will not change and we can state that the external field (within the air gap between layers) is unaffected by the layers surrounding it. The field is only dependent on the permeability of the material at the surface of the cylinder so the field value within all the air spaces will be H_a whilst the field value within all the sample layers will be given by H_s from equation (4.10). The field values are independent of the number of layers or position within the stack.

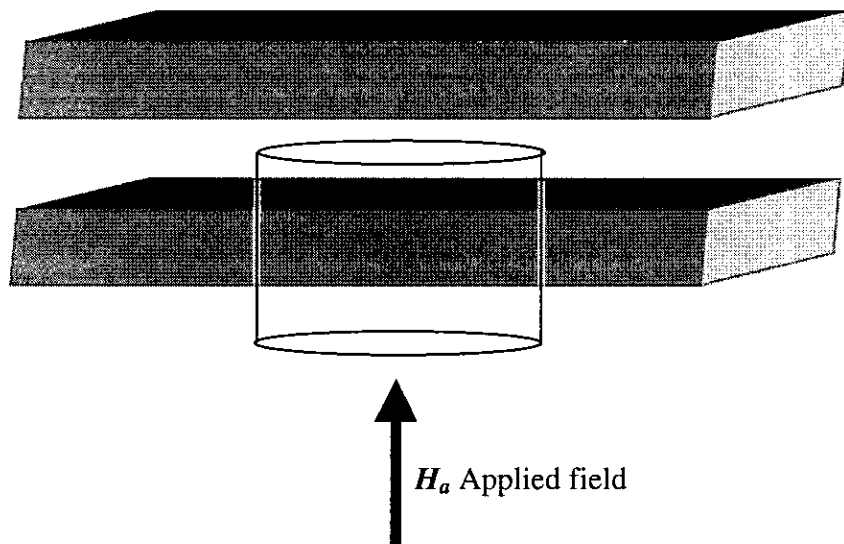


Figure 4-4 B/μ is the same for both ends of the cylinder so the external field is unchanged by the sample

The above conditions are true where the samples are considered to be infinite sheets and the flux remains parallel through the sample. Near the edges of the sample, however, the flux lines would curve towards the sample to minimise the energy of the field, resulting in some flux cutting through the sides of the Gaussian cylinder. In order to test the assumption that the edge effects could be neglected, a series of measurements of transverse susceptibility peaks were made using samples assembled from different

numbers of tape layers. These showed (Figure 4-5) that the position of the transverse susceptibility peak was independent of the number of layers in the sample.

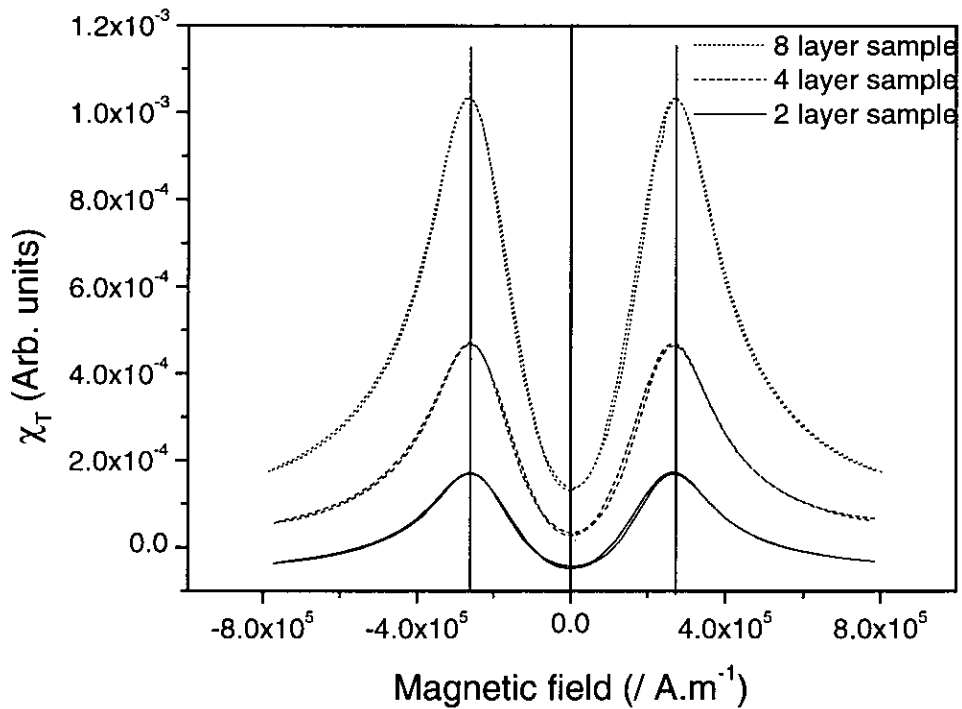


Figure 4-5 Transverse susceptibility response of layered samples showing peak position independent of number of layers

4.4 Measurement of MP samples

Samples were prepared by assembling 300-layer thick stacks of a number of commercial and development metal particle (MP) tapes. Development tapes manufactured to the linear tape open (LTO) format were supplied with magnetic layers of differing thickness. The effects of diffusion of magnetic particles into the ‘non-magnetic’ layer, and the change in the magnetic layer thickness during the drying and calendaring processes, were not known. Also it was not possible to delaminate the magnetic layer from the non-magnetic under-layer to make mechanical thickness measurements.

The MP samples were identified by nominal $M_r t$ (remanent magnetisation \times magnetic layer thickness) values, as determined by the manufacturer. The $M_r t$ values were also checked by measurement with a VSM along with other standard characterisation measurements which are given in Table 4-1.

| Sample | | M_{rf} / memu·cm ⁻² | M_{rf} / mA·m ⁻² | M_{sf} / mA·m ⁻² | H_c / kA·m ⁻¹ | Squareness | OR |
|--------------------|--------|-------------------------------------|----------------------------------|----------------------------------|-------------------------------|------------|-----|
| Hi8 MP videotape | | 24.39 | 243.9 | 284.5 | 73.5 | 0.86 | 2.2 |
| 3590 MP data tape | | 52.10 | 521.0 | 638.2 | 128 | 0.82 | 2.0 |
| LTO Commercial | | 6.328 | 63.28 | 75.3 | 153 | 0.84 | 2.2 |
| Development LTO | Mrt3 | 3.53 | 35.3 | 40.5 | 155 | 0.87 | 2.2 |
| | Mrt4 | 4.03 | 40.3 | 47.9 | 152 | 0.84 | 2.0 |
| | Mrt4.5 | 4.60 | 46.0 | 54.9 | 151 | 0.84 | 2.0 |
| | Mrt6 | 6.24 | 62.4 | 74.1 | 151 | 0.84 | 2.0 |

(VSM sweep rate = 3.1kAm⁻¹s⁻¹, Maximum field 560kAm⁻¹)

Table 4-1 Static characteristics of tape samples

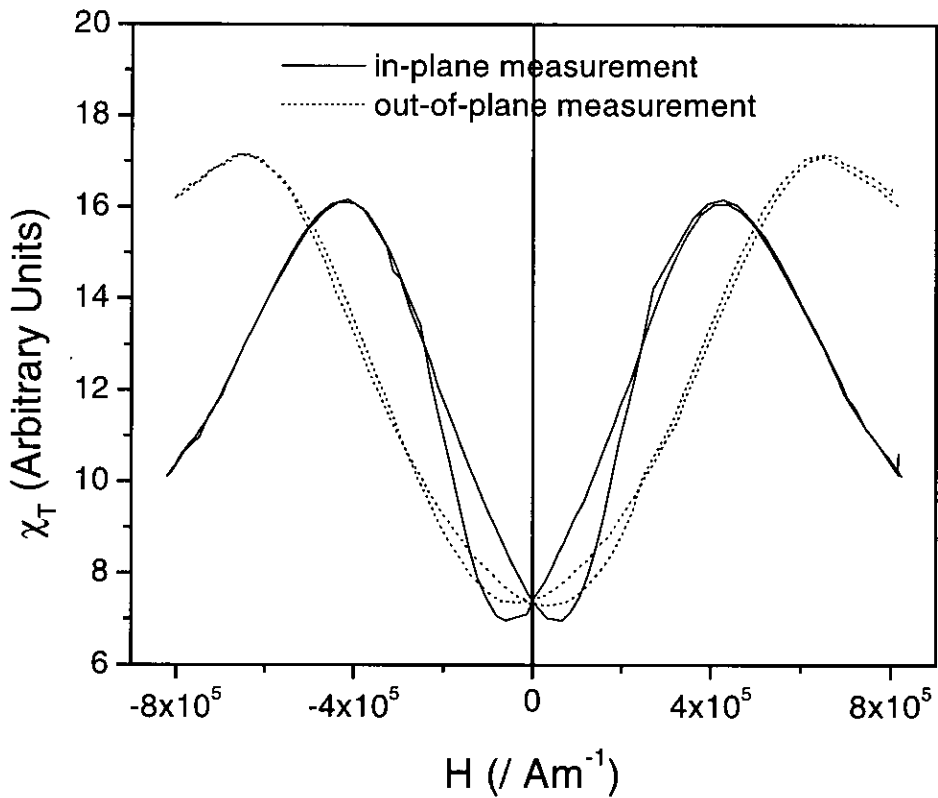


Figure 4-6 Typical measurement (sample Mrt6) showing change in peak position

The magnetic layer thicknesses of the samples were determined using the techniques described in section 4.1 and Figure 4-6 shows a comparison of the χ_t response for the two orientations of a typical sample.

The preliminary results for all of the samples are detailed in Table 4-2 and Figure 4-7 shows a comparison between the measured thickness and $M_r t$ values of the development samples. The trend is reasonably linear, as we would expect assuming that the samples were manufactured using the same magnetic dispersion and that the only difference between them was the magnetic layer thickness.

Although the results looked reasonable, the assumption that the particulate magnetic layer could be approximated by a layer of magnetically homogeneous material was questionable for modern media, where the magnetic layer thickness was of the same order of magnitude as the size of the particles. In order to investigate the error in the determination due to this assumption a numerical model of the effective demagnetising factors of MP3 and MP4 particulate tapes was constructed.

| | Sample | H_d / $\text{kA}\cdot\text{m}^{-1}$ | t / μm |
|--------------------|-------------------------------------|--|------------------------|
| Commercial | Hi8 MP | 146 | 1.63 |
| | 3590 | 232 | 2.56 |
| | LTO | 227 | 0.29 |
| Development | LTO $M_r t_3$ | 239 | 0.15 |
| | LTO $M_r t_4$ | 208 | 0.21 |
| | LTO $M_r t_{4.5}$ | 212 | 0.23 |
| | LTO $M_r t_6$ | 226 | 0.30 |

Table 4-2 Results of demagnetising field and magnetic layer thickness calculations

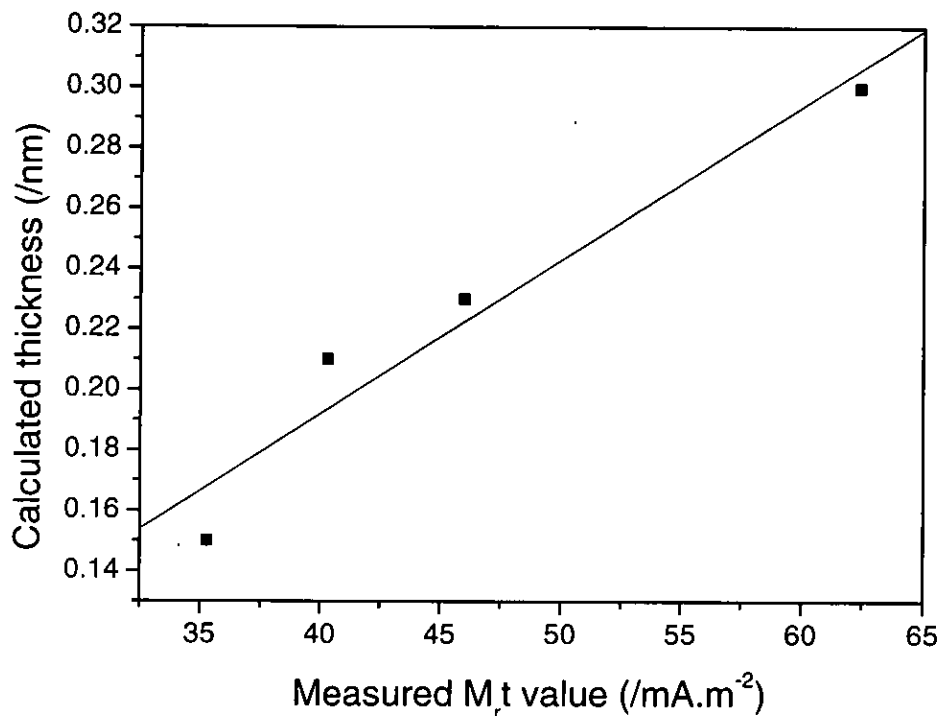


Figure 4-7 Comparison of calculated thickness with M_t values

4.5 Demagnetising field model

The original work of Sollis & Bissell [6] in determining magnetic film thickness assumed that the magnetic coating of a recording tape sample was approximated by a homogeneous layer of magnetic material. This approximation allowed the known demagnetising factors of a homogeneously magnetised layer to be used in the thickness determination and was acceptable for traditional recording tapes where the magnetic layer thickness was large compared to the dimensions of the magnetic particles.

With the advance of magnetic recording techniques and the requirement to increase the areal bit-density of magnetic tapes it has been necessary to make the magnetic layer progressively thinner. Although the size of magnetic particles in the layer has also been reduced, the layer thickness for modern media is of the same order of magnitude as the particle dimensions. In this case, the particulate nature of the magnetic layer becomes more evident and the assumption that the demagnetising factors will be the same as those of a homogeneously magnetised layer is questionable.

In order to determine the demagnetising factors of a particulate layer compared to those of a homogeneous layer, and hence determine the error in the homogeneous assumption,

a model was developed to determine the magnetostatic self-field of the system of particles.

4.5.1 Design of model

The model was designed using the following criteria: (See Figure 4-8)

1. The particles were positioned equally spaced on a regular lattice.
2. The model was run using two sets of particle parameters. Those of the current generation of MP tape (MP3), and those of the next proposed generation (MP4).
3. The long axes of the particles were all perfectly aligned along the y-axis of the model tape.
4. The particles were considered to be magnetically saturated along the z-axis for the out-of-plane calculations and along the x-axis for the in-plane calculations.

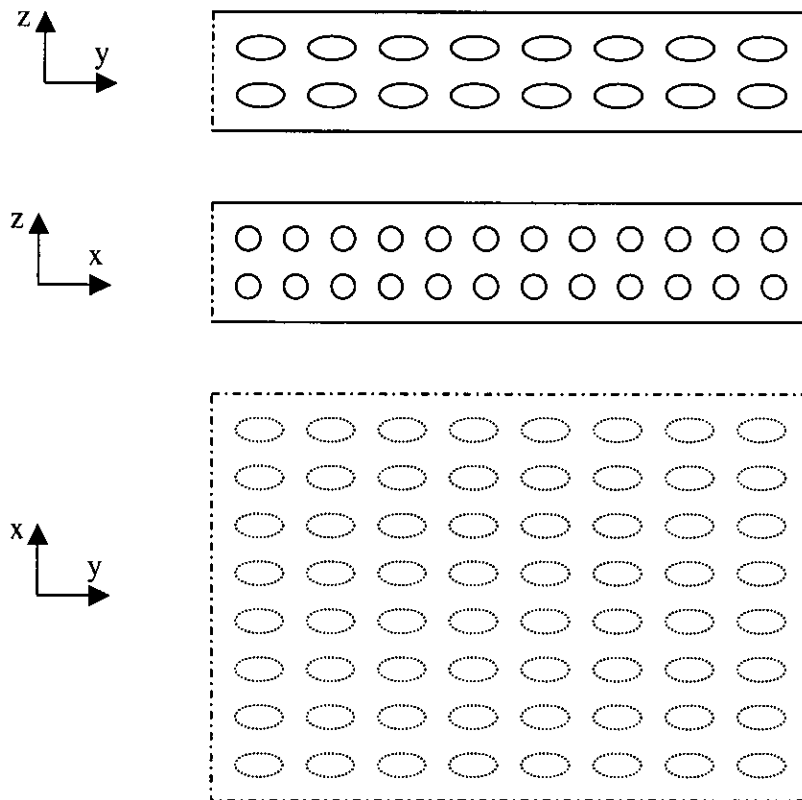


Figure 4-8 Axis definition and particle layout for demagnetising field model

As the purpose of the model was to compare the effective demagnetising factors of the particulate tape samples with those of a homogeneous layer there was no requirement to

model any dynamic changes to the applied field or magnetisation. As the demagnetising factor relates the mean magnetisation of the sample to its demagnetising field the applied field was ignored and the particles were considered to be saturated in the hard-axis direction at all times. In order to simplify the model the particles were all considered identical in size and shape, arranged in a regular lattice, and all perfectly aligned along the y-axis. As the model was not used to determine switching or remanent behaviour it was assumed that the use of such a system of particles would give a reasonable estimate of the demagnetising fields of the real system.

4.5.2 Calculation of effective demagnetising field

In order to calculate the demagnetising field, the magnetic layer was considered as a stack of two-dimensional lattices referred to as 'sheets', where each sheet is a regular lattice of particles in the x - y plane, all with a common z ordinate. The sheets were considered to be infinite in the x - y plane.

If we now consider an arbitrary particle in a sheet, the demagnetising field acting upon it consists of the sum of the following;

1. The field due to the moment of the particle itself,
2. The field due to the moments of all the other particles in the sheet.
3. The field due to the moments of all the other sheets other than the one containing the particle of interest.

The lattice parameter in the z direction was defined as a_z , the field due to the sheet containing the selected particle was calculated (sheet $z = 0$), then the field due to a sheet one lattice parameter removed from the particle (sheet $|z| = a_z$), then two layers removed (sheet $|z| = 2a_z$) etc. Different combinations of these values were added to calculate the demagnetising field as a function of depth through the magnetic layer for a number of different layer thicknesses. Note that the field due to a sheet at a particular distance from the particle of interest is the same whether it is above, or below the particle of interest

For the four sheet thick magnetic layer illustrated in Figure 4-9, the total demagnetising field, $H_d(\text{layer})$, seen by the shaded particle is given by equation (4.11);

$$H_d(\text{layer}) = H_d(z = 0) + 2 \cdot H_d(|z| = a_z) + H_d(|z| = 2a_z) \quad (4.11)$$

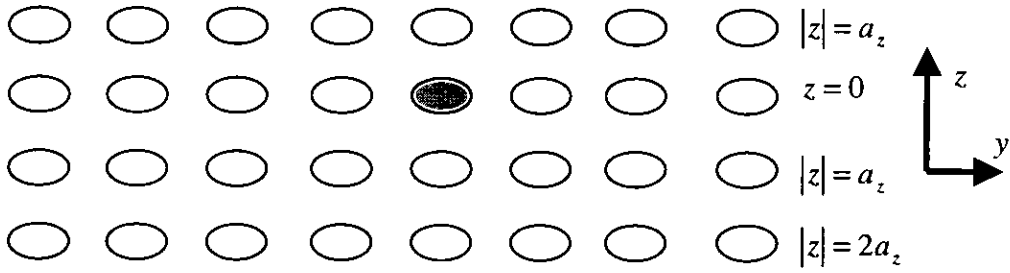


Figure 4-9 Four-sheet magnetic layer (particle of interest shaded)

4.5.2.1 Contribution of individual sheets

The contribution to the demagnetising field due to each single thickness sheet of particles was calculated by selecting a particle then summing the demagnetising field due to each particle in a $([2n+1] \times [2n+1])$ array centred on the particle considered (so particles at the edge of the array were considered to be n particles distant from the centre). The value of n was increased from 0 to 100 in steps of 5.

For the more distant particles we assumed that the field due to each particle was similar to the field from a small dipole acting on the particle at an angle of 90° from its direction of magnetisation. The field due to a distant particle decreases as a function of $(\text{distance})^3$, but the number of particles in the sheet increases as a function of $(\text{distance})^2$. Hence we expect the field due to the distant particles to follow the relation shown in equation (4.12),

$$H_d \propto \frac{n^2}{n^3} = \frac{1}{n}. \quad (4.12)$$

At large values of n , by plotting H_d vs. $1/n$ we obtained a straight line which was extrapolated back to $1/n = 0$ to find the value of H_d for an infinite sheet.

The above operation was repeated for the required number of sheets, from sheet ($z=0$) to sheet ($z=[N-1]a_z$), where N is the number of sheets required to make up the final magnetic layer thickness.

4.5.2.2 Contribution due to individual particles

As described above the contribution to the local field of each sheet was found by summing the field due to an $([2n+1] \times [2n+1])$ array of particles.

The field due to individual particles (including the central particle considered) was found by assuming the particles to be magnetised with constant magnetisation throughout their volume (true only for ellipsoids of revolution). For the prolate ellipsoid MP4 particles this assumption is true, however, the MP3 particles are more cylindrical in shape and so the magnetisation will vary slightly throughout the particle volume due to end effects.

The charge distribution on the surface of the particles was calculated and the field due to each particle was found by integrating the field due to surface charges over the surface of the particle. Both the positive charges on the $+z$ (out of plane calculation, $+x$ for in plane calculation) surface of the particle and negative charges on the $-z$ side were integrated to determine the total field.

The integral was defined in terms of a local co-ordinate system (o,p,q) for the particle, then global co-ordinates (x,y,z) were added so that the same integral could be transposed to any location to find the field due to a particle at that point. Also the field calculations were divided through by the particle magnetisation, M_p , to express the results directly as a contribution to the demagnetising factor, N_d .

The integral for the demagnetising factor due to a particle magnetised in the $+q$ direction of the (o,p,q) co-ordinate system was derived as follows;

Pole strength, P , at the surface of a cross sectional area element da is given in equation (4.13),

$$P = M_p \cdot da, \quad (4.13)$$

and the field due to an isolated pole is given by

$$H = \frac{P}{d^2}, \quad (4.14)$$

where d is the distance between the pole and the point where the field is measured.

Hence, if the origin is at the centre of a particle, the demagnetising field due to point (o,p,q) on the surface is given by,

$$H = M_p \frac{da}{(o^2 + p^2 + q^2)}. \quad (4.15)$$

If we recall that $H_d/M = N_d$ (demagnetising factor), and also that because of the symmetry of the sheet we only need to consider the component of field in the q direction, we can rearrange equation (4.15) as follows,

$$\begin{aligned}
 N_d &= \frac{q}{d} \cdot \frac{da}{(o^2 + p^2 + q^2)}, \\
 &= \frac{q \cdot da}{\sqrt{(o^2 + p^2 + q^2)} \cdot (o^2 + p^2 + q^2)}, \\
 &= \frac{q \cdot da}{(o^2 + p^2 + q^2)^{\frac{3}{2}}}.
 \end{aligned} \tag{4.16}$$

Hence, for the ellipsoid MP4 particles we integrate over the elliptical projected area of the particle, and for MP3 we integrate over the rectangular projected area of the cylinder.

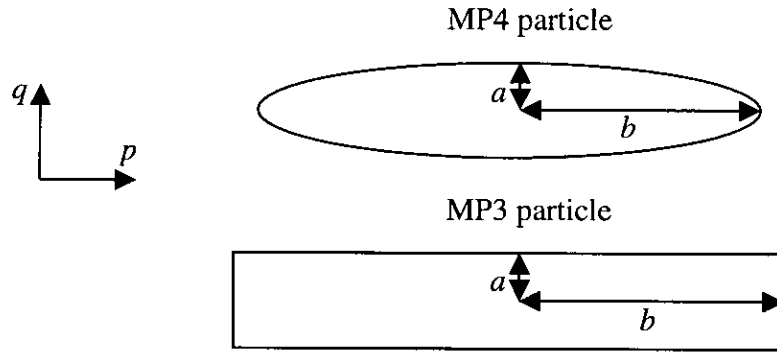


Figure 4-10 MP3 and MP4 particle shapes (not to scale)

So for the MP3 particle of dimensions $a=1$ and $b=5$, the value of q at a point (o,p) on the surface is given by,

$$q_{\text{MP3}}(o, p) = \pm \sqrt{a^2 - o^2}. \tag{4.17}$$

Hence, we can substitute this into equation (4.16) and build the integral for both the positive charged and negative charged surface of the particle. If we assume that the positive charges exist on the $+q$ side of the particle we obtain,

$$N_d = \int_{-b}^b \int_{-a}^a \frac{-q_{\text{MP3}}(o, p)}{\left[o^2 + p^2 + (-q_{\text{MP3}}(o, p))^2 \right]^{\frac{3}{2}}} - \frac{q_{\text{MP3}}(o, p)}{\left[o^2 + p^2 + (+q_{\text{MP3}}(o, p))^2 \right]^{\frac{3}{2}}} do \cdot dp. \tag{4.18}$$

For the MP4 elliptical particle of dimensions $a=1$ and $b=5$, the value of q at point (o,p) on the surface is given by,

$$q_{\text{MP4}}(o, p) = \sqrt{a^2 \left(1 - \frac{p^2}{b^2}\right) - o^2}. \quad (4.19)$$

Also, the limits of p as a function of o for integration of the projection of the surface are,

$$\lim p(o) = \sqrt{b^2 \left(1 - \frac{o^2}{a^2}\right)}. \quad (4.20)$$

Hence, substituting into equation (4.16) for positive and negative charges we obtain the integral,

$$N_d = \int_{o=-a}^a \int_{p=-\lim p(o)}^{\lim p(o)} \frac{-q_{\text{MP4}}(o, p)}{\left[o^2 + p^2 + (-q_{\text{MP4}}(o, p))^2\right]^{\frac{3}{2}}} - \frac{q_{\text{MP4}}(o, p)}{\left[o^2 + p^2 + (q_{\text{MP4}}(o, p))^2\right]^{\frac{3}{2}}} dp \cdot do. \quad (4.21)$$

The above equations, (4.18) and (4.21), give the component of the demagnetising factor at the origin due to a particle centred on the origin. By simply adding x , y and z to o , p and q respectively we can transpose the particle so that the equations give the component of the demagnetising factor at the origin for a particle centred on co-ordinates (x,y,z) . So the equation for the cylindrical MP3 particle array becomes,

$$N_d(x, y, z) = \int_{-b}^b \int_{-a}^a \frac{z - q_{\text{MP3}}(o, p)}{\left[(x+o)^2 + (y+p)^2 + (z - q_{\text{MP3}}(o, p))^2\right]^{\frac{3}{2}}} - \frac{z + q_{\text{MP3}}(o, p)}{\left[(x+o)^2 + (y+p)^2 + (z + q_{\text{MP3}}(o, p))^2\right]^{\frac{3}{2}}} do \cdot dp \quad (4.22)$$

Finally, we add a scaling factor m so that we can represent the lattice with only integer values of x , y and z . So, if we define $m=1$ as the spacing where each cylinder just

touches its neighbour, consecutive x and z values must be separated by $2ma$, whereas consecutive y values will be separated by $2mb$, thus we have the final formula,

$$N_d(x, y, z) = \int_{-b}^b \int_{-a}^a \frac{2m \cdot a \cdot z - q_{MP3}(o, p)}{\left[(2m \cdot a \cdot x + o)^2 + (2m \cdot b \cdot y + p)^2 + (2m \cdot a \cdot z - q_{MP3}(o, p))^2 \right]^{\frac{3}{2}}} \frac{2m \cdot a \cdot z + q_{MP3}(o, p)}{\left[(2m \cdot a \cdot x + o)^2 + (2m \cdot b \cdot y + p)^2 + (2m \cdot a \cdot z + q_{MP3}(o, p))^2 \right]^{\frac{3}{2}}} do \cdot dp \quad (4.23)$$

Following the same steps we obtain the final MP4 equation from equation (4.21);

$$N_d(x, y, z) = \int_{o=-a}^a \int_{p=-\lim p(o)}^{\lim p(o)} \frac{2m \cdot a \cdot z - q_{MP4}(o, p)}{\left[(2m \cdot a \cdot x + o)^2 + (2m \cdot b \cdot y + p)^2 + (2m \cdot a \cdot z - q_{MP4}(o, p))^2 \right]^{\frac{3}{2}}} \frac{2m \cdot a \cdot z + q_{MP4}(o, p)}{\left[(2m \cdot a \cdot x + o)^2 + (2m \cdot b \cdot y + p)^2 + (2m \cdot a \cdot z + q_{MP4}(o, p))^2 \right]^{\frac{3}{2}}} dp \cdot do \quad (4.24)$$

The contribution to the demagnetising factor due to a $([2n+1] \times [2n+1])$ sheet of particles, z layers distant from the origin (see section 4.5.2), is now calculated as,

$$N_d[\text{sheet}](z, n) = \sum_{x=-n}^n \sum_{y=-n}^n N_d(x, y, z). \quad (4.25)$$

4.5.3 Programming model

Initially attempts were made to program the model described above using the Fortran programming language, however, on running the programs it was found that the standard numerical integration routines could not converge on a solution to the particle surface integration. Attempts to solve the integral by simple summing over the surface took a prohibitively long time (in the order of minutes for each particle) and were of a

low accuracy (checked against the known demagnetising factor of a single particle from tables [132]).

A number of software packages were tried in order to solve the integral and this was eventually achieved using Mathcad7[®] which solved the central particle integral in 18 seconds, and converged on the solution for the outer particles in successively less time, falling to 2 seconds for the most distant particles. For the full model of 11 sheets with each sheet 200×200 particles this would still result in a run time of approximately 11 days for each packing density.

In order to reduce the overall run time of the model two further refinements were made as follows:

- Reducing the number of integrations required through symmetry
- Increasing the speed of calculation for distant particles by replacing the integrations by a single dipole estimate for each particle.

4.5.3.1 Reducing integrations through symmetry

By looking at the symmetry of particles in each sheet, we know that any components of the field that are not parallel to the direction of magnetisation will cancel each other out. We can also see that using symmetry we need only calculate the field due to half of the particles in each sheet.

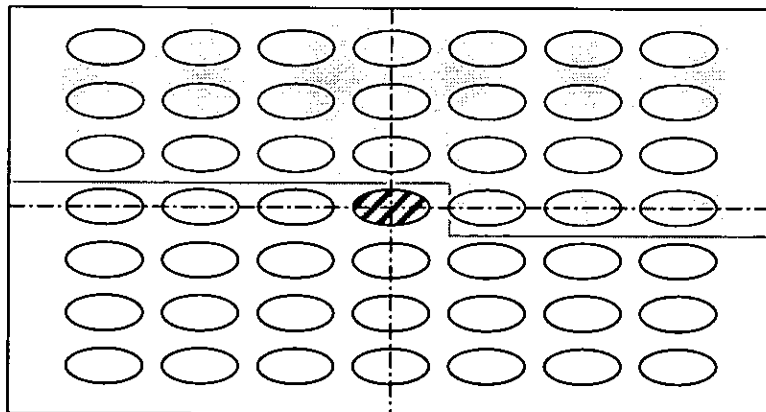


Figure 4-11– Symmetry of particle sheet

Hence, looking at Figure 4-11 the demagnetising factor of the sheet is equal to the demagnetising factor of the central particle plus two times that due to the particles in the shaded area.

4.5.3.2 Using dipole estimates for distant particles

In order to speed up calculation of the model it is possible to consider each particle as a single dipole, where the dipole moment is given by $M \times$ particle volume. For particles close to the origin this approximation is not accurate for the following reasons:

- Using the dipole approximation replaces the broad distribution of charge due to near particles with a few large point charges at discrete angles, which distort the balance between positive and negative field contributions,
- The formula for the field due to a dipole is itself an approximation, which is only valid where the distance to the dipole from the origin is large, compared with the dipole length.

In order to determine at what distance the dipole approximation could be used without causing significant errors a comparison was made between the field given by the exact integration method, and the field given by the dipole method, for particles as a function of distance from the origin (Figure 4-12).

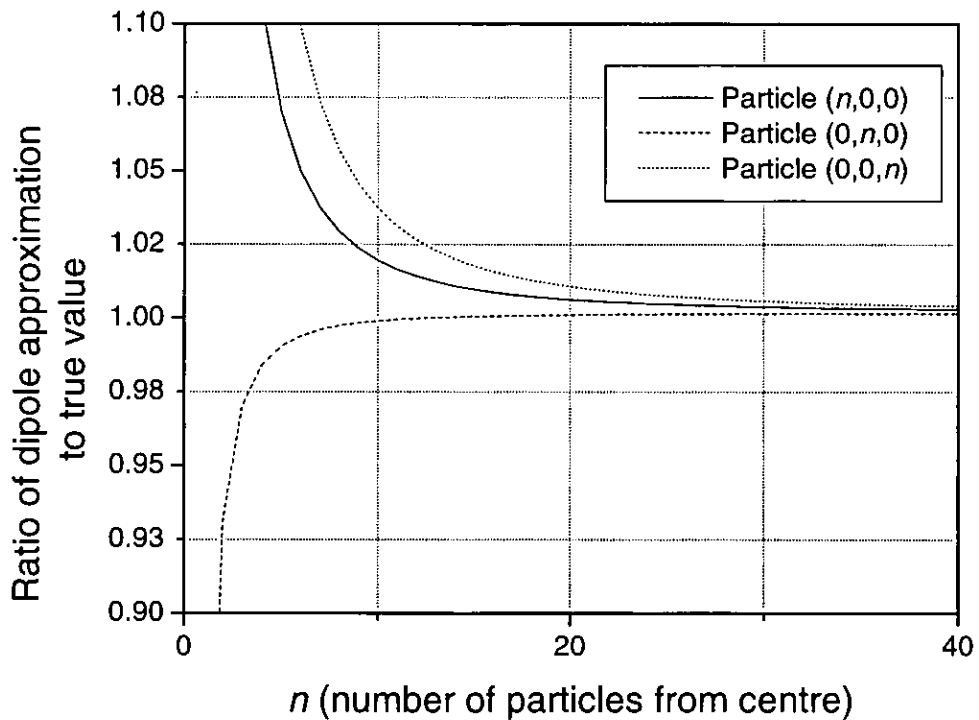


Figure 4-12 Error in dipole estimate as a function of particle distance

From this comparison it was found that the error due to the dipole approximation fell to less than 2% for particles greater than $15a$ distant from the selected particle in the x and z direction or $15b$ distant from the selected particle in the y direction. Hence, the central (31×31) particle square of each sheet was calculated using the integration technique, then the remainder of the sheet was calculated using the simpler dipole approximation, whereby the z component of the demagnetising factor due to a particle at (x, y, z) is given;

$$N_d(x, y, z) = vol \cdot \left(\frac{2}{\left[(2m \cdot a \cdot x)^2 + (2m \cdot b \cdot y)^2 + (2m \cdot a \cdot z)^2 \right]^{\frac{3}{2}}} - \frac{3 \left[(2m \cdot a \cdot x)^2 + (2m \cdot b \cdot y)^2 \right]}{\left[(2m \cdot a \cdot x)^2 + (2m \cdot b \cdot y)^2 + (2m \cdot a \cdot z)^2 \right]^{\frac{5}{2}}} \right) \quad (4.26)$$

Where vol is the volume of the magnetic core of the particle.

The use of the dipole estimate, for the outer particles, reduced the running time of the model to approximately 6 hours for 11 sheets, with a maximum n value of 200.

4.5.3.3 Determination of effective demagnetising factor

The results of the model give us the magnetostatic field in the centre of each particle due to itself and all the other particles in the system extended to an infinite plane. As the particle dilution increases and the layer thickness decreases we find that the field within each particle increases, although it remains well below the magnetisation of the particle. This is true for both in-plane and out-of-plane directions of magnetisation. In order to interpret this data we must relate it to the macroscopic experimental measurements.

4.5.4 Calculation of volume packing fraction

The volume packing fraction was given by the volume of the particle divided by the volume of the unit cell of the matrix that it occupied.

As the model was only concerned with the magnetic cores of the particles an allowance was also made for the non-magnetic shell of the particle in order to calculate the equivalent volume packing fraction.

The volume of the MP3 (cylindrical) particle cores was given by,

$$V_{core_{MP3}} = 2\pi a^2 b. \quad (4.27)$$

The volume of the ellipsoid MP4 cores was given by,

$$V_{core_{MP4}} = \frac{4}{3}\pi a^2 b. \quad (4.28)$$

The volume of the cuboid, which just enclosed the particle, multiplied by m^3 , gave the volume of the unit cell. Hence for both particle types,

$$V_{cell} = 8a^2 b \cdot m^3. \quad (4.29)$$

The volume packing fraction of the cores was therefore,

$$vpf_{Core} = \frac{V_{core}}{V_{cell}}. \quad (4.30)$$

In order to estimate what fraction of the particle volume was taken up by the magnetic core we used the measured bulk magnetisation of the particles compared with the standard value for the magnetisation of the magnetic core (both values supplied by the tape manufacturer).

As magnetisation is a measure of moment per unit volume, the ratio of magnetisation is equal to the ratio of volumes. Hence,

$$\frac{M_{Core}}{M_{Particle}} = \frac{\left(\frac{\mu}{V_{core}}\right)}{\left(\frac{\mu}{V_{particle}}\right)} = \frac{V_{particle}}{V_{core}}. \quad (4.31)$$

So, substituting into equation (4.30) we have,

$$\begin{aligned} \frac{M_{Core}}{M_{Particle}} &= \frac{V_{particle}}{vpf_{Core} \cdot V_{cell}} \\ vpf_{Core} \cdot \frac{M_{Core}}{M_{Particle}} &= \frac{V_{particle}}{V_{cell}} \\ \therefore vpf_{Particle} &= vpf_{Core} \cdot \frac{M_{Core}}{M_{Particle}}. \end{aligned} \quad (4.32)$$

4.5.5 Results of model

The above model was run using particle parameters supplied by the MP tape manufacturer. (See Table 4-3)

| Particle Type | Shape | Semi-major dimension (b) / nm | Semi-minor dimension (a) / nm | Bulk M_S (M_{Particle}) / Tesla | Core M_S (M_{Core}) / Tesla |
|---------------|-----------|-------------------------------|-------------------------------|--|--|
| MP3 | Cylinder | 50 | 10 | 10.4 | 22.6 |
| MP4 | Ellipsoid | 32 | 6 | 8.80 | 22.6 |

Table 4-3 Particle parameters for demagnetising field model

It is important to note that the results of the model are related to actual tape thicknesses using the particle parameters given in Table 4-3. Due to the proprietary nature of commercial particle manufacture, little information has been published on the particle parameters and the stated values must be treated with some caution. The paper of Hisano and Saito[133] gives parameters for particles produced up to 1997 by the Dowa Mining Co., Ltd., but does not state the density of the particles so the M_S values cannot be directly compared with those given in Table 4-3. The M_S value and length of sample g in the paper of Okamoto *et al*[134] is broadly in agreement with the values given for MP4 particles in Table 4-3 although the aspect ratio is considerably smaller at 3.4 suggesting a semi-minor dimension of 9.4 nm.

The values of bulk and core M_S from Table 4-3 were used to calculate back through equations (4.29) to (4.32) and determine values for the m parameter which corresponded to vpf_{Particle} values of 0.2, 0.4 and 0.6 .

The model was run for the above three VPF values and the average effective demagnetising factor was calculated for layers ranging from one sheet of particles thick, to eleven sheets of particles thick. As the spacing between adjacent sheets was dependent on the volume packing fraction, the total layer thickness was a function of both VPF and the number of sheets.

The results of the demagnetising field model for MP3 and MP4 type particles are shown in Figure 4-13 and Figure 4-14 respectively. The results show that the effective demagnetising factor increases as the layer thickness decreases, and as the vpf decreases. The thicknesses are shown in terms of the number of sheets in the particular model. This increase in effective demagnetising factor compared to a homogeneous

sheet results in the magnetic thickness determinations being lower than the actual values. In order to determine the size of the error it was necessary to determine the number of model layers with which to represent the real samples. The remaining sections of the chapter describe the correction of the thickness measurements using the model results.

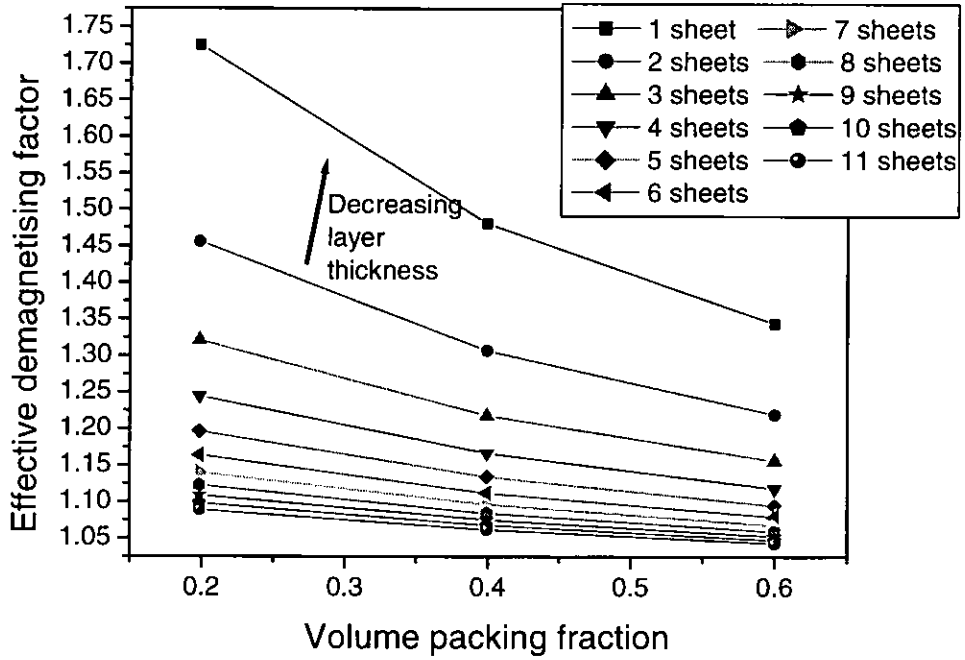


Figure 4-13 MP3 particles effective demagnetising factor against VPF for varying layer thickness

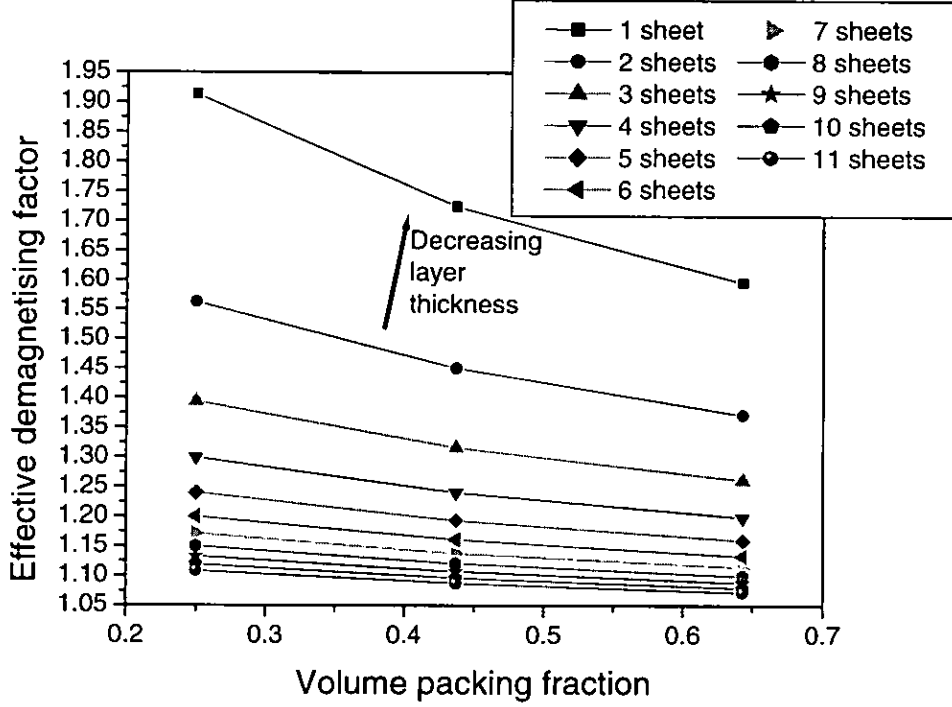


Figure 4-14 MP4 particles effective demagnetising factor against VPF for varying layer thickness

4.5.5.1 Layer thickness

In order to determine the thickness of the magnetic layer represented by the model we multiply the number of sheets by the thickness of each sheet. The thickness of an individual sheet of particles, t_s , is given by,

$$t_s = 2ma, \quad (4.33)$$

and by rearranging equations (4.29) to (4.32) we obtain an expression for m ,

$$m = \sqrt[3]{\frac{V_{particle}}{8a^2b \cdot vpf_{Particle}}}. \quad (4.34)$$

Hence,

$$t_s = \sqrt[3]{\frac{a V_{particle}}{b vpf_{Particle}}}. \quad (4.35)$$

So for MP3 particles,

$$V_{particle}_{MP3} = 2\pi a^2 b \left(\frac{M_{Core}}{M_{Particle}_{MP3}} \right), \quad (4.36)$$

and the sheet thickness is given,

$$t_{S_MP3} = a \cdot \sqrt[3]{\frac{2\pi}{Vpf_{\text{Particle}}} \left(\frac{M_{\text{Core}}}{M_{\text{Particle}}} \right)_{\text{MP3}}} \quad (4.37)$$

In the case of the ellipsoidal MP4 particles,

$$V_{\text{particle}}_{\text{MP4}} = \frac{4}{3} \pi a^2 b \left(\frac{M_{\text{Core}}}{M_{\text{Particle}}} \right)_{\text{MP4}} \quad (4.38)$$

So the sheet thickness is given,

$$t_{S_MP4} = a \cdot \sqrt[3]{\frac{4\pi}{3Vpf_{\text{Particle}}} \left(\frac{M_{\text{Core}}}{M_{\text{Particle}}} \right)_{\text{MP4}}} \quad (4.39)$$

By inserting the appropriate values of a , M_{Core} and M_{Particle} from Table 4-3 into equations (4.37) and (4.39) we may obtain values for the thickness of the magnetic layers as a function of VPF and number of sheets thick. See Table 4-4, Table 4-5 and Figure 4-15.

| Number of sheets | | | | | | | | | | | |
|------------------|----|----|----|-----|-----|-----|-----|-----|-----|-----|-----|
| VPF | 1 | 2 | 3 | 4 | 5 | 6 | 7 | 8 | 9 | 10 | 11 |
| 0.2 | 32 | 63 | 95 | 126 | 158 | 189 | 221 | 252 | 284 | 316 | 347 |
| 0.4 | 25 | 50 | 75 | 100 | 125 | 150 | 175 | 200 | 225 | 250 | 275 |
| 0.6 | 22 | 44 | 66 | 88 | 109 | 131 | 153 | 175 | 197 | 219 | 241 |

Table 4-4 Magnetic layer thickness (/nm) for MP3 particle model

| Number of sheets | | | | | | | | | | | |
|------------------|----|----|----|----|----|----|-----|-----|-----|-----|-----|
| VPF | 1 | 2 | 3 | 4 | 5 | 6 | 7 | 8 | 9 | 10 | 11 |
| 0.2 | 17 | 33 | 50 | 66 | 83 | 99 | 116 | 132 | 149 | 165 | 182 |
| 0.4 | 13 | 26 | 39 | 53 | 66 | 79 | 92 | 105 | 118 | 131 | 144 |
| 0.6 | 11 | 23 | 34 | 46 | 57 | 69 | 80 | 92 | 103 | 115 | 126 |

Table 4-5 Magnetic layer thickness (/nm) for MP4 particle model

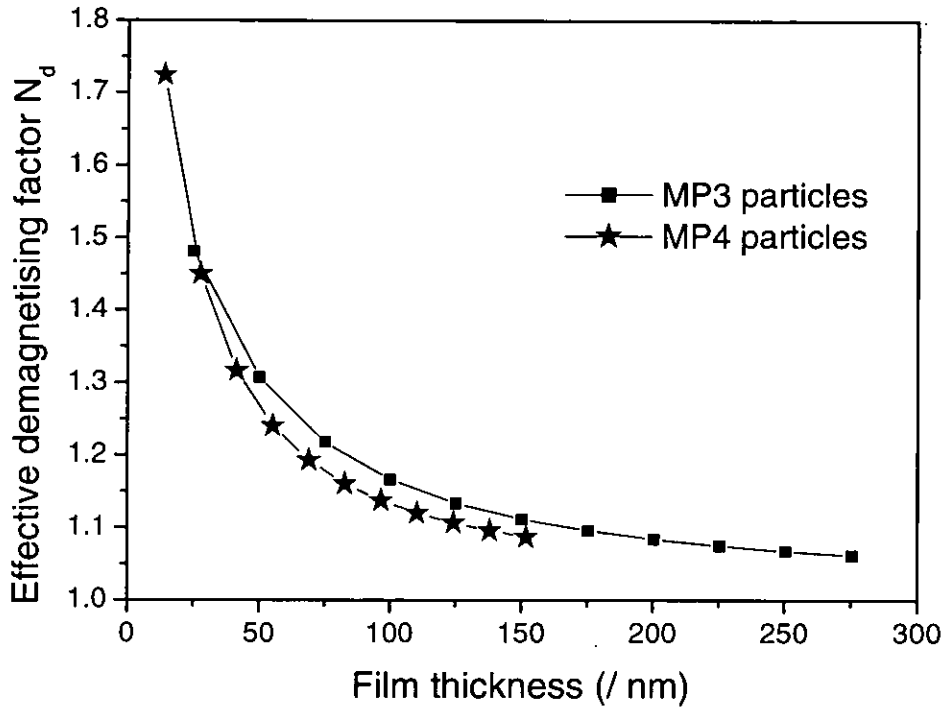


Figure 4-15 Effective N_d vs. thickness for VPF=0.4 (assumed typical)

4.6 Interpretation of model results

The model described in section 4.5 showed the error in the assumed demagnetising factor for tapes as a function of tape VPF and magnetic layer thickness. Unfortunately, the assumed demagnetising factor is used to calculate the layer thickness. Hence, in order to determine the error in the calculated thickness we must use an iterative approach.

By definition we know that the demagnetising field is given,

$$H_d = N_d M . \quad (4.40)$$

Substituting for M in equation (4.6) we obtain,

$$t = \frac{N_d \mu}{H_d A} . \quad (4.41)$$

If we now let the error in N_d (compared with the assumed value) be represented by x , equation (4.41) becomes,

$$t = \frac{N_d \mu}{H_d A} + \frac{x \mu}{H_d A} . \quad (4.42)$$

So, for a reasonably small change in N_d we can say,

$$\frac{\Delta t}{\Delta x} \approx \frac{dt}{dx} = \frac{\mu}{H_d A} \quad (4.43)$$

Hence,

$$\Delta t = \frac{\mu}{H_d A} \Delta x \quad (4.44)$$

Using equation (4.44) we can correct the thickness values presented in Table 4-2 by repeatedly adjusting t , and reading the value of x for each iteration from Figure 4-15.

4.6.1 Corrected thickness values

It was found that only three iterations were required to correct the $M_r t=3, 4$ and 4.5 sample results to the nearest nm, and the iterations for the $M_r t=3$ sample are shown in Table 4-6

| Pass number | t (/ m) | Δx | $t + \Delta t$ (/ m) |
|-------------|------------|------------|----------------------|
| 1 | 1.4962E-07 | 0.1126 | 1.6647E-07 |
| 2 | 1.665E-07 | 0.011 | 1.6812E-07 |
| 3 | 1.6812E-07 | 0.0008 | 1.6824E-07 |
| 4 | 1.6824E-07 | 0 | 1.6824E-07 |

Table 4-6 Correction of thickness iterations for $M_r t=3$

Applying the above iterative technique for the samples with $M_r t$ values of 3, 4 and 4.5 we obtain the results shown in Table 4-7.

| Tape | Uncorrected t (/m) | Corrected t (/m) | Error (%) |
|----------------|----------------------|--------------------|-----------|
| LTO $M_r t3$ | 1.496E-07 | 1.682E-07 | 12.4 |
| LTO $M_r t4$ | 2.095E-07 | 2.277E-07 | 8.7 |
| LTO $M_r t4.5$ | 2.331E-07 | 2.515E-07 | 7.9 |

Table 4-7 Thickness measurements corrected using results of model

4.7 Other magnetic methods of determining layer thickness

Although the method for determining magnetic layer thickness was developed using transverse susceptibility measurements it has been shown that various other techniques normally used to estimate the anisotropy field of a sample may also be used to determine the magnetic layer thickness [135]. All that is required is a response which can be associated with a fixed internal field value, and which is independent of the in-plane / out-of-plane orientation of the sample. By observing the applied field value of the feature in the in-plane and out-of-plane orientations we can determine the demagnetising field and hence the layer thickness as described above. Two suitable techniques are the Flanders & Shtrikman [64] torque or remanent magnetisation technique, and the determination of the closure point of the transverse hysteresis loop which can be carried out using simple VSM measurements. A co-worker at Preston, Marian Vopsaroiu, developed the extension of the Flanders & Shtrikman technique for the measurement of magnetic layer thickness. Full details of the technique and the hysteresis loop closure method are given in Bissell *et al* [135] and Vopsaroiu *et al* [67]. We would expect the accuracy of the hysteresis closure method to be less than the others due to the subjectivity of the determination of the value of the field at a loop closure. Also for Stoner-Wohlfarth particles the loop closure point would be determined by the anisotropy of those particles aligned with the applied field, therefore being influenced by differences in texture between the in-plane transverse and out-of-plane directions. In practice we find that the coercivity of MP particles is generally less than that predicted by the Stoner-Wohlfarth model, indicating that reversals of particles with easy axes parallel to the applied field are non-coherent. In this case the loop closure will be due to the switching of particles with easy axes nearly orthogonal to the applied field (see Figure 1-7) and hence, the same particles will define closure in the two measured orientations. The main advantage of the hysteresis closure measurement is that it is a fast technique, which can be made in any laboratory equipped with a VSM. A comparison of the three techniques (after Bissell *et al* [135]) is shown in Figure 4-16.

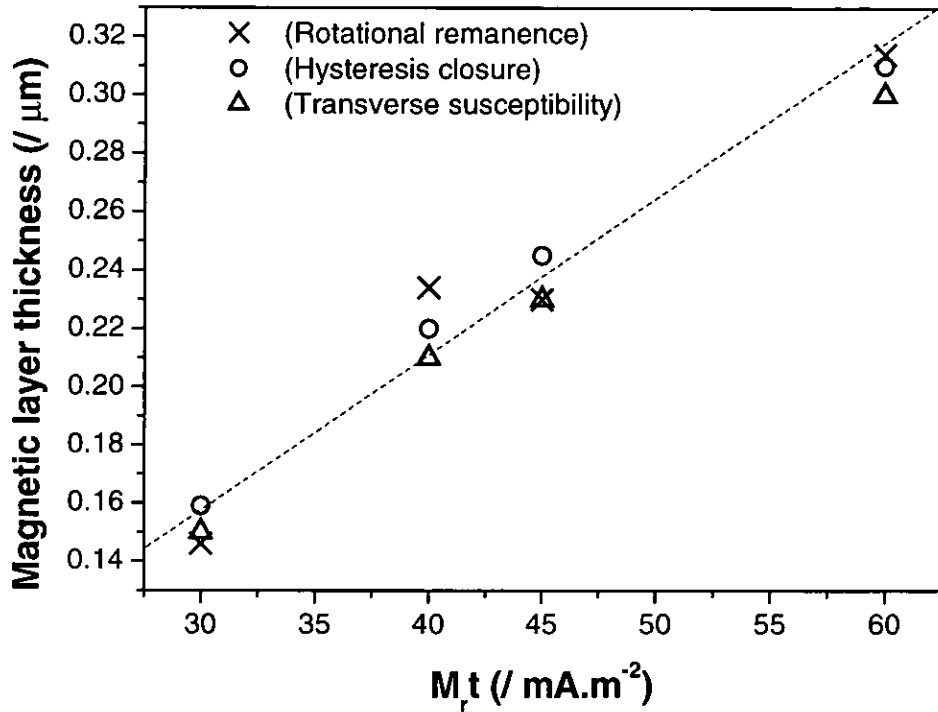


Figure 4-16 Comparison of magnetic thickness evaluation techniques after Bissell *et al*

4.8 Discussion

The determination of magnetic layer thickness for modern tape media has been demonstrated using transverse susceptibility measurements. The equivalence of stacked samples to single tape layers in determining out-of-plane susceptibility measurements has been demonstrated both theoretically and experimentally, allowing larger moment composite samples to be used for low areal-moment modern media.

A number of commercial and development metal particle tapes have been measured using the technique down to a thickness of approximately 170nm. The results have not been compared to a mechanical measurement due to the difficulty in delaminating the magnetic layer from the under-layer although previous measurements using single layer coated media showed a good agreement with mechanical measurements[108]. The results have been compared to measurements made using other magnetic methods to determine the out-of-plane demagnetising field of the samples and the results compare well (Figure 4-16).

A computer model has been developed to determine the effective demagnetising factor ratio of MP3 and MP4 particulate media as a function of magnetic layer thickness and

particle volume packing fraction. The effective factor increases as the layer becomes more dilute and as the thickness reduces with respect to the particle dimensions.

Although new generations of magnetic particles are becoming smaller this is not at the same rate as the reduction in layer thicknesses resulting in increasingly particulate layers and increasing errors in the determination of layer thickness using magnetic techniques.

The thickness values determined for the tape samples were corrected using the results of the model and assuming a typical VPF of 0.4. The error in the thickness determination ranged from 8% to 12% for the sample with the thinnest layer. The uncorrected results tended to underestimate the layer thickness.

The magnetic techniques for the determination of magnetic layer thickness are particularly useful in characterising modern media where magnetic layers cannot be delaminated and the extent of diffusion into under-layers is not known. However, care must be taken when particle size approaches that of layer thickness and models of the system are required in order to correct the result in these cases.

5 Non-linear transverse susceptibility

The non-linear transverse susceptibility was first observed in soft magnetic materials (FeSi steel) by Lütke-Stetzkamp *et al* in 1988[136]. In 1989, the theoretical paper of Chantrell *et al*[7] proposed the phenomenon as a technique for investigating the anisotropy distribution and orientational texture of magnetic recording media. However, subsequent attempts to measure the non-linear susceptibility of recording media were unsuccessful[108], probably due to the relatively small signal size.

This chapter reviews the basic theory of the non-linear transverse susceptibility and describes modifications made to the susceptometer at Preston to allow the non-linear transverse susceptibility of magnetic recording tapes and magnetic powders to be investigated. The response of the susceptometer to variation of the ac probe field was investigated and was found to be non-linear in accordance with the predictions of the theory.

Results are presented for a number of commercial recording tapes with Co- γ -Fe₂O₃ and CrO₂ based particle systems. Results are also presented for γ -Fe₂O₃, CrO₂, and metal particle powders. Attempts were made to measure metal particle tape samples but the sample moments were too low to achieve repeatable results. The results for powder samples show anisotropy peaks in all cases, even where these peaks were suppressed in the linear transverse susceptibility, such as γ -Fe₂O₃ and MP randomly oriented powders, indicating that the technique is a useful tool for determining the mean anisotropy field of systems where the peak is suppressed by texture effects in the linear transverse susceptibility.

The non-linear susceptibility plots also contained peaks associated with the particle switching which were visible in most samples independent of texture. The switching peaks were associated with reversal of particles, and comparison of the peak position with the sample coercivity gave an indication of the reversal mode of the system. An investigation of the change in the susceptibility plot as the sample easy axis was rotated within the ac / dc field plane showed large differences associated with the dominant switching mode.

5.1 Theory

The non-linear transverse susceptibility is a measurement of the same perturbation of the magnetic moment of a sample as that measured by linear transverse susceptibility. The difference between the two techniques is that in the case of non-linear transverse susceptibility the changing moment of the sample is measured in a direction parallel to the dc field direction. The effect of the magnetic fields on the particle moment is identical to that of linear transverse susceptibility (see Figure 3-4).

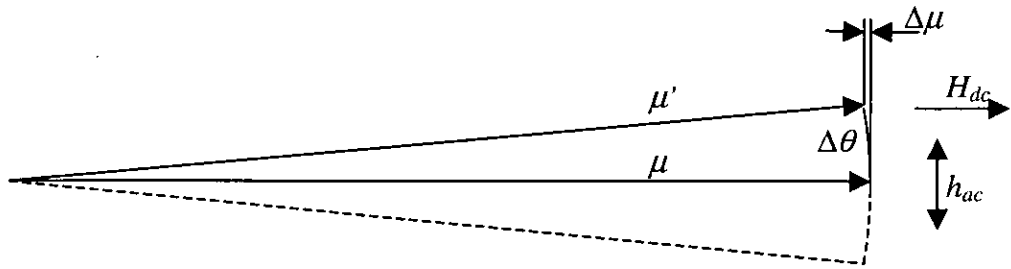


Figure 5-1 Change in moment in dc field direction due to action of ac field

In the measurement of the linear transverse susceptibility the change in moment was measured in the ac field direction at the ac probe field frequency, f_{ac} . In the case of the non-linear transverse susceptibility the changing moment is measured in the direction of the dc field ($\Delta\mu$ of Figure 5-1). Referring to Figure 5-1 we see that for each sweep direction of the magnetic moment vector, μ , the measured quantity, $\Delta\mu$, goes through a complete cycle, returning to its starting value at the end of the sweep. Each sweep direction of the magnetic moment is associated with half a cycle of the ac probe field, so for each full cycle of the ac field, $\Delta\mu$ will undergo two cycles. This gives the acquired signal a frequency of $2f_{ac}$. It is also apparent that the measured change in moment will be considerably smaller than that measured in the ac field direction for linear transverse susceptibility measurements.

The response of the non-linear transverse susceptibility, χ_{nl} , for a uniaxial Stoner-Wohlfarth particle was calculated by Chantrell *et al*[7] as,

$$\chi_{nl} = \frac{1}{2} \frac{\cos^3 \theta_M \cos^2 \phi_H}{[\cos 2(\theta_M - \psi) + h \cos \theta_M]^2}, \quad (5.1)$$

where the coordinate system was that shown in Figure 5-2.

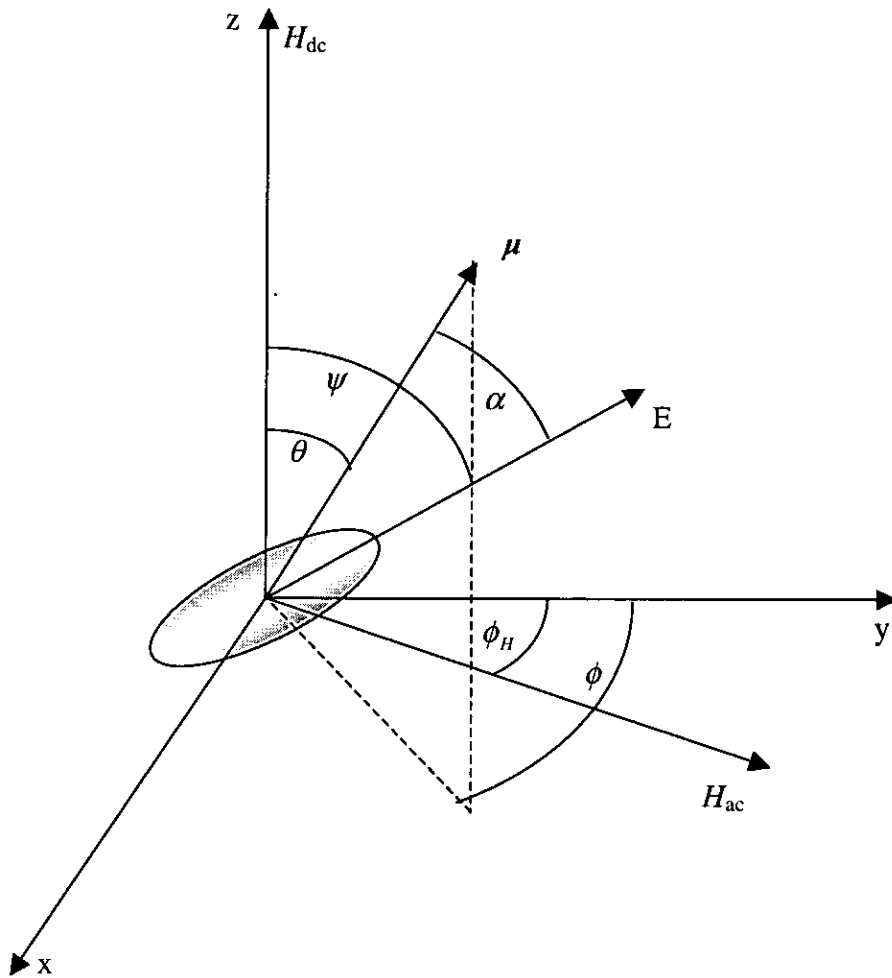


Figure 5-2 Coordinate system for particle with easy axis direction E after Chantrell *et al*[7].

The response of equation (5.1) was found to be divergent when H_{dc} was equal to the switching field of the particle, or when H_{dc} was equal to the anisotropy field of a particle with easy axis parallel to H_{ac} . In order to model the response of a system of particles the response for a single particle shown in equation (5.1) was integrated over a texture function, which simulated a Gaussian angular distribution of easy axis directions ($\sigma = 2.5^\circ$) centred on the ac field direction. The inter-particle interactions and distribution of anisotropy field values were neglected in the model. The response for the symmetrically distributed system of particles is shown in Figure 5-3 and is compared with the χ_i response calculated for the same distribution of easy axis directions. The model showed that the non-linear response had a much greater divergence at the anisotropy field,

suggesting that the peaks in the χ_{nl} response due to the anisotropy information were much less likely to be suppressed by broad texture distributions than they were in the χ_t measurements.

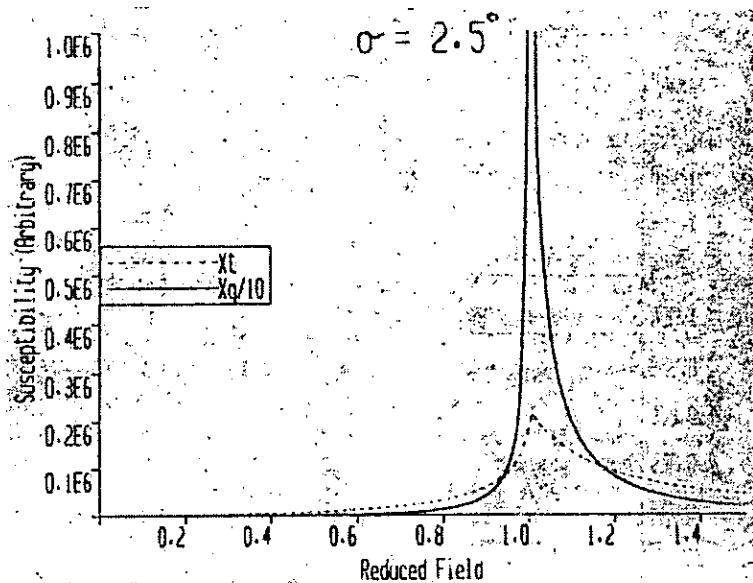


Figure 5-3 Modelled comparison of $\chi_{nl}/10$ (solid line) to χ_t (dashed line) after Chantrell *et al*[7]

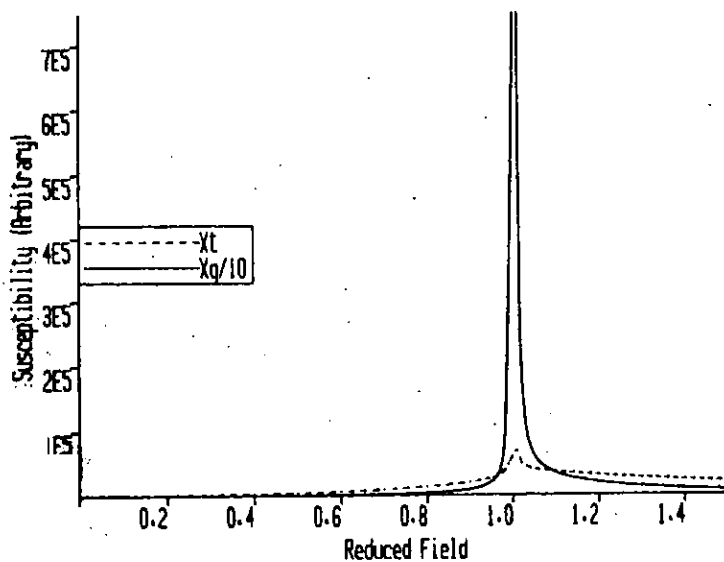


Figure 5-4 Modelled comparison of $\chi_{nl}/10$ to χ_t with texture symmetry axis at 5° to ac field after Chantrell *et al*[7]

A further integration was made with the easy axis texture distribution centre offset from the ac field direction by 5° . As both the χ_{nl} and χ_t divergent response at $h=1$ was due only to those particles with easy axes at 90° to the dc bias field, this misalignment resulted in many fewer of the particles in the system exhibiting a divergent response.

The results of the χ_{nl} and the χ_t response were again compared and are shown in Figure 5-4. The results showed that the divergence of χ_{nl} at the anisotropy field was less likely to be suppressed than that of χ_t by texture distributions and also showed that the χ_{nl} response was still very sensitive to those particles with easy axes at 90° to the bias field (previously shown for χ_t by Le Dang *et al*[97]). Given the above results it was apparent that the measurement of χ_{nl} would give a singular point detection technique for the determination of anisotropy field distributions that was less sensitive to sample texture than the χ_t determination.

5.2 Modification of susceptometer

In order to measure the χ_{nl} response of magnetic samples it was necessary to modify the transverse susceptometer to measure the changes in magnetisation in the sample in the direction of the dc field. To achieve this a new sample holder assembly was manufactured. Mechanically the new sample holder was identical to the existing component, locating in the centre of the ac solenoid former. In place of the coaxial sense coil described in section 2.3.3 a single 300 turn formerless coil was manufactured with the same core dimensions as the coaxial assembly. The coil was attached to the sample holder rod with the coil axis parallel to the dc field direction. The arrangement is shown in Figure 5-5.

As the measured signal was at a frequency of $2f_{ac}$ it was reasoned that the compensation coil would not be required as any component of the signal directly induced by the ac field would be at f_{ac} and would be removed by the lock-in amplifier. In practice the signal induced at f_{ac} was large enough to saturate the lock-in amplifier, so a 20 turn compensating coil coaxial with the ac solenoid (see Figure 5-5) was used to minimise the induced signal.

In order to set the lock-in amplifier phase a nickel sample was inserted into the sense coil and the phase was adjusted to maximise the signal at $H_{dc}=0$. It was not possible to match the required signal phase to the phase of the ac probe field due to their different frequencies and it was known from standard χ_t measurements that soft magnetic materials such as nickel had a very strong signal at $H_{dc}=0$.

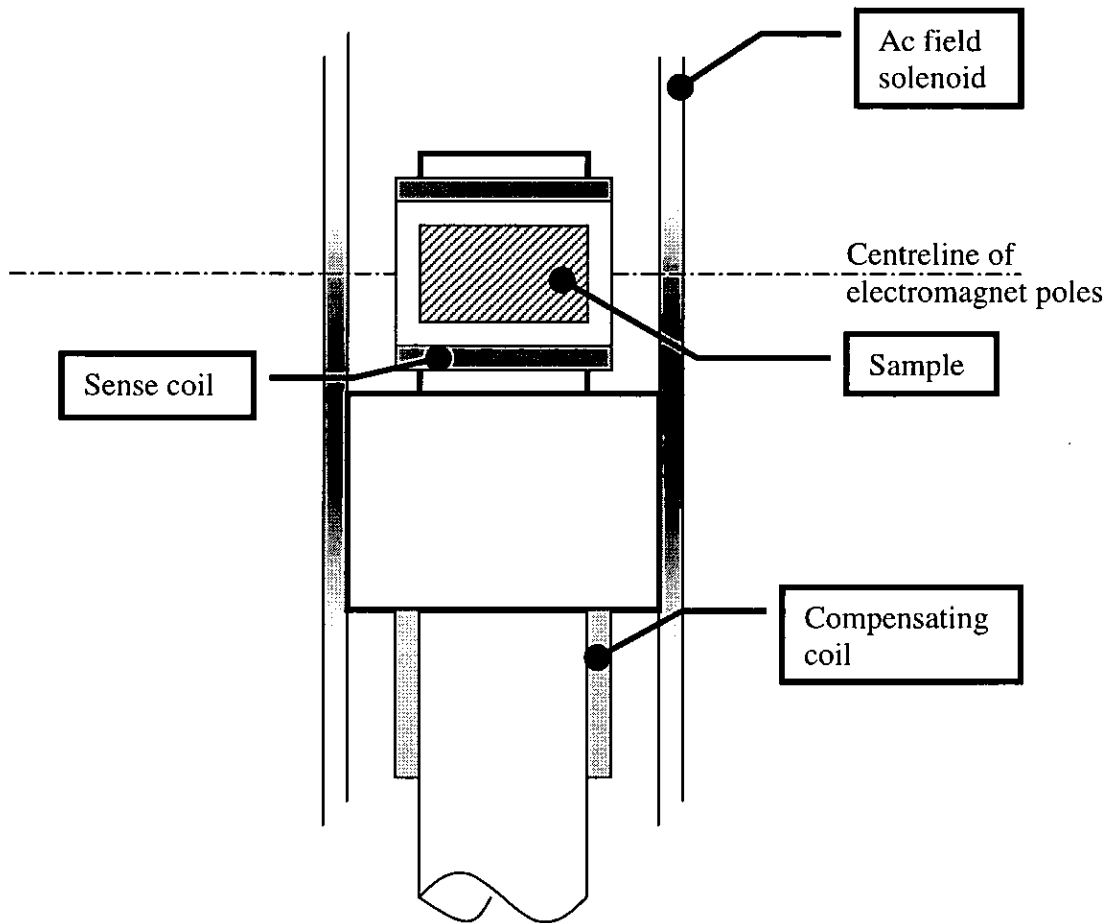


Figure 5-5 Sensing and compensating coil layout for χ_{nl} measurement

5.3 Response to variation of ac field

Using the same approach as for linear transverse susceptibility in section 3.3, we may suppose that for a small perturbing field ($\Delta h_{ac} \rightarrow 0$) with the dc field constant, the displacement angle, $\Delta\theta$, (shown in Figure 3-4) will be proportional to Δh_{ac} , such that,

$$\Delta\theta = k_1 \Delta h_{ac}, \quad (5.2)$$

where k_1 is a constant.

The change in magnetic moment, $\Delta\mu$, measured in the dc field direction is given by,

$$\begin{aligned} \Delta\mu &= \mu - \mu \cos \Delta\theta \\ \Delta\mu &= \mu (1 - \cos \Delta\theta) \end{aligned} \quad (5.3)$$

(see Figure 5-1).

From the series expansion of $\cos\Delta\theta$,

$$\cos \Delta\theta = 1 - \frac{(\Delta\theta)^2}{2!} + \frac{(\Delta\theta)^4}{4!} - \frac{(\Delta\theta)^6}{6!} \dots, \quad (5.4)$$

we can approximate $\cos\theta$ for a small angle as $1 - (\Delta\theta)^2/2!$. Hence, the change in moment becomes,

$$\begin{aligned} \Delta\mu &= \mu \left(1 - \left[1 - \frac{(\Delta\theta)^2}{2} \right] \right), \\ \Delta\mu &= \frac{\mu}{2} (\Delta\theta)^2. \end{aligned} \quad (5.5)$$

Substituting from equation (5.2) we obtain,

$$\begin{aligned} \Delta\mu &= \frac{\mu}{2} (k_1 \Delta h_{ac})^2, \\ \Delta\mu &= k_1^2 \Delta h_{ac}^2. \end{aligned} \quad (5.6)$$

Where k_1^2 is constant.

From equation (5.6), the susceptometer coil output for a sample with a constant applied dc field should be proportional to Δh_{ac}^2 . In order to test the predicted response the dc bias field was set to the anisotropy peak value of a control sample and the ac probe field was varied. The measured response for the sample as a function of the solenoid current is shown in Figure 5-6. The correlation between the measurements and the quadratic least squares fit was very high with a Pearson's correlation coefficient of $r > 0.999$.

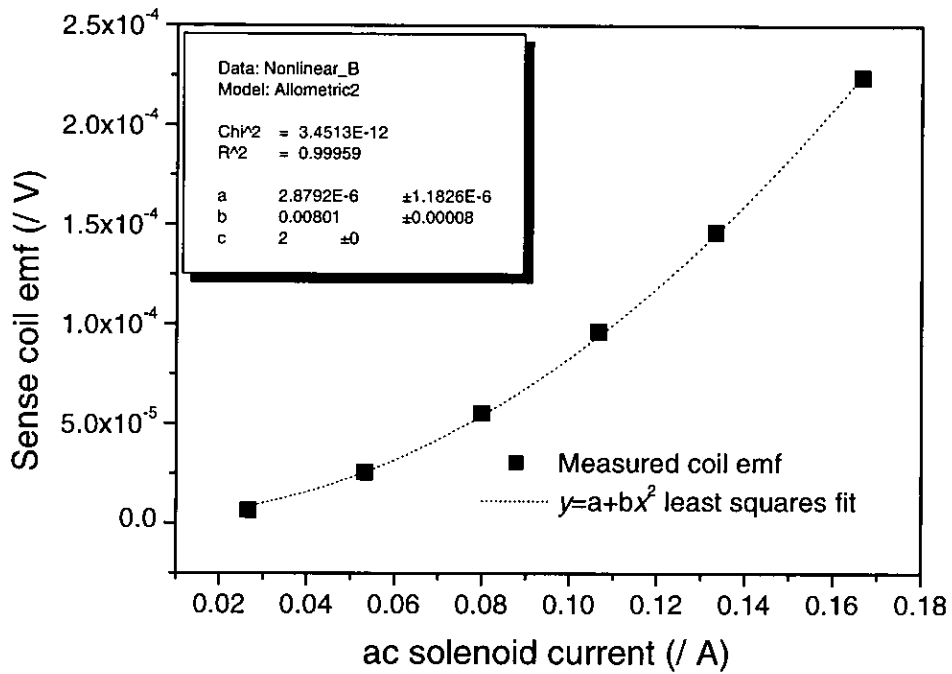


Figure 5-6 χ_q sense coil voltage as a function of ac solenoid current

5.4 Investigation of tape and powder samples

χ_{nl} investigations were made on a number of magnetic recording tape and magnetic particle powder samples. The samples used were the same as those investigated in chapter 3 and again the samples were positioned with the sample plane parallel to the ac / dc field plane to minimise the error due to sample demagnetising fields. In the investigation of the metal-particle powders the geometry of the sense coil (see Figure 5-5) allowed the samples to be arranged with their long axes parallel to the dc field direction, which also minimised the error due to demagnetising fields for these samples. It is likely, however, that the anisotropy peak values for these samples were inflated due to their relatively low aspect ratio (approximately 5:1) which, if we assume that the cylindrical sample was approximated by a prolate spheroid, would have a demagnetising factor of approximately 0.06[132] ($\cong 0.06 / 4\pi$ for cgs system).

A comparison of the χ_{nl} and the χ_t plots for the same (CrO_2 TK50 data tape) sample is shown in Figure 5-7. A number of tape samples were investigated using the new arrangement. The plots showed two peaks (A,B) [Figure 5-7] and one trough (C) for the positive to negative field sweep direction and two troughs (C,D) and one peak (A) for the negative to positive field sweep direction. The sense of the curve was reversed for

the reverse sweep direction, giving the plots second order rotational symmetry rather than the line symmetry of the χ_t plots. Considering the positive to negative sweep direction, the first peak (A) occurred in the positive field at a relatively high field value and the second peak (B) occurred in the negative branch at a lower absolute field value. The trough (C) was an inversion of the first peak in the negative field. The higher-field peak and the trough (A and C) were attributed to the anisotropy field effects of those particles aligned with the ac field, whilst the peak at the lower reversed field (B) was attributed to the switching field effects of particles with easy axes not aligned with the ac field. See section 3.2 for a discussion of the physical origin of anisotropy and switching peaks.

According to theory the χ_{nl} anisotropy peak is divergent even when a distribution of easy axis directions is applied (compared with the theoretical cusp of χ_t , see Figure 5-3 and Figure 5-4).

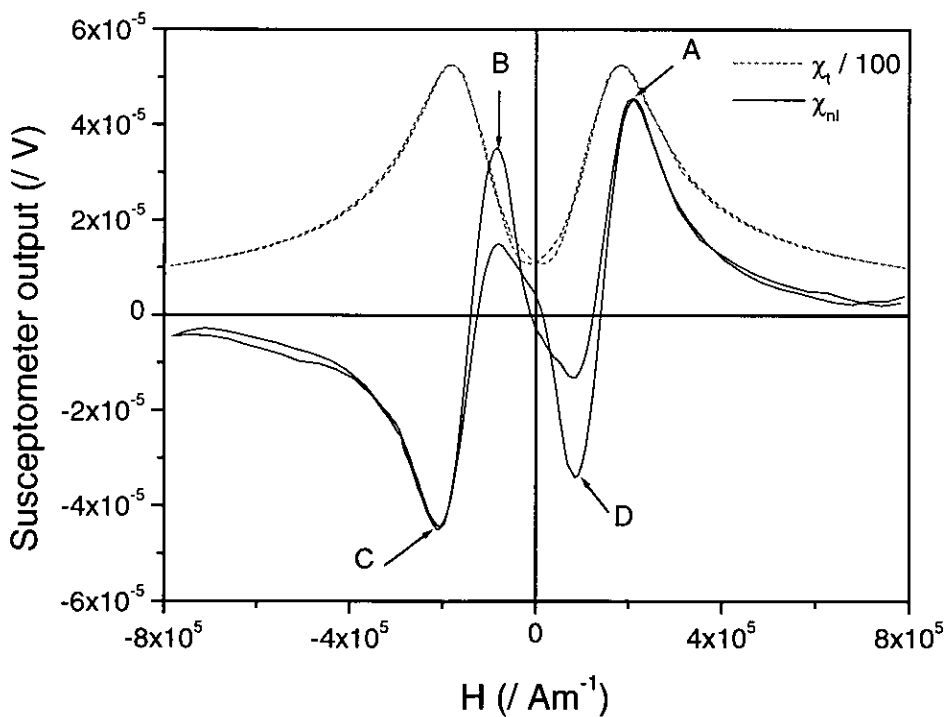


Figure-5-7 Comparison of χ_t and χ_{nl} plots for CrO₂ TK50 data tape

The measured anisotropy peaks are clearly not divergent. However, the effects of thermal activation, inter-particle interaction and a distribution of anisotropy field values were not taken into account in the model.

The effect of thermal activation would be to cause thermal switching between the two minima just before they merged at $h=1$ (see Figure 1-5). If the barrier were sufficiently small compared to the thermal energy the relaxation time would be low allowing reversible switching in phase with the ac signal and thus contributing to the output signal. A larger barrier compared to the thermal energy would result in the relaxation time increasing and this is the process by which the imaginary χ_t response occurs (see section 3.7). The thermal energy of particles within a system is not constant (following a Boltzmann distribution) so there would be a distribution of fields at which particles started to reverse below the anisotropy field value, which would contribute to some spreading of the anisotropy peak.

The effect of inter-particle interactions on the anisotropy response of the system is difficult to quantify. Particles in particulate recording media are not generally considered to be in close enough contact for 'exchange' interactions to be significant so the primary interactions would be magnetostatic, causing variations in the local applied field due to the effect of neighbouring particles. Such interactions are highly dependent on the physical dispersion and texture of the magnetic particles. The general effect of such interactions is to cause a spreading of the anisotropy peak as individual particles within the system are subject to a distribution of local fields, which modify the applied field value.

Probably the most significant factor omitted from the model of Chantrell *et al* is a distribution of anisotropy field values. The model used a single anisotropy field value for all particles resulting in a divergence at the anisotropy field in χ_{nl} and a cusp in χ_t . Previous work by Hoare *et al*[113] has shown that the application of an anisotropy distribution to the theoretical χ_t response results in a broader rounded peak very similar in form to that observed experimentally. It may be that in a similar way the χ_{nl} anisotropy peak shape is largely due to the distribution of particle anisotropy fields within the sample. If this is the case, and the thermal activation and inter-particle interaction effects are sufficiently small, we would expect the peak to be a direct measurement of the anisotropy field distribution, as theory indicates that the χ_{nl}

response remains divergent even for a textured system. This implies that the difficult deconvolution required to obtain the anisotropy distribution from χ_t plots may not be required in the case of χ_{nl} .

Comparison of the plots in Figure 5-7 shows that the χ_{nl} anisotropy peak is considerably narrower than the χ_t peak which is consistent with the proposition that the χ_{nl} response is less susceptible to broadening by texture effects. This accounts for the anisotropy peak in the χ_{nl} response being at a slightly higher field value, as we would expect the peak value in the χ_t response to be depressed for all but perfectly aligned systems. We also find that the switching peaks are greatly enhanced in the χ_{nl} plot compared to the χ_t plot where only a slight hysteresis effect is observed rather than peaks.

One feature of the χ_{nl} curve which is different from theory was the inversion of the signal for the reverse field-sweep direction. This effect is easily explained by the reversal of the moments relative to the direction of measurement of the susceptibility, which does not occur in χ_t where the susceptibility is measured at 90° to the dc bias field. The change in sense of the χ_{nl} signal when the moment switches is explained by reference to Figure 5-8.

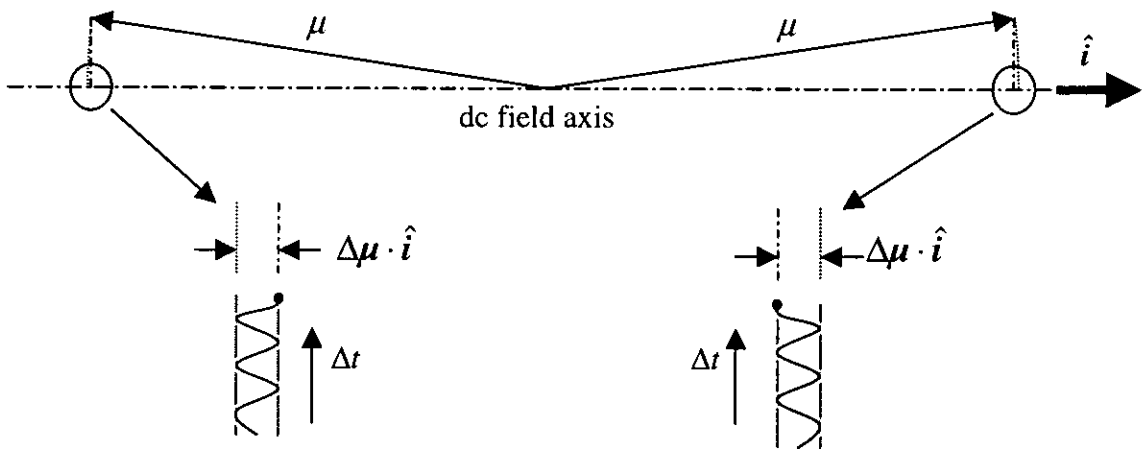


Figure 5-8 Phase change in measurement with moment switching

If we take the unit vector \hat{i} to be the direction in which we measure the change in moment of the sample, and also to be parallel to the dc field, the change in moment we are measuring is given by $\Delta\mu \cdot \hat{i}$. We can think of this as the locus of the intersect between the dc field axis line and a line normal to it which passes through the tip of the moment vector, μ . If we plot the locus against time for the moment parallel and anti-

parallel to \hat{i} we find that they are in anti-phase (see Figure 5-8). Thus, when moments are switched into the opposite direction from that to which the lock-in amplifier phase was set, the output becomes negative.

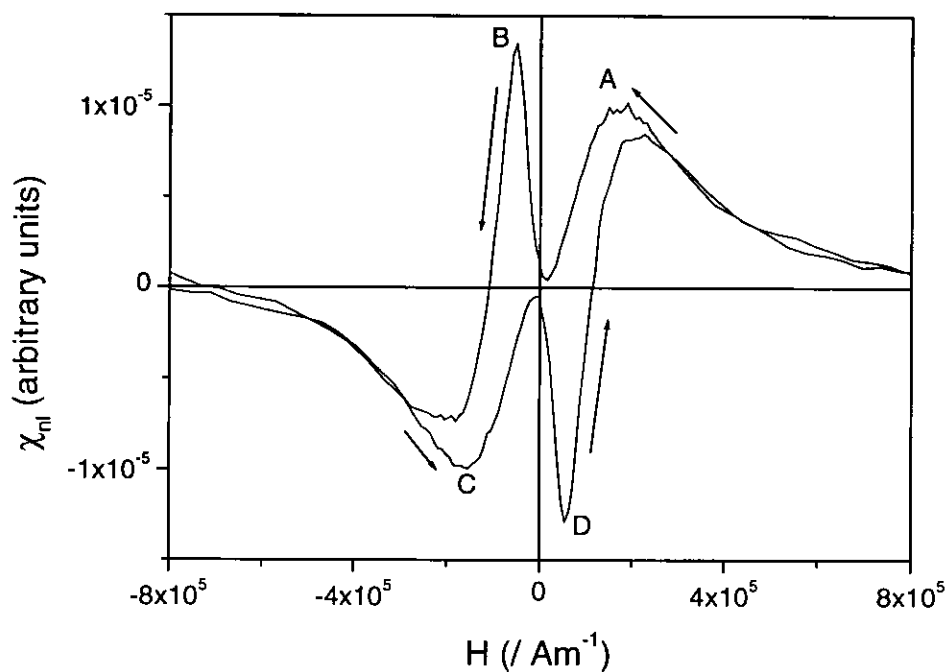


Figure 5-9 Co- γ -Fe₂O₃ commercial VHS tape χ_{nl} plot

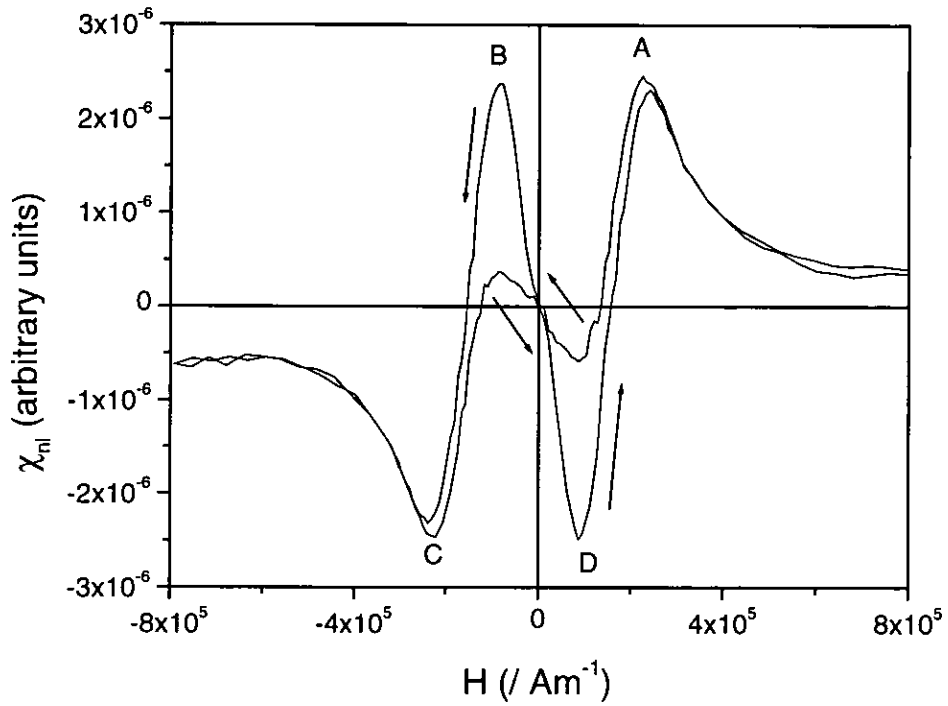


Figure 5-10 Mixed $\gamma\text{-Fe}_2\text{O}_3 / \text{CrO}_2$ commercial VHS tape χ_{nl} plot

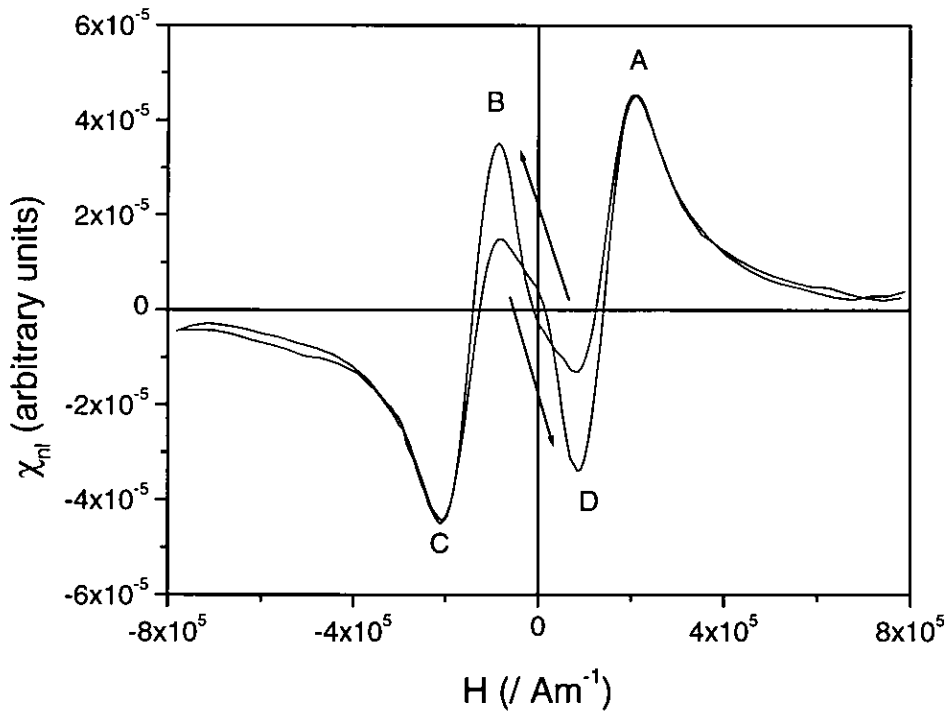


Figure 5-11 Commercial CrO_2 TK50 data tape χ_{nl} plot

Susceptibility plots for a Co- $\gamma\text{-Fe}_2\text{O}_3$ tape system, a mixed $\gamma\text{-Fe}_2\text{O}_3 / \text{CrO}_2$ tape system and a pure CrO_2 tape system are shown in Figure 5-9, Figure 5-10 and Figure 5-11

respectively. The plots of the three tape samples are all similar in their main features each showing two peaks associated with the anisotropy information (peaks A and C) and a peak associated with the switching information (peaks B and D) in each sweep direction. However, the relative height and sharpness of the peaks differed between the samples. The Co- γ -Fe₂O₃ VHS sample (Figure 5-9) had a broad anisotropy peak and a very sharp 'switching' peak. The switching peak susceptibility was higher than the anisotropy peak and the irreversible part of the curve extended from zero to beyond the peak anisotropy value in both field directions, indicating some overlap between the switching field and anisotropy distributions. The mixed γ -Fe₂O₃ / CrO₂ VHS sample had a narrower anisotropy peak and a broader switching peak which were both of a similar height. In this case the irreversible part of the curve only just extended beyond the anisotropy peaks indicating a greater separation of the switching and anisotropy field distributions. The CrO₂ sample plot was similar to that of the mixed sample in terms of peak widths but the anisotropy peak susceptibility was this time higher than that of the switching peak and the irreversible loop closed below the anisotropy peak, suggesting greater separation of the anisotropy and switching field distributions.

| Sample | $H_k(\chi_{nl})$ peak (/ kAm⁻¹) | $H_k(\chi_t)$ peak (/ kAm⁻¹) | Switching(χ_{nl}) peak (/ kAm⁻¹) | $H_c(\text{trans})^*$ (/ kAm⁻¹) |
|--|--|---|--|--|
| Co-γ-Fe₂O₃ | 171 | 125 | 53.5 | 40.0 |
| Mixed γ-Fe₂O₃ / CrO₂ | 227 | 200 | 85.7 | 38.3 |
| CrO₂ | 208 | 183 | 87.5 | 33.5 |

*(H_c transverse to play direction, VSM sweep rate = 3.1kAm⁻¹s⁻¹, Maximum field 560kAm⁻¹)

Table 5-1 Comparison of χ_{nl} peak values with χ_t peaks and VSM measurements

Comparing the χ_{nl} peak values with the values of the χ_t peaks and the transverse coercivity of the samples we find a number of differences (see Table 5-1). The H_k peaks in the χ_{nl} plots are at higher fields than those in the χ_t plots. This is consistent with the observation that the χ_t anisotropy peaks are shifted to lower fields as the easy axis

distribution widens[75,120] and with the theoretical prediction that the χ_{nl} anisotropy response is less influenced by such texture distributions than that of the χ_t [7]. Comparing the switching peak value with the transverse coercivity we find that the field values are very different with the χ_{nl} peak occurring at a significantly higher field than the coercivity. The CrO_2 and mixed $\gamma\text{-Fe}_2\text{O}_3 / \text{CrO}_2$ samples in particular have χ_{nl} peaks at approximately double the coercive field. This suggests that the χ_{nl} response at the switching field is not equal for all of the particles within these samples. We may expect the χ_{nl} response at the switching field to differ according to the switching angle, θ_c , (see section 1.5.1) with respect to the ac field, but this would give a similar deviation of the switching peak for all samples with a similar orientational texture which is not the case. The theoretical formulation of the χ_{nl} and χ_t response assumes that particles reverse in a coherent, Stoner-Wohlfarth, manner. However, by means of a simple thought experiment we can see that particles reversing by non-coherent means will have a lower total moment and hence a lower transverse susceptibility response than those reversing coherently. This sensitivity of transverse susceptibility to particles reversing coherently may explain why the switching peak in χ_{nl} is so much higher than the coercivity for certain classes of particle systems. Where a distribution of easy axis directions exists it is often energetically favourable for those particles with low switching angles with respect to the applied field to reverse incoherently. This is because flux closures can be achieved within the particle during switching without moments directly opposing the applied field. As the switching angle increases incoherent reversal mechanisms require a fraction of the particle moment to directly oppose the applied field so coherent reversal becomes more energetically favourable. The result of this is that coherent reversal is favoured by particles with large switching angles (i.e. θ_c close to 90° or 270°). Reference to Figure 1-7 shows that these high switching angles also have a high switching field so a measurement technique which is weighted in favour of coherent reversals will tend to be skewed towards the high side of the switching field distribution.

Another feature of the χ_{nl} plots of the systems containing CrO_2 particles is the area of negative χ_{nl} in the first branch of the curve as the field is decreased from saturation to zero. The negative signals in the curve increasing from negative saturation are easily explained in terms of reversed particles which give a negative χ_{nl} response. However, in

the region from positive saturation to zero field we would not expect any switching, so we would not expect any of the particles to give a negative signal. The implication of the negative signal is either that particles have switched into the negative direction, or that the particle moments are moving in anti-phase to the ac field. Neither of these propositions seems to be physically likely and these effects may be due to non-coherent rotations and inter-particle interaction effects which are neglected by the existing theory. Further theoretical study is required in this area to determine the implications of different switching modes, interactions and thermal relaxation / phase lag effects on the transverse susceptibility.

5.4.1 Powders

χ_{nl} measurements were made of $\gamma\text{-Fe}_2\text{O}_3$ powder (non cobalt modified), CrO_2 powder and the four metal particle powder samples described in section 3.5 with the characteristics shown in Table 3-5.

The $\gamma\text{-Fe}_2\text{O}_3$ and the CrO_2 plots are shown in Figure 5-12 and Figure 5-13 respectively. Anisotropy peaks (A and C) and switching peaks (B and D) are evident on both of the plots. As with the tape samples the switching peak is the larger in the $\gamma\text{-Fe}_2\text{O}_3$ system whereas the anisotropy peak is the larger in the CrO_2 system. Comparing the plots with the χ_t plots for the same samples, Figure 3-12 and Figure 3-14, we can see that the anisotropy peaks which were suppressed on the $\gamma\text{-Fe}_2\text{O}_3$ χ_t plot are clearly resolved in the χ_{nl} plot of the sample.

| Powder sample | $H_k(\chi_{nl})$ peak (/ kAm^{-1}) | $H_k(\chi_t)$ peak (/ kAm^{-1}) | Switching(χ_{nl}) peak (/ kAm^{-1}) |
|--------------------------------|--|---|--|
| $\gamma\text{-Fe}_2\text{O}_3$ | 97 | - | 19.8 |
| CrO_2 | 219 | 178.15 | 22.5 |

Table 5-2 Comparison of anisotropy and switching peak values for $\gamma\text{-Fe}_2\text{O}_3$ and CrO_2 powders

The comparisons between the χ_{nl} and χ_t anisotropy peak values and the χ_{nl} switching peak values are shown in Table 5-2. Again, the χ_{nl} anisotropy peak is at a higher field than the χ_t peak for the same sample. Conclusions cannot be drawn from a comparison between the tape and powder samples as the powders are not from the same source as

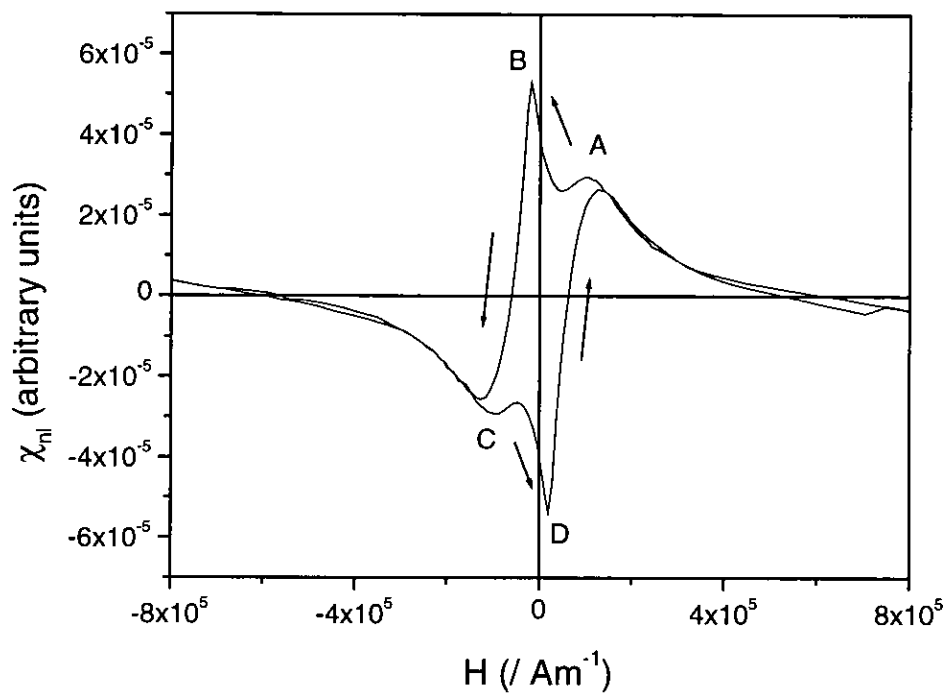


Figure 5-12 $\gamma\text{Fe}_2\text{O}_3$ powder χ_{nl} plot

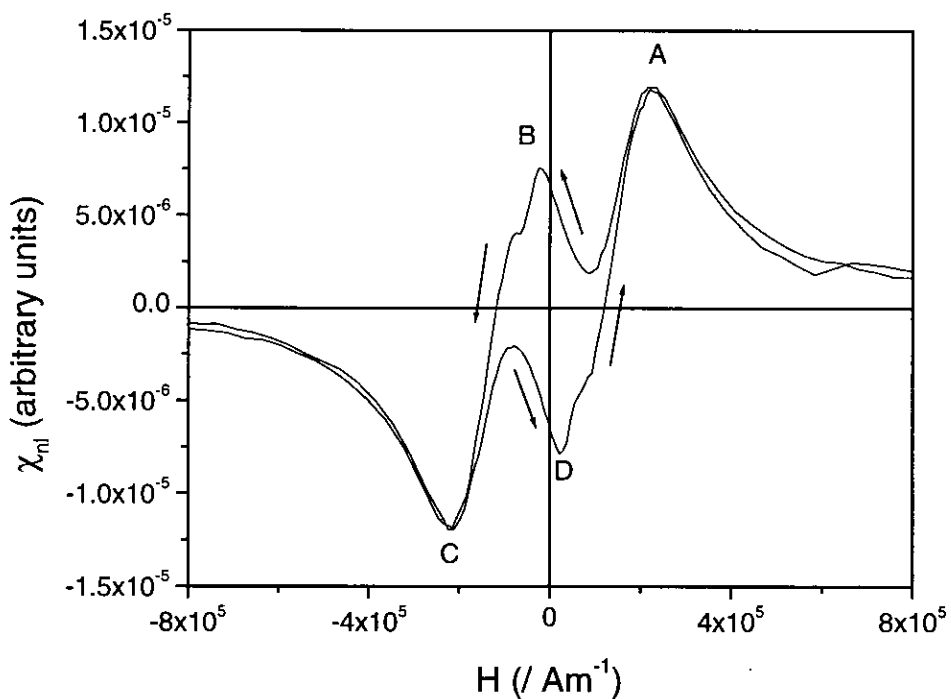


Figure 5-13 CrO_2 powder χ_{nl} plot

those used to manufacture the tape and will differ in anisotropy, shape and volume distribution. The MP powder sample plots are shown in Figure 5-14, Figure 5-15, Figure

5-16 and Figure 5-17. The measurement of the MP powder samples required a change in the sensing coil arrangement of the susceptometer as the samples would not fit into the flat coils which were designed so that small samples of tape filled the core of the sense coil. The cylindrical coils used for MP powders had to be made with a greater number of turns to give them the necessary mechanical strength to support themselves. The result of this was that the system was more susceptible to external electrical noise and drift than the normal arrangement.

All of the χ_{nl} plots for the MP powder samples showed both anisotropy peaks (A and C) and switching peaks (B and D) although the switching peak of sample 2 was not well defined. The relative amplitudes and shapes of the peaks varied widely. The χ_t plots of the same samples did not show any anisotropy peak information and it seemed likely that χ_{nl} plots would allow anisotropy information to be observed in all the cases where it was normally suppressed in the χ_t response.

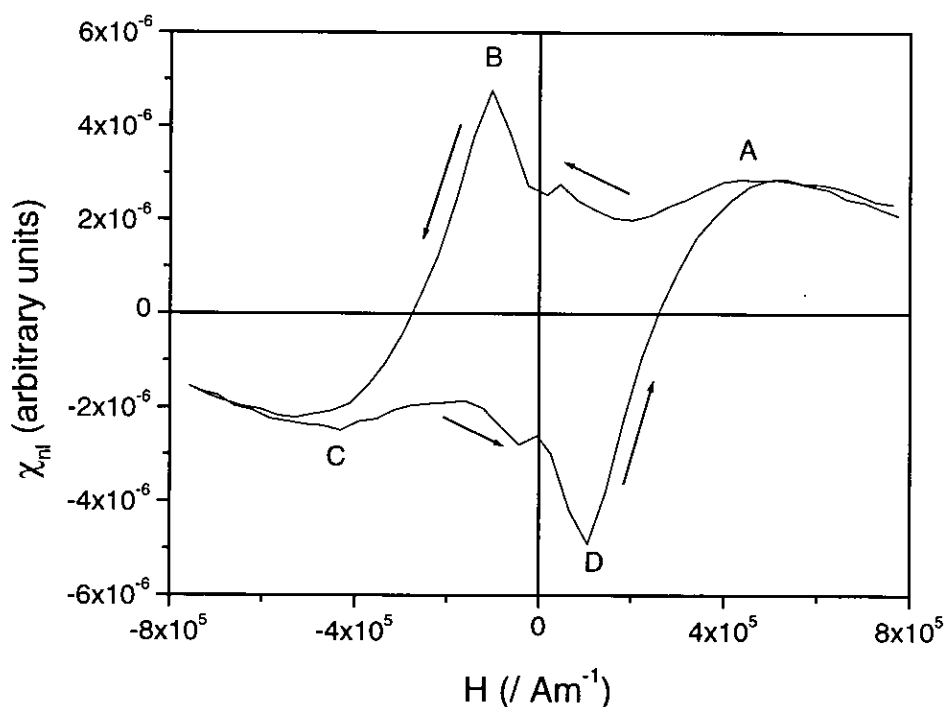


Figure 5-14 MP powder sample 1 χ_{nl} plot

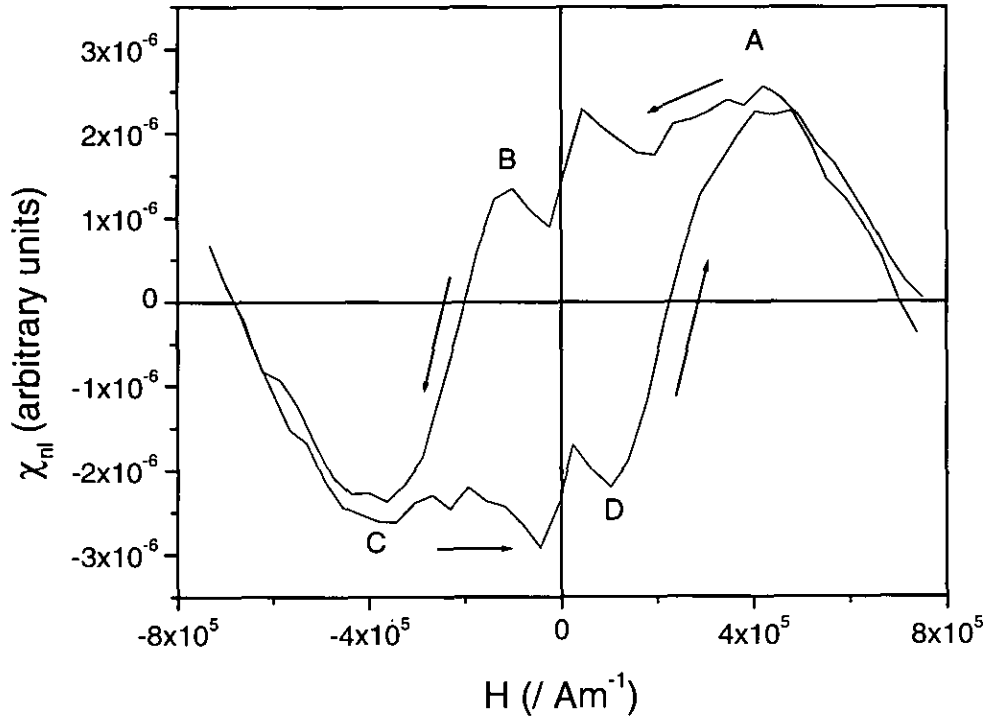


Figure 5-15 MP powder sample 2 χ_{nl} plot

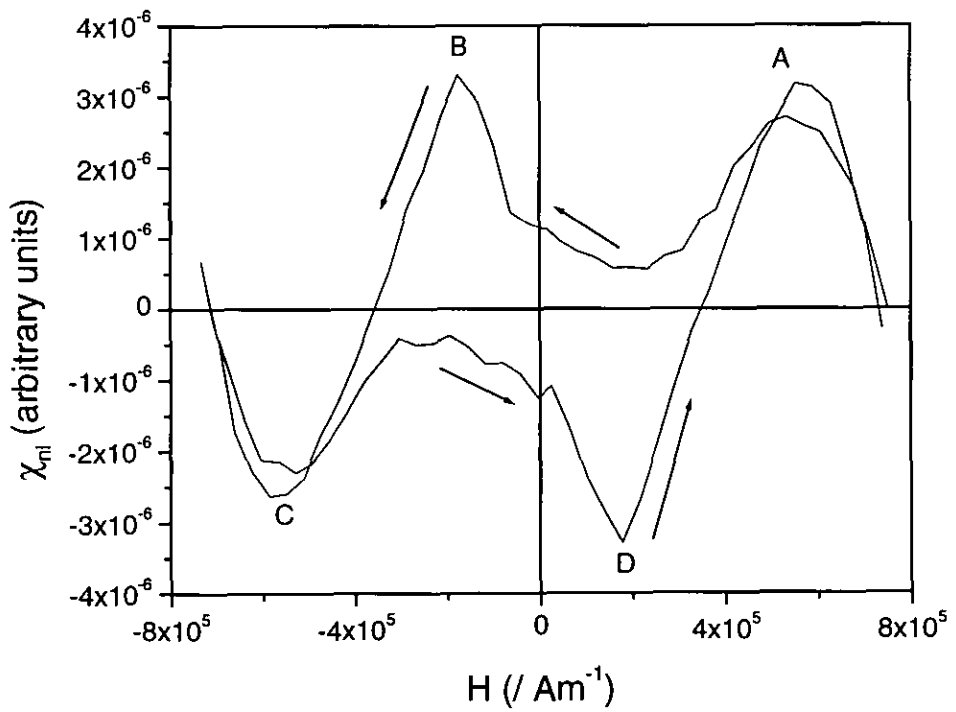


Figure 5-16 MP powder sample 3 χ_{nl} plot

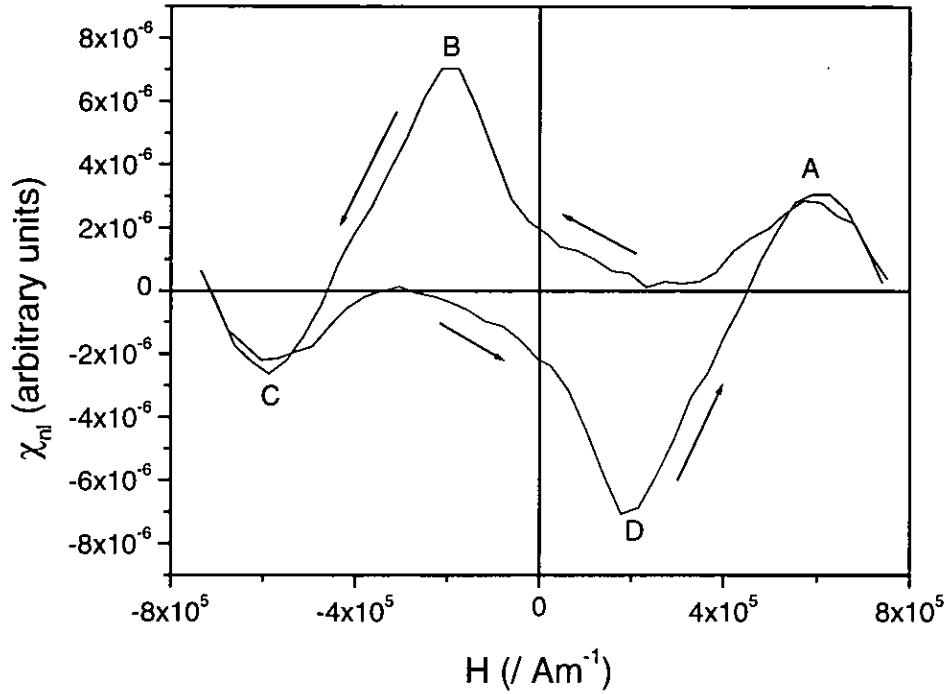


Figure 5-17 MP powder sample 4 χ_{nl} plot

| MP powder sample | $H_k(\chi_{nl})$ peak (/ kAm ⁻¹) | Switching(χ_{nl}) peak (/ kAm ⁻¹) | H_c^* (/ kAm ⁻¹) | $H_c / H_k(\chi_q)$ | SFD* (/ kAm ⁻¹) |
|------------------|--|--|--------------------------------|---------------------|-----------------------------|
| 1 | 441 | 106 | 109 | 0.25 | 111 |
| 2 | 386 | 102 | 130 | 0.34 | 171 |
| 3 | 530 | 176 | 171 | 0.32 | 157 |
| 4 | 587 | 195 | 183 | 0.31 | 151 |

* (From Table 3-5)

Table 5-3 χ_{nl} peak positions of metal particle powder samples

Table 5-1 shows the peak positions in the χ_{nl} plots and the measured coercivity and switching field distribution of the MP samples. Looking at the results in Table 5-3 the three switching peaks for samples 1, 3 and 4 are in good agreement with the measured sample coercivities. The switching peak for sample 2 is approximately 25% lower than the measured coercivity. The height of the switching peak in sample 2 is also very low relative to the anisotropy peak when compared with the other three samples. It may be that the switching peak in sample 2 is suppressed due to the wide switching field distribution of this sample broadening the peak although we would expect the switching

peak of sample 1 to be very pronounced if this were the case as this sample has a much smaller SFD than the others.

In order to investigate further the switching component of the response the curves in opposite sweep directions were subtracted from one another to remove the reversible components.

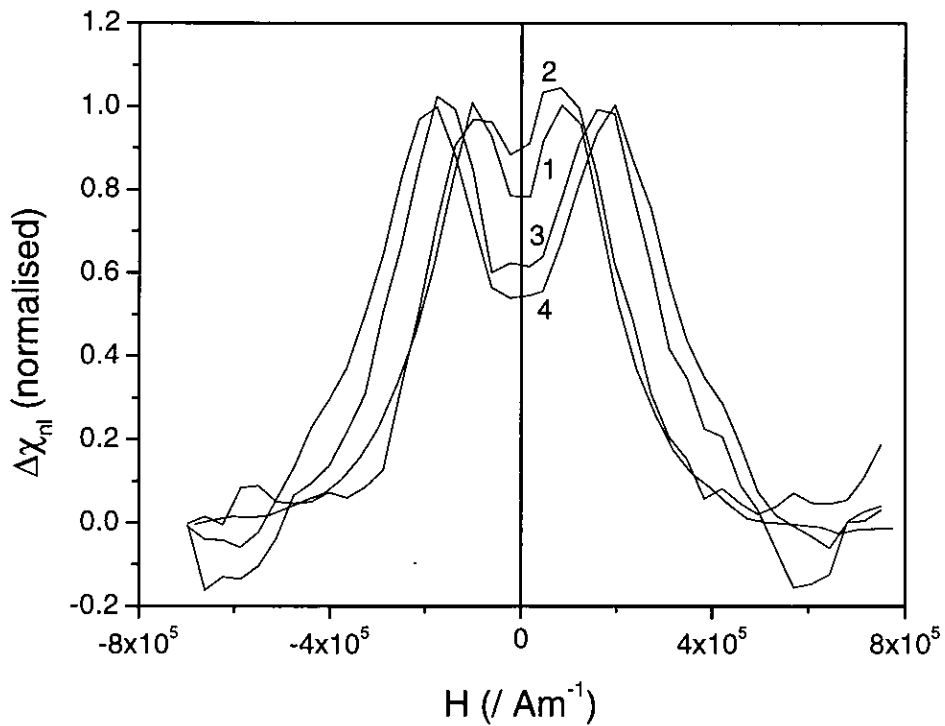


Figure 5-18 χ_{nl} difference curves for MP powder samples showing irreversible response

Figure 5-18 shows the difference in χ_{nl} response between the two field sweep directions for the MP powder samples. The samples appear to split into two groups with similar shaped difference curves, samples 1 and 2 forming one group and samples 3 and 4 forming the other. The similarity of the difference curves for samples 1 and 2 is surprising given the lack of obvious similarity in the χ_{nl} plots and suggests that there are underlying reversible features also present in the plot which may obscure the switching information. The difference curves prepared in the same way from χ_t measurements show no obvious differences between the four samples (see Figure 5-19).

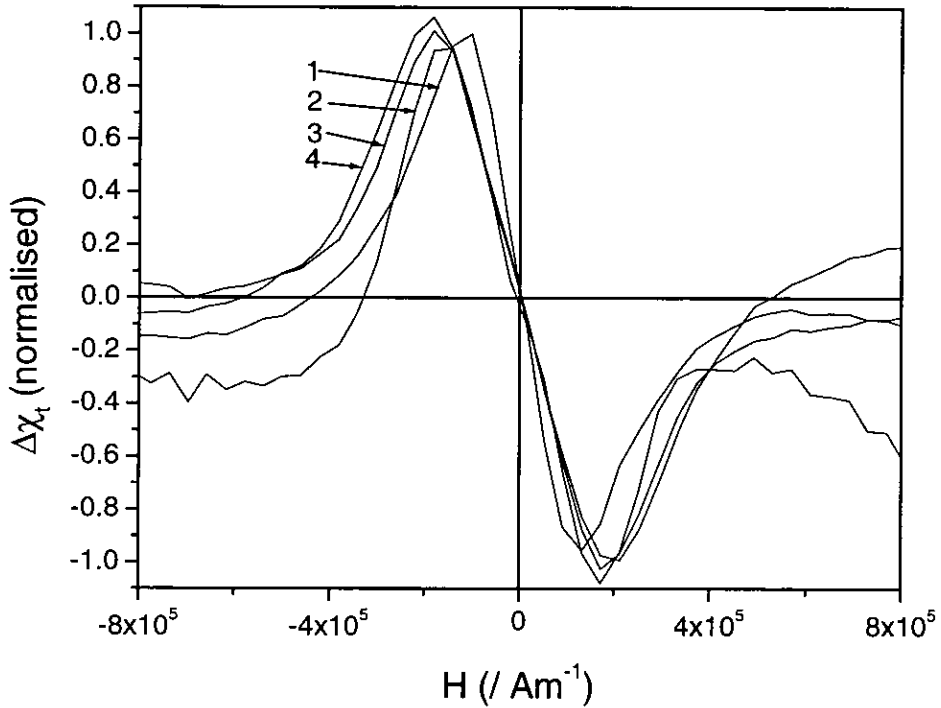


Figure 5-19 χ_t difference curves for MP powder samples showing irreversible response

In order to investigate the reversible features of the χ_{nl} curve the mean curve for both sweep directions was also produced. By taking the mean we reduce the features due to switching whilst leaving the reversible features intact. Figure 5-20 is a sketch of a mean χ_{nl} curve (solid line) for an idealised sample, with the underlying reversible anisotropy peaks and irreversible switching peaks shown dashed.

The mean χ_{nl} curves for samples 1, 3 and 4 are shown in Figure 5-20 and these curves are similar to the idealised form shown in Figure 5-20. The features of these χ_{nl} curves can be explained fully as the sum of appropriate anisotropy and switching peaks.

The mean χ_{nl} plot of sample 2 is shown in Figure 5-22. This curve does not have the expected form shown in Figure 5-20. As the field approaches zero from the anisotropy peak we would expect the mean susceptibility plot to change sign as the switching component becomes dominant but instead the curve rises to form a small peak at low field in the same sense as the anisotropy peak. The difference plot of this sample (see Figure 5-18) indicates that the switching peaks are present and normal in shape, which suggests that some other reversible effect is responsible for the extra peaks in this sample.

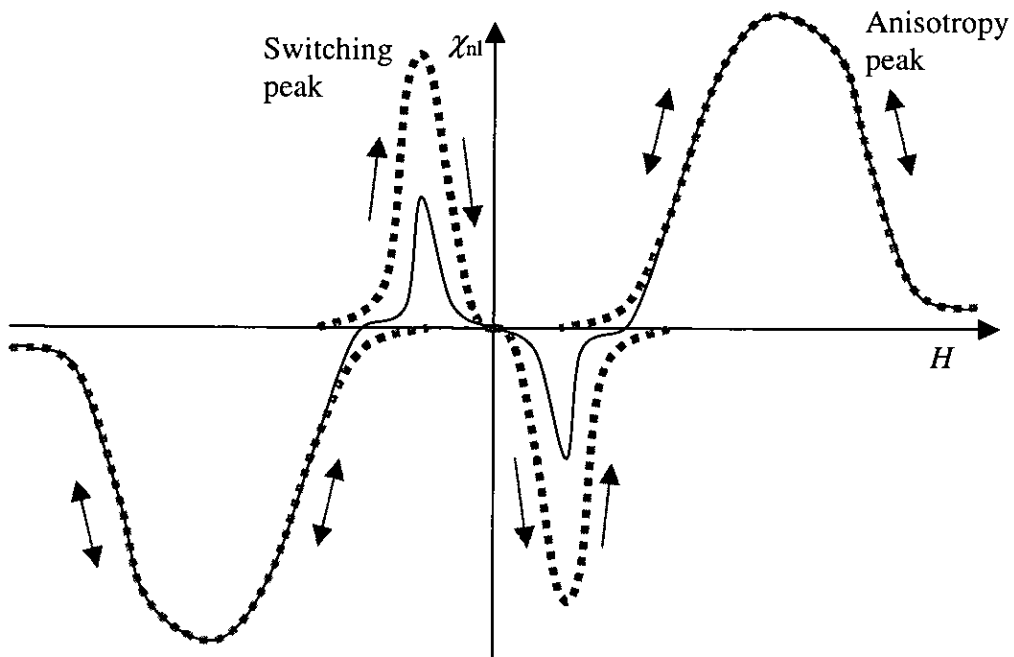


Figure 5-20 Idealised form of mean χ_{nl} curve (solid line), dashed lines show underlying features

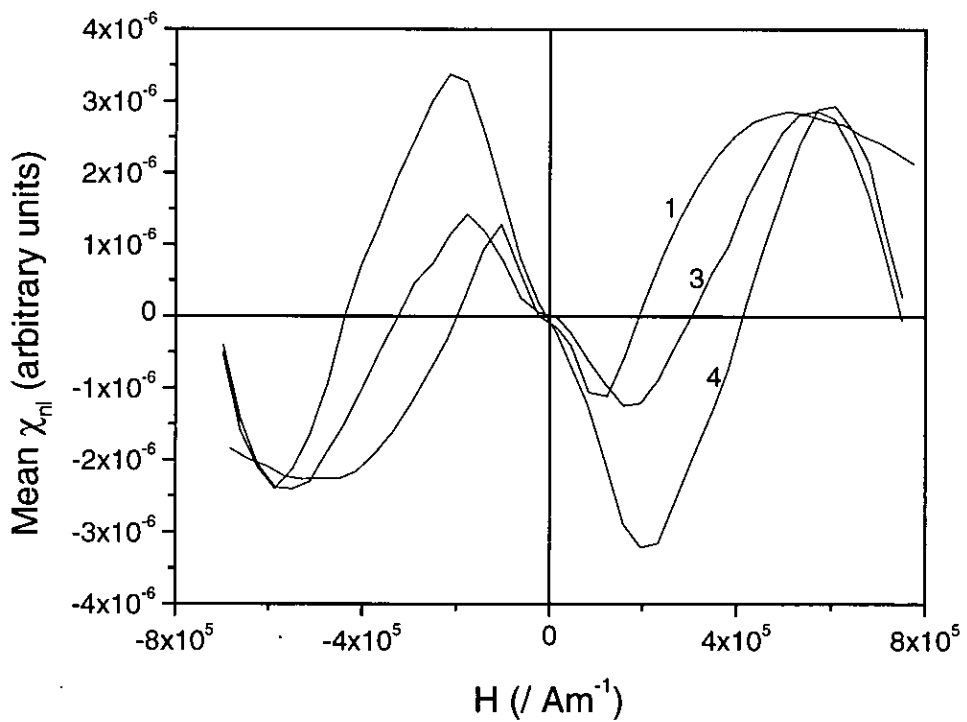


Figure 5-21 Mean χ_{nl} curves for MP powder samples 1, 3 and 4

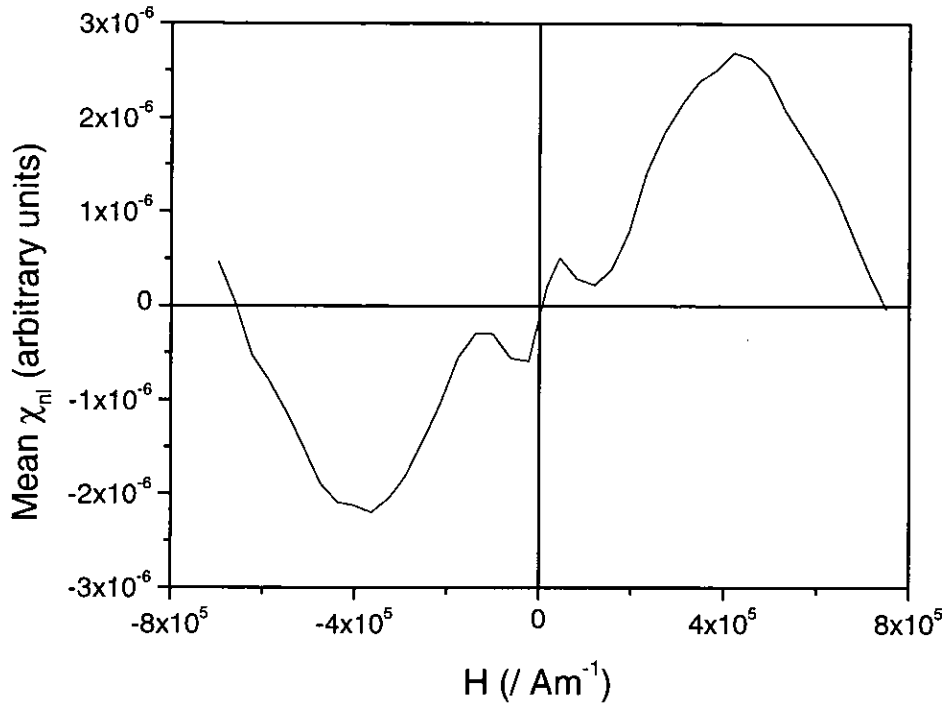


Figure 5-22 Mean χ_{nl} plot for MP powder sample 2

One possible mechanism by which the additional peaks could be produced in the χ_{nl} plot for sample 2 is the response of the particles aligned with the dc field. Because of their alignment orthogonal to the ac field the moments of these particles will oscillate in the ac field. These oscillations will increase as the dc field is reduced until the negative switching field of the particle is reached when they will change sign and the oscillations reduce. The energy diagram of such a particle in Figure 5-23 shows how the energy minimum broadens as the field reduces from saturation until the switching point where the moment switches to the other narrow minimum. The energy diagram shows the switching occurring at $H_{dc} = H_k$ in accordance with Stoner-Wohlfarth theory for particles aligned with the applied field. In practice we would expect the switching mode of many particles to be incoherent at this switching angle resulting in a lower H_c value.

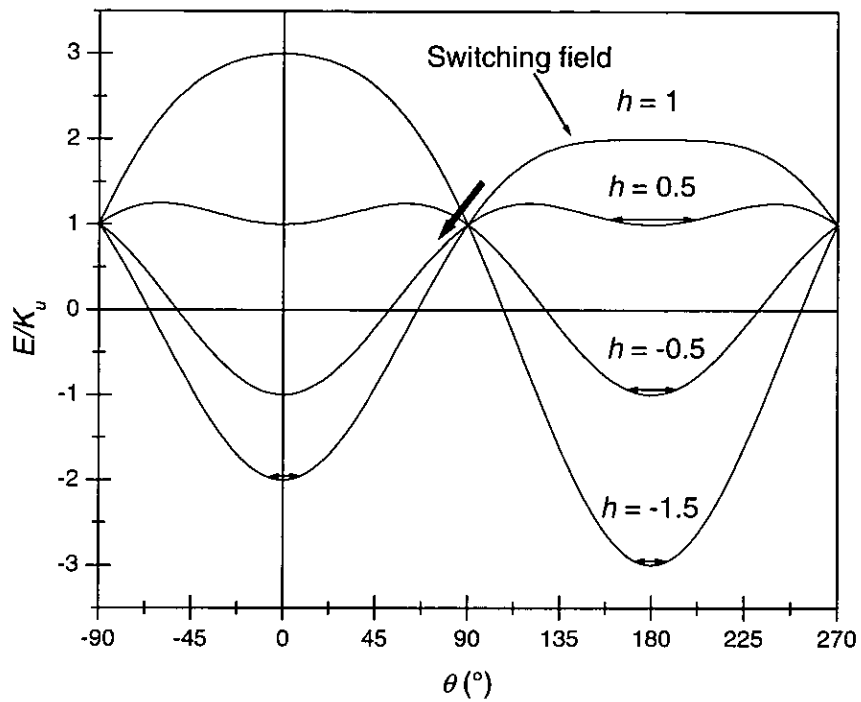


Figure 5-23 Energy diagram for particle aligned with dc field

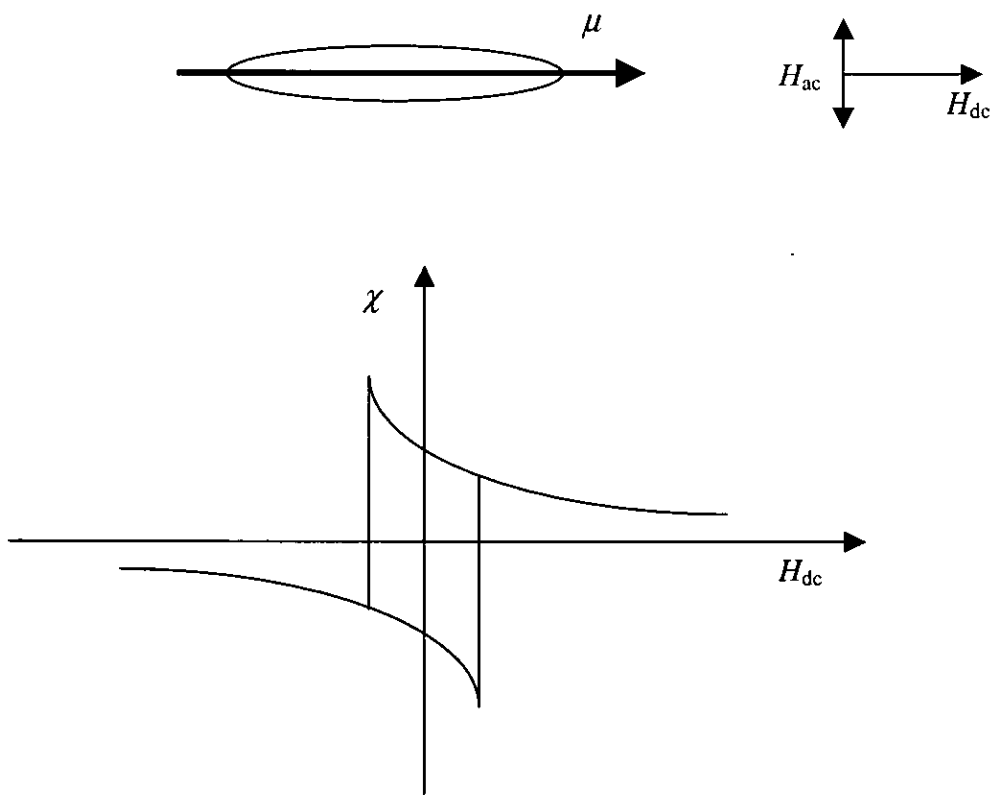


Figure 5-24 Predicted susceptibility of a particle with easy axis parallel to the dc field direction

A sketch of the predicted χ_{nl} response to such particles is shown in Figure 5-24. We can see that as the applied field reduces there is a steady reversible increase in the susceptibility signal. As the field reaches the reverse switching field the moment switches and the susceptibility changes sign. If we think of the mean value of the susceptibility over both cycle directions we can see that this effect could produce peaks in the same sense as the anisotropy peaks in the low field region, similar to those observed in Figure 5-22, if the switching field were sufficiently low. The reason why these peaks are only apparent in sample 2 is not known but may be due to the broad switching field distribution (see Table 5-3) of this sample broadening the switching peak which might otherwise mask this effect.

5.5 Variation in response with sample alignment

In order to further investigate the effects of texture, measurements were made of χ_{nl} as a function of the angle, β , between the sample easy axis direction and the ac field axis (see Figure 3-22). The sample plane was parallel to the ac/dc field plane for all measurements. For these plots samples of Co- γ -Fe₂O₃ videotape and CrO₂ TK50 data tape were used. The samples were fixed in the sample holder at a number of values of β and plots were recorded as a function of the sample angle.

The plots of χ_{nl} as a function of β are shown in Figure 5-25 and Figure 5-27 and show marked differences between the two particle systems. For the Co- γ -Fe₂O₃ system (Figure 5-25) with the sample easy axis aligned with the ac field (i.e. $\beta = 0^\circ$), both the anisotropy peak (A) in the positive field and a sharp peak associated with the switching behaviour (B) in the negative field were observed. As β increased both of the peaks were shifted to lower fields, with the anisotropy peak broadening and reducing in height whilst the switching peak increased. For alignment angles approaching $\beta = 90^\circ$ the switching peak dominated the plot and the anisotropy peak was suppressed. The shift in anisotropy peak may have been due to a change in the anisotropy field distribution of the particles as a function of the texture, as the anisotropy response is dominated by those particles with easy axes orthogonal to the ac field. However, a more likely cause was the response of the particles aligned with the dc field which would increase as the sample was rotated towards $\beta = 90^\circ$ and the number of particles aligned with the dc field increased. Particles with easy axes in the dc field direction will oscillate as their

moments are subject to a torque from the orthogonal ac field. These oscillations will increase as the dc field is reduced (from saturation), due to widening of the local energy minimum, until the negative switching field of the particle is reached when they will change sign and reduce as discussed in 5.4.1 and illustrated in Figure 5-23 and Figure 5-24. The presence of this response is confirmed by looking at the χ_{nl} plot for $\beta = 90^\circ$ in isolation shown in Figure 5-26, which is very similar to the predicted response sketched in Figure 5-24. A combination of this response increasing and the normal anisotropy field response reducing (due to a reduction of the number of particles with easy axes in the ac field direction) as the samples were rotated would account for the changes observed as a function of β in Figure 5-25.

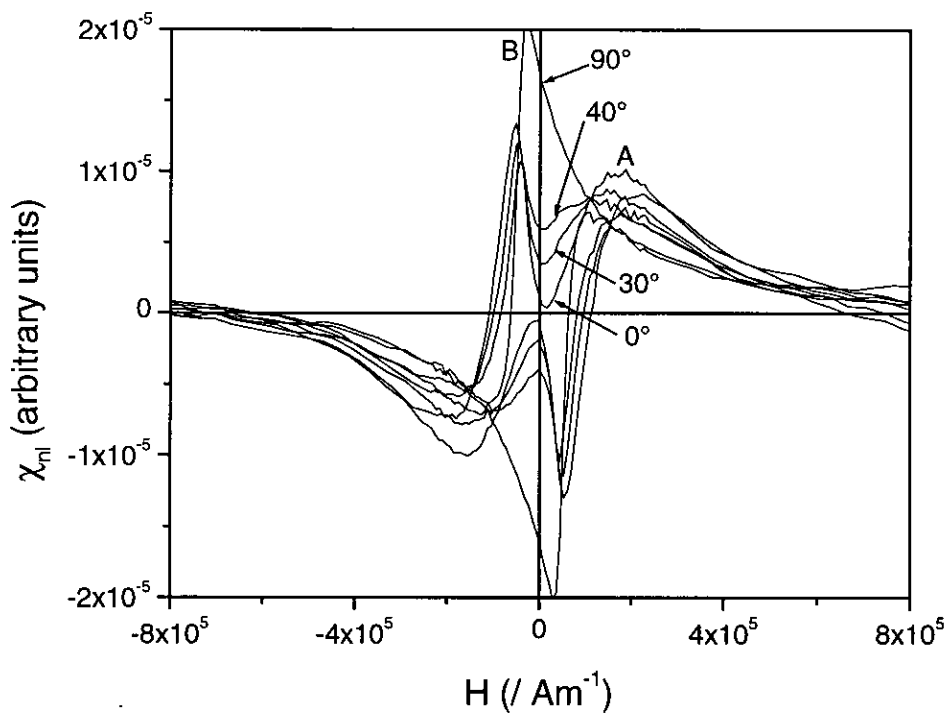


Figure 5-25 Co- γ -Fe₂O₃ VHS video tape, variation of χ_{nl} response with sample alignment

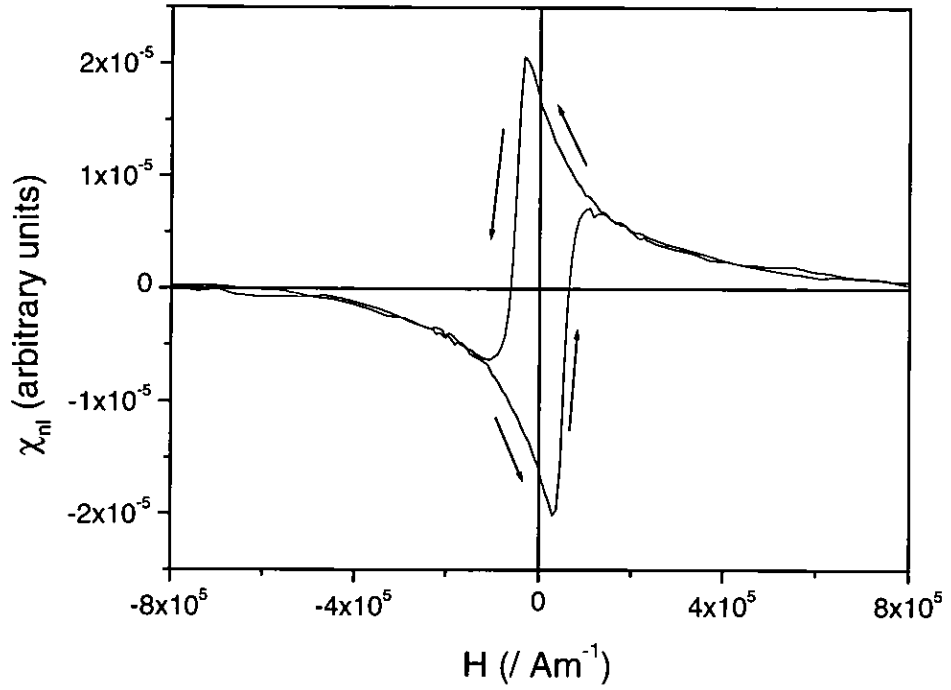


Figure 5-26 Co- γ -Fe₂O₃ VHS video tape, alignment angle $\beta = 90^\circ$

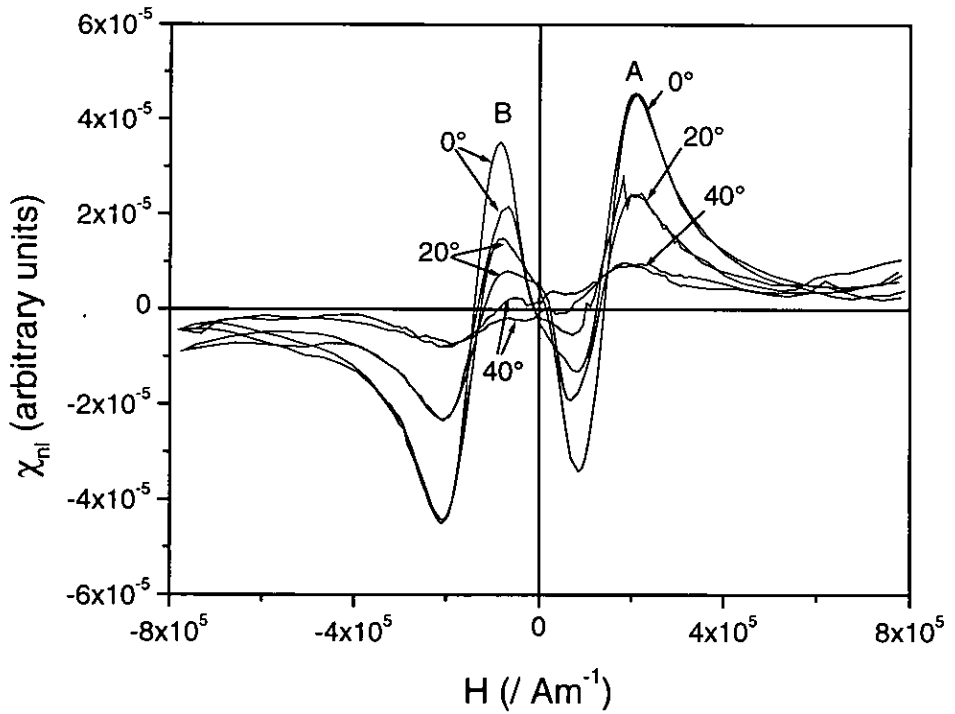


Figure 5-27 CrO₂ TK50 data tape, variation of χ_{nl} response with sample alignment

Figure 5-27 shows the variation in χ_{nl} with sample alignment for a CrO₂ TK50 data tape sample. In this case both the anisotropy (A) and the switching peak (B) rapidly reduced as the angle between the easy axis and the ac field was increased. Also, the switching peak field reduced as the angle increased, but the anisotropy peak remained at the same field irrespective of angle. It appeared that the predicted response for particles aligned with the dc field, shown in Figure 5-24, was not present in this sample. A likely explanation for this was that the particles in this sample tended to reverse by a non-coherent mechanism when the angle between the dc field and the particle easy axis was low. Particles with easy axes close to 90° from the dc field direction would still reverse coherently as incoherent reversals would require a fraction of the particle moments to directly oppose the applied field (see section 1.6). Incoherent reversals would not be readily detected in the susceptibility of the sample due to internal flux closure reducing the flux change in the sense coil. The result of this effect is that as the angle between the dc field and the sample easy axis is reduced, the number of particles with easy axes parallel to the ac field decreases, reducing the anisotropy peak (as predicted by theory, Figure 5-4). Also, the number of particles with easy axes near 90° to the dc field direction, for which coherent reversal is energetically favourable, will decrease, reducing the switching peak.

5.6 Discussion

A susceptometer has been developed to investigate the non-linear transverse susceptibility of magnetic recording media, proposed as an investigative technique for the study of recording media by Chantrell *et al*[7]. The output of the susceptometer as a function of the input probe field was found to be in good agreement with the predicted quadratic relationship.

Investigation of tape and powder samples showed peaks associated with anisotropy field and switching field distributions of the particles. The switching peaks for Co- γ -Fe₂O₃ tapes were at a similar field to the sample coercivity, suggesting that the switching peak was equivalent to the switching field distribution of those particles as predicted by theory. The switching peaks for CrO₂ tapes were much higher than the sample coercivity value suggesting that not all switching events were contributing equally to the switching peak for this sample. As the switching peak was much higher than the

sample coercivity this suggested that the switching peak was weighted in favour of the switching mode of the particles with the highest switching field. It is proposed that these are those particles with easy axes nearly orthogonal to the applied bias (dc) field, which will have a switching angle (θ_c) close to 90° and hence a high switching field and will favour switching by coherent rotation. This proposition is supported by the study of χ_{nl} as a function of the sample easy axis angle with respect to the ac field axis. The study shows that for the CrO_2 sample (Figure 5-27) the switching peak reduces as the sample easy axis becomes more aligned with the dc field, suggesting that the mode of switching for particles aligned with the dc field is different than that for particles orthogonal to the dc field and does not contribute to the χ_{nl} signal.

The study of χ_{nl} as a function of the sample easy axis angle with respect to the ac field axis for the $\gamma\text{-Fe}_2\text{O}_3$ system shows a strong response for the switching of particles with easy axes closely aligned with the dc field which increases as the sample easy axis is moved towards alignment with the dc field. The shape of the response is consistent with that predicted by the theory and the similarity of the sample coercivity and the switching peak maximum values suggests that virtually all of the switching events contribute equally to the switching peak and hence that the majority of the particles switch by the same mechanism which, due to its large contribution to the χ_{nl} signal, is probably coherent rotation. Experimental observations of the rotation of $\gamma\text{-Fe}_2\text{O}_3$ particles within systems have shown that they reverse by predominantly coherent reversal [13], although the study was limited to particles with a true prolate spheroid form. The difference in the switching peak field relative to the coercivity for the samples may be useful as a test for the switching mode of magnetic recording media samples. Further work is required in this area to identify the effect of different switching modes on the transverse susceptibility output.

The theory of non-linear transverse susceptibility predicted that the anisotropy field response would remain divergent even for a system with a distribution of easy axis directions in contrast with linear transverse susceptibility which forms a 'cusp' when an orientational texture is applied to a system of particles. The implication of this is that the anisotropy peak measured would be a direct measure of the anisotropy field distribution of the sample and would not require the deconvolution which is required to obtain the anisotropy field distribution from χ_t measurements. The investigation of CrO_2

TK50 tape as a function of sample alignment (Figure 5-27) tends to support this proposition as the shape and position of the anisotropy peak remains the same for all sample alignment angles with only the peak height changing due to the reduction in number of particles aligned with the ac field axis as the sample is rotated. This suggests that the peak in this sample is a direct measure of the anisotropy field distribution of the sample and that the changing peak height as the sample is rotated could be used as a measure of the easy axis distribution of the sample. Unfortunately, the anisotropy peak of the $\gamma\text{-Fe}_2\text{O}_3$ sample shown in Figure 5-25 does not show the same invariance for differing sample orientation angles and hence cannot be considered to be a direct measure of the anisotropy field distribution. It seems likely that the underlying anisotropy response of this sample is invariant, but the oscillating (i.e. pre-switching) response of particles aligned with the dc field, sketched in Figure 5-24, is also present in the χ_{nl} signal which tends to skew the anisotropy peak. As the relative strengths of the anisotropy signal and the dc-aligned oscillating signal are dependent on sample texture and orientation the anisotropy field distribution could not be obtained from these plots without deconvolution which took into account the specific texture and orientation of the sample.

The difference between the sample coercivity and the switching peak appears to give a reasonable indication of whether the switching peak is a measure of all, or just selected switching events. In those samples where the switching peak field is close to the coercivity it seems unlikely that the anisotropy peak will be a true representation of the anisotropy field distribution, however, comparison with χ_t investigations of the same samples show that χ_{nl} anisotropy peaks still occur at a higher field than χ_t and should therefore be regarded as a more accurate indicator of the modal H_k value than the χ_t determination, which is known to give a depressed H_k value for all but perfectly aligned systems.

The greater divergence of the anisotropy signal in χ_{nl} allows the technique to be used to detect anisotropy information in random samples where the peak is suppressed in χ_t investigations. In this way anisotropy field information can be extracted from $\gamma\text{-Fe}_2\text{O}_3$ and MP powders which do not give any anisotropy information under χ_t investigation. Some care is required in the interpretation of χ_{nl} plots as it is not always obvious which features are due to switching processes and which are due to anisotropy field processes.

The subtraction of the two sweep directions can be used to isolate the irreversible behaviour due to switching, but it is important to note that there is also a significant reversible component due to particles with easy axes close to the dc field direction, which is nominally related to switching rather than anisotropy. This reversible component can be seen in Figure 5-24 and Figure 5-26 and is probably the effect which has obscured the switching peak in Figure 5-15. The effect can be observed for this sample when the two sweep directions are averaged (Figure 5-22) but in other samples the effect could be difficult to isolate from the anisotropy peak and may result in an undetected skew towards lower field values in both the anisotropy peak and the switching peak. The effect can be detected in highly aligned samples by measuring the χ_{nl} response with the sample easy axis parallel to the dc field axis as shown in Figure 5-26.

Further work is required to test the proposition that the χ_{nl} plot gives a direct measure of the anisotropy field distribution for incoherently rotating systems. Independent tests are required such as deconvolution of the χ_t response for a CrO_2 powder sample[121,123] and comparison with the χ_{nl} plot, or comparison with an independent anisotropy measurement technique. The non-linear susceptometer was not developed until relatively late in the programme of work described in this thesis leaving insufficient time to develop such independent comparisons.

6 Conclusions & further work

The transverse susceptibility has been investigated as a potential source of information on the anisotropy distribution of magnetic materials since its first experimental demonstration by Pareti and Turilli[4]. This thesis describes the development of a highly sensitive transverse susceptometer and details the analysis of information obtained from investigations of magnetic recording media. The results of the investigations are compared with current theory.

In the design and manufacture of the susceptometer described in Chapter 2 it has been shown that the instrument baseline and noise were largely due to coupling between the ac probe field and the electromagnet. Such coupling resulted in the ac probe field changing as a function of the saturation of the electromagnet components. In order to reduce this effect, a coaxial solenoid was developed which reduced the external stray field to approximately 1% of its former value. In addition the sample and compensating coils were wound coaxially to ensure that any residual changes in the ac probe field would be similar for each. The net result of the modifications to the susceptometer design was a cumulative reduction of the baseline compared to the signal of a factor of 525. A reduction of the random noise on the susceptometer response was also observed although this was not measured quantitatively. The increase in the sensitivity of the susceptometer allowed a number of investigations to be carried out which had not been possible previously including,

- The investigation of modern advanced metal particle tapes,
- The investigation of the imaginary component of transverse susceptibility,
- The investigation of the non-linear transverse susceptibility, χ_{nl} .

The work reported for the latter two techniques was the first experimental demonstration of these measurements on magnetic recording media.

Although the sensitivity of the susceptometer had been greatly increased it was still not possible to measure the χ_{nl} response of modern advanced metal particle tapes due to their relatively low sample moment and the small signal size of χ_{nl} compared to χ_t .

Attempts were also made to investigate the χ_t response of thin film media but no peaks were observed. It is possible that the investigation of thin films using χ_{nl} would give anisotropy and switching information but the sensitivity of the susceptometer would

have to be increased in order to measure the non-linear response of such samples. Further changes to the susceptometer that could improve the sensitivity of the instrument include,

- The use of a super-conducting solenoid or a wide pole-gap electromagnet to further reduce the coupling between solenoid and electromagnet,
- Improvements to the balancing of the sample and compensating coil to eliminate the need for the balancing circuit,
- Replacement of the compensating coil for the χ_{nl} system with a coil parallel to the sample coil (as used in the measurement of MP powders) to reduce the pick-up of electrical noise.

The results of χ_t measurements of control sample tapes on the improved susceptometer showed that the H_k peak value had increased compared with those measured previously on the unmodified system. It is thought that the use of large multi-layer samples had lowered the earlier H_k values as misalignment between sample layers effectively broadened the sample texture. Although the use of smaller samples reduced this misalignment on the modified system some lowering of the measured H_k values is still likely where multi-layer samples are used. Further improvements to the sensitivity of the susceptometer are required before the ideal case is achieved, where all samples can be characterised from a single layer.

Analysis of the H_c / H_k ratio, χ_t plots and χ_{nl} plots all suggested that the coherent reversal mode was dominant for the Co- γ -Fe₂O₃ tape sample, the MP tape samples, the γ -Fe₂O₃ powder and the metal particle powders. Some form of incoherent reversal was proposed as the dominant reversal mode for the mixed γ -Fe₂O₃ / CrO₂ tape, pure CrO₂ tape and CrO₂ powder. The χ_{nl} results were particularly useful in the analysis of the switching mode as in many cases the switching peaks could be observed directly on the χ_{nl} plot and compared with the sample coercivity measured using a vibrating sample magnetometer (VSM). It was proposed that the χ_{nl} signal was particularly sensitive to coherent reversal processes, but less sensitive to incoherent processes due to internal flux closure in the particles. Hence, comparison of the switching peak field with the coercivity, H_c , gave an indication of the dominant reversal mode. For coherently reversing particles we would expect the switching peak to be at a similar field to the sample coercivity. Systems dominated by incoherent reversal would have switching

peaks higher than the sample coercivity as coherent reversals only occur in such systems at the higher values of the switching field distribution. For some samples the switching peaks were not immediately obvious (see Figure 5-15) due to reversible features associated with particles with easy axes parallel to the dc field direction (see Figure 5-24 and Figure 5-26). However, subsequent subtraction of the plot in the reverse sweep direction was used to isolate the switching peak from the reversible component.

Unfortunately, the conclusion that the $\gamma\text{-Fe}_2\text{O}_3$ based systems are switching in a predominantly coherent mode is controversial, and reference to the published literature reviewed in section 1.6 shows that whilst there is still some debate on this subject, the widely accepted view is that $\gamma\text{-Fe}_2\text{O}_3$ particles, and most metal particles rotate by predominantly incoherent processes. There are few macroscopic parameters which can be measured experimentally to determine the method of reversal. The most obvious parameter affected by the reversal mode is the coercivity of the particle. Calculations of the coercivities of particles typical of those discussed in this thesis are shown for Stoner-Wohlfarth (C), chain-of-spheres coherent (B) and chain-of-spheres ‘fanning’ (A) reversal in Table 6-1.

| Particle type | σ_s Am ² /kg | Aspect Ratio | ρ kg/m ³ | H_c (C) kA/m | H_c (B) kA/m | H_c (A) kA/m | H_c (meas) kA/m |
|------------------------------------|-----------------------------------|----------------|-----------------------------|-------------------|-------------------|-------------------|----------------------|
| MP3 | 221.7 ^a | 5 ^a | 7874 | 727 | 384 | 166 | 152 |
| MP4 | 221.7 ^a | 5 ^a | 7874 | 727 | 384 | 166 | - |
| Co- $\gamma\text{-Fe}_2\text{O}_3$ | 76 ^b | 8 ^b | 4670 ^c | 154 | 80 | 35 | 53 |
| CrO ₂ | 90 ^c | 9 ^d | 4830 ^c | 202 | 100 | 43 | 37 |

^aParticle data from tape manufacturer[131]. ^bTypical videotape particle values[137], quoted $H_c=52.5$.

^cTypical data[138]. ^dTypical BASF CrO₂ tape particle[42].

Table 6-1 Calculated coercivities of typical recording particles for Stoner-Wohlfarth (C), chain-of-spheres coherent (B) and chain-of-spheres ‘fanning’ (A) reversal modes

Looking at the calculated coercivities in the table we can see that the chain-of-spheres ‘fanning’ model gives the closest value to the measured coercivity. However, we must also remember that the calculated model coercivities are the maximum switching field of an individual particle and have not taken into account the effects of inter-particle interactions, imperfect alignment or thermally assisted switching, which some investigations have suggested may lower the coercivity by a considerable amount.

Taken in isolation the discrepancy between the measured coercivity and the transverse susceptibility switching peak position for some systems certainly indicates that the transverse susceptibility is more sensitive to certain types of switching process than others. Also the transverse susceptibility switching peak being at a higher field than the coercivity in these systems, and being absent in CrO₂ systems with easy axes aligned with the dc field all suggest that the technique does not show a large response for incoherent reversals. However, it seems unlikely, given the weight of contrary evidence, that particles such as Co- γ -Fe₂O₃ could be switching in a completely coherent mode. The true behaviour of the particles during reversal is probably some mixture of the very simple modes described. It must be remembered that the reason for the assumptions in the models [a) that particle shapes are spheroids of revolution, and b) that all, or certain sections of the particle rotate coherently] is to simplify the models by avoiding difficult calculations of exchange interaction and variations of magnetisation within the particle. Micromagnetic calculations may offer more realistic models of reversal, although as with analytical models the lack of proven experimental techniques for determining switching modes from macroscopic measurements makes it difficult to establish which models are the most appropriate. It seems that the transverse susceptibility, and particularly the non-linear transverse susceptibility are particularly sensitive to the behaviour of magnetic systems during reversal and with further research could provide a powerful tool for the investigation of particle rotation modes.

Comparison of the χ_t and the χ_{nl} response demonstrated that the anisotropy peaks in the χ_{nl} have a greater independence to sample texture than those in the χ_t . In particular the investigation of χ_t and χ_{nl} as a function of the sample orientation axis angle for a sample of TK50 CrO₂ data tape, shown in Figure 3-24 and Figure 5-27 respectively, demonstrated that the anisotropy peak field of the χ_t response was highly dependent on the sample orientation whilst the χ_{nl} was independent of orientation. This is consistent with the theoretical model of Chantrell *et al*[7] which suggests that the χ_{nl} anisotropy response is sufficiently divergent to overcome orientational texture effects. This result for the sample shown in Figure 5-27 suggests that the measured peak is a direct measurement of the anisotropy field distribution, and the comparative heights of the peak as the sample is rotated are similarly a measure of the orientational texture of the sample. Unfortunately, due to the non-linear element of the susceptometer being

developed relatively late in the experimental programme, there was insufficient time to confirm this by comparison with the anisotropy field distribution of the sample determined by an alternative technique. If we assume that the peaks observed in Figure 5-27 are a direct measurement of the anisotropy field distribution then the non-linear transverse susceptibility offers a very simple method of anisotropy field distribution and orientational texture determination for such samples. The change in anisotropy peak shape as a function of orientation and texture in the χ_{nl} response of other samples measured appears to be due to coherent switching processes which produce a large signal due to those particles with easy axes aligned with the dc field. The signal due to such particles extends over a wide range of field values and a significant part of the signal is reversible which prevents its isolation from the anisotropy information. Although this effect distorts the anisotropy information in samples with a distribution of easy axis directions, which reverse by coherent rotation, the anisotropy peaks can still be seen in randomly oriented samples, unlike χ_t measurements where they are completely suppressed. This implies that even for coherently rotating samples, the χ_{nl} response is less affected by texture than that of the χ_t , and the measurement of H_k using χ_{nl} will be more accurate than that determined using χ_t . This proposition is supported by the comparison of H_k values determined using the two techniques (shown in Table 5-1 and Table 5-2). In each case the H_k value determined using χ_{nl} is at a higher field. This is consistent with the technique being a more accurate method as texture and interaction effects are known to reduce the value of H_k in χ_t determinations. Hence, the method giving the higher H_k value is likely to be the most accurate. For both techniques the most accurate determination of H_k is given by using a highly textured sample with the easy-axis parallel to the ac field direction. Further work is required to extend the theoretical model of χ_{nl} to broader texture distributions. The existing theory shows that the response remains divergent at the anisotropy field for a system with a Gaussian distribution of easy-axes with $\sigma = 2.5^\circ$ but the experimental results of Chapter 5 show that for much wider texture distributions the reversible response of coherently reversing particles with easy axes aligned with the dc field can skew the anisotropy response. Further work is required to determine the range of distributions for which the coherent reversing behaviour can be neglected, and the anisotropy field distribution can be obtained without the need to deconvolve the results.

Earlier work on the imaginary susceptibility of ferrofluids was reported by Fannin *et al*[139,140] based on the Debye theory of rotational Brownian motion. In the work of Fannin *et al*, however, the imaginary response was related to the physical rotation of the particles in a viscous fluid, whereas the Papusoi model discussed in section 3.7 postulates the imaginary response due to the thermal relaxation of magnetic moments over an energy barrier in a static particle based on the theory of Néel[141]. The detection of the imaginary component of the χ_i response and its close agreement with the theoretical predictions of Papusoi (section 3.7) suggests that thermally activated reversible switching occurs between the energy minima at fields below the anisotropy field. The reversible switching field is dependent on the widths of the anisotropy field and particle volume distributions. Further extension of the theory in this area could yield information about the anisotropy and volume distributions from the differences in response between the real and imaginary components. Correspondence with the author of the theoretical work[142] suggests that the presence of the imaginary signal casts doubt on the classification of χ_i measurement as a ‘stiffness’ technique of anisotropy measurement (as the signal is partly due to thermally activated switching) which could lead to the underestimate of H_k associated with ‘switching’ methods of anisotropy measurement. However, assessment of the quality of anisotropy measurement techniques by division into ‘stiffness’ and ‘switching’ categories is rather an oversimplification. The observations that switching techniques give lower values of anisotropy field are far from definitive, being based on comparisons of only a few of the available techniques. It has been shown that some of the switching techniques give lower anisotropy field values but the reasons for this are not fully understood. No study has compared all of the techniques, and in several of the studies χ_i measurements have been classified as ‘stiffness’ and have compared closely with other ‘stiffness’ techniques[60,75]. Whilst the model of Papusoi shows the effect of thermal activation on the real component of the χ_i signal the effect has not been modelled with respect to χ_{nl} and it may be that with the greater divergence of the anisotropy information in non-linear measurements the thermal activation component becomes insignificant. Further work is required in this area to determine the effect of thermal activation on both linear and non-linear transverse susceptibility measurements.

Determination of magnetic layer thicknesses using χ_t has been demonstrated for modern advanced metal particle tapes using stacked samples to increase the magnetic moment. The technique has been used to measure layer thicknesses down to 170nm and is particularly useful with the advent of dual-coating techniques where mechanical measurements of the layer thickness are difficult. The development of a computer model has shown that the assumption that demagnetising factors of the magnetic layer are approximated by those of a homogeneous sheet is increasingly in error as the layer becomes thinner and as the packing fraction decreases. The model provides corrections to the demagnetising factor ratio for MP3 and MP4 type particles as a function of packing fraction and layer thickness. Other related methods have been developed to measure the layer thickness using the Flanders & Shtrikman and transverse loop-closure techniques. The results of the techniques compare favourably (see Figure 4-16) and the latter technique is particularly useful as it can be performed using a standard VSM. The technique of transverse susceptibility measurement has much to offer in terms of the measurement of anisotropy field distribution, switching mode and texture. Further work on the imaginary component may also lead to information on particle volume distributions. Transverse susceptibility is particularly suited to automation and 'in-process' monitoring techniques due to its robust nature, and lack of moving parts. The technique has not been successful in the characterisation of thin films and the reason for this is not fully understood. The lack of χ_t peaks in the thin film response may just be due to the planar random texture suppressing the peaks as it has been shown to do in coherently switching randomly oriented powders. In this case it is possible that the peaks would be visible in the χ_{nl} measurement if the sensitivity of the susceptometer were increased and noise reduced sufficiently to measure such samples.

Bibliography

1. Gans,R. 4. Zur Theorie des Ferromagnetismus. 3. Mitteilung: Die reversible longitudinale und transversale Permeabilität. *Annalen der Physik* **29**, 301-315 (1909).
2. Stoner,E.C. & Wohlfarth,E.P. A Mechanism of Magnetic Hysteresis in Heterogeneous Alloys. *Phil.Trans.Roy.Soc A* **240**, 599-642. 1948.
3. Aharoni,A., Frei,E.H., Shtrikman,S. & Treves,D. The reversible susceptibility tensor of the Stoner-Wohlfarth model. *Bull. Res. Counc. of Israel* **6A**, 215-238 (1957).
4. Pareti,L. & Turilli,G. Detection of Singularities in the reversible transverse susceptibility of an uniaxial ferromagnet. *Journal Of Applied Physics* **61**(11), 5098-5101. 1987.
5. Papusoi,C. The complex transverse susceptibility. *Physics Letters A* **265**, 391-402 (2000).
6. Sollis,P.M. & Bissell,P.R. A novel method for absolute magnetization measurement in longitudinal recording media using transverse-susceptibility measurements. *Journal Of Physics D-Applied Physics* **24**, 1891-1893 (1991).
7. Chantrell,R.W., Hoare,A., Melville,D., Lutke-Stetzkamp,H.J. & Methfessel,S. Transverse Susceptibility of a Fine Particle System. *IEEE Transactions On Magnetics* **25**(5), 4216-4218. 1989.
8. Sharrock,M.P. Particulate magnetic recording media - a review. *IEEE Transactions On Magnetics* **25**, 4374-4389 (1989).
9. Chantrell,R.W. & O'Grady,K. Magnetic Characterization of Recording Media. *Journal Of Physics D-Applied Physics* **25**, 1-23 (1992).

10. Cullity,B.D. Introduction to Magnetic Materials. Cohen,M. (ed.), pp. 207-247 (Addison Wesley, California,1972).
11. Cullity,B.D. Introduction to Magnetic Materials. Cohen,M. (ed.), pp. 287-356 (Addison Wesley, California,1972).
12. Parker,F.T., Berkowitz,A.E. & Slade,S.B. H_k distributions and H_c calculations for magnetic recording particles. *Journal Of Applied Physics* **75**, 1681-1688 (1994).
13. Salling,C., Obarr,R., Schultz,S., Mcfadyen,I. & Ozaki,M. Investigation of the Magnetization Reversal Mode for Individual Ellipsoidal Single-Domain Particles of Gamma-Fe₂O₃. *Journal Of Applied Physics* **75**, 7989-7992 (1994).
14. Jacobs,I.S. & Bean,C.P. An Approach to Elongated Fine-Particle Magnets. *Physical Review* **100**, 1060-1067 (1955).
15. Cullity,B.D. Introduction to Magnetic Materials. Cohen,M. (ed.), pp. 383-438 (Addison Wesley, California,1972).
16. Frei,E.H., Shtrikman,S. & Treves,D. Critical size and nucleation field of ideal ferromagnetic particles. *Physical Review* **106**, 446-455 (1957).
17. Aharoni,A. Nucleation modes in ferromagnetic prolate spheroids. *Journal of Physics-Condensed Matter* **9**, 10009-10021 (1997).
18. Jacobs,I.S. & Luborsky,F.E. Magnetic Anisotropy and Rotational Hysteresis in Elongated Fine-Particle Magnets. *Journal Of Applied Physics* **28**, 467-473 (1957).
19. Brown,W.F. & Morrish,A.H. Effect of a cavity on a single-domain magnetic particle. *Physical Review* **105**, 1198-1201 (1957).
20. Aharoni,A. Some recent developments in micromagnetics at the Weizmann Institute of Science. *Journal Of Applied Physics* **30**, 70S-78S (1959).

21. Johnson,C.E. & Brown,W.F. Shape Distribution of Magnetite Powders. *Journal Of Applied Physics* **30**, 136S-137S (1959).
22. Wohlfarth,E.P. Angular variation of the coercivity of partially aligned elongated ferromagnetic particles. *Journal Of Applied Physics* **30**, 117S-119S (1959).
23. Luborsky,F.E. High coercive materials. *Journal Of Applied Physics* **32**, 171S-183S (1961).
24. Bottoni,G., Candolfo,D., Cecchetti,A. & Masoli,F. Influence of extreme dilutions on the magnetic properties of single-domain particle aggregates. *IEEE Transactions On Magnetism* **8**, 770-772 (1972).
25. Knowles,J.E. Magnetic-Properties of Individual Acicular Particles. *IEEE Transactions On Magnetism* **17**, 3008-3013 (1981).
26. Sharrock,M.P. & Mckinney,J.T. Kinetic Effects in Coercivity Measurements. *IEEE Transactions On Magnetism* **17**, 3020-3022 (1981).
27. Sharrock,M.P. Particle-Size Effects on the Switching Behavior of Uniaxial and Multiaxial Magnetic Recording Materials. *IEEE Transactions On Magnetism* **20**, 754-756 (1984).
28. Bottoni,G., Candolfo,D., Cecchetti,A., Masoli,F. & Corradi,A.R. The Effect of Multiple Anisotropies in Fine Particles. *Journal Of Magnetism And Magnetic Materials* **45**, 91-99 (1984).
29. Andress,S.J., Benedetti,A., Corradi,A.R. & Fagherazzi,G. The Microstructure of Gamma-Fe₂O₃ and Its Effects on the Magnetization Properties. *IEEE Transactions On Magnetism* **22**, 1341-1348 (1986).
30. Ishii,Y. & Sato,M. Rotational Hysteresis of Elongated-Single-Domain Particles by Chain-Of-Spheres Model. *Journal Of Applied Physics* **61**, 311-318 (1987).
31. Richter,H.J. & Hempel,K.A. Extension of the Chain of Spheres Model. *IEEE Transactions On Magnetism* **24**, 1826-1828 (1988).

32. Schabes, M.E. & Bertram, H.N. Ferromagnetic Switching in Elongated Gamma-Fe₂O₃ Particles. *Journal Of Applied Physics* **64**, 5832-5834 (1988).
33. de Witte, A.M., O'Grady, K., Coverdale, G.N. & Chantrell, R.W. Activation Volumes of Reversal in Ultrafine Particles and Recording Media. *Journal Of Magnetism And Magnetic Materials* **88**, 183-193 (1990).
34. Pankhurst, Q.A. Measurement of Magnetic-Anisotropy in Ferrimagnetic Powders by Applied Field Mossbauer-Spectroscopy. *Journal Of Magnetism And Magnetic Materials* **101**, 291-292 (1991).
35. Bottoni, G. Influence of the Magnetic-Interactions on the Reversal Mode of Magnetic Recording Particles. *Journal Of Applied Physics* **69**, 4499-4501 (1991).
36. Lederman, M., Schultz, S. & Ozaki, M. Measurement of the Dynamics of the Magnetization Reversal in Individual Single-Domain Ferromagnetic Particles. *Physical Review Letters* **73**, 1986-1989 (1994).
37. Braun, H.B. Thermally Activated Magnetization Reversal in Elongated Ferromagnetic Particles. *Physical Review Letters* **71**, 3557-3560 (1993).
38. Braun, H.B. & Bertram, H.N. Nonuniform Switching of Single-Domain Particles at Finite Temperatures. *Journal Of Applied Physics* **75**, 4609-4616 (1994).
39. Morales, M.P., El Hilo, M. & O'Grady, K. Time-Dependence Effects and Reversal Mechanisms in Gamma-Fe₂O₃ Particles. *Journal Of Magnetism And Magnetic Materials* **140**, 2211-2212 (1995).
40. Bottoni, G. Rotational hysteresis in particles for magnetic recording with different switching modes. *Journal Of Magnetism And Magnetic Materials* **155**, 16-18 (1996).
41. McConochie, S.R., Bissell, P.R., Parker, D.A. & Gotaas, J.A. Angular dependence of magnetization reversal in gamma-Fe₂O₃ single particles: an experimental and modelling study. *IEEE Transactions On Magnetics* **33**, 3043-3045 (1997).

42. Keller,R. & Schmidbauer,E. Rotational hysteresis and magnetization of elongated Fe-doped CrO₂ particles. *Journal Of Magnetism And Magnetic Materials* **187**, 160-168 (1998).
43. Morales,M.P.Walton,S.A., Prichard,L.S., Serna,C.J., Dickson,D.P.E., O'Grady,K. Characterisation of advanced metal particle recording media pigments. *Journal Of Magnetism And Magnetic Materials* **190**, 357-370 (1998).
44. Igaki,M., Nagamori,H., Shimatsu,T. & Takahashi,M. Magnetic anisotropy and switching field of spindle-shaped metal particles for particulate recording media. *Journal Of Magnetism And Magnetic Materials* **183**, 209-219 (1998).
45. Bottoni,G. Switching volumes in high-density recording materials with different magnetization reversal modes. *Journal Of Magnetism And Magnetic Materials* **197**, 602-603 (1999).
46. Sharrock,M.P. Recent advances in metal particulate recording media: Toward the ultimate particle. *IEEE Transactions On Magnetics* **36**, 2420-2425 (2000).
47. Bottoni,G., Candolfo,D. & Cecchetti,A. Some aspects of the intrinsic magnetic behavior of metal particles for advanced recording media. *Journal Of Magnetism And Magnetic Materials* **242**, 335-337 (2002).
48. Poulsen,V. (8961). 1899. UK.
Ref Type: Patent
49. Koster,E. & Arnoldussen,T.C. Magnetic Recording - Technology. Mee,C.D. & Daniel,E.D. (eds.), pp. 98-243 (McGraw-Hill, New York,1987).
50. Spratt,G.W.D., Bissell,P.R., Chantrell,R.W. & Wohlfarth,E.P. Static and Dynamic Experimental Studies of Particulate Recording Media. *Journal Of Magnetism And Magnetic Materials* **75**, 309-318 (1988).
51. Wohlfarth,E.P. Relations between different modes of acquisition of the remanent magnetisation of ferromagnetic particles. *Journal Of Applied Physics* **29**, 595-596 (1958).

52. Kelly,P.E., O'Grady,K., Mayo,P.I. & Chantrell,R.W. Switching Mechanisms in Cobalt-Phosphorus Thin-Films. *IEEE Transactions On Magnetics* **25**, 3880-3883 (1989).
53. Zhu,J.G. & Bertram,H.N. Magnetization Reversal in CoCr Perpendicular Thin-Films. *Journal Of Applied Physics* **66**, 1291-1307 (1989).
54. Zhu,J.G. & Bertram,H.N. Recording and Transition Noise Simulations in Thin-Film Media. *IEEE Transactions On Magnetics* **24**, 2706-2708 (1988).
55. Mayo,P.I., O'Grady,K., Chantrell,R.W., Cambridge,J.A., Sanders,I.L., Yogi,T., Howard,J.K. Magnetic Measurement of Interaction Effects in CoNiCr and CoPtCr Thin-Film Media. *Journal Of Magnetism And Magnetic Materials* **95**, 109-117 (1991).
56. Bean,C.P. & Meiklejohn,W.H. *Bulletin of the American Physical Society. Series II* **1**, 148 (1956).
57. Berkowitz,A.E. & Flanders,P.J. Magnetic Analysis of the Precipitation of Iron from Beta Brass. *Acta Metallurgica* **8**, 823-832 (1960).
58. Doyle,W.D., Rudisill,J.E. & Shtrikman,S. Angular Dependence of Torque in Anisotropic Permalloy Films. *Journal Of Applied Physics* **32**, 1785-1787 (1961).
59. Paige,D.M., Hoon,S.R., Tanner,B.K. & O'Grady,K. High-precision torque hysteresis measurements on fine particle- systems. *IEEE Transactions On Magnetics* **20**, 1852-1854 (1984).
60. Gornert,P. Schuppel,W., Sinn,E., Schumacher,F., Hempel,K.A.; Turilli,G.; Paoluzi,A. & Rosler,M. Comparitive measurements of the effective anisotropy-field H_A for barium ferrites. *Journal Of Magnetism And Magnetic Materials* **114**, 193-201 (1992).
61. Takahashi,M., Shimatsu,T., Suekane,M., Miyamura,M., Yamaguchi,K. & Yamasaki,H. Magnetization reversal mechanism evaluated by rotational

- hysteresis loss analysis for the thin-film media. *IEEE Transactions On Magnetism* **28**, 3285-3287 (1992).
62. Futamoto,M., Inaba,N., Hirayama,Y., Ito,K. & Honda,Y. Compositional microstructure and micromagnetics of Co based thin film media. *Materials Research Society Symposium Proceedings* **517**, 243-254 (1998).
 63. Inaba,N., Uesaka,Y. & Futamoto,M. Comparison between different methods of determining anisotropy constants of thin film media. *IEEE Transactions On Magnetism* **35**, 2670-2672 (1999).
 64. Flanders,P.J. & Shtrikman,S. Experimental Determination of the Anisotropy Distribution in Ferromagnetic Powder. *Journal Of Applied Physics* **33**, 216-219 (1962).
 65. Sharrock,M.P. Anisotropy and switching behavior of recording media - comparison of barium ferrite and acicular particles. *IEEE Transactions On Magnetism* **26**, 225-227 (1990).
 66. Papusoi,C., Stancu,A. & Papusoi,C.S. Magnetic Method for Anisotropy Axis Distribution Analysis. 2000. (in press)
 67. Vopsaroiu,M., Cookson,R. & Bissell,P.R. Anisotropy field measurements using an extended rotational remanence technique. *Physica Status Solidi A-Applied Research* **189**, 759-762 (2002).
 68. Papusoi,C. & Suzuki,T. Anisotropy field distribution measurements for high-density recording media. *Journal Of Magnetism And Magnetic Materials* **240**, 568-570 (2002).
 69. Pfeiffer,H. Determination of anisotropy-field distribution in particle assemblies taking into account thermal fluctuations. *Physica Status Solidi A-Applied Research* **118**, 295-306 (1990).

70. Pfeiffer,H. Influence of thermal fluctuations on the magnetic-properties of particle assemblies. *Physica Status Solidi A-Applied Research* **122**, 377-389 (1990).
71. Geshev,J., Martinez,L.M., Munoz,J.S., Schmidt,J.E. & Mikhov,M. Evaluation of the anisotropy field for fine-particle systems from low-field thermomagnetic curves. *IEEE Transactions On Magnetics* **35**, 1019-1023 (1999).
72. Hoon,S.R. & Paige,D.M. The use of torque magnetometry in determining particle anisotropy and orientation distributions in magnetic tape materials. *IEEE Transactions On Magnetics* **23**, 183-185 (1987).
73. Lee,Y.H., Kim,H.J., Noh,T.H., Kang,I.K. & Kim,C.S. A New Measurement System for Magnetic-Anisotropy with Pulsed Rotation Field. *IEEE Transactions On Magnetics* **26**, 2055-2057 (1990).
74. Li,N. & Lairson,B.M. Use of Rotational Transverse Magnetometry to Measure Anisotropy Energy. *Journal Of Applied Physics* **85**, 5142-5144 (1999).
75. Jones,G.R., Prichard,L.S., Hutchings,J.A., Laidler,H. & O'Grady,K. Determination of Anisotropy fields in recording media. *Journal Of Applied Physics* **87**(9), 5711-5713. 2000.
76. Johnson,C.E. & Brown,W.F. Magnetic Determination of Shape Distribution of Single Domain Powders. *Journal Of Applied Physics* **29**, 313-314 (1958).
77. Papusoi,C. & Suzuki,T. Magnetic anisotropy field dispersion characterization of advanced perpendicular and longitudinal media. *IEEE Transactions On Magnetics* **38**, 1687-1692 (2002).
78. Berkowitz,A.E. & Flanders,P.J. Magnetic Analysis of the Precipitation of Iron from Beta Brass. *Acta Metallurgica* **8**, 823-832 (1960).
79. Suran,G. & Ounadjela,K. Magnetically induced anisotropy in amorphous $\text{Co}_{1-x}\text{Ti}_x$ thin-films studied by various techniques. *Journal Of Magnetism And Magnetic Materials* **54-7**, 237-238 (1986).

80. Asti,G. & Rinaldi,S. Nonanalyticity of the Magnetization Curve: Application to the Measurement of Anisotropy in Polycrystalline Samples. *Physical Review Letters* **28**, 1584-1586 (1972).
81. Asti,G. & Rinaldi,S. Singular points in the magnetization curve of a polycrystalline ferromagnet. *Journal Of Applied Physics* **45**(8), 3600-3610. 1974.
82. Asti,G. Singularities in the magnetization processes of high anisotropy materials. *IEEE Transactions On Magnetics* **30**, 991-996 (1994).
83. Barandiaran,J.M., Vazquez,M., Hernando,A., Gonzalez,J. & Rivero,G. Distribution of the Magnetic-Anisotropy in Amorphous-Alloys Ribbons. *IEEE Transactions On Magnetics* **25**, 3330-3332 (1989).
84. Bottoni,G., Candolfo,D., Cecchetti,A. & Masoli,F. Magnetic anisotropy distribution in Ba ferrite particles. *Journal Of Magnetism And Magnetic Materials* **193**, 326-328 (1999).
85. Bottoni,G., Candolfo,D. & Cecchetti,A. The characteristics of the anisotropy field distribution in magnetic recording media. *Journal Of Magnetism And Magnetic Materials* **195**, 754-758 (1999).
86. Franco,V. & Conde,A. Magnetic anisotropy obtained from demagnetization curves: Influence of particle orientation and interactions. *Applied Physics Letters* **74**, 3875-3877 (1999).
87. Bottoni,G., Candolfo,D. & Cecchetti,A. Analysis of the magnetic anisotropy in advanced metal particles for recording media. *Physica Status Solidi A-Applied Research* **186**, 437-443 (2001).
88. Artman,J.O. Magnetic anisotropy and structure of magnetic recording media. *Journal Of Applied Physics* **61**(8), 3137-3142. 1987.

89. Surig,C., Zimmerman,G. & Hempel,K.A. Transverse susceptibility and ferromagnetic-resonance of Hi-8 metal evaporated tape. *Journal Of Applied Physics* **75**, 5981-5983 (1994).
90. Orth,T., Moller,M., Pelzl,J., Schmitt,W. & Kohler,B.U. Characterization of the Anisotropy Behavior of Different Cobalt Modified Gamma-Fe₂O₃. *Journal Of Magnetism And Magnetic Materials* **145**, 243-254 (1995).
91. Calleja,J.F., Gutierrez,M.O., Suran,G., Corrales,J.A. & Contreras,C. Comparison of the in-plane magnetic anisotropy dispersion obtained using transverse biased initial susceptibility technique performed by magneto-optical Kerr effect and ferromagnetic resonance technique: The role of the large angle ripple. *Japanese Journal of Applied Physics Part 1-Regular Papers Short Notes & Review Papers* **37**, 6384-6389 (1998).
92. Zijlstra,H. *Review Of Scientific Instruments* **32**, 634 (1961).
93. Richter,H.J., Hempel,K.A., Schulz,R., Maurer,R. & Hibst,H. Application of the torsion pendulum method to barium ferrite media. *IEEE Transactions On Magnetism* **25**, 3405-3407 (1989).
94. Richter,H.J. Determination of magnetic-anisotropy of magnetically hard materials. *Journal Of Applied Physics* **67**, 3081-3087 (1990).
95. Richter,H.J. Transverse susceptibility measurements of particulate media. *IEEE Transactions On Magnetism* **26**, 1882-1884 (1990).
96. Zimmermann,G. Determination of magnetic-anisotropy by transverse susceptibility measurement - an application to NdFeB. *Journal Of Applied Physics* **73**, 8436-8440 (1993).
97. LeDang,K., Veillet,P., Suran,G. & Ounadjela,K. Study of induced uniaxial anisotropy in magnetic thin-films by transverse susceptibility. *Journal Of Applied Physics* **62**, 3328-3330 (1987).

98. Sollis,P.M. Hoare,A., Peters,A., Orth,T., Bissell,P.R., Chantrell,R.W. & Pelzl,J.. Experimental and theoretical-studies of transverse susceptibility in recording media. *IEEE Transactions On Magnetics* **28**, 2695-2697 (1992).
99. Sollis,P.M., Bissell,P.R. & Chantrell,R.W. Transverse susceptibility and remanence characteristics of barium ferrite hand spread coatings as a function of milling time. *IEEE Transactions On Magnetics* **30**, 4101-4103 (1994).
100. Sollis,P.M., Bissell,P.R. & Matsutake,Y. An experimental investigation of the influence of interactions on anisotropy field. *IEEE Transactions On Magnetics* **33**, 3046-3048 (1997).
101. Bottoni,G., Candolfo,D. & Cecchetti,A. Comparison between different methods for evaluating the anisotropy field distribution in recording systems. *IEEE Transactions On Magnetics* **36**, 2441-2443 (2000).
102. Spinu,L. Srikanth,H., Wiemann,J.A., Li,S., Tang,J. & O'Connor,C.J. Superparamagnetism and transverse susceptibility in magnetic nanoparticle systems. *IEEE Transactions On Magnetics* **36**, 3032-3034 (2000).
103. Turilli,G. Measurement of the Magnetic-Anisotropy Field by Performing the 2Nd Derivative of the Magnetization Curve in A Continuous Field. *Journal Of Magnetism And Magnetic Materials* **130**, 377-383 (1994).
105. Miyajima,H., Sato,K. & Mizoguchi,T. Simple analysis of torque measurement of magnetic thin films. *Journal Of Applied Physics* **47**(10), 4669-4671. 1976.
106. Uesaka,Y., Fukushima,H. & Inaba,N. Accuracy of 45 degrees torque method for obtaining anisotropy constant of 2D random films. *IEEE Transactions On Magnetics* **35**, 2673-2675 (1999).
107. Corrales,J.A., Rivas,M., Calleja,J.F., Iglesias,I. & Contreras,M.C. Highly sensitive magneto-optic transverse Kerr effect measurement system for the detection of perpendicular anisotropy and magnetic phases in thin films. *Journal Of Applied Physics* **79**, 5217-5219 (1996).

108. Sollis,P.M. Transverse susceptibility measurements on particulate recording media. 30-8-1995. University of Central Lancashire, Preston, UK.
109. Srikanth,H., Wiggins,J. & Rees,H. Radio-frequency impedance measurements using a tunnel-diode oscillator technique. *Review Of Scientific Instruments* **70**, 3097-3101 (1999).
110. Spratt,G.W.D. Particle interactions in fine particle magnetic systems. 103-125. 1987. University of Central Lancashire.
Ref Type: Thesis
111. Heuser,T. Determination of the transverse ac susceptibility for magnetic samples. 11-1-2002.
Ref Type: Unpublished Work
112. Sollis,P.M. Bissell,P.R., Mayo,P.I., Chantrell,R.W., Gilson,R.G. & O'Grady,K. Characterization of the dispersion process using transverse susceptibility measurements. *Journal Of Magnetism And Magnetic Materials* **120**, 94-96 (1993).
113. Hoare,A., Chantrell,R.W., Schmitt,W. & Eiling,A. The reversible transverse susceptibility of particulate recording media. *Journal Of Physics D-Applied Physics* **26**, 461-468 (1993).
114. Lu,J.J., Huang,H.L., Chang,C.R. & Klik,I. Reversible transverse susceptibility of particulate recording media. *Journal Of Applied Physics* **75**, 5499-5501 (1994).
115. Huang,H.L. & Lu,J.J. Textural and sweep rate effects on transverse susceptibility of magnetic particles. *Journal Of Magnetism And Magnetic Materials* **140**, 1917-1918 (1995).
116. Huang,H.L. & Lu,J.J. Thermal relaxation, textural and sweep-rate effects on reversible transverse susceptibility of magnetic particles. *Journal Of Applied Physics* **77**, 3323-3330 (1995).

117. Lee, J., Klik, I. & Chang, C.R. The reversible transverse susceptibility of coupled uniaxial systems. *Journal Of Magnetism And Magnetic Materials* **129**, L141-L145 (1994).
118. Chang, C.R. & Yang, J.S. Detection of anisotropy in the reversible transverse susceptibility. *Applied Physics Letters* **65**, 496-498 (1994).
119. Zimmermann, G. Transverse susceptibility of particulate recording media in different remanence states. *Journal Of Applied Physics* **77**, 2097-2101 (1995).
120. Sollis, P.M., Bissell, P.R. & Chantrell, R.W. The effects of texture and interactions on transverse susceptibility measurements of particulate media. *Journal Of Magnetism And Magnetic Materials* **155**, 123-125 (1996).
121. Chantrell, R.W., Bissell, P.R., Sollis, P., Hoare, A. & Orth, T. Deconvolution of anisotropy field distributions from transverse susceptibility measurements. *Journal Of Magnetism And Magnetic Materials* **177**, 894-895 (1998).
122. Jones, H.V., Duller, A.W.G., Chantrell, R.W., Hoare, A. & Bissell, P.R. A neural network approach to the determination of anisotropy distributions. *Journal Of Physics D-Applied Physics* **31**, 3028-3035 (1998).
123. Jones, H.V., Duller, A.W.G., Chantrell, R.W., Hoare, A. & Bissell, P.R. Application of neural networks to the determination of h-k distributions from transverse susceptibility data. *Journal Of Magnetism And Magnetic Materials* **193**, 416-419 (1999).
124. Spinu, L., Srikanth, H., Carpenter, E.E. & O'Connor, C.J. Dynamic Radio-Frequency Transverse Susceptibility in Magnetic Nanoparticle Systems. *Journal of Applied Physics*. **87**(9), 5490-5492 (2000)
125. Inaba, H., Ejiri, K., Abe, N., Masaki, K. & Araki, H. The advantages of the thin magnetic layer on a metal particulate tape. *IEEE Transactions On Magnetics* **29**, 3607-3612 (1993).

126. Veitch,R.J., Ilmer,A., Lenz,W. & Richter,V. MP technology for a new generation of magnetic tapes. *Journal Of Magnetism And Magnetic Materials* **193**, 279-283 (1999).
127. Berkov,D.V. & Chantrell,R.W. Transverse Susceptibility for the Fanning Mode of Magnetization Reversal. *Journal Of Magnetism And Magnetic Materials* **120**, 200-202 (1993).
128. Mercer,T. Particulate dispersions for magnetic recording media. 2001.
Ref Type: Thesis/Dissertation
129. Bissell,P.R. Proportions of components in γ -Fe₂O₃ / CrO₂ VHS tape. 2002.
Ref Type: Personal Communication
130. Pankhurst,Q.A. & Pollard,R.J. Fine-Particle Magnetic Oxides. *Journal of Physics-Condensed Matter* **5**, 8487-8508 (1993).
131. Sharrock,M.P. MP3 and MP4 particle details. Cookson, R. 10-9-2000.
Ref Type: Personal Communication
132. Cullity,B.D. Introduction to Magnetic Materials. Cohen,M. (ed.), pp. 618-620 (Addison Wesley, California,1972).
133. Hisano,S. & Saito,K. Research and development of metal powder for magnetic recording. *Journal Of Magnetism And Magnetic Materials* **190**, 371-381 (1998).
134. Okamoto,K., Okazaki,Y., Nagai,N. & Uedaira,S. Advanced metal particles technologies for magnetic tapes. *Journal Of Magnetism And Magnetic Materials* **155**, 60-66 (1996).
135. Bissell,P.R., Vopsaroiu,M., Cookson,R.D. & Sharrock,M.P. A magnetic evaluation of recording tape thickness. *Journal Of Magnetism And Magnetic Materials* **242-245**, 331-334 (2002).

136. Lutkestetzkamp,H.J., Methfessel,S. & Chantrell,R.W. Relation between the transverse ac susceptibility and anisotropy distribution in fesi. *Journal De Physique* **49**, 1313-1314 (1988).
137. AUVICO magnetic iron oxide grades / for video tapes. 2003.
<http://www.titan.ab.psiweb.com/english/auvico.htm>, **Titan Kogyo Kabushiki Kaisha**.
Ref Type: Website
138. Craik,D. Magnetism - Principles and Applications., pp. 377-408 (John Wiley & Sons Ltd., Chichester,1995).
139. Fannin,P.C., Scaife,B.K.P. & Charles,S.W. New Technique for Measuring the Complex Susceptibility of Ferrofluids. *Journal Of Physics E-Scientific Instruments* **19**, 238-239 (1986).
140. Fannin,P.C., Scaife,B.K.P. & Charles,S.W. A Study of the Complex Susceptibility of Ferrofluids and Rotational Brownian-Motion. *Journal Of Magnetism And Magnetic Materials* **65**, 279-281 (1987).
141. Neel,L. *Annales de Geophysique* **5**, 99-136 (1949).
142. Papusoi,C. Discussion of imaginary transverse susceptibility results. 17-12-2001.
Ref Type: Personal Communication

Appendix – Susceptometer control system software

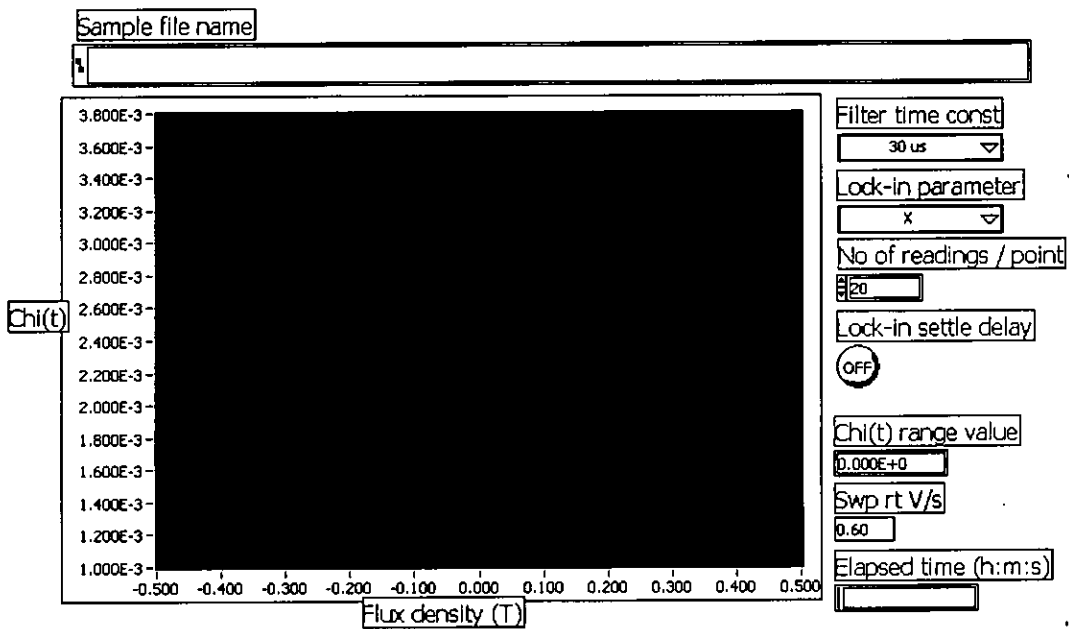
| | |
|---|-----|
| Main loop | 202 |
| Field control routine | 205 |
| Global variables..... | 208 |
| Initialise Serial Port..... | 209 |
| Read magnetic moment..... | 210 |
| Elapsed time | 213 |
| Get results filename..... | 214 |
| Get baseline array from file..... | 215 |
| creep field..... | 216 |
| set time const.vi..... | 218 |
| wait for lock-in to settle.vi | 219 |
| Warm up magnet | 220 |
| Look up | 222 |
| change polarity | 223 |
| get magnet current setting | 226 |
| switch sense..... | 227 |
| set new current | 229 |
| increment caculation | 230 |
| overload detect and sensitivity adjust.vi | 231 |
| Burst read | 232 |
| Date string | 234 |
| Reduce field..... | 235 |
| Increase field | 237 |
| Write string to lockin.vi | 239 |
| set magnet to zero..... | 241 |
| creep set current | 242 |
| read magnet direction | 243 |
| read lockin parameter..... | 244 |
| Round to 0.001 | 246 |
| Read magnet voltage | 247 |
| Read string from lockin.vi..... | 248 |
| Clear Buffer.vi..... | 250 |

Main loop

Connector Pane

Test
Loop

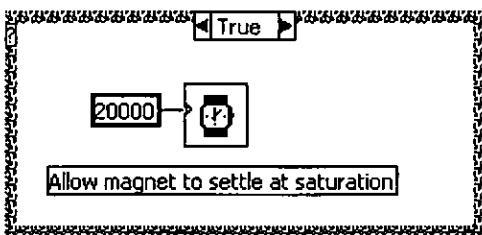
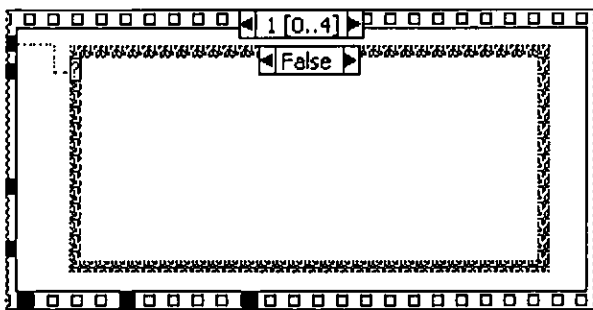
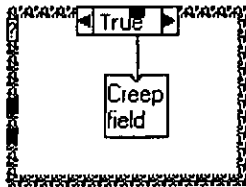
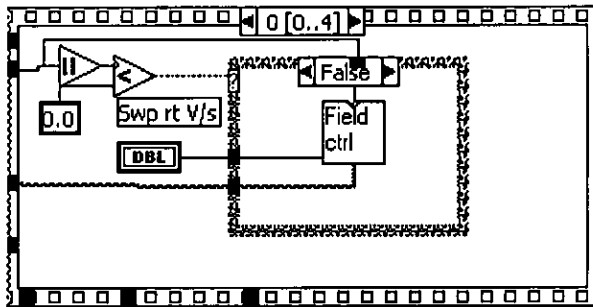
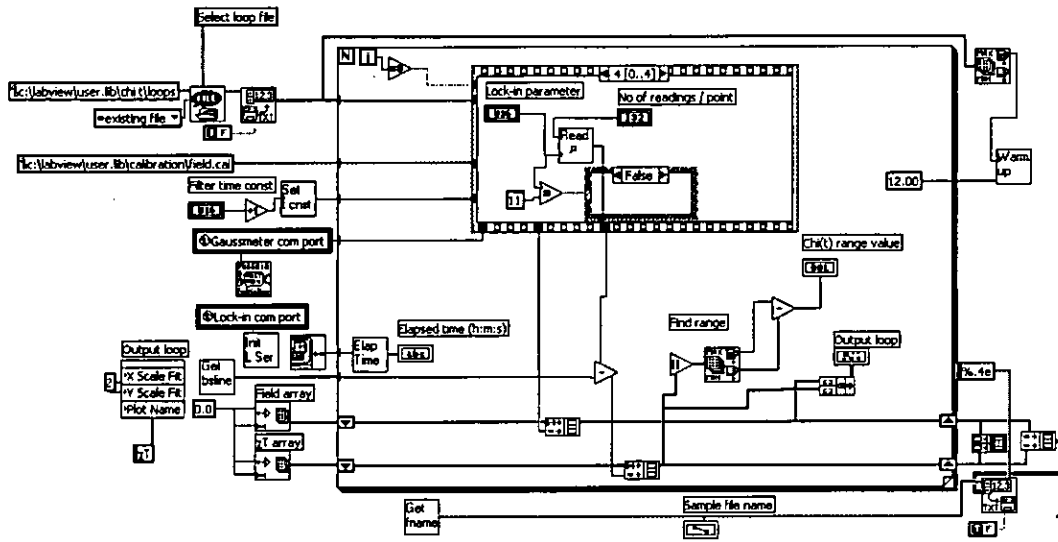
Front Panel

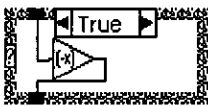
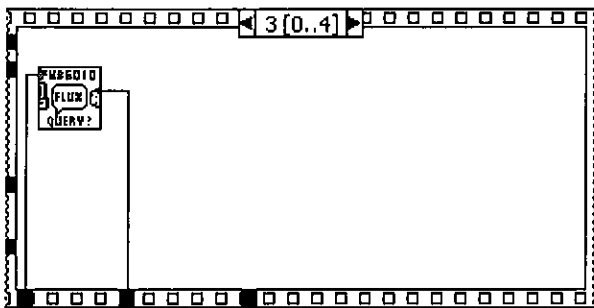
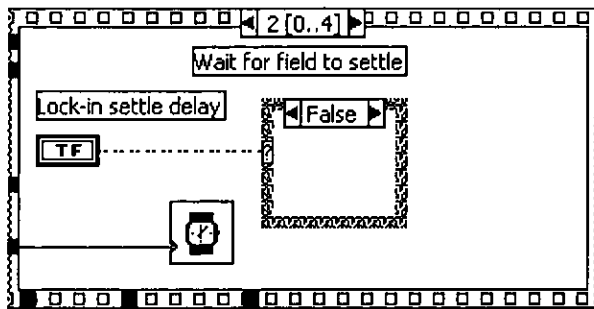


Controls and Indicators

- U16** Lock-in parameter
 - U16** Filter time const
 - DBL** Swp rt V/s
 - I32** No of readings / point
 - TF** Lock-in settle delay
 - RF** Output loop
 - abc** Elapsed time (h:m:s)
 - File** Sample file name
 - DBL** Chi(t) range value
-

Block Diagram





List of SubVIs



Read From Spreadsheet File.vi

C:\Program Files\National Instruments\LabVIEW\vi.lib\Utility\file.lib\Read From Spreadsheet File.vi



Field control routine

C:\Labview\USER.LIB\Magnet control.lib\Field control routine



Global variables

D:\USER.LIB\Magnet control.lib\Global variables



Initialise Serial Port

D:\USER.LIB\SR810\Sr810.lib\Initialise Serial Port



FWB6010 Initialize.vi

C:\Labview\USER.LIB\6010\fwb6010.lib\FWB6010 Initialize.vi



FWB6010 Flux Query.vi

C:\Labview\USER.LIB\6010\fwb6010.llb\FWB6010 Flux Query.vi



Read magnetic moment

C:\Labview\USER.LIB\Transverse Susceptibility.llb\Read magnetic moment



Elapsed time

C:\Labview\USER.LIB\Utilities.llb\Elapsed time



Get results filename

C:\Labview\USER.LIB\Utilities.llb\Get results filename



Write To Spreadsheet File.vi

C:\Program Files\National Instruments\LabVIEW\vi.lib\Utility\file.llb\Write To Spreadsheet File.vi



Get baseline array from file

C:\Labview\USER.LIB\Transverse Susceptibility.llb\Get baseline array from file



creep field

D:\USER.LIB\Magnet control.llb\creep field



set time const.vi

D:\USER.LIB\SR810\Sr810.llb\set time const.vi



wait for lock-in to settle.vi

C:\Labview\USER.LIB\Utilities.llb\wait for lock-in to settle.vi



Warm up magnet

C:\Labview\USER.LIB\Transverse Susceptibility.llb\Warm up magnet

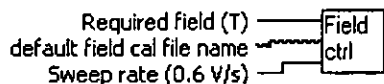
History

"Main loop History"

Current Revision: 48

Field control routine

Connector Pane



Front Panel

Field Control VI

Inputs: Magnet current, required field and sweep rate (V/s)

Sweeps current from present value to required value at sweep rate

Current setting output

0.00

Required field (T)

0.00

default field cal file name

c:\labview\user.lib\calibration\field.cal

Sweep rate (0.6 V/s)

0.60

Controls and Indicators

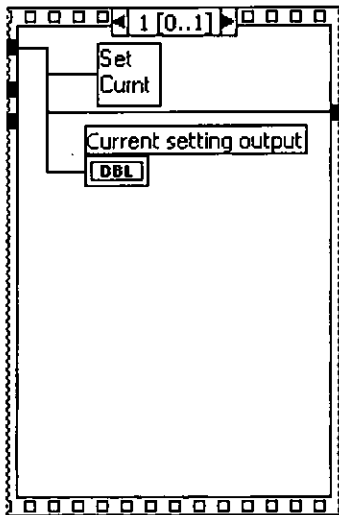
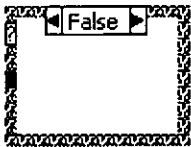
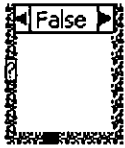
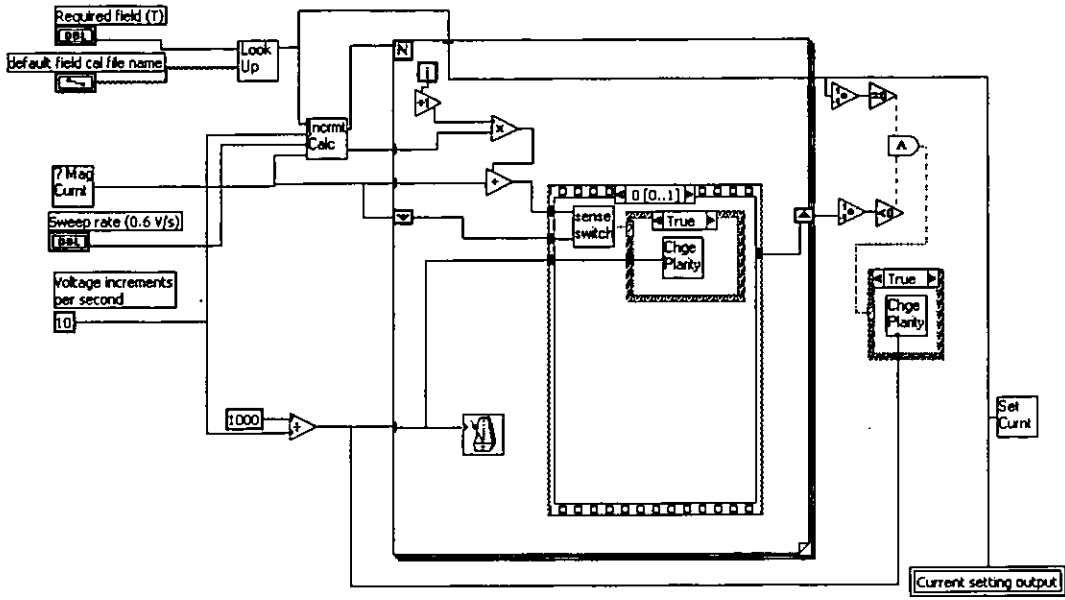
DBL Required field (T)

DBL Sweep rate (0.6 V/s)

 default field cal file name

DBL Current setting output

Block Diagram



List of SubVIs

Look up

D:\USER.LIB\Magnet control.llb\Look up

Chge
Polarity

change polarity

C:\Labview\USER.LIB\Magnet control.llb\change polarity

? Mag
Currt

get magnet current setting

D:\USER.LIB\Magnet control.llb\get magnet current setting

sense
switch

switch sense

D:\USER.LIB\Magnet control.llb\switch sense

Set
Currt

set new current

D:\USER.LIB\Magnet control.llb\set new current

Incrmt
Calc

increment caculation

D:\USER.LIB\Magnet control.llb\increment caculation

History

"Field control routine History"

Current Revision: 25

Global variables

Connector Pane



Front Panel

Lock-in com port

COM2 ▾

Power supply zero offset

0.040

Gaussmeter com port

COM1 ▾

Controls and Indicators

U16 Lock-in com port

U16 Gaussmeter com port

DBL Power supply zero offset

List of SubVIs

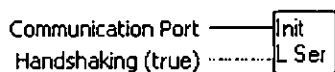
History

"Global variables History"

Current Revision: 4

Initialise Serial Port

Connector Pane



Front Panel

Initialise Lock-in amplifier

Communication Port:

Com 1 ▾

Handshaking (true):

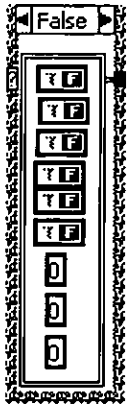
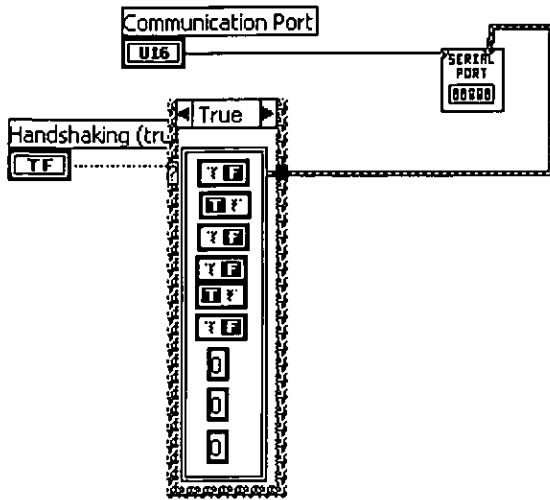
ON

Controls and Indicators

U16 Communication Port

TF Handshaking (true)

Block Diagram



List of SubVIs



Serial Port Init.vi

C:\Program Files\National Instruments\LabVIEW\vi.lib\Instr\Serial.lib\Serial Port Init.vi

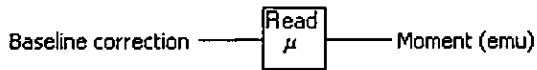
History

"Initialise Serial Port History"

Current Revision: 6

Read magnetic moment

Connector Pane



Front Panel

Read magnetic moment

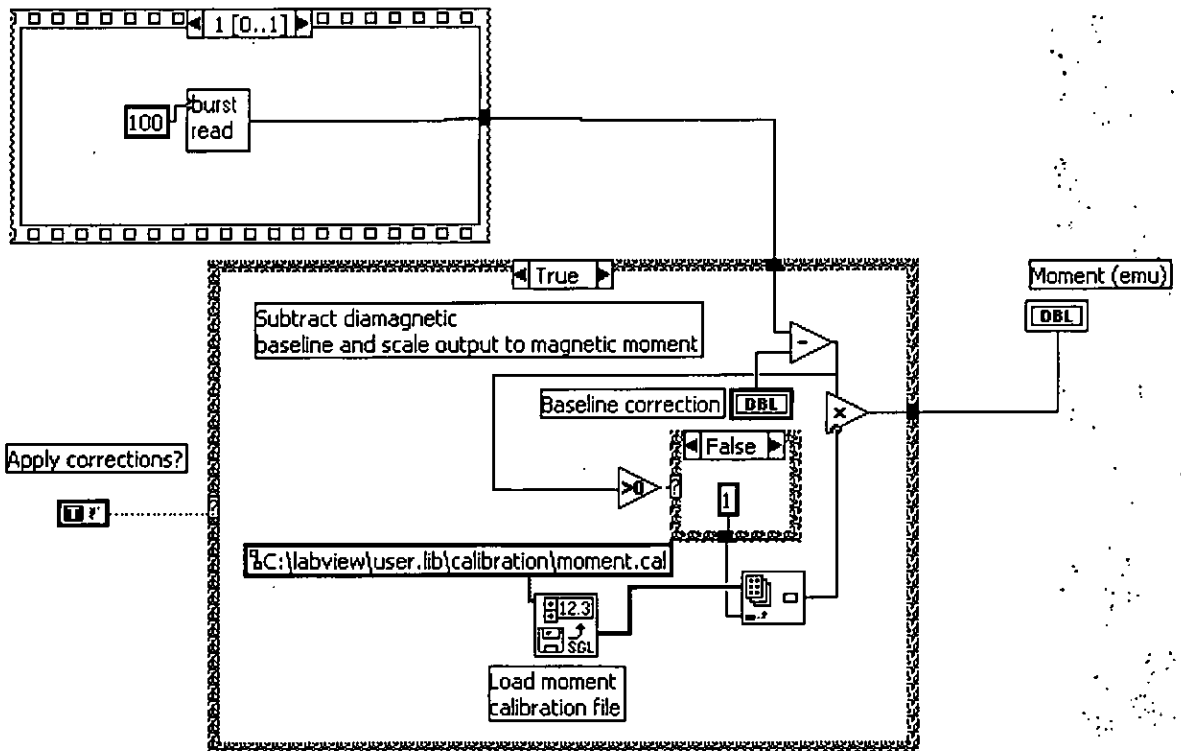


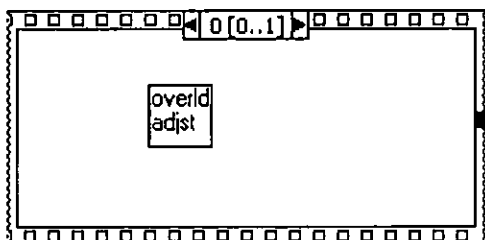
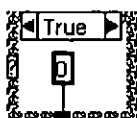
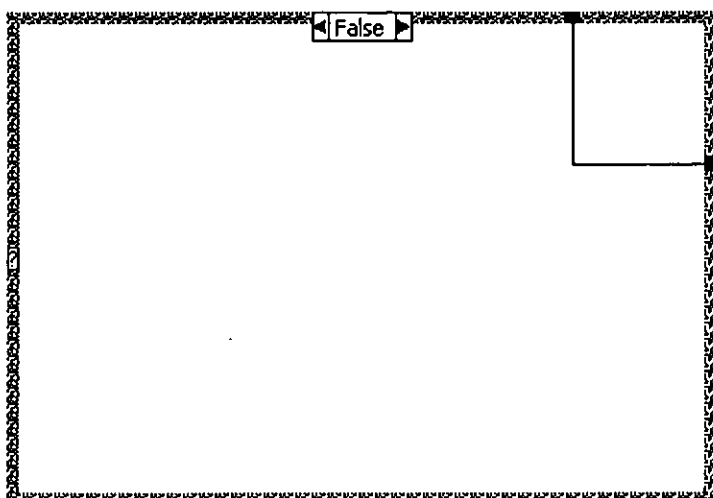
Controls and Indicators

- DBL** Baseline correction
- DBL** Moment (emu)

Block Diagram

adjust gain, Read coil voltage





List of SubVIs



Read From SGL File.vi

C:\Program Files\National Instruments\LabVIEW\vi.lib\Utility\file.lib\Read From SGL File.vi



overload detect and sensitivity adjust.vi

C:\Labview\USER.LIB\SR810\Sr810.lib\overload detect and sensitivity adjust.vi



Burst read

C:\Labview\USER.LIB\SR810\Sr810.lib\Burst read

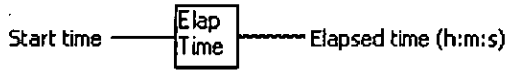
History

"Read magnetic moment History"

Current Revision: 21

Elapsed time

Connector Pane

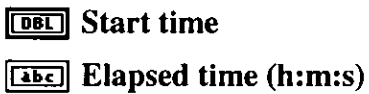


Front Panel

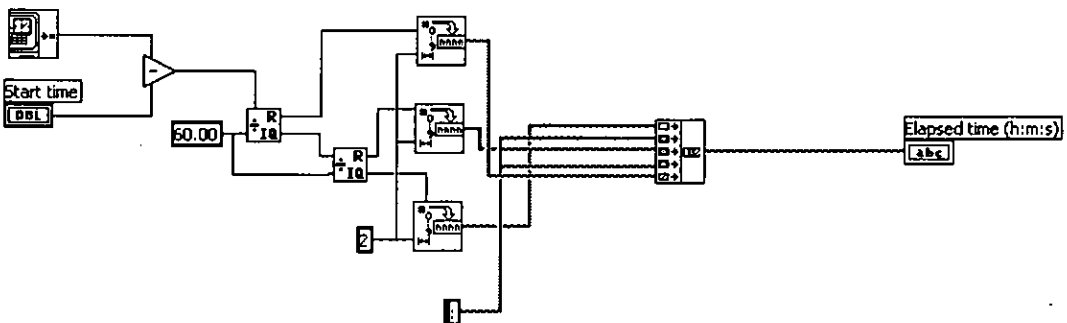
Elapsed time calculator



Controls and Indicators



Block Diagram



List of SubVIs

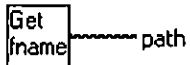
History

"Elapsed time History"

Current Revision: 1

Get results filename

Connector Pane



Front Panel

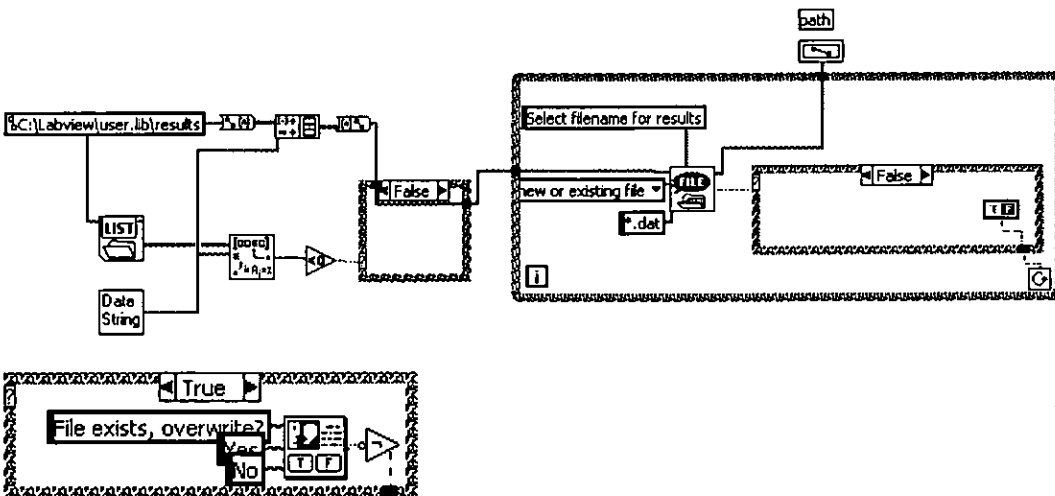
Find filename for saving data

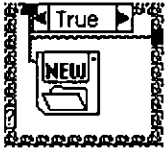


Controls and Indicators



Block Diagram





List of SubVIs



Date string

C:\Labview\USER.LIB\Utilities.llb\Date string

History

"Get results filename History"

Current Revision: 1

Get baseline array from file

Connector Pane



Baseline

Front Panel

Get baseline array from results file



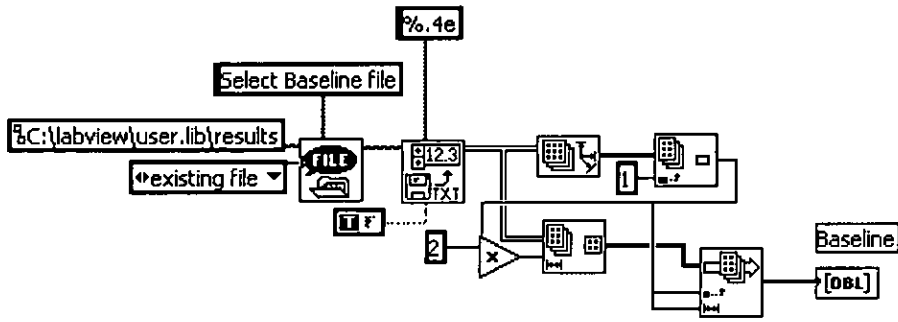
Controls and Indicators



Baseline



Block Diagram



List of SubVIs

Read From Spreadsheet File.vi

C:\Program Files\National Instruments\LabVIEW\vi.lib\Utility\file.lib\Read From Spreadsheet File.vi

History

"Get baseline array from file History"

Current Revision: 1

creep field

Connector Pane

Required field — Creep field
Increment — field

Front Panel

Creeps field by minimum increments until within 2% of reqd value

Required field

0.00

Increment

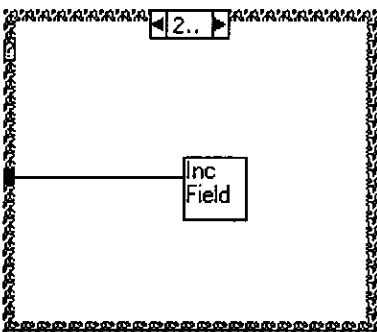
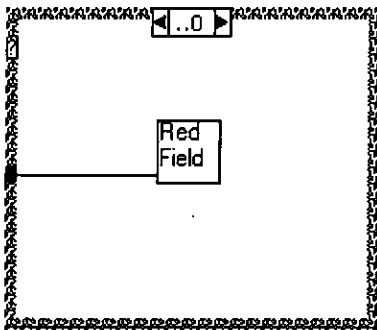
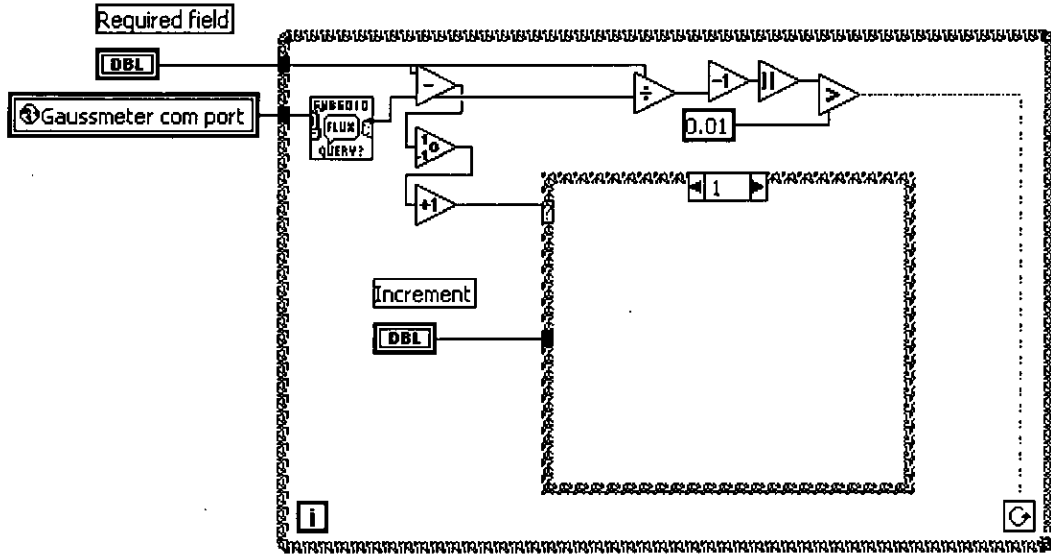
0.001

Controls and Indicators

DBL Required field

DBL Increment

Block Diagram



List of SubVIs



Reduce field

D:\USER.LIB\Magnet control.llb\Reduce field



Increase field

D:\USER.LIB\Magnet control.llb\Increase field



FWB6010 Flux Query.vi

C:\Labview\USER.LIB\6010\fwb6010.llb\FWB6010 Flux Query.vi



Global variables

D:\USER.LIB\Magnet control.llb\Global variables

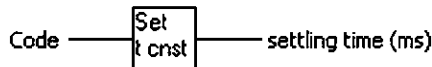
History

"creep field History"

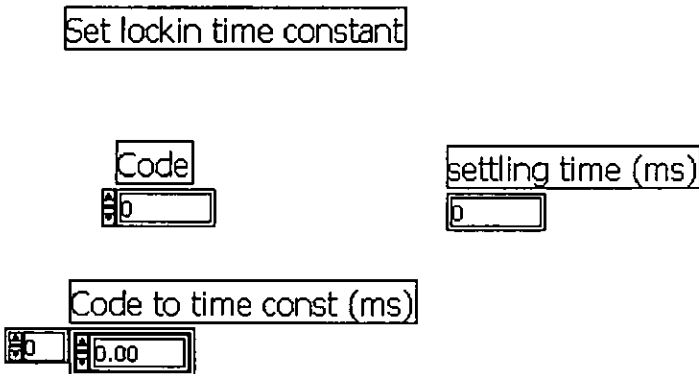
Current Revision: 7

set time const.vi

Connector Pane



Front Panel



Controls and Indicators

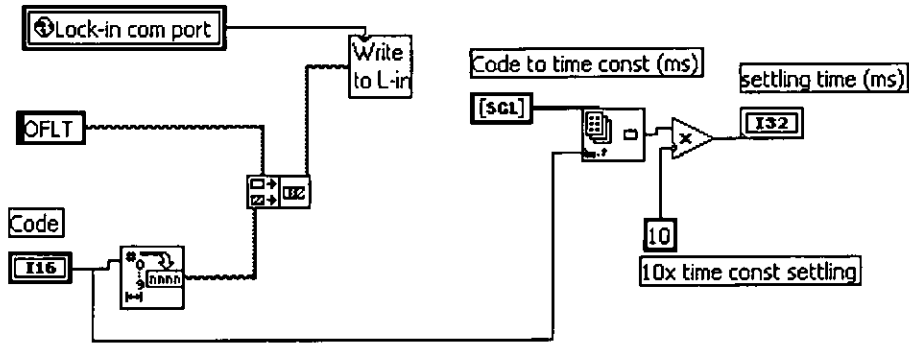
I16 Code

[scl] Code to time const (ms)

[scl]

I32 settling time (ms)

Block Diagram



List of SubVIs

Write to L-in Write string to lockin.vi

D:\USER.LIB\SR810\Sr810.llb\Write string to lockin.vi

Global variables

D:\USER.LIB\Magnet control.llb\Global variables

History

"set time const.vi History"

Current Revision: 4

wait for lock-in to settle.vi

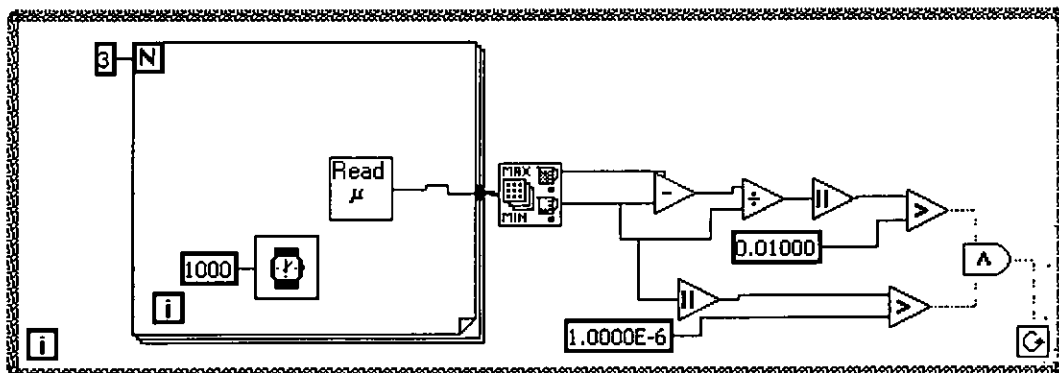
Connector Pane

lockin
settle

Front Panel

Controls and Indicators

Block Diagram



List of SubVIs

 Read magnetic moment

C:\Labview\USER.LIB\Transverse Susceptibility.llb\Read magnetic moment

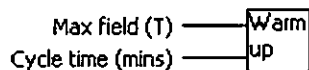
History

"wait for lock-in to settle.vi History"

Current Revision: 15

Warm up magnet

Connector Pane



Front Panel

Warm up routine Continuously cycles field at rate specified

Max field (T)

1.00

Elapsed time

Cycle time (mins)

12.00

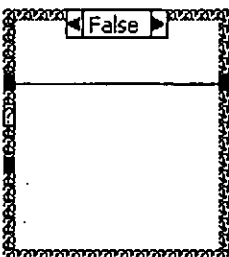
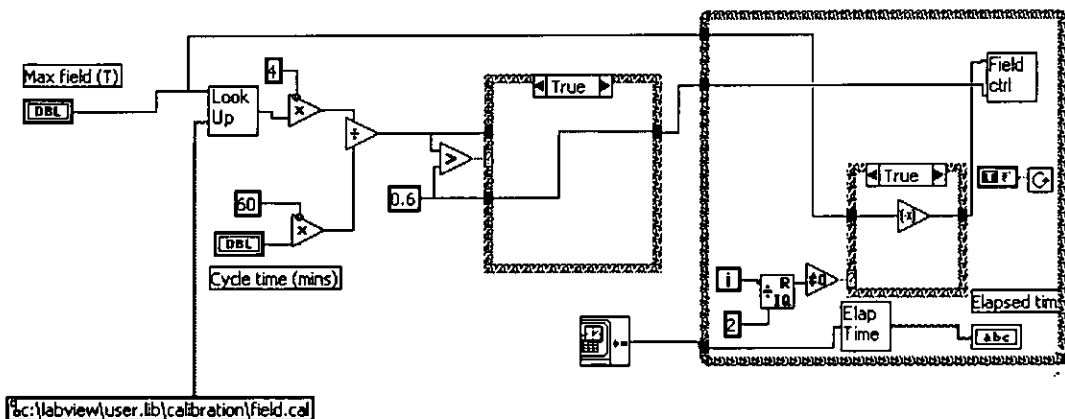
Controls and Indicators

Max field (T)

Cycle time (mins)

Elapsed time

Block Diagram



List of SubVIs

- Field control routine**
C:\Labview\USER.LIB\Magnet control.llb\Field control routine
- Look up**
D:\USER.LIB\Magnet control.llb\Look up
- Elapsed time**
C:\Labview\USER.LIB\Utilities.llb\Elapsed time
-

History

"Warm up magnet History"

Current Revision: 4

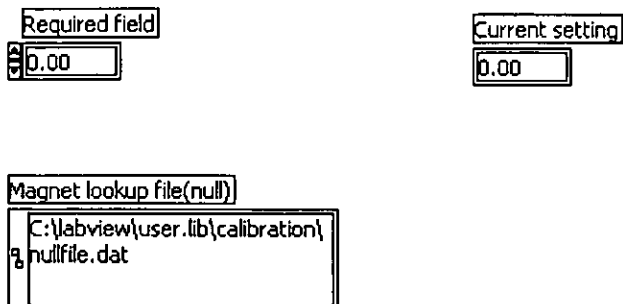
Look up

Connector Pane



Front Panel

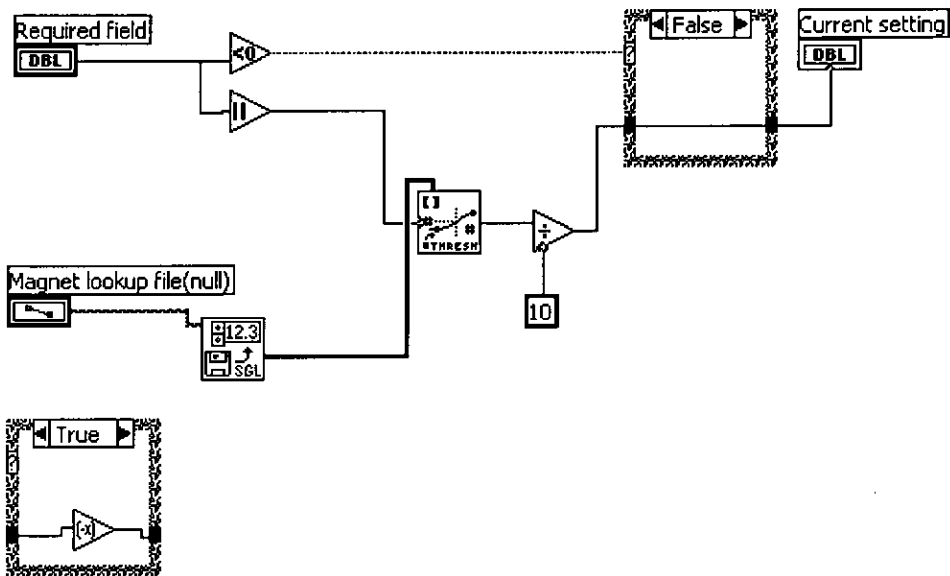
Lookup routine, passes required current for specified field.
If no lookup file is specified, passes input to output unchanged



Controls and Indicators

-  Required field
 -  Magnet lookup file(null)
 -  Current setting
-

Block Diagram



List of SubVIs

-  Read From SGL File.vi

C:\Program Files\National Instruments\LabVIEW\vi.lib\Utility\file.lib\Read From SGL File.vi

History

"Look up History"

Current Revision: 7

change polarity

Connector Pane

Increment time (ms) — Chge
Polarity

Front Panel

Polarity change

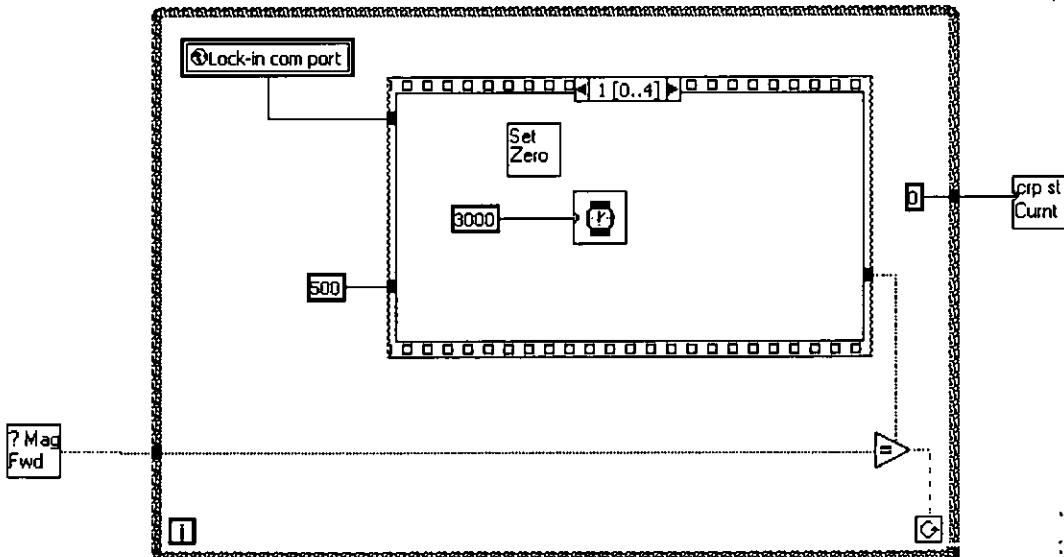
Increment time (ms)

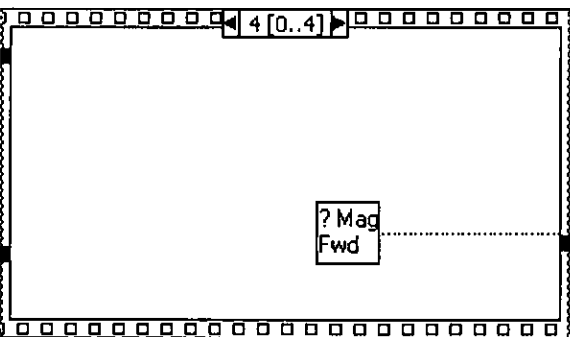
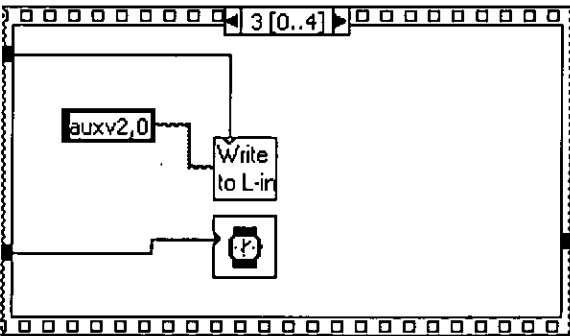
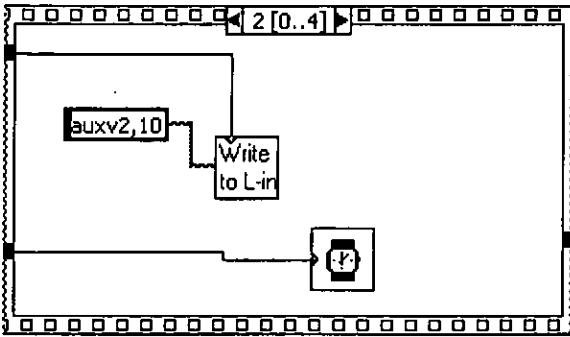
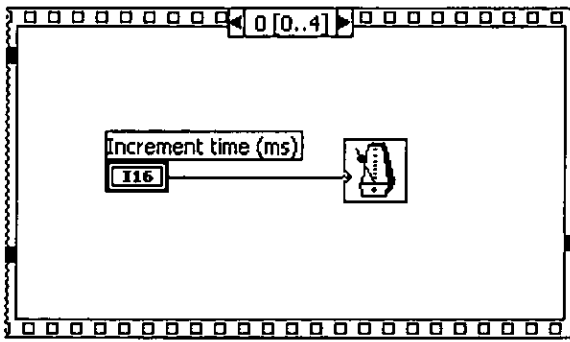
0

Controls and Indicators

116 Increment time (ms)

Block Diagram





List of SubVIs



Write string to lockin.vi

D:\USER.LIBSR810\Sr810.lib\Write string to lockin.vi



Global variables

C:\Labview\USER.LIB\Magnet control.llb\Global variables

Set
Zero

set magnet to zero

D:\USER.LIB\Magnet control.llb\set magnet to zero

crp st
Curnt

creep set current

D:\USER.LIB\Magnet control.llb\creep set current

? Mag
Fwd

read magnet direction

C:\Labview\USER.LIB\Magnet control.llb\read magnet direction

History

"change polarity History"

Current Revision: 20

get magnet current setting

Connector Pane

? Mag
Curnt

Current setting (V)

Front Panel

Get magnet current setting

Current setting (V)

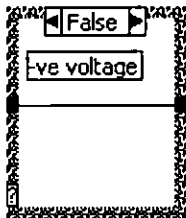
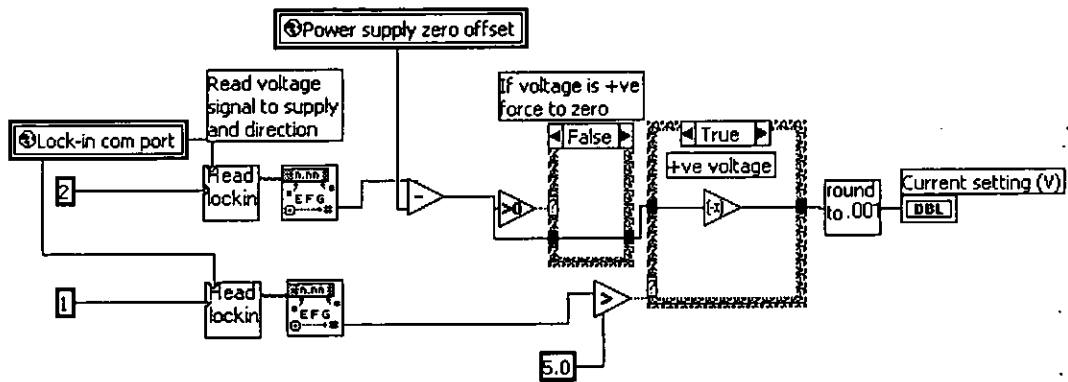
0.0000

Controls and Indicators

DBL

Current setting (V)

Block Diagram



List of SubVIs

- 
Global variables
 C:\Labview\USER.LIB\Magnet control.llb\Global variables
 - 
read lockin parameter
 D:\USER.LIB\SR810\SR810.llb\read lockin parameter
 - 
Round to 0.001
 D:\USER.LIB\Magnet control.llb\Round to 0.001
-

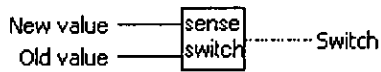
History

"get magnet current setting History"

Current Revision: 6

switch sense

Connector Pane



Front Panel

Polarity change selector



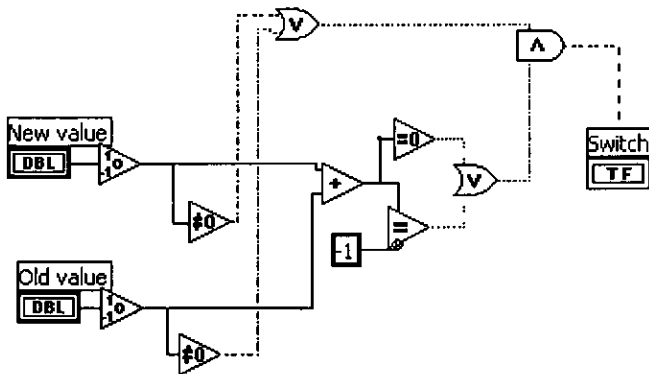
Controls and Indicators

DBL New value

DBL Old value

TF Switch

Block Diagram



List of SubVIs

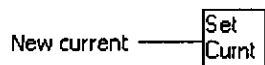
History

"switch sense History"

Current Revision: 2

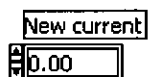
set new current

Connector Pane



Front Panel

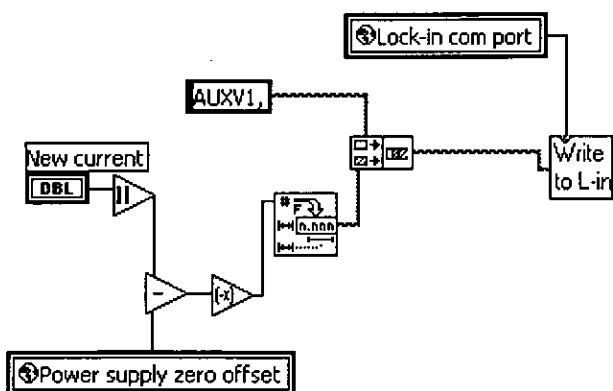
Send new current value to Lockin



Controls and Indicators

DBL New current

Block Diagram



List of Sub VIs

Write to L-in Write string to lockin.vi

D:\USER.LIB\SR810\Sr810.llb\Write string to lockin.vi



Global variables

C:\Labview\USER.LIB\Magnet control.llb\Global variables

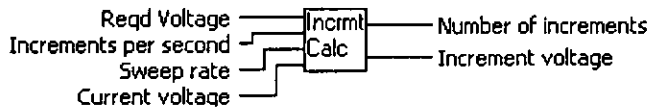
History

"set new current History"

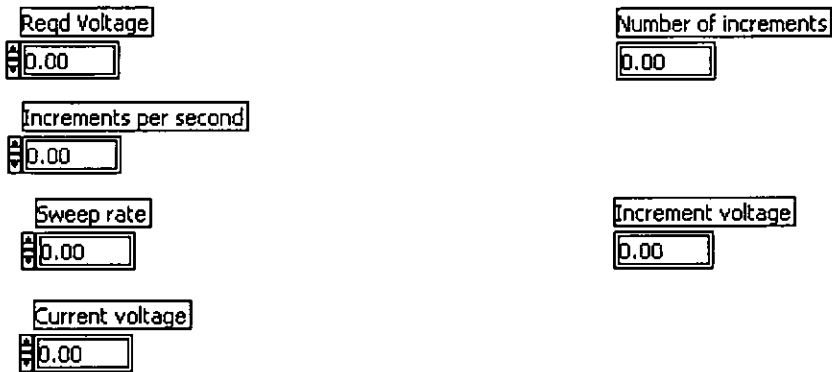
Current Revision: 6

increment caculation

Connector Pane



Front Panel

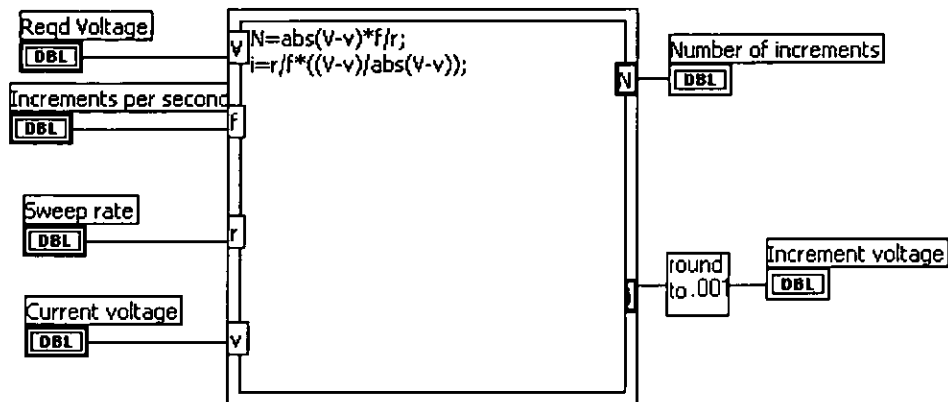


Controls and Indicators

- Reqd Voltage**
- Increments per second**
- Sweep rate**
- Current voltage**
- Number of increments**

DBL Increment voltage

Block Diagram



List of SubVIs

round to .001

D:\USER.LIB\Magnet control.lib\Round to 0.001

History

"increment caculation History"

Current Revision: 1

overload detect and sensitivity adjust.vi

Connector Pane

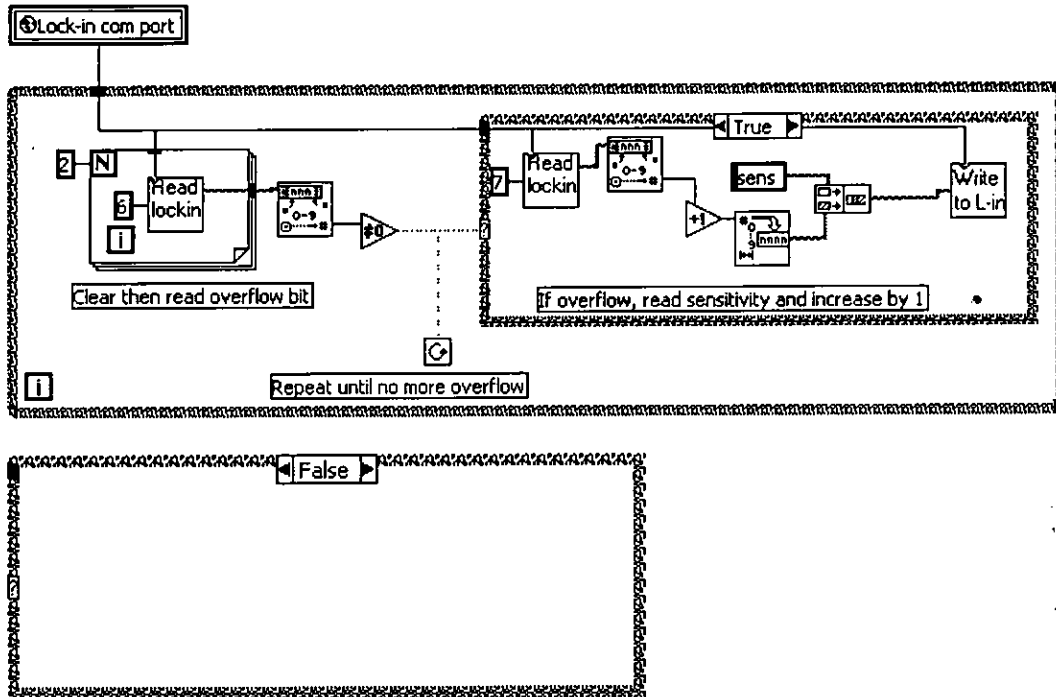
overld
adjst

Front Panel

Check for overflow and increase range if exceded

Controls and Indicators

Block Diagram



List of Sub VIs

- 
Global variables
 C:\Labview\USER.LIB\Magnet control.llb\Global variables
- 
read lockin parameter
 D:\USER.LIB\SR810\Sr810.llb\read lockin parameter
- 
Write string to lockin.vi
 D:\USER.LIB\SR810\Sr810.llb\Write string to lockin.vi

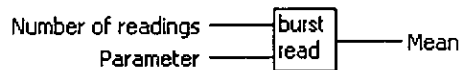
History

"overload detect and sensitivity adjust.vi History"

Current Revision: 2

Burst read

Connector Pane



Front Panel

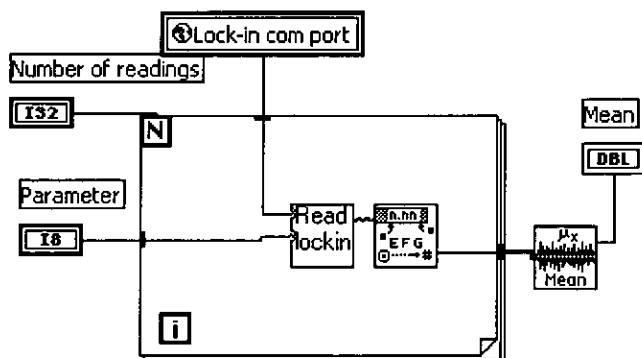
Take a burst of readings and report the average



Controls and Indicators

- [I32] Number of readings
 - [I8] Parameter
 - [DBL] Mean
-

Block Diagram



List of SubVIs

- Read lockin read lockin parameter

D:\USER.LIB\SR810\Sr810.llb\read lockin parameter



Global variables

C:\Labview\USER.LIB\Magnet control.llb\Global variables



Mean.vi

C:\Program Files\National
Instruments\LabVIEW\vi.lib\Analysis\5stat.llb\Mean.vi

History

"Burst read History"

Current Revision: 5

Date string

Connector Pane

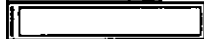


date string

Front Panel

Select results file name

date string

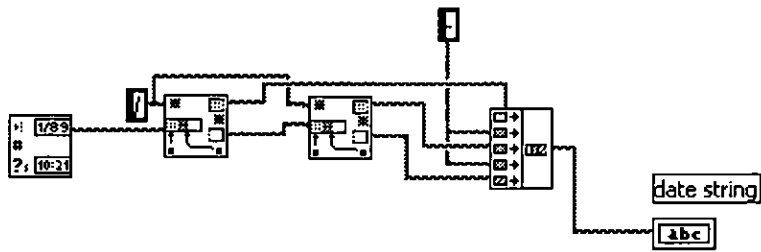


Controls and Indicators



date string

Block Diagram



List of SubVIs

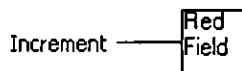
History

"Date string History"

Current Revision: 2

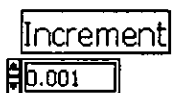
Reduce field

Connector Pane



Front Panel

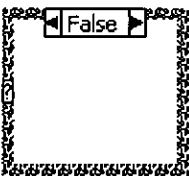
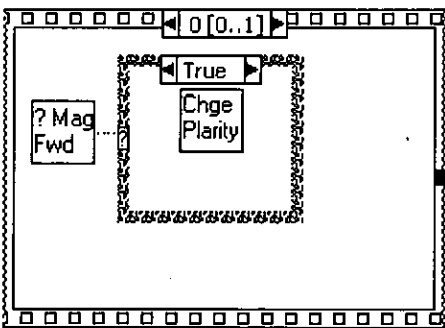
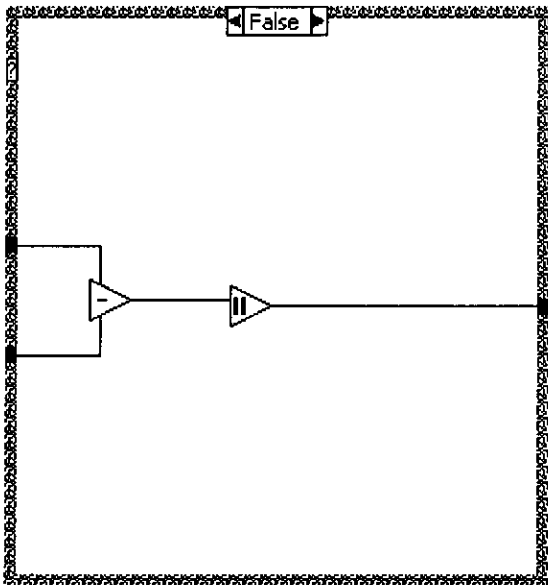
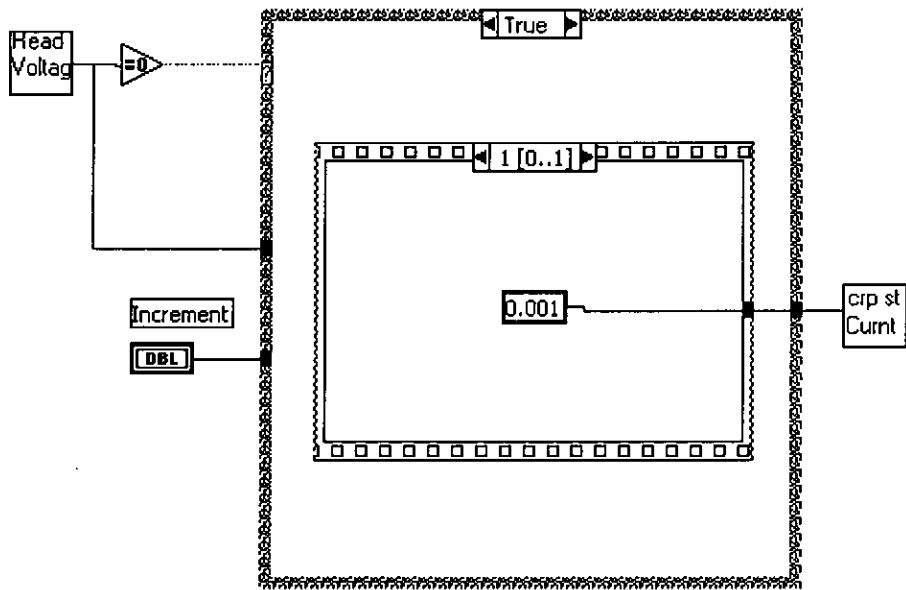
Decrease field (in absolute terms) by increment



Controls and Indicators

DBL Increment

Block Diagram



List of SubVIs

Read
Voltage

Read magnet voltage

D:\USER.LIB\Magnet control.llb\Read magnet voltage

Chge
Polarity

change polarity

C:\Labview\USER.LIB\Magnet control.llb\change polarity

? Mag
Fwd

read magnet direction

D:\USER.LIB\Magnet control.llb\read magnet direction

crp st
Curnt

creep set current

D:\USER.LIB\Magnet control.llb\creep set current

History

"Reduce field History"

Current Revision: 4

Increase field

Connector Pane

Increment

Inc
Field

Front Panel

Increase field (in absolute terms) by increment

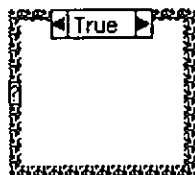
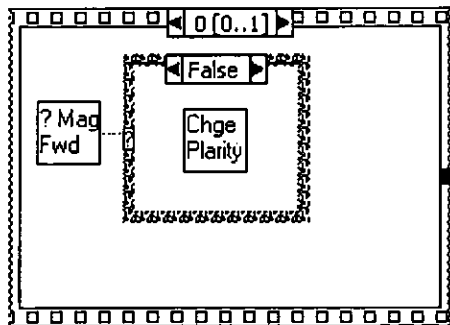
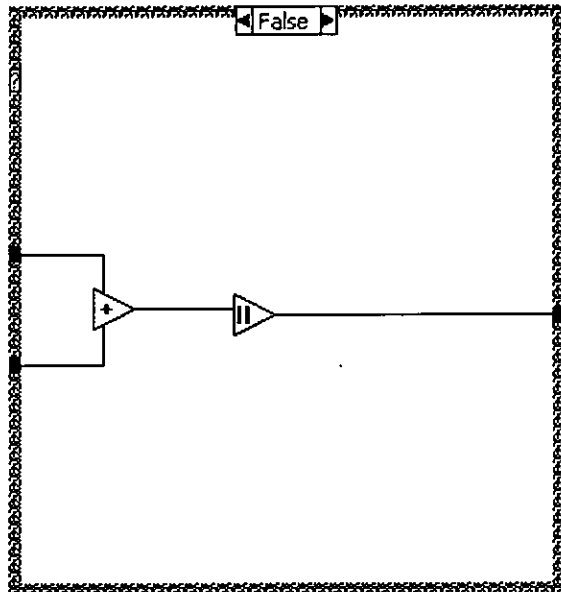
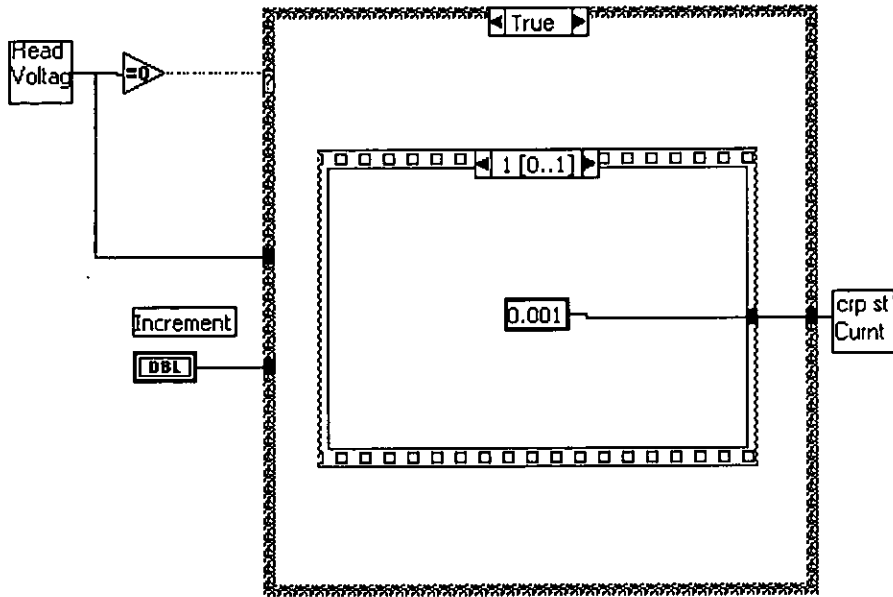
Increment

0.001

Controls and Indicators

DBL Increment

Block Diagram



List of SubVIs

Head
Voltage

Read magnet voltage

D:\USER.LIB\Magnet control.llb\Read magnet voltage

Chge
Polarity

change polarity

C:\Labview\USER.LIB\Magnet control.llb\change polarity

? Mag
Fwd

read magnet direction

D:\USER.LIB\Magnet control.llb\read magnet direction

crp st
Curnt

creep set current

D:\USER.LIB\Magnet control.llb\creep set current

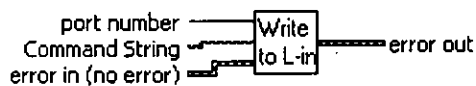
History

"Increase field History"

Current Revision: 5

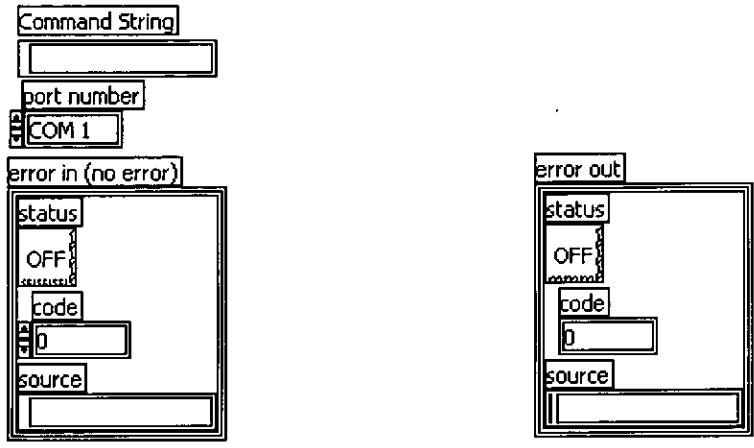
Write string to lockin.vi

Connector Pane



Front Panel

Send commands to lock-in



Controls and Indicators

abc Command String

Y32 port number

ES1 error in (no error)

TF status

Y32 code

abc source

ES1 error out

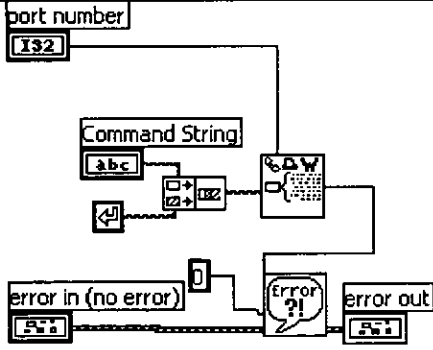
TF status

Y32 code

abc source

Block Diagram

Add carriage return to command string and send to correct port for Lock-in amplifier



List of SubVIs



Serial Port Write.vi

C:\Program Files\National Instruments\LabVIEW\vi.lib\Instr\Serial.lib\Serial Port Write.vi



Simple Error Handler.vi

C:\Program Files\National Instruments\LabVIEW\vi.lib\Utility\error.lib\Simple Error Handler.vi

History

"Write string to lockin.vi History"

Current Revision: 6

set magnet to zero

Connector Pane

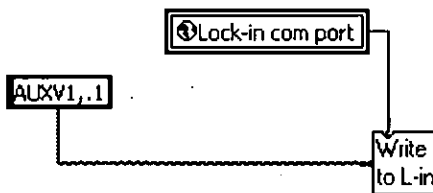


Front Panel

Set magnet to zero

Controls and Indicators

Block Diagram



List of SubVIs



Write string to lockin.vi

D:\USER.LIB\SR810\SR810.lib\Write string to lockin.vi



Global variables

C:\Labview\USER.LIB\Magnet control.lib\Global variables

History

"set magnet to zero History"

Current Revision: 11

creep set current

Connector Pane

New current —

Front Panel

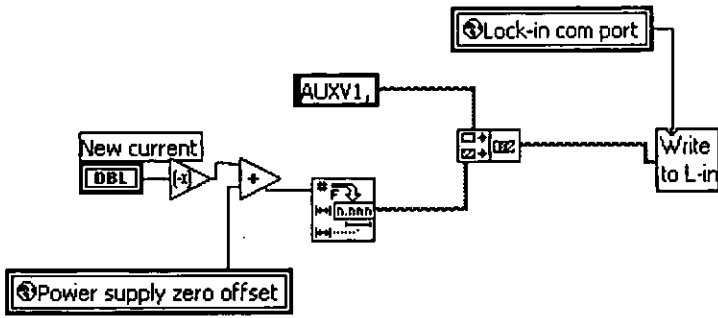
Send new current value to Lockin

New current

Controls and Indicators

New current

Block Diagram



List of SubVIs



Write string to lockin.vi

D:\USER.LIB\SR810\Sr810.llb\Write string to lockin.vi



Global variables

C:\Labview\USER.LIB\Magnet control.llb\Global variables

History

"creep set current History"

Current Revision: 8

read magnet direction

Connector Pane



..... Fwd?

Front Panel

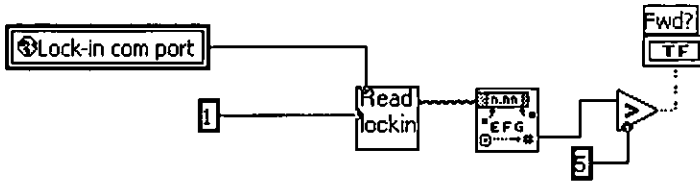
Read magnet supply polarity



Controls and Indicators

TF Fwd?

Block Diagram



List of SubVIs

Read lockin read lockin parameter

D:\USER.LIB\SR810\Sr810.lib\read lockin parameter

1 Global variables

C:\Labview\USER.LIB\Magnet control.lib\Global variables

History

"read magnet direction History"

Current Revision: 4

read lockin parameter

Connector Pane



Front Panel



Controls and Indicators

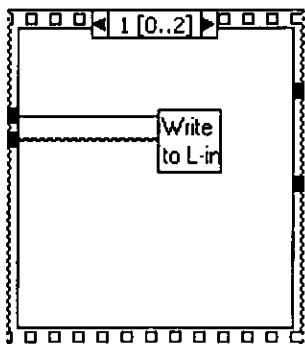
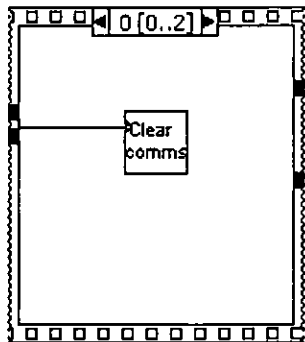
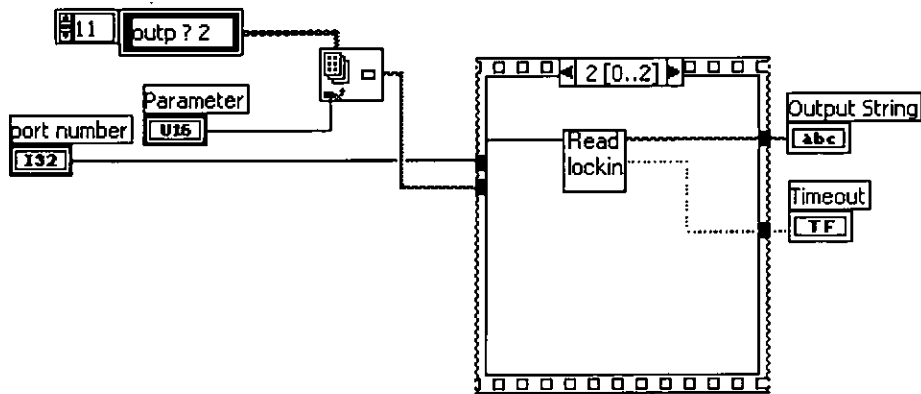
I32 port number

U16 Parameter

abc Output String

TF Timeout

Block Diagram



List of SubVIs

Write
to L-in

Write string to lockin.vi

D:\USER.LIB\SR810\Sr810.lib\Write string to lockin.vi

Read
lockin

Read string from lockin.vi

D:\USER.LIB\SR810\Sr810.lib\Read string from lockin.vi

Clear
comms

Clear Buffer.vi

D:\USER.LIB\SR810\Sr810.lib\Clear Buffer.vi

History

"read lockin parameter History"

Current Revision: 8

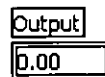
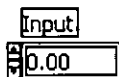
Round to 0.001

Connector Pane



Front Panel

Round to nearest 0.001

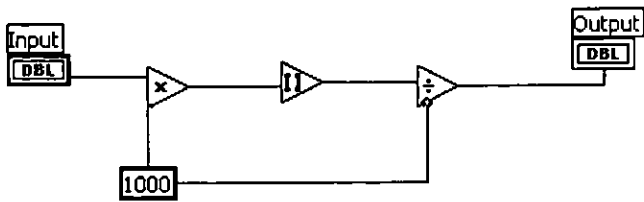


Controls and Indicators

OBL Input

OBL Output

Block Diagram



List of SubVIs

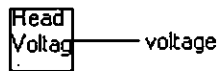
History

"Round to 0.001 History"

Current Revision: 4

Read magnet voltage

Connector Pane



Front Panel

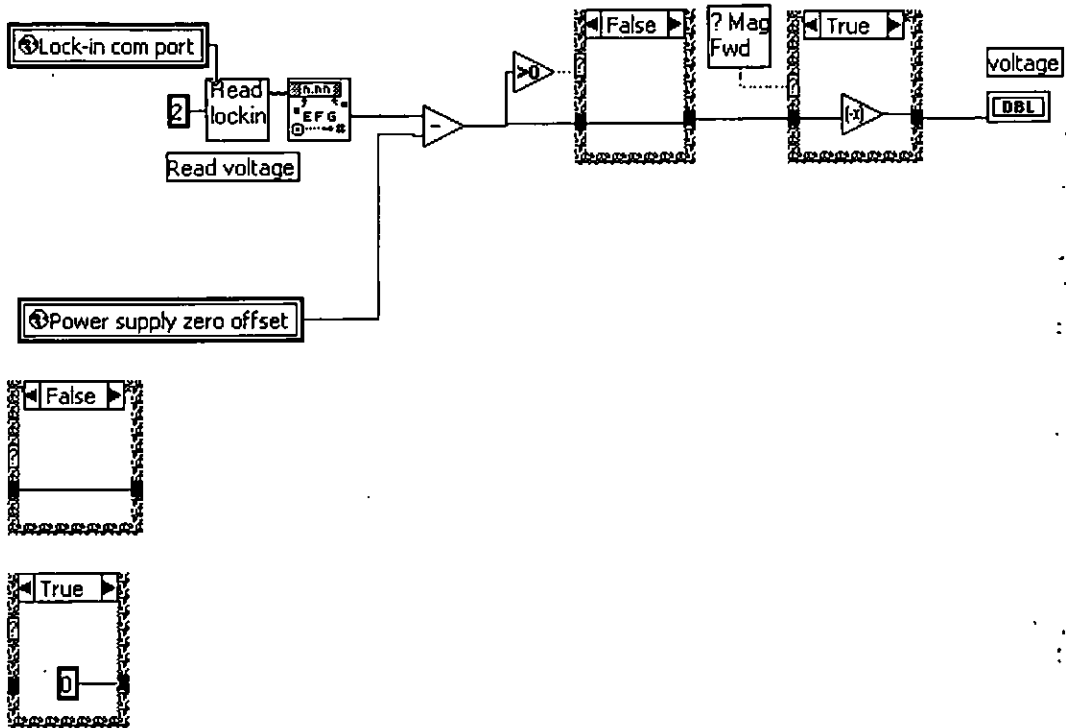
Reads magnet voltage and polarity setting and expresses it as a voltage from -10 to +10V
 (Takes into account any zero offset on the power supply)



Controls and Indicators



Block Diagram



List of SubVIs

- Read lockin **read lockin parameter**
 D:\USER.LIB\Sr810\Sr810.llb\read lockin parameter
 - 1 **Global variables**
 C:\Labview\USER.LIB\Magnet control.llb\Global variables
 - ? Mag Fwd **read magnet direction**
 D:\USER.LIB\Magnet control.llb\read magnet direction
-

History

"Read magnet voltage History"

Current Revision: 3

Read string from lockin.vi

Connector Pane



Front Panel

Read String from Lock-in

Lock-in amplifier Coms port

0

Output String

Timeout



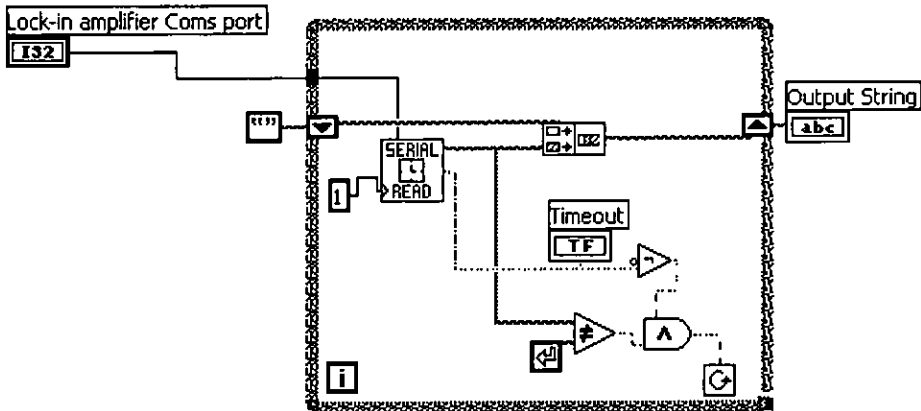
Controls and Indicators

I32 Lock-in amplifier Coms port

abc Output String

TF Timeout

Block Diagram



List of SubVIs

SERIAL READ Serial Read with Timeout.vi

C:\Program Files\National Instruments\LabVIEW\EXAMPLES\NSTR\smp1ser1.llb\Serial Read with Timeout.vi

History

"Read string from lockin.vi History"

Current Revision: 7

Clear Buffer.vi

Connector Pane



Front Panel

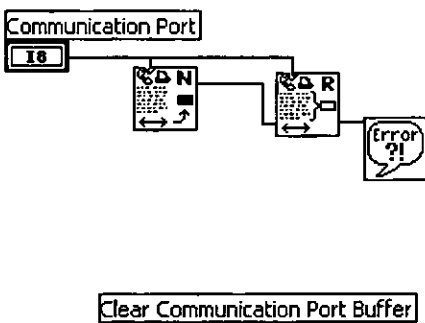


Clears any characters out of the buffer of the selected serial port

Controls and Indicators



Block Diagram



List of SubVIs



Simple Error Handler.vi

C:\Program Files\National Instruments\LabVIEW\vi.lib\Utility\error.lib\Simple Error Handler.vi



Serial Port Read.vi

C:\Program Files\National Instruments\LabVIEW\vi.lib\Instr\Serial.lib\Serial Port Read.vi



Bytes At Serial Port.vi

C:\Program Files\National Instruments\LabVIEW\vi.lib\Instr\Serial.lib\Bytes At Serial Port.vi

History

"Clear Buffer.vi History"

Current Revision: 5